Generalized holographic dualities for metric gravity & Quantum geometry based on area variables

by

Seth Kurankyi Asante

A thesis
presented to the University of Waterloo
in fulfillment of the
thesis requirement for the degree of
Doctor of Philosophy
in
Physics

Waterloo, Ontario, Canada, 2020

Examining Committee Membership

The following served on the Examining Committee for this thesis. The decision of the Examining Committee is by majority vote.

External Examiner: John Barrett
Professor, Dept. of Mathematics, University of Nottingham, United Kingdom

Supervisors: Bianca Dittrich
Faculty, Perimeter Institute for Theoretical Physics
Adjunct Faculty, Department of Physics and Astronomy
University of Waterloo

Lee Smolin
Faculty, Perimeter Institute for Theoretical Physics
Adjunct Faculty, Department of Physics and Astronomy
University of Waterloo

Committee Members: Niayesh Afshordi
Associate Professor, Department of Physics and Astronomy
University of Waterloo

Erik Schnetter
Adjunct Faculty, Department of Physics and Astronomy
University of Waterloo

Internal-External Member: Florian Girelli
Associate Professor, Department of Applied Mathematics
University of Waterloo

Author's Declaration

This thesis consists of material all of which I authored or co-authored: see Statement of Contributions included in the thesis. This is a true copy of the thesis, including any required final revisions, as accepted by my examiners.

I understand that my thesis may be made electronically available to the public.

Statement of Contributions

Part I of this thesis contains materials from the paper [1], which I co-authored with Bianca Dittrich and Florian Hopfmueller. In Chapter 4, I have used results from [2] to be published, co-authored with Bianca Dittrich. Also the paper [3] which is co-authored with Bianca Dittrich and Hal M. Haggard motivated the work in Chapter 4.

Part II of this thesis is based on two papers [4,5], both co-authored with Bianca Dittrich and Hal M. Haggard.

Work in [6] which I co-authored with Bianca Dittrich, Florian Girelli, Aldo Riello, and Panagiotis Tsimiklis is not directly part of the thesis.

Abstract

Holography holds promise for simplifying computations in quantum gravity. In part I of this thesis, we construct holographic boundary theories for linearized gravity, for a general family of finite or quasi-local boundaries, which capture diffeomorphisms acting on the boundary. These boundary theories are directly derived from the dynamics of general relativity by computing the effective action for a geometric boundary observable, which measures the geodesic length from a given boundary point to some centre in the bulk manifold. We identify the general form for these boundary theories and find that these are Liouville–like with a coupling to the boundary Ricci scalar. This is illustrated with various examples, each of which offers interesting insights into the structure of holographic boundary theories. We also compute the gravitational one-loop partition function for 4D linearized gravity, including graviton degrees of freedom via a recursion relation method.

Furthermore, discretization of general relativity is a promising route towards quantum gravity. Discrete geometries have a finite number of degrees of freedom and can mimic aspects of quantum geometry. However, the selection of the correct discrete freedoms and description of their dynamics has remained a challenging problem. Again, several approaches to four-dimensional quantum gravity, such as loop quantum gravity and holography, situate areas as their fundamental variables. With these motivations, we explore in part II classical area Regge calculus, an alternative to standard Regge calculus where instead of lengths, the areas of a simplicial discretization are fundamental. There are a number of surprises: though the equations of motion impose flatness, we show that diffeomorphism symmetry is broken for a large class of area Regge geometries. This is due to degrees of freedom not available in the length Regge calculus. We enumerate and characterize these non-metric, or 'twisted', degrees of freedom and provide tools for understanding their dynamics. The non-metric degrees of freedom also lead to fewer invariances of the area Regge action—in comparison to the length action—under local changes of the triangulation (Pachner moves). This means that invariance properties can be used to classify the dynamics of spin foam models. Our results lay a promising foundation for understanding the dynamics of the non-metric degrees of freedom in loop quantum gravity and spin foams. In the quantum theory, the choice of area variables kinematics can easily lead to gravitational dynamics peaked on flat space–times. We show that this is due to how regions are glued in the gravitational path integral via a discrete spin foam model. We introduce a family of 'effective' spin foam models that incorporate a quantum area spectrum, impose gluing constraints as strongly as possible, and leverage the discrete general relativity action to specify amplitudes. These effective spin foam models avoid flatness in a restricted regime of the parameter space.

Acknowledgements

My first thanks are to God almighty for giving me the hope, the wisdom and the strength to undertake my PhD studies. *For with God nothing shall be impossible.*

I want to express my deepest thanks to my advisor, Bianca Dittrich, for giving me the opportunity to work under her supervision in a prestigious place as the Perimeter Institute (PI). Bianca has been immensely kind to me throughout my studies. This thesis would not be possible without her support, guidance and patience towards me. She truly has my best interest at heart, and for that, I am forever grateful.

I am very grateful to Hal Haggard for his collaborations which led to the second part of this thesis. It is always a pleasure working with Hal. I am also thankful for my graduate committee members: Lee Smolin, Niayesh Afshordi, Florian Girelli, Erik Schnetter, who gave me encouragement and advice in my research. A special thanks to John Barrett for accepting and taking the time to examine my thesis.

During my PhD studies, I enjoyed and learnt a lot from working with Florian Girelli, Aldo Riello and two fellow students Florian Hopfmueller and Panagiotis Tsimiklis (Peter). Discussions and meetings with members of the quantum gravity group at PI were always insightful. I thank everyone from the quantum gravity group, especially Sebastian Steinhaus, Wolfgang Wieland and Prince Koree, with whom I had very stimulating discussions. My studies at PI were successful because of the constant encouragement and discussions I had with my wonderful friends over the years, especially with Pablo Bosch (the best office mate), Abdulmajid Osumanu, Eugene Adjei, Andrés Schlief, Monica Rincon, Qiaoyin Pan and many others. Cheers to them all.

Throughout my PhD studies, the Waterloo SDA church family became a vital part of my support system. They made me feel at home in the Waterloo region. I am incredibly grateful to Mary Tassoni, Samwel Manasse and all the youth members, to mention a few, whose encouragement and prayers kept me going.

I want to thank all my family members for their love and support over the years. I immensely appreciate my loving parents Ernest Asante and Esther Addo, for their sacrifices and trust in me. A very special thanks to my fiancée Rowena Cornelius, for her love, unflinching support and constant care for me always. I am truly blessed to have all these wonderful friends and family who positively influence my life.

Lastly, I was supported by an NSERC grant awarded to Bianca Dittrich. Research at Perimeter Institute is supported in part by the Government of Canada through the Department of Innovation, Science and Economic Development Canada and by the Province of Ontario through the Ministry of Colleges and Universities.

Dedication

In loving memory of my late grandfather Ps. Stephen Addo.

Table of Contents

List of Tables

List of Figures

Chapter 1

Introduction

The theory of general relativity has for over a century served as the theoretical underpinning for the nature of space, time and gravitation. This theory unifies the geometry of space and time with the gravitational field. Precisely, it describes the effects of gravitation as the curvature of space–time. As a consequence, this led to a paradigm shift from how space and time was described by Newtonian physics. In Einstein's theory, space–time is no longer considered a static background on which matter fields propagate, rather, the geometry of space–time is itself dynamical. Different geometries of space–time correspond to different histories of the universe.

The *fundamental degrees of freedom* of general relativity are encoded in a quantity known as the metric tensor which describes the geometry and causal structure of space–time. Its dynamics is governed by the Einstein field equations which describe the relation between space–time geometry and the distribution of matter content within. Thus general relativity provides a precise relationship between the geometry of space–time and the properties of matter.

Since its inception, the theory of general relativity has enjoyed many rich theoretical and physical applications. For example, the study of astrophysics, cosmology, black hole physics and most recently gravitational wave physics are all based on the principles of general relativity. It has also provided many successful predictions of gravitational phenomena such as time dilation, precession of Mercury's orbit, bending of light, gravitational waves and several others.

In spite of all these great accomplishments, general relativity remains incomplete as a fundamental theory of nature. The incompleteness is manifested in the breakdown of the theory due to the presence of singularities in the context of gravitational collapse

inside black holes. *Quantum theory*—a framework which describes the behaviour of atoms and molecules in the universe—underlies the descriptions of three out of the four known fundamental forces of nature with the exception of gravity. The frameworks of general relativity and quantum theory are incompatible with each other. These challenges can be overcome possibly by finding a *quantum theory of gravity* which is capable of providing a quantum description of the gravitational field.

The formulations of general relativity and quantum field theory are both based on the notion of classical space–time. Since the properties of gravity are encoded in the geometry of space–time, one expects a quantum theory of gravity to be based on *quantum geometries* or the geometry of a *quantum space–time*. Finding a consistent theory of quantum gravity which is valid over small and large energy scales is currently one of the unsolved problems in physics.

One of the critical questions in the theory of quantum gravity and quantum space–time is; what are the fundamental degrees of freedom described by? In this thesis, we shall explore two themes which are capable of addressing this question. The first theme is *holographic dualities*—based on the *holographic principle*—which suggests that the degrees of freedom of a quantum theory of gravity in a d dimensional space–time region can be encoded on its $(d-1)$ dimensional boundary. The holographic principle was motivated by black hole thermodynamics which conjectures that the maximal entropy of a space–time region scales as the area of its boundary surface rather than its volume.

The second theme is concerned with discrete approaches to the theory of quantum gravity. In these approaches there exist different notions of quantum geometries and which one is best suited for quantum gravity is unclear. In particular, it is not obvious what geometric variables account for the fundamental degrees of freedom of quantum geometry. We expound on the two themes separately in the next two sections. Specifically, we will review some literatures that serves as motivations to the aspects of the two themes which we shall focus on in this thesis.

1.1 Holographic dualities

The most explored example of holographic dualities is the AdS/CFT correspondence which proposes that a quantum gravity theory in anti-de Sitter space–time can be dually described by a conformal field theory on its asymptotic boundary. That is, the partition functions of such dual boundary field theories, which would depend on the (asymptotic) boundary metric, can be interpreted as a partition function for gravity, which is however restricted to asymptotic boundary data.

In the first part of this thesis, we will be interested in extending such holographic dualities to finite and more general boundaries of space–time. One reason is that the partition function with boundary can also serve as the vacuum (physical) wave function for gravity [7]. Thus aiming to employ holography to construct such physical wave functions, we need to understand such dualities for arbitrary boundaries.

A holographic boundary field theory would allow an easier access to the partition function of quantum gravity: instead of solving the full bulk dynamics of quantum gravity for given boundary data, and deal with the diffeomorphism gauge theory, one would have to "just" solve the dynamics of the boundary field theory. For this to be a useful approach, the boundary field theory should be ideally local or an approximation to a local theory, with finitely many fields. Note that otherwise the notion of holographic boundary field theory is quite empty, as one can construct boundary field theories by integrating out almost all bulk fields, except some degrees of freedom that one can attribute to the boundary. This will however generically lead to non–local boundary field theories, which could be converted to local ones at the price of introducing infinitely many fields.

The construction of "quasi-local" holographic dualities has already been quite successful for 3D gravity. Here, due to the topological nature of the theory, one can indeed expect to encounter a local field theory, if one goes through the procedure which will be describe in this thesis. Thus there are a number of approaches in which such boundary field theories for gravity can be constructed. Moreover, again due to the fact that there are no propagating bulk degrees of freedom, the boundary field theories describe so-called boundary degrees of freedom, which in the case of gravity can often be understood as encoding the shape of the boundary in the embedding space time.

We briefly review some of the developments which serve as motivation to this current work. Most of these works are based on asymptotic boundaries. This starts with the relation between the Chern–Simons description of AdS_3 gravity [8] to its Wess-Zumino-Witten (WZW) boundary theory [9–11], which however relies on connection boundary data. Restricting to asymptotically AdS_3 boundary conditions, one obtains a constrained (chiral) WZW model which is equivalent to Liouville theory [12–16]. Liouville boundary field theory also appears for asymptotically flat boundary conditions as the flat limit of asymptotic AdS_3 [17].

Carlip in [18] has argued that a dual Liouville boundary theory arises from the breaking of (normal) diffeomorphisms by the presence of the asymptotic boundary also in AdS_3 gravity in metric formulation. There are also other derivations [18–20] of Liouville theory from the asymptotic AdS_3 boundary based on metric gravity.

The Euclidean partition function has been computed for AdS_3 [21] and flat space–

time [22] with torus boundaries at asymptotic infinity. These computations were done in the metric formulation using heat kernel methods. In both cases, the results were found to be one-loop exact and given by the vacuum character of the gravitational asymptotic symmetry groups: Virasoro group for AdS_3 and Bondi-Metzner-Sachs (BMS_3) group for flat space–time.

Using metric boundary data, [23] showed that a Liouville like dual field theory can also be identified more directly for finite boundaries. This work considered a specific background space time, the twisted thermal flat space [24], and employed (linearized) Regge calculus [25], a discretization of gravity, in which the variables are given by edge lengths in a piecewise flat geometry. Thus these variables can be identified as geodesic lengths. Using discretization independence of the one-loop partition function of the theory [26], one can choose a discretization in which a class of variables describes the geodesic lengths from the boundary to some central axis. These can be taken as boundary field variables, and one can thus easily integrate out all variables except these boundary field variables. In [23], the authors also computed the one-loop partition function for a finite boundary, which led to the similar result as for asymptotically flat boundaries [22].

In the approach of [23], the boundary field theory is directly derived from gravity and obtained as an effective action for a geometric observable, which encodes the shape of the boundary.[1] Thus one has the advantage that the boundary field theory gives direct access to the dynamics of a geometric observable, which allows a "bulk reconstruction". Such effective actions for geometric observables have also been studied independently from holographic considerations [29, 30].

The choice of the geodesic distance from the boundary to a centre also resonates with Carlip's arguments [18]. In fact, we will see that the geodesic distance captures the change in the shape of the boundary that arises from diffeomorphisms generated by vector fields normal to the boundary.

Quasi-local holographic dualities have also been derived in a completely non-perturbative framework [31–36], in particular for the Ponzano-Regge model [37] of 3D quantum gravity. This model constitutes a quantization of first order (Palatini) gravity. It offers precise control on the (quantum) boundary conditions and their (quantum) geometric interpretations via loop quantum gravity techniques [38]. In particular one can again choose (quantum) metric boundary conditions. Different kinds of boundary field theories arise, e.g. in the form of spin chain models, or in the form of sigma models, depending on the precise choice

[1] Note that this is not a Dirac observable, as Dirac observables should be independent of the shape of the boundary, and are very hard to come by, see e.g. [27, 28]. Here the chosen geometrical observable should rather encode the shape of the boundary.

of (quantum) boundary conditions and the choice of geometric variable that describes the embedding of the boundary. In particular [34] provides a fully non-perturbative version of having the geodesic lengths as a boundary field, in which case one obtains so–called rigid solid on solid models as boundary theories. In [32], the authors performed the semiclassical analysis for a particular family of boundary conditions, which are encoded in a particular choice of boundary wave functions [39]. This led to a confirmation of the one-loop partition function found in [22,23], albeit with Planckian corrections, which arise due to the fact that the Ponzano–Regge framework allows for an arbitrary winding number of the boundary around the central axis.

To a great extent these works rely on the topological nature of 3D gravity. Thus the question arises whether these constructions can be also applied to 4D gravity. A first step to answer this question can be found in [3] of which I am a co–author. There, we used again (linearized) Regge calculus to consider a background space–time, which is a 4D version of twisted thermal flat space. Restricting to boundary data which induce a 4D flat solution, [3] finds a 3D Liouville-type boundary theory. However, due to the fact that 4D Regge calculus does not feature a local discretization independent measure [40], it is hard to extend this result to the (one-loop) quantum theory.[2]

To extend these results to more general backgrounds and to tackle the main task, namely including gravitons, we need a framework that is applicable to 4D gravity and for which we can expect to solve the dynamics. Being particularly interested in length observables, we will therefore consider (linearized) metric gravity. As the geodesic lengths has so far been shown to be a convenient choice for the boundary field, which moreover is connected to obtaining Liouville (like) boundary theories, we will stick with this choice. This does however present us with a challenge, namely to compute the effective action for a composite observable.

In part I of this thesis, we develop and test a general framework in which such effective actions can be computed. As we will see this allows us to consider more general backgrounds and boundaries in general dimensions and to systematize and greatly extend the results which have been obtained so far. The challenge is to describe observables which capture graviton propagating degrees of freedom.

We shall now shift gears and discuss aspects of discrete approaches to quantum geometry which we will consider in part II of this thesis.

[2]One can consider a model for quantum flat space [41], for which a discretization independent model does exist. In this case one can compute the one-loop partition function [3], which captures the effect of the boundary degrees of freedom.

1.2 Quantum geometry

The quantization of space–time geometry is an interplay between its symplectic and metrical features. In three dimensions, alignment between these two facets of geometry allows construction of a discrete, simplicial path integral formulation of quantum gravity, the Ponzano-Regge model [37]. In this model, space–time is decomposed into a large collection of tetrahedra that are glued along a subset of edges with matched lengths. The metrical and symplectic aspects of this geometry nicely align: the lengths encode the intrinsic metric and the dihedral angles of the tetrahedra encode the extrinsic geometry and these two sets of variables are canonically conjugated to each other [23, 42]. In the Euclidean signature case the angles are compact, which leads to discrete spectra for the lengths.

In four dimensions the situation is more subtle, and there is tension between the symplectic and the metrical aspects. In a space–time split, the metric has two natural discretizations: (i) the lengths of edges, and (ii) the extrinsic curvature angles, which are defined on 2D faces. These variables are not canonically conjugate. This is manifested in the different versions of Regge calculus, a discrete formulation of general relativity, based on edge lengths [25] and face areas [43] respectively. A Regge formulation based on areas and angles [44] also exists.

If the lengths are taken as fundamental, then the conjugate variables are contractions of the curvature angles with certain area-length derivatives [45]. If the curvature angles are taken to be fundamental, the conjugate variables are the face areas— whose quantization should then give a discrete area spectrum. The area version of Regge calculus is equivalent to length Regge calculus if one implements constraints that ensure that the configurations arise from a consistent length assignment [44, 46, 47]. Weakening these constraints or not implementing them at all leads, however, to a different dynamics based on a configuration space of generalized discrete geometries.

Area variables arise naturally in connection reformulations of general relativity (e.g. with gauge group SU(2) or SO(3, 1), [48]). In Loop Quantum Gravity (LQG), the curvature of a space–time is encoded in the (Ashtekar-Barbero) connection variables which are exponentiated to holonomies. The natural conjugated variables are electric (or triad) fields, which are integrated over two-dimensional faces—from these variables one constructs the areas of these faces [49–51]. The same structure of canonically conjugated variables appears in lattice gauge field theories.

The conjugated variables that appear in the construction of the phase space for (3+1)-dimensional simplicial geometries are areas of triangles with dihedral angles hinging on them [52, 53]. The dihedral angles and areas encode the extrinsic curvature and intrinsic

curvature respectively.

Spin foam models [54]—discrete geometry path integral quantization—of LQG focus on this set of 'curvature-area' variables. This focus has led to a rich set of results e.g., discrete area and volume spectra [49–51,55–57]. Area variables also play a central role in holography [58,59], in particular for the reconstruction of geometry from entanglement [60,61]. Discrete area spectra are key in many approaches to black hole entropy counting [62–65].

In spite of these motivating arguments, questions about area and area-angle Regge calculus abound. Even for a small simplicial complex, the areas greatly outnumber the edge lengths. What is the nature of these extra degrees of freedom? In particular, there are multidimensional families of area configurations that have no corresponding description in the length Regge calculus. What are these 'non-metric' area Regge configurations? Do they have a correspondent in continuum general relativity? Most importantly, can we understand the dynamics of these degrees of freedom? These questions and several others are discussed in the second part of this thesis.

LQG is a well developed theory of quantum geometry. At the classical level, various phase space descriptions of simplicial geometries have been constructed [53, 66–71] In the quantum theory, rigorous representations of geometric observables as operators on continuum Hilbert spaces are available [72–75]. And in the covariant theory spin foam amplitudes [76–81] describe the dynamics for these quantum geometries. The quantum geometries can be analyzed in a semiclassical limit [55, 82–89], which here means that the discrete areas become large in comparison to the Planck areas. These works show that the Regge action [25] emerges in this semiclassical limit.

The classical limit of the first four-dimensional spin foam model for gravity, the Barrett–Crane model, was suggested to describe area Regge calculus [90]. However, it was pointed out that area Regge calculus does *not* describe general relativity [43]. This is because the equations of motions impose flatness and area variables describe a bigger configuration space than that provided by (piecewise) simplicial geometries.

Recent arguments show that the Barrett-Crane model cannot lead to general relativity dynamics [91], see also the discussion [92].[3] This has motivated 'new' models [77–81], whose boundary Hilbert space matches those of canonical LQG. However, these models describe a class of generalized simplicial geometries. In particular, they identify a well-defined length geometry and a matching of areas along faces of glued triangles. However, the shapes of the glued triangles need not to match. The constraints that impose the matching of these

[3] In fact, we will later in this thesis propose a model which provides a 'correction' to the Barett-Crane model.

shapes have been worked out in [44] and are known as gluing conditions or shape matching constraints. Figure 1.1 illustrates these generalized geometries for two pairs of tetrahedra.

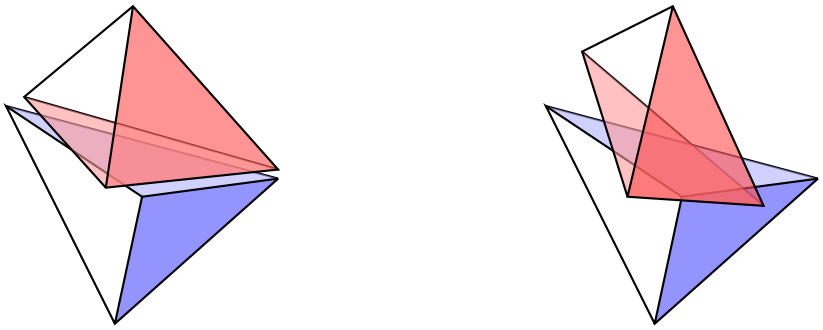

Figure 1.1: Two examples of the generalized simplicial geometries considered in quantum gravity. In both cases the pairs of tetrahedra are glued along their pale shaded faces and the areas of these triangles agree. On the left the shape mismatch is mild, while on the right it is more extreme.

Intriguingly, shape matching constraints are *not* automatically implemented in a classical version of LQG, that is, in the description of the phase space of $(3+1)$-dimensional simplicial geometries [53]. This has been linked, in [66], to the much discussed question of whether one should implement, in addition to the primary simplicity constraints, secondary simplicity constraints in spin foam models or not [93–95]. References [67] and [96] show that the enlarged space of simplicial geometries can also explain the appearance of the Barbero-Immirzi parameter in LQG.[4]

The work [71] described these same generalized simplicial geometries in a phase space parametrization that included a 'twisting angle' and provided a derivation from canonical LQG, using the phase space associated to the cotangent bundle $T^*\mathrm{SU}(2)$ of each triangle. (See [97] for an earlier derivation of the twisting angles from spin foams.) This led to the term 'twisted' geometries, which is now the most common name for this class of generalized simplicial geometries.[5] Indeed a link to twistors has been proposed in [99, 100], and extended further in [101]. A proposal for a 4-simplex action for twisted geometries beyond the shape-matched sector appears in [102]. Secondary simplicity constraints do arise in this context [103] and, intriguingly, only admit solutions in the sector of shape matched configurations. On the other hand, in [104] the authors describe a splitting of the connection for the generalized spatial geometry into torsion and torsionless parts which is solved

[4] That is, the fact that the Barbero-Immirzi parameter appears in the spectrum of geometric observables, despite the fact that classically it only parametrizes a canonical transformation of the theory's variables.

[5] See also [98] for an alternative interpretation of twisted geometries in terms of 'spinning' geometries.

for shape matched configurations. This highlights the question of what kind of dynamics one can attribute to these generalized geometries and it is one of our central themes.

While [104] provides a construction for a Levi–Civita connection for the twisted geometries, in a sense, they identify an exponentiated version of the symmetric part of a more general connection. There is a left-over part of the connection's holonomy that acts within the plane of the triangle along which two tetrahedra are glued. This can be understood as the non-symmetric part and therefore as describing torsion degrees of freedom. This provides yet another alternative interpretation for the additional degrees of freedom that appear for the generalized or twisted geometries. Another viewpoint is confirmed in analysis of a higher gauge topological BFCG action [6] where we interpreted edge simplicity constraints as torsionless conditions.

We shall refer to these degrees of freedom as non-metric, in the sense that they extend the space of simplicial, piecewise linear and piecewise flat (or homogeneously curved) geometries beyond a length description.

One has thus reached quite a detailed understanding of the generalized space of geometries that underlies LQG. So far this understanding is strictly on the kinematical level and there is not a clear understanding of what kind of dynamics the spin foam models prescribe for the additional degrees of freedom present in these non-metric geometries. This understanding is necessary to clarify whether the current spin foam models can describe the dynamics of general relativity, or whether additional constraints need to be added to suppress the non-metric degrees of freedom. Again, see [103] for a canonical analysis of this question.

The examples of length Regge calculus and area Regge calculus show that such an enlarged configuration space of geometries can lead to a danger of having flat dynamics. Indeed this possibility of a flat dynamics has arisen in the semiclassical analysis of spin foam amplitudes [83, 88, 105–109]. The semiclassical analysis allows only limited information on how strongly the constraints are imposed, this is one reason why the so-called flatness problem has yet to receive a satisfactory resolution [109]. Indeed, we will see in chapter 9 of this thesis that the discreteness of the areas prevents a sharp imposition of these constraints.

It is important in the analysis of spin foams to find out if they lead to area Regge calculus or length Regge calculus dynamics. To this end we will consider in part II of this thesis a rigorous study of area Regge calculus. Even on the classical level, the dynamics (and kinematics) of area Regge calculus remains poorly understood [110–112]. But, area Regge calculus does provide a dynamics for the non-metric degrees of freedom, which also appear in spin foams. The action of area Regge calculus numerically coincides with that of

length Regge calculus (on configurations which can be matched to each other), and as we have noted above the Regge action (in variables that include areas) appears as the classical limit of Barrett-Crane-type spin foam models. In fact, area Regge calculus is still the best candidate for the classical limit of the Barrett-Crane model. The semiclassical analysis of the newer spin foam models feature the appearance of dominating saddle points that describe so-called vector geometries [89,113,114]. Additional shape mismatched configurations and generalized Regge actions appear also at the saddle point of non-simplicial spin foams, as shown in [115] for regular hypercuboids and in [89] more generally. While area Regge calculus will shed light on the dynamics of all these spin foams, we expect that a better candidate for their classical limit is area-angle Regge calculus [89], which includes the three-dimensional dihedral angles as independent variables [44].

In part II of this thesis, we aim at a broader understanding of the possible dynamics of such generalized geometries arising from LQG. This can provide effective descriptions for quantum gravity models, which will help to understand their dynamics and to improve the models. We also aim to provide a foundation and tools for future studies of the dynamics of area-angle Regge calculus.

Theories in which areas are the fundamental variables are also interesting in a wider context. The investigations of area metrics in the continuum by Schuller et al [116] are motivated by string theory. Recently it has been suggested that quantum gravity and a notion of quantum geometry can be rebuilt from the entanglement structure of (possibly matter) quantum fields [117,118]. In particular Ryu and Takayanagi [119] propose that in a holographic setup the entanglement of the dual boundary field can be used to measure the areas (in (3+1) dimensions) of surfaces extending into the bulk. Thus, also here, areas appear to be more fundamental. In some sense areas are more natural than length in $(3+1)$ dimensions as the flow of a vector field through a surface can be used to measure the area of this surface.

Outline of thesis

In part I of this thesis, we shall discuss the holographic dualities for linearized gravity using the metric formulation. We begin in chapter 2 with a computation of the effective action for geodesic distances. A first key result will be the computation of the Hamilton–Jacobi functional for (linearized) gravity, restricting only to dynamics which describes

diffeomorphisms, for a large family of boundaries[6], in section 2.1. It turns out that a convenient way to express this Hamilton–Jacobi function is in terms of the diffeomorphism generating vector field that generates the on-shell metric perturbations. In fact, the Hamilton–Jacobi functional is local in terms of these vector fields. Note however that the vector fields themselves are non-local functionals of the boundary metric data.

This allows us to propose in section 2.2 a field theory for a scalar field defined on the boundary, whose Hamilton–Jacobi functional reproduces the one for gravity (restricted to the diffeomorphism sector) and whose equation of motion imposes that the scalar field equals the geodesic lengths from the boundary to some centre. To compute more directly the effective action for the geodesic lengths we introduce in section 2.3 a Lagrange multiplier method.

In chapter 3, we compute explicitly the dual boundary actions for three different examples of three dimensional backgrounds. We will see in section 3.1 and 3.2 that a priori this method does *not* lead to the expected results for the cases of backgrounds with intrinsically flat boundaries, such as the torus boundaries appearing for the twisted thermal flat space–time and AdS_3, which form our first two examples. The reason is that the geodesic lengths turn out to be in a certain sense a degenerate observable. This can be changed however by carefully implementing smoothness conditions at the central axis of the solid torus. This procedure will lead to an effective action, which differs from the one proposed in section 2.2 by the insertion of a non-local operator. This insertion also implements a remnant of the diffeomorphism symmetry of the gravitational theory, which turns the precise location of the central axis into a gauge degree of freedom, also for the boundary field theory.

The third example, which we consider in section 3.3, is a three dimensional spherical boundary in flat space (and thus with intrinsic background curvature), which has so far not been discussed in the literature. Here the mechanism for constructing the effective action differs slightly from the one with flat boundaries, as the smoothness conditions at the centre play less of a key role. The effective action will be local and agree with the proposed one from section 2.2.

Using our framework, we will also consider an example of a background in four dimensions given by the twisted thermal flat space–time in chapter 4. We will compute the dual boundary field theory for the gauge sector and also compute the Hamilton–Jacobi functional for the boundary metric data featuring gravitons.

We will close with a discussion and outlook in chapter 5. To avoid deviating from the key points in the main body of the thesis, we deferred all more involved calculations and

[6]We consider boundaries with homogeneous intrinsic curvature $D_A{}^b R = 0$ and with non-vanishing extrinsic curvature.

proofs to the appendices. This includes the defining formulas for the parametrization of the diffeomorphism sector in Appendix A.1, and the calculation of the restricted Hamilton–Jacobi functional in Appendix A.2. In appendix B, we proof some useful formulas which are needed for subsequent appendices. We discuss the derivation of solutions to the linearized Einstein equations with a Lagrange multiplier term in Appendices C. In particular, we find solutions for backgrounds with intrinsic flat boundaries in section C.1 and with spherical boundaries in section C.2. In Appendix E we derive the smoothness conditions which we need to implement at the centre of the bulk manifolds. Appendix F discusses the computation of effective actions for observables, which in a certain sense are degenerate. Finally, Appendix G collects definitions for spherical vector and tensor harmonics, which are useful to discuss the example with spherical boundary in section 3.3.

In part II of this thesis we revisit area Regge calculus. In Chapter 6, we address an ambiguity problem that arises in the original formulation of the theory, which makes the action ill-defined for configurations with right angles. We circumvent this problem by constructing a first order formulation. In Section 6.3 we analyze certain aspects of the dynamics of linearized area Regge calculus. Here we consider, in particular, setups that are helpful in distinguishing between length-Regge-type dynamics and area-type dynamics in spin foams. To this end we consider configurations that describe Pachner moves, that is, local changes in the triangulation in Section 7.1. We will indeed see that length and area Regge calculus behave differently under these Pachner moves. We provide a canonical analysis of the dynamics using tent moves in Section 7.2. Tent moves also allow a comparison of the counting of (propagating or physical) degrees of freedom between length and area Regge calculus. We will see that area Regge calculus has generically more propagating degrees of freedom than length Regge calculus, and that the additional degrees of freedom can be matched to specific variables describing the non-matching of the shapes of (glued) triangles.

In Chapter 8 we show that non-metricity (torsion) also breaks diffeomorphism symmetry. In particular, we show that certain three-dimensional dihedral angles can be used to capture the peculiar non-metricity of area Regge calculus and to parametrize the extent of the diffeomorphism breaking.

To tackle the question of whether a discrete, locally independent area spectrum is consistent with the dynamics of general relativity, we propose a family of 'effective' models in chapter 9. These models contain all the necessary ingredients and are relevant for spin foams. We will explore the implications of all of these findings in chapter 10.

Part I

Generalized Holography

Chapter 2

Effective actions for geodesic lengths

In this chapter we will determine directly from the *diffeomorphism sector* of (linearized) Einstein's metric gravitational theory, dual boundary field theories for a variety of backgrounds and boundaries with different topologies. These boundary field theories arise as effective theories for geodesic lengths variables. The computations can be performed for quasi-local boundaries at finite distance, and allow for negative, vanishing or positive cosmological constant. The limit to asymptotic boundaries can be considered easily in this framework by imposing the appropriate boundary conditions at infinity. These dual boundary field theories allow for an easy computation of the gravitational (one-loop) partition function restricted to the diffeomorphism sector for quasi-local boundaries at finite distance.

2.1 The Hamilton–Jacobi action for linearized gravity

One key ingredient needed to determine the dual boundary theories is the Hamilton–Jacobi functional, that is the on-shell action for gravity. Later, we will show how the linearized gravitational Hamilton–Jacobi functional can be used to compute the one-loop partition function for gravity. Thus, in this section, we will determine the (restricted) Hamilton–Jacobi functional for linearized gravity, for a large class of boundaries.

To start, we will summarize our conventions and define the type of boundaries we will be considering here. We will then introduce a convenient parametrization of the boundary metric perturbations in terms of diffeomorphism generating vector fields and curvature excitation (graviton) fields. This allows to split the metric perturbations into

diffeomorphism sector– the part that is described by the diffeomorphism vector fields– and graviton sector–the part described by the graviton fields.

The first key result we will present is to invert the relationship between boundary metric perturbations and the vector fields, that is to express the vector field components in terms of the boundary metric perturbations for the diffeomorphism sector.

Using our first result, we will evaluate the Hamilton–Jacobi functional restricted to the diffeomorphism sector. (This amounts to the classical limit of the physical vacuum wave function associated to the given boundary when restricted to the diffeomorphism sector.) This is our second key result. It turns out that the restricted Hamilton–Jacobi functional is a local functional, if we use the parametrization in terms of diffeomorphism generating vector fields. To avoid deviating from the key points in this section, we have deferred most of the involved computations and proofs to the appendices.

2.1.1 Assumptions and conventions

We consider linearized gravity in dimensions $d \geq 3$ with Euclidean signature, on a space–time manifold $(\mathcal{M}, \boldsymbol{g}_{ab})$ with a cosmological constant term Λ and a smooth closed boundary $(\partial\mathcal{M}, \boldsymbol{h}_{ab})$. The (Euclidean) Einstein-Hilbert action with the Gibbs-Hawking-York (GHY) boundary term is given by

$$S \;=\; -\frac{1}{2\kappa}\int_{\mathcal{M}} d^d x\,\sqrt{\boldsymbol{g}}\,(\boldsymbol{R}-2\Lambda) \;-\; \frac{1}{\kappa}\int_{\partial\mathcal{M}} d^{(d-1)}y\;\epsilon\sqrt{\boldsymbol{h}}\,\boldsymbol{K} \quad , \tag{2.1}$$

where $\kappa = 8\pi G_N$, G_N is Newton's constant. We have used $\boldsymbol{R}$ to denote the Ricci scalar and $\boldsymbol{K}$ the trace of the extrinsic curvature. The parameter $\epsilon = \pm 1$ depends on the sign convention for boundary extrinsic curvature, we will later specify our convention.

We choose the background solution to be expressed in Gaussian normal coordinates

$$ds^2 = g_{ab}dx^a dx^b = dr^2 + h_{AB}dy^A dy^B \tag{2.2}$$

where the space–time coordinates have the form $x^a = (\perp, y^A)$ with $\perp$ as an index for the radial coordinate $r \in \mathbb{R}^+$. We will assume $r = 0$ to define a bulk submanifold and the boundary to be given by a set of points with fixed radial coordinate $r = r_{\text{bdry}}$. Also, we will allow the manifold to have two boundary components ("inner" and "outer") at two different radial coordinates. Here, we denote the space–time indices by $a, b, \ldots$ and the 'spatial' indices $A, B, \ldots$ for the $r =$ const. hypersurfaces.

With the use of Gaussian coordinates, the extrinsic curvature is defined by $\boldsymbol{K}_{AB} = \frac{1}{2}\partial_\perp \boldsymbol{h}_{AB}$. This differs however by a sign from the extrinsic curvature tensor associated to an "inner" boundary, which has outward pointing normal $n^a = (-1, 0, \ldots)$. We have therefore used the variable $\epsilon = \pm 1$ to make this sign explicit.

We consider perturbations around a background metric

$$\boldsymbol{g}_{ab} = g_{ab} + \delta \boldsymbol{g}_{ab} = g_{ab} + \gamma_{ab} \quad , \tag{2.3}$$

and describe with $\gamma_{\perp\perp}, \gamma_{\perp A}$ and γ_{AB} the various components of the metric perturbations according to the foliation defined by the $r =$ const surfaces. The linearized action will be given by expanding the Lagrangian density up to quadratic order in the perturbation variables γ_{ab}. Under a linearized coordinate transformation with change of coordinates $x^a \mapsto x^a + \xi^a$, the metric perturbations transform as $\mathcal{L}_\xi g_{ab}$.

The non-vanishing components of the Christoffel symbols associated with the metric in Gaussian coordinates

$$\Gamma^\perp_{AB} = -\boldsymbol{K}_{AB}\,, \quad \Gamma^A_{\perp B} = \boldsymbol{K}^A_B\,, \quad \Gamma^A_{BC} = {}^{\mathrm{b}}\Gamma^A_{BC} \quad , \tag{2.4}$$

allow to express the relation between the space–time covariant derivatives ∇ on $(\mathcal{M}, \boldsymbol{g}_{ab})$ and spatial covariant derivatives D on radial foliations $(\Sigma_\perp, \boldsymbol{h}_{AB})$.

We will use bold Latin fonts to denote space–time, spatial tensors and normal Latin fonts to denote background tensors except for the Christoffel symbols denoted with Γ. For example $\boldsymbol{K}_{AB}$, K_{AB} represent the full extrinsic curvature and background extrinsic curvature respectively. We will also denote the curvature tensors on the $r =$ const boundary hypersurface with the superscript ${}^{\mathrm{b}}$, so that ${}^{\mathrm{b}}\boldsymbol{R}$ is the boundary Ricci scalar.

We shall consider a family of background solutions whose Weyl curvature tensor associated to the metric vanishes. In d dimensions, the Riemann curvature tensor can be decomposed in terms of the Ricci tensor as

$$R_{abce} = C_{abce} - \frac{2}{(d-1)(d-2)} R g_{a[c} g_{e]b} + \frac{2}{(d-2)} \left(g_{a[c} R_{e]b} + R_{a[c} g_{e]b} \right) \quad , \tag{2.5}$$

where C_{abce} is the Weyl curvature tensor which is traceless and conformally invariant. Taking the trace of the vacuum Einstein equations gives the Ricci scalar $R = \frac{2d\Lambda}{(d-2)}$ and inserting the vacuum Einstein equations into the decomposition (2.5) (if $C_{abce} = 0$), yields

$$R_{abce} = \frac{4\Lambda}{(d-1)(d-2)} g_{a[c} g_{e]b} \quad . \tag{2.6}$$

These background solutions describe homogeneously curved or maximally symmetric (isotropic and homogeneous) space–times also referred to as Einstein manifolds. These solutions can therefore be classified by the sign of the cosmological constant. For $\Lambda > 0$, we will have space–times that are locally spherical, $\Lambda < 0$ describe locally hyperbolic space–times and $\Lambda = 0$ describe locally (Euclidean) flat space–times. For dimensions $d = 3$, the Weyl tensor vanishes identically by dimension analysis and hence all vacuum solutions have homogeneous curvature. Thus the class of background solutions we consider captures all vacuum solutions in three dimensions.

Finally, we will assume for the background intrinsic curvature for the boundary manifold at the $r = \text{const}$ hypersurfaces to be covariantly constant ($D_A\, {}^{\text{b}}R^B{}_{CDE} = 0$).

Gauss–Codazzi Relations

We will make use of the Gauss-Codazzi relations which ensure an embedding of the hypersurfaces into the vacuum solutions. The Gauss relations, which relate the Riemann tensor of the $d-$dimensional manifold and the Riemann tensor of the $(d-1)-$dimensional hypersurfaces is given by

$$ {}^{\text{b}}R_{ABC}{}^{D} = R_{ABC}{}^{D} + K_{AC}K_{B}{}^{D} - K_{BC}K_{A}{}^{D} \quad , \tag{2.7} $$

where ${}^{\text{b}}R_{ABC}{}^{D}$ is the $(d-1)-$dimensional Riemann tensor associated to the boundary metric h. For vacuum solutions to the Einstein equations, the Ricci tensor and Ricci scalar satisfy

$$ R_{ab} = \frac{2\Lambda}{d-2} g_{ab} \qquad \text{and} \qquad R = \frac{2d\Lambda}{d-2} \tag{2.8} $$

and for such solutions the contracted Gauss relations become

$$ {}^{\text{b}}R_{AB} = \frac{2\Lambda}{d-1} h_{AB} + K K_{AB} - K_{A}{}^{C} K_{CB} \quad , \tag{2.9} $$

$$ {}^{\text{b}}R = 2\Lambda + K^2 - K_{AB}K^{AB} \quad . \tag{2.10} $$

The last equation (2.10) which is also referred to as the scalar Gauss relation coincides with the Hamiltonian constraint, that is the $(\perp\perp)$ component of the vacuum Einstein equations.

Furthermore, the Codazzi relations state that

$$ \begin{aligned} D_A K_{BC} - D_B K_{AC} &= R_{ABCe} n^e \underset{\text{max. sym. sol.}}{=} 0 \,, \\ D_A K_B{}^{A} - D_B K_A{}^{A} &= R_{Be} n^e \underset{\text{vac.-sol.}}{=} 0 \quad . \end{aligned} \tag{2.11} $$

The equations $D_A K_B{}^A - D_B K_A{}^A = 0$ in the last line (contracted Codazzi relations) coincide with the momentum constraints, that is the $(\perp A)$–components of the Einstein equations.

2.1.2 Perturbative expansion of the action

To compute the linearized Hamilton–Jacobi functional (HJF) up to quadratic order, we will need to expand the action (2.1) up to second order terms of metric perturbations (2.3). We therefore compute this expansion in this section.

Zeroth, first and second order contributions

The zeroth term is given by the action evaluated on the (background) solution. Using our assumption of homogeneous curvature background with $R = \frac{2d}{(d-2)}\Lambda$, the zeroth order action is given by

$$S^{(0)} = -\frac{1}{\kappa}\frac{2\Lambda}{(d-2)}{}^{d}V - \frac{1}{\kappa}\int_{\partial\mathcal{M}} d^{(d-1)}y\,\epsilon\,\sqrt{h}\,K \tag{2.12}$$

where ${}^{d}V$ is the volume of the manifold $\mathcal{M}$.

The first order variation of the bulk term in the action (2.1) gives

$$\delta(S_{\text{bulk}}) = \frac{1}{2\kappa}\int_{\mathcal{M}} d^d x\,\sqrt{g}\left(G^{ab}+\Lambda g^{ab}\right)\delta\boldsymbol{g}_{ab} + \frac{1}{2\kappa}\int_{\partial\mathcal{M}} d^{(d-1)}y\,\sqrt{h}\left(2\delta\boldsymbol{K} + K^{AB}\delta\boldsymbol{g}_{AB}\right)\Big)\ . \tag{2.13}$$

This bulk variation together with the variation of the $\sqrt{\boldsymbol{h}}\boldsymbol{K}$ term in the boundary action gives the first variation of the action ($\gamma_{ab} = \delta\boldsymbol{g}_{ab}$)

$$S^{(1)} = \frac{1}{2\kappa}\int_{\mathcal{M}} d^d x\,\sqrt{g}\left(G^{ab}+\Lambda g^{ab}\right)\gamma_{ab} + \frac{1}{2\kappa}\int_{\partial\mathcal{M}} d^{(d-1)}y\,\epsilon\,\pi^{AB}\gamma_{AB} \tag{2.14}$$

and determines the (background) equations of motions as well as the first order of the on-shell action. It also determines the background momentum $\pi^{AB} = \sqrt{h}(K^{AB} - Kh^{AB})$ which is conjugated to the metric.

The variation of the first order bulk and boundary terms of the action give the second order bulk and boundary terms respectively

$$\begin{aligned} -\kappa S^{(2)} &= -\frac{1}{2}\int d^d x\ \delta\left(\sqrt{\boldsymbol{g}}\left(\boldsymbol{G}^{ab}+\Lambda \boldsymbol{g}^{ab}\right)\right)\delta \boldsymbol{g}_{ab} - \frac{1}{2}\int_{\partial\mathcal{M}} d^{(d-1)}y\,\epsilon\,\delta(\sqrt{\boldsymbol{h}}(\boldsymbol{K}^{AB} - \boldsymbol{K}\boldsymbol{h}^{AB}))\delta \boldsymbol{g}_{AB} \\ &= \frac{1}{2}\int d^d x\sqrt{g}\ \gamma_{ab}\ \left(V^{abcd}\gamma_{cd} + \tfrac{1}{2}G^{abcdef}\nabla_c\nabla_d\gamma_{ef}\right) \\ &\quad + \frac{1}{2}\int_{\partial\mathcal{M}} d^{(d-1)}y\,\epsilon\,\gamma_{ab}\left((B_1)^{abcd}\gamma_{cd} + (B_2)^{abecd}\nabla_e\gamma_{cd}\right) \end{aligned} \tag{2.15}$$

The expressions for all the background tensors appearing in the second order action (2.15) are detailed in Appendix C. (See also the appendix in [23] for a derivation of the second order action). From the bulk term we get the linearized equations of motion for the metric perturbations

$$\hat{G}^{ab} := V^{abcd}\gamma_{cd} + \tfrac{1}{2}G^{abcdef}\nabla_c\nabla_d\gamma_{ef} \;=\; 0 \quad . \tag{2.16}$$

The linearized equations are not all independent but satisfy the divergence equation

$$\nabla_a\hat{G}^{ab} = 0 \quad , \tag{2.17}$$

which follows from the Bianchi identity. This dependence is attributed to diffeomorphism symmetry: the d dependencies suggest that the equations of motion leave d parameters in the metric undetermined– indeed these are the gauge degrees of freedom implied by the diffeomorphism symmetry of the action.

2.1.3 Mode decomposition of the boundary metric perturbations

Here, we will consider a convenient splitting of the boundary metric perturbations. In general dimensions, the boundary data determines two different classes of solutions – those which are equivalent to a solution diffeomorphism equivalent to the background and those which include (linearized) curvature excitations on top of the background, that is bulk gravitons. We split the induced boundary metric fluctuations γ_{AB} accordingly into the diffeomorphism sector ζ_{AB} and the graviton sector χ_{AB}.

The diffeomorphism sector can be defined via a symmetric projector $\zeta_{AB} = {}^{\mathrm{D}}\mathbf{P}^{CD}_{AB}\gamma_{CD}$ which projects the metric perturbations onto the part generated by linearized diffeomorphisms

$$\begin{aligned} \zeta_{AB} = [\mathcal{L}_\xi \boldsymbol{g}]_{AB} &= 2K_{AB}\xi^\perp + D_A\xi_B + D_B\xi_A \\ &= 2K_{AB}\xi^\perp + [\mathcal{L}_{\xi^\parallel}\boldsymbol{h}]_{AB} \quad . \end{aligned} \tag{2.18}$$

The graviton sector is defined as being invariant under the action of linearized diffeomorphisms on the metric fluctuations via a symmetric projector $\chi_{AB} = {}^{\mathrm{G}}\mathbf{P}^{CD}_{AB}\gamma_{CD}$. The two sectors are orthogonal with respect to the inner product on the space of symmetric tensors on the hypersurface $\Sigma_\perp$ defined by

$$\langle \gamma, \gamma' \rangle := \frac{1}{{}^{(d-1)}V} \int_{\Sigma_\perp} d^{(d-1)}y \, \sqrt{h} \, \gamma_{AB} h^{AC} h^{BD} \gamma'_{CD} \quad , \tag{2.19}$$

where ${}^{(d-1)}V$ is the $(d-1)$-dimensional volume of the hypersurface $\Sigma_\perp$. Using the inner product, we get that the graviton metric perturbations satisfy

$$D^A \chi_{AB} = 0 \quad , \qquad K^{AB} \chi_{AB} = 0 \quad . \tag{2.20}$$

where we have used the assumption that the boundary hypersurface is closed.[1] The first condition implies that graviton modes are transversal, the second condition implies that the "$K-$trace" vanishes. If $K_{AB} \sim g_{AB}$, the graviton sector is described by transverse traceless modes.

In summary, the induced metric perturbations can be parametrized as

$$\gamma_{AB} = {}^{\mathrm{D}}\mathbf{P}^{CD}_{AB}\gamma_{CD} + {}^{\mathrm{G}}\mathbf{P}^{CD}_{AB}\gamma_{CD} = \zeta_{AB} + \chi_{AB} \tag{2.21}$$

where ${}^{\mathrm{G}}\mathbf{P}^{CD}_{AB} = \mathbb{I}^{CD}_{AB} - {}^{\mathrm{D}}\mathbf{P}^{CD}_{AB}$, with $\mathbb{I}$ the identity operator on symmetric tensors.

In dimensions $d \geq 4$, the graviton sector will feature propagating local degrees of freedom. Constructing the HJF will require (case dependent) solutions to the equations of motion. The diffeomorphism sector on the other hand can be discussed in general terms for backgrounds satisfying the assumptions in section 2.1.1. In the next sub-section we will therefore concentrate on the diffeomorphism sector and keep the discussion general.

2.1.4 The diffeomorphism sector

Let us require that the relationship between the metric fluctuations projected onto the diffeomorphism sector ζ_{AB} and the diffeomorphism inducing vector field $(\xi^\perp, \xi^A)$ in (2.18) is invertible. Using the shorthand $\tilde{\pi}^{AB} = \left(K^{AB} - K h^{AB}\right)$ which is the de-densitized conjugate momentum $\tilde{\pi}^{AB} = h^{-1/2}\pi^{AB}$, we will now state our first result.

[1] If the manifold $\partial\mathcal{M}$ has a boundary, we can still choose appropriate boundary conditions such that the conditions (2.20) still hold.

Result 1: The diffeomorphism vector field components can be determined from the following equations

$$\begin{aligned} \Pi^{AB}\zeta_{AB} &= \Delta\,\xi^{\perp} \quad , \\ 2\tilde{\pi}^{BC}\delta' {}^{\mathrm{b}}\Gamma^{A}_{BC} &= \mathcal{D}^{A}{}_{B}\xi^{B} + Q^{AB}D_{B}\xi^{\perp} \end{aligned} \tag{2.22}$$

where

$$\begin{aligned} \Pi^{AB} &= \left(h^{AC}h^{BD} - h^{AB}h^{CD}\right) D_C D_D - {}^{\mathrm{b}}R^{AB} \quad , \\ \delta' {}^{\mathrm{b}}\Gamma^{A}_{BC} &= \frac{1}{2}h^{AD}\left(D_B\zeta_{CD} + D_C\zeta_{BD} - D_D\zeta_{BC}\right) \quad , \\ \Delta &= 2\tilde{\pi}^{AB}D_A D_B - 2\,{}^{\mathrm{b}}R^{AB}K_{AB} \quad , \\ \mathcal{D}^{A}{}_{B} &= 2\tilde{\pi}^{CD}\left(D_C D_D h^{A}_{B} + {}^{\mathrm{b}}R^{A}{}_{CBD}\right) \quad , \\ Q^{AB} &= 2\left(2\tilde{\pi}^{BC}K^{A}_{C} - \tilde{\pi}^{CD}K_{CD}h^{AB}\right) \quad . \end{aligned} \tag{2.23}$$

The proof of **Result 1** can be found in Appendix A.1. Note that we have used δ' to denote the restriction of the metric variations to the diffeomorphism sector ($\delta' \boldsymbol{g}_{AB} \equiv \zeta_{AB}$).

To obtain $\xi^{\perp}$ and ξ^{A} we need to invert the operators Δ (on the space of spatial scalars) and $\mathcal{D}^{A}_{B}$ (on the space of spatial vectors). Thus the vector components are non-local functionals of the spatial metric perturbations. Note that by construction, $\xi^{\perp}$ is a functional of the boundary metric perturbations, which is invariant under (linearized) boundary tangential diffeomorphisms. This suggest a relation of $\Pi^{AB}\zeta_{AB}$ to the first variation of the boundary Ricci scalar, which is also vanishing on boundary tangential diffeomorphisms. In fact, the variation of the boundary Ricci scalar satisfies

$$\delta({}^{\mathrm{b}}\boldsymbol{R}) = \left(D^{A}D^{B} - h^{AB}D_C D^{C}\right)\gamma_{AB} - {}^{\mathrm{b}}R^{AB}\gamma_{AB} = \Pi^{AB}\gamma_{AB} \tag{2.24}$$

where the operator Π^{AB} is given in (2.23). If we restrict to the metric perturbations to the diffeomorphism sector, we get a relation between between the first variation of the Ricci scalar and the normal component $\xi^{\perp}$, that is $\delta'({}^{\mathrm{b}}\boldsymbol{R}) = \Pi^{AB}\zeta_{AB} = \Delta\xi^{\perp}$.

Using the Gauss-Codazzi relations and the assumption of the background, we can further expand Q^{AB} as

$$Q^{AB} = 2\left(\left({}^{\mathrm{b}}R h^{AB} - 2\,{}^{\mathrm{b}}R^{AB}\right) - 2\Lambda\frac{(d-3)}{(d-1)}h^{AB}\right) \quad . \tag{2.25}$$

In dimensions $d = 3$, the background tensor Q^{AB} vanishes automatically since the Ricci scalar for two dimensional surfaces satisfies ${}^{2}R_{AB} = \frac{1}{2}{}^{2}R h_{AB}$.

Having found the components $\xi^\perp$ and ξ^A as functions of the boundary metric components ζ_{AB}, we can express the lapse $\zeta_{\perp\perp}$ and shift $\zeta_{\perp A}$ as functions of generating vector fields $\left(\xi^\perp, \xi^A\right)$ and thus in terms of ζ_{AB}. This can be computed from the components $\hat{G}^{\perp\perp}, \hat{G}^{\perp A}$ of the linearized equations (2.16), and they are given by,

$$\begin{aligned} \zeta_{\perp\perp} &= 2\partial_\perp \xi^\perp \\ \zeta_{\perp A} &= \nabla_\perp \xi_A + \nabla_A \xi_\perp \\ &= D_A \xi^\perp + h_{AB}\partial_\perp \xi^B \quad . \end{aligned} \tag{2.26}$$

We now determine the first and second order Hamilton–Jacobi functional (HJF) for general backgrounds (satisfying the assumptions of section 2.1.1), if we restrict to the diffeomorphism sector. This appears in a particular simple form if we use the parametrization of this sector in terms of the vector field components $(\xi^\perp, \xi^A)$. This is our second result.

Result 2: The first and second order Hamilton–Jacobi functional for the diffeomorphism sector (using our assumptions in section 2.1.1) are given by

$$\begin{aligned} {}^{\mathrm{D}}S^{(1)}_{\mathrm{HJ}} &= -\frac{1}{\kappa}\int_{\partial\mathcal{M}} d^{(d-1)}y\, \sqrt{h}\, \epsilon\, \left({}^{\mathrm{b}}R - 2\Lambda\right)\, \xi^\perp \quad , \\ {}^{\mathrm{D}}S^{(2)}_{\mathrm{HJ}} &= -\frac{1}{2\kappa}\int_{\partial\mathcal{M}} d^{(d-1)}y\, \sqrt{h}\epsilon \Big(\xi^\perp(\Delta + Q^{AB}K_{AB})\xi^\perp + \xi^\perp Q^{AB} D_A \xi_B - \\ &\qquad\qquad \xi_A Q^{AB} D_B \xi^\perp - \xi^A \mathcal{D}_{AB} \xi^B \Big) \quad . \end{aligned} \tag{2.27}$$

The differential operators Δ and $\mathcal{D}_{AB}$ are defined in (2.23) and the background tensor Q^{AB} is given in equation (2.25). We provide a derivation of these results in Appendix A.2. We remind the reader that ϵ is a sign that depends on the orientation of the normal vector to the boundary.

The HJF contributions given in (2.27) are local functionals, as expressed in terms of the vector field components $(\xi^\perp, \xi^A)$. These are however non-local functionals of the induced metric perturbations. The second order HJF will decouple into normal and tangential terms only when Q^{AB} vanishes, for example in three dimensions.

As we will see the lengths of geodesics which are normal (in the background geometry) to the boundary will be basically given by $\xi^\perp$ when restricted to the diffeomorphism sector. The differential operator Δ will therefore also be a key ingredient in the effective action for the geodesic lengths.

2.2 Dual boundary field theories

For the diffeomorphism sector, there are no local physical degrees of freedom. However, diffeomorphisms can affect the metric on the boundary and its derivatives: as we have seen, this contributes to the Hamilton–Jacobi functional (HJF). In 3D or in higher dimensions restricted to the diffeomorphism sector, this is the only contribution to the HJF. In this sense, all dynamics is captured by the boundary. The dynamics been captured by the boundary space–time, makes it a perfect playground for explicit realizations of the bulk/boundary correspondence. Here we are interested in defining a (local) field theory that is defined in terms of local fields on the boundary manifold, whose HJF agrees with that of gravity. We will refer to such a field theory as dual boundary field theory.

We shall look for boundary fields directly related to the observables of the gravitational theory. The gravitational HJF measures the extrinsic curvature of the boundary and describes the deformation of the shape of the boundary. Therefore, we shall consider boundary fields which describe the embedding of the boundary in the (homogeneously curved) bulk solution.

One such choice is the geodesic distance between two space–time points. More precisely, we consider a geodesic from a point (r_{out}, y^A) on the boundary $\partial\mathcal{M}$ to a point $(r = 0, y^A)$ (central bulk axis). We can therefore understand the geodesic length as a field defined on the boundary itself.

Since the metric is of Gaussian form with respect to the radius and the boundary is a $r = \text{const.}$ surface, the tangent vector to the background geodesic is orthogonal to the boundary. For this reason the geodesic length will be to first order in the (boundary) metric perturbations invariant under boundary tangential diffeomorphisms. Thus we can only expect to reproduce the part of the gravitational HJF, which is invariant under these boundary tangential diffeomorphisms, that is the part quadratic in $\xi^\perp$. On the other hand, knowing that the first order of the geodesic lengths is boundary diffeomorphism invariant, we can suspect that it is proportional to $\xi^\perp$ evaluated on the boundary, which in turn is related to the first variation of the boundary Ricci scalar.

In the following we will determine the (first order of the) geodesic length as a function of the boundary metric. This will allow us to 'guess' a candidate for a dual field theory, which (i) reproduces the equation of motion for this geodesic length and (ii) reproduces the boundary diffeomorphism invariant part of the gravitational HJF. In the process we will encounter a subtlety, namely that the geodesic lengths is also affected by the position of the central axis or point. This position is determined by the bulk metric perturbations, which are however gauge degrees of freedom.

In general, the positions of a central point or axis do however require d degrees of freedom for a central point and d degrees of freedom per axis point, whereas the boundary field describes one degree of freedom per boundary point. Indeed, we will see later, that this arbitrariness affects only certain momentum modes of the boundary field. But this feature will be also responsible for a certain modification which arise, if we determine the action for the geodesic length more directly from the gravitational action.

In section 2.2.2 we will furthermore find dual fields which reproduce the parts of the gravitational HJF which describe tangential boundary diffeomorphisms.

2.2.1 Action for the geodesic length

To start, we need to know the lengths of geodesics $(r(\tau), y^A)$ as a functional of the metric perturbations to first order. As a second step we express these lengths as functionals of the boundary metric.

Note that the parametrized curves $x^a(\tau) = (r_{\rm in}+(r_{\rm out}-r_{\rm in})\tau, 0, \ldots)$ between two points $(r_{\rm in}, y^A)$ and $(r_{\rm out}, y^A)$ with $\tau \in [0,1]$ are affinely parametrized geodesics with respect to background metrics of the form (2.2). This follows from the geodesic equation

$$\frac{dx^a}{d\tau}\nabla_a\frac{dx^b}{d\tau} = \Gamma^b_{\perp\perp}(r_{\rm out}-r_{\rm in})^2 = 0 \quad . \tag{2.28}$$

We now consider a geodesic $z^a(\tau)$ with respect to the full metric $\boldsymbol{g}_{ab}$ with fixed endpoints $z^a(0)$ and $z^a(1)$. As explained in Appendix D its length is given to first order in metric perturbations by

$$\ell_{\rm g} = \frac{1}{2(r_{\rm out}-r_{\rm in})}\int_0^1 d\tau\,\frac{dx^a}{d\tau}\frac{dx^b}{d\tau}\gamma_{ab}(x(\tau)) = \frac{1}{2}\int_{r_{\rm in}}^{r_{\rm out}} dr\,\gamma_{\perp\perp}(r) \quad . \tag{2.29}$$

For a solution generated by a diffeomorphism parametrized by a vector field ξ^a, the first order metric perturbation is given by

$$\gamma_{\perp\perp} \equiv \zeta_{\perp\perp} = (\mathcal{L}_\xi g)_{\perp\perp} \underset{(2.2)}{=} 2\partial_\perp\xi^\perp. \tag{2.30}$$

We thus find

$$\ell_{\rm g} = \xi^\perp(r_{\rm out}) - \xi^\perp(r_{\rm in}) \quad . \tag{2.31}$$

With (2.22) and the expression for the variation of the boundary Ricci scalar, we can express the $\xi^\perp$ component as a functional of the boundary metric

$$\xi^\perp \;=\; \frac{1}{\Delta}\Pi^{AB}\zeta_{AB} \;=\; \frac{1}{\Delta}\delta'({}^{\mathrm{b}}\boldsymbol{R}) \quad . \tag{2.32}$$

But we see that the geodesic lengths needs the metric γ_{AB} at the outer boundary at r_{out} and inner boundary at r_{in}. In the following, we will assume that $r_{\mathrm{in}} = 0$ describes a central axis or point. We will later see that in these cases, making certain smoothness assumptions on the metric perturbations and Fourier transforming in the spatial y^A coordinates, $\xi^\perp(r=0)$ is indeed vanishing for almost all momentum modes. The following will hold for momentum modes for which $\xi^\perp(r=0)$ is vanishing. For these modes we have that $\ell_{\mathrm{g}} = \xi^\perp(r_{\mathrm{out}})$ is a functional of the (outer) boundary metric only.

Let us consider the action

$${}^{D}S_\rho \;=\; \frac{1}{2\kappa}\int d^{(d-1)}y\,\sqrt{h}\left(\rho\,(\Delta + Q^{AB}K_{AB})\,\rho - 2\rho\,(\Delta + Q^{AB}K_{AB})\frac{1}{\Delta}\delta'({}^{\mathrm{b}}\boldsymbol{R})\right) \tag{2.33}$$

which leads to the equation of motion

$$\rho \;=\; \frac{1}{\Delta}\delta'({}^{\mathrm{b}}\boldsymbol{R}) \;=\; \xi^\perp \quad . \tag{2.34}$$

This shows that on-shell $\rho = \ell_{\mathrm{g}}$, and that the on-shell action

$${}^{D}S_\rho \underset{\text{solu}}{=} -\frac{1}{2\kappa}\int d^2y\sqrt{h}\,\xi^\perp(\Delta + Q^{AB}K_{AB})\xi^\perp \tag{2.35}$$

does indeed reproduce the boundary tangential invariant part of the gravitational Hamilton–Jacobi functional.

The action (2.33) is the guessed dual boundary action with a quadratic term defined by $(\Delta + Q^{AB}K_{AB})$ and a Liouville-like coupling to the boundary Ricci scalar. For backgrounds with $Q^{AB} = 0$, this boundary action will be a local functional of the field ρ. One subtlety is that the δ' projection to the diffeomorphism sector might be considered non-local (but it acts on γ_{AB} and not on ρ).

In chapters 3 and 4 we will derive effective actions for the geodesic length observable more directly from the gravitational action. That is, we integrate out from the gravitational action all fields excepts for a degree of freedom describing the geodesic lengths. This resulting effective action will be very similar to (2.33), but there will be also a non-local modification. This modification will take into account that $\xi^\perp(r = 0)$ might be non-vanishing for certain momentum modes.

2.2.2 Action for the boundary tangential diffeomorphisms

So far we have found a boundary theory which reproduces the boundary diffeomorphism invariant part of the gravitational on-shell action. Its equation of motion for the field ρ imposes that $\rho = \xi^\perp$, where $\xi^\perp$ is understood as a functional of the boundary metric. Similarly we can find an action which reproduces the remaining parts of the gravitational on-shell action, which are quadratic in the tangential boundary diffeomorphism parameters ξ^A. The dynamical variable is a boundary vector field σ^A and the equations of motion will impose that $\sigma^A = \xi^A$.

To this end remember that the relation between ξ^A and the boundary metric perturbations is given by

$$2\tilde{\pi}^{BC}\,\delta'\,{}^{\mathrm{b}}\Gamma^A_{BC} - Q^{AB}D_B\left(\Delta^{-1}\Pi^{CD}\zeta_{CD}\right) \;=\; \mathcal{D}^A{}_B\,\xi^B \quad . \tag{2.36}$$

The action

$${}^{D}S_\sigma = -\frac{1}{2\kappa}\int d^{(d-1)}y\,\sqrt{h}\left(\sigma^A\mathcal{D}_{AB}\sigma^B - 2\sigma^A h_{AD}\left(2\tilde{\pi}^{BC}\,\delta'\,{}^{\mathrm{b}}\Gamma^D_{BC} - Q^{BD}D_B\left(\Delta^{-1}\Pi^{CE}\zeta_{CE}\right)\right)\right) \tag{2.37}$$

leads to the equation of motion

$$\mathcal{D}_{AB}\sigma^B = h_{AD}\left(2\tilde{\pi}^{BC}\delta'{}^{\mathrm{b}}\Gamma^D_{BC} - Q^{BD}D_B\left(\Delta^{-1}\Pi^{CE}\zeta_{CE}\right)\right) \tag{2.38}$$

which are solved by $\sigma^A = \xi^A$. On-shell the action evaluates to

$${}^{D}S_\sigma \underset{\text{solu}}{=} \frac{1}{2\kappa}\int d^{(d-1)}y\,\sqrt{h}\,\xi^A\mathcal{D}_{AB}\xi^B. \tag{2.39}$$

Hence we can define a boundary theory, with a scalar field ρ and vector field σ^A with action given by a combination of the actions ${}^{D}S_{(\rho,\sigma)} = {}^{D}S_\rho + {}^{D}S_\sigma$. The non-local terms (Δ^{-1}) appearing in both actions vanish when Q^{AB} vanishes. The combined action ${}^{D}S_{(\rho,\sigma)}$ reproduces the normal and tangential components of the second order gravitational on-shell action

$${}^{D}\tilde{S}^{(2)}_{\mathrm{HJ}} \;=\; -\frac{1}{2\kappa}\int d^{(d-1)}y\,\sqrt{h}\,\left(\xi^\perp\left(\Delta + Q^{AB}K_{AB}\right)\,\xi^\perp \,-\, \xi^A\mathcal{D}_{AB}\,\xi^B\right) \tag{2.40}$$

but without the mixed terms.

2.3 The effective action for the geodesic length

We have seen that we can postulate an action for a boundary field theory, such that the boundary field variable evaluates to the geodesic lengths on solutions, and the action reproduces the (boundary diffeomorphism invariant part of the) Hamilton–Jacobi functional (HJF) of gravity restricted to the diffeomorphism sector. Later we will encounter examples for which the postulated action will differ in some subtle ways from the effective action for the geodesic lengths. This effective action is obtained by integrating out all degrees of freedom from the gravitational action, except those parametrizing the geodesic lengths. These differences concern in particular the proper reflection of the (gauge) symmetries of the theory, and are, as we will discuss, important for the one-loop correction for the gravitational partition function.

Integrating out all variables except for the geodesic lengths is difficult to do directly[2], as the geodesic length is a composite observable in terms of the metric perturbations. Instead we will add a Lagrange multiplier term to the second order action,

$$\begin{aligned} -\kappa S_\lambda^{(2)} \;=\; & \frac{1}{2}\int_M d^d x\sqrt{g}\;\gamma_{ab}\left(V^{abcd}\,\gamma_{cd} \;+\; \tfrac{1}{2}\,G^{abcdef}\,\nabla_c\nabla_d\gamma_{ef}\right) \;+ \\ & \frac{1}{2}\int_{\partial\mathcal{M}} d^{(d-1)}y\sqrt{h}\,\epsilon\,\gamma_{ab}\left(\,(B_1)^{abcd}\gamma_{cd} + \,(B_2)^{abcde}\nabla_c\gamma_{de}\right) \;+ \\ & \frac{1}{2}\int_{\partial\mathcal{M}} d^{(d-1)}y\;\lambda(y)\,(\rho(y)-\ell_{\rm g}[\gamma_{\perp\perp}]) \end{aligned} \tag{2.41}$$

where λ is a scalar density with respect to the boundary metric, which we treat as first order variable. The boundary field ρ is a scalar, and the λ equation of motion imposes that, evaluated on solutions, it gives the geodesic length

$$\ell_{\rm g} = \frac{1}{2}\int_{r_{\rm in}}^{r_{\rm out}} dr\;\gamma_{\perp\perp} \quad . \tag{2.42}$$

Here we allow for now to have either one outer boundary or one outer and an inner boundary. In the latter case we consider geodesics which go from the point $(r_{\rm out}, y)$ on the outer boundary to the point $(r_{\rm in}, y)$ on the inner boundary. In the case where we have only an outer boundary the geodesic goes from $(r_{\rm out}, y)$ to a bulk point $(r=0, P_{r\to 0}(y))$ where $P_{r\to 0}(y)$ is a projection of the y–coordinate to the set of points described by $r=0$.

[2]This can be achieved in Regge calculus [3, 23], but requires to employ a discretization of the theory, which might break the underlying diffeomorphism symmetry for backgrounds with curvature [52, 120].

Varying the action (2.41) with respect to the metric components we find the equations of motion

$$\hat{G}^{ab} := \left(V^{abcd}\,\gamma_{cd} \;+\; \tfrac{1}{2}\,G^{abcdef}\,\nabla_c\nabla_d\gamma_{ef}\right) \;=\; \frac{1}{4}\frac{\lambda(y)}{\sqrt{h}}\delta^a_\perp\delta^b_\perp \quad , \tag{2.43}$$

where we have used that with our choice of Gaussian coordinates $\sqrt{g} = \sqrt{h}$.

At this point one might wonder about the fate of the contracted Bianchi identities

$$\nabla_a \hat{G}^{ab} = 0 \tag{2.44}$$

which guarantee that d number of the (vacuum) Einstein equations are redundant. But the divergence is also vanishing for the right hand side of (2.43)

$$\nabla_a \frac{\lambda(y)}{\sqrt{h}}\delta^a_\perp\delta^b_\perp \;=\; \left(\lambda(y)\partial_\perp\frac{1}{\sqrt{h}} + \frac{\lambda(y)}{\sqrt{h}}\Gamma^A_{A\perp}\right)\delta^\perp_b \;=\; 0 \quad . \tag{2.45}$$

Hence we still have d number of redundancies between the equations of motion. In the examples, we will consider in the following, it is sufficient to consider the equations (2.43) for $a = \perp$ and $b = \perp, A$.

In the next two chapters we will work through several examples in three dimensions and four dimensions. Specifically, we shall consider a torus boundary embedded into three dimensional flat space–time, a torus boundary embedded into hyperbolic space–time, and a spherical boundary embedded into three dimensional flat space–time. We shall also later consider a four dimensional flat space with a 3-torus boundary embedded in flat space–time. The cases with a torus boundary have a boundary internal curvature ${}^{\mathrm{b}}R = 0$ and we will see that these cases are qualitatively different from the spherical boundary where ${}^{\mathrm{b}}R \neq 0$.

In particular for the cases with ${}^{\mathrm{b}}R = 0$ the solution for the lapse $\gamma_{\perp\perp}$ resulting from (2.43) will not depend on λ. (See Appendix C.1 for the proof.) This prevents us from finding a solution for λ, and the resulting action will be simply the gravitational HJF with the Lagrange multiplier term added.

There is however a resolution, if we consider only having an outer boundary and thus include $r = 0$ into the bulk manifold $\mathcal{M}$. In this case one has to take into account smoothness conditions for the metric perturbations at $r = 0$. These conditions will constraint certain Taylor expansion coefficients of the 'spatial' metric components γ_{AB}, and in case we have a Lagrange multiplier term, render these λ–dependent. This mechanism will allow us to find an effective action for the geodesics lengths which can also serve as a gravitational dual boundary field theory. The subtle point here is that certain properties of this boundary field theory are determined by the smoothness conditions at $r = 0$, even if we consider an asymptotic boundary $r_{\mathrm{out}} \to \infty$.

Chapter 3

Holographic dualities for 3D gravity

In this chapter, we will focus mainly on three dimensional examples of background space–times which satisfy our initial assumptions in section 2.1.1 and compute their dual boundary field theories as effective action for geodesic lengths. We will also compute the one-loop partition function directly from the dual boundary theory. The examples will consist of flat space–time with vanishing cosmological constant, hyperbolic space–time with a torus boundary and also a flat space–time with a spherical boundary.

In three dimensions, there are no local propagating gravitational degrees of freedom for pure Einstein's gravity due to the vanishing of the Weyl curvature. All vacuum solutions are therefore equivalent to homogeneous curvature solutions. This leads to the fact that the boundary metric perturbations of the linearized theory feature only the diffeomorphism sector (there are no gravitational waves) $\gamma_{AB} = \zeta_{AB}$.

Using the parametrization given in terms of diffeomorphism vector fields (2.18) for the boundary metric, we get a simplified Hamilton–Jacobi functional (HJF). The three dimensional second-order HJF is given by

$$S^{(2)}_{\mathrm{HJ}} = -\frac{1}{2\kappa}\int_{\partial\mathcal{M}} d^2y \, \left(\xi^{\perp}\Delta\,\xi^{\perp} - \xi^{A}\mathcal{D}_{AB}\,\xi^{B}\right) \quad . \tag{3.1}$$

The differential operators appearing in the HJF are given in (2.23), where Q^{AB} vanishes automatically in 3D. Let us now consider our background examples.

3.1 Twisted thermal flat space with torus boundary

As our first example, we consider a background flat geometry (vanishing cosmological constant) known as the twisted or thermal spinning flat space. An effective action for the geodesic lengths has been found in [23] using a Regge discretization of gravity.

The metric of thermal spinning flat space is given by

$$ds^2 \;=\; dr^2 + dt^2 + r^2 d\theta^2 \tag{3.2}$$

with periodic identification $(r, t, \theta) \sim (r, t+\beta, \theta+\gamma)$ in addition to the usual identification $\theta \sim \theta + 2\pi$ for the angular variable. This particular space–time has been considered in [22] with the boundary at asymptotic infinity where the authors computed the one-loop partition function using heat kernel methods.

For space–time with $0 \leq r \leq r_{\text{out}}$, we obtain a solid-torus with a torus topology at the boundary. Cycles contractible in the bulk manifold include curves described by $t = \text{const}$, $r = \text{const}$ and non–contractible cycles are given by curves along $\theta = \text{const}$ and $r = \text{const}$. The solid-torus can be obtained by identifying the top and bottom discs of a cylinder of height β, with a twisting angle (or angular potential) γ. See figure (3.1).

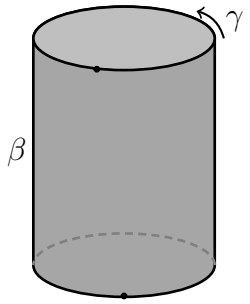

Figure 3.1: A twisted torus flat space–time obtained by identifying the top and bottom of the cylinder of height β with a twist γ along the $t = \text{const}$ surface.

There is one non-vanishing component of the (background) extrinsic curvature given by $K_{\theta\theta} = r$ and the trace of the extrinsic curvature given by $K = \frac{1}{r}$. The boundary (background) intrinsic curvature vanishes, i.e., ${}^2R = 0$. Hence we obtain for the differential operators $\Delta = -\frac{2}{r}\partial_t^2$ and $\mathcal{D}_B^A = -\frac{2}{r}\partial_t^2\, h_B^A$. These only involve derivatives in t–direction.

As the intrinsic curvature is vanishing we can define a Fourier transform for the metric perturbation components. We have to be however careful to implement the periodicity

$(r,t,\theta) \sim (r,t+\beta,\theta+\gamma)$ of these functions into the Fourier transform. This can be done by 'twisting' the phase factors for the Fourier transform so that these have the same periodicity:

$$\gamma_{ab}(r,k_t,k_\theta) = \frac{1}{\sqrt{2\pi\beta}}\int_{-\beta/2}^{\beta/2} dt \int_{-\pi}^{\pi} d\theta\, \gamma_{ab}(r,t,\theta)\, e^{-\mathrm{i}\theta k_\theta} e^{-\mathrm{i}\frac{2\pi t}{\beta}(k_t' - \frac{\gamma}{2\pi}k_\theta)} \quad , \tag{3.3}$$

where we will use the abbreviation $k_t := \frac{2\pi}{\beta}(k_t' - \frac{\gamma}{2\pi}k_\theta)$, and $k_\theta, k_t' \in \mathbb{Z}$. The inverse transform is given by

$$\gamma_{ab}(r,t,\theta) = \frac{1}{\sqrt{2\pi\beta}}\sum_{k_t,k_\theta} \gamma_{ab}(r,k_t,k_\theta)\, e^{\mathrm{i}\theta k_\theta} e^{\mathrm{i}\frac{2\pi t}{\beta}(k_t' - \frac{\gamma}{2\pi}k_\theta)} \quad . \tag{3.4}$$

We shall now discuss the equations of motions for the modified action (2.41) with a Lagrange multiplier term and compute from it the dual boundary action.

3.1.1 Equations of motion

Using the Fourier transform the equations of motion (2.43)

$$\hat{G}^{ab} = \frac{1}{4}\frac{\lambda(y)}{\sqrt{h}}\delta^a_\perp \delta^b_\perp \quad , \tag{3.5}$$

can be straightforwardly evaluated. The radial components $G^{\perp\perp}, G^{\perp A}$ of the equations of motion can be use to solve for the lapse and shift components $\gamma_{\perp\perp}, \gamma_{\perp A}$ of the metric perturbations. (See also Appendix C.1, which discusses the solutions for general backgrounds with flat spatial slices, that is with ${}^{\mathrm{b}}R = 0$.)

One finds

$$\begin{aligned}
\gamma_{\perp\perp} &= 2\partial_\perp\left(\frac{1}{2r}\left(\gamma_{\theta\theta} + \frac{k_\theta^2}{k_t^2}\gamma_{tt} - 2\frac{k_\theta}{k_t}\gamma_{\theta t}\right)\right) \\
&= 2\partial_\perp \xi^\perp \quad , \\
\gamma_{\perp\theta} &= \mathrm{i}k_\theta \frac{1}{2r}\left(\gamma_{\theta\theta} + \frac{k_\theta^2}{k_t^2}\gamma_{tt} - 2\frac{k_\theta}{k_t}\gamma_{\theta t}\right) + r^2\partial_\perp\left(\frac{\mathrm{i}}{r^2}\left(\frac{k_\theta}{2k_t^2}\gamma_{tt} - \frac{1}{k_t}\gamma_{\theta t}\right)\right) - \mathrm{i}k_\theta\lambda\frac{1}{4k_t^2} \\
&= \mathrm{i}k_\theta\xi^\perp + r^2\partial_\perp\xi^\theta - \mathrm{i}k_\theta\lambda\frac{1}{4k_t^2} \quad , \\
\gamma_{\perp t} &= \mathrm{i}k_t \frac{1}{2r}\left(\gamma_{\theta\theta} + \frac{k_\theta^2}{k_t^2}\gamma_{tt} - 2\frac{k_\theta}{k_t}\gamma_{\theta t}\right) + \partial_\perp\left(-\frac{\mathrm{i}}{2k_t}\gamma_{tt}\right) - \mathrm{i}k_t\lambda\frac{1}{4k_t^2} \\
&= \mathrm{i}k_t\xi^\perp + \partial_\perp\xi^t - \mathrm{i}k_t\lambda\frac{1}{4k_t^2} \quad .
\end{aligned} \tag{3.6}$$

For $\lambda = 0$ these confirm the relations (2.26) between the metric perturbations and the diffeomorphism generating vector ξ^a. Note also that the λ dependence can be described by replacing $\xi^\perp$ by

$$\hat{\xi}^\perp = \xi^\perp - \frac{1}{2\Delta}\frac{\lambda}{\sqrt{h}} = \xi^\perp - \frac{1}{4k_t^2}\lambda \quad . \tag{3.7}$$

Using the solutions for lapse and shift perturbations in the remaining equations $\hat{G}^{AB} = 0$, one finds that these are automatically satisfied, see also the discussion in section 2.3.

Thus, if we are solving the equations for $r \in [r_{\rm in}, r_{\rm out}]$ with $r_{\rm in} > 0$, we can conclude that the metric perturbations γ_{AB}, can be freely chosen in the bulk. If we consider only an outer boundary and thus include $r = 0$ in $\mathcal{M}$, we will however argue that we have to impose some smoothness conditions on the metric components at $r = 0$. We will see that this restricts certain Taylor expansion coefficients (arising from an expansion around $r = 0$) of the spatial metric components.

We have one remaining equation, coming from the variation of the Lagrange multiplier, namely

$$\rho = \frac{1}{2}\int_{r_{\rm in}}^{r_{\rm out}} dr\, \gamma_{\perp\perp} = \xi^\perp(r_{\rm out}) - \xi^\perp(r_{\rm in}) \quad , \tag{3.8}$$

where[1]

$$\xi^\perp = \frac{1}{2r}\left(\gamma_{\theta\theta} + \frac{k_\theta^2}{k_t^2}\gamma_{tt} - 2\frac{k_\theta}{k_t}\gamma_{\theta t}\right) \tag{3.9}$$

does not depend on λ, at least not for non-vanishing radius. Considering the case with non-vanishing $r_{\rm in}, r_{\rm out}$ this equation only involves fixed boundary data and the field ρ, which we treat here as parameter, and not as a variable to solve for. There is no variable left, for which we can solve (3.8) and thus λ remains a free parameter.

3.1.2 Evaluating the action on solutions

We proceed by inserting the solutions (3.6) into the action with Lagrange multiplier term (2.41). Let us first consider the case that we have an outer boundary at $r_{\rm out}$ and an inner boundary at $r_{\rm in}$.

[1] We could also write $\rho = \hat{\xi}^\perp(r_{\rm out}) - \hat{\xi}^\perp(r_{\rm in})$ with a λ-dependent $\hat{\xi}^\perp(r)$ defined in (3.7). However, note that the λ-dependent terms drop out, as the λ–dependent term in $\hat{\xi}^\perp(r)$ is r-independent.

From the bulk term of the action we get a contribution

$$-\kappa S^{(2)}_{\rm bulk} = \frac{1}{2}\int_{\mathcal{M}} d^3x\sqrt{g}\ \gamma_{ab}\,\hat{G}^{ab} = \frac{1}{8}\int_{\mathcal{M}} d^2y dr\ \gamma_{\perp\perp}(r,y)\lambda(y) = \frac{1}{4}\int_{\partial\mathcal{M}} d^2y\,\lambda(y)\,\epsilon\xi^{\perp}\,, \quad (3.10)$$

where $\epsilon = +1$ for the outer boundary component and $\epsilon = -1$ for the inner boundary component.

The boundary terms split into two parts: the first part arises from the vacuum solution (without λ), and the second part appears due to the presence of λ. We have determined the first part $S^{(2)}_{\rm HJ}$ in (3.1) (and for general backgrounds in Appendix A.2). The λ–dependent part is derived in Appendix C.3, (for flat boundaries and also for spherical boundaries) where it is shown that it amounts also to a boundary integral over $\epsilon\lambda\xi^{\perp}$. We thus have

$$-\kappa S^{(2)}_{\rm bdry} = -\kappa S^{(2)}_{\rm HJ} - \frac{1}{4}\int_{\partial\mathcal{M}} d^2y\,\epsilon\lambda(y)\xi^{\perp} \quad . \quad (3.11)$$

We see that the λ–dependent terms cancel from the gravitational action[2]. We are left with the gravitational HJF and the Lagrange multiplier term

$$-\kappa S^{(2)}_{\lambda} \underset{\rm solu}{=} -\kappa S^{(2)}_{\rm HJ} + \frac{1}{4}\int_{(\partial\mathcal{M})_{\rm out}} d^2y\ \lambda(y)\,(\rho(y) - \ell_{\rm g}[(\gamma_{AB})_{\rm out},(\gamma_{AB})_{\rm in}]) \quad (3.12)$$

where the geodesic lengths $\ell_{\rm g}$ is now understood as a functional of the boundary metric perturbations.

This is an effective action for the geodesic lengths as the boundary field ρ evaluates to the geodesic length on solutions. But we cannot interpret (3.12) as a proper dual boundary field theory for gravity.

Note that the same cancellation between the λ-dependent terms in the bulk and boundary contributions to the action seems to appear if we have only an outer boundary, that is in the case where the 3-manifold $\mathcal{M}$ is the full solid torus. This however conflicts with the result of [23], which used a Regge calculus set-up. There the geodesic length variables can be explicitly identified with certain edge lengths, which serve as basic variables in Regge calculus. This allows to integrate out all variables except for those edge lengths identified with the geodesic lengths. This results in an effective action, which can be interpreted as a dual boundary field theory.

In fact, adopting the approach of [23] to the case of an outer and inner boundary, that is to a torus ring, one finds the same result as in (3.12). As one now deals with a

[2]The cancellation of the λ–dependent terms happens in general for backgrounds with a flat boundary.

finite dimensional system one can identify the reason for this behaviour. To this end one splits the variables into two sets. The first set of variables $\mathcal{L}$ give the geodesic lengths, the other set $\mathcal{E}$ contains all remaining edge lengths. The linearized action has a Hessian with non–vanishing[3] determinant, which allows to integrate out all variables. However, the subdeterminant associated to the variables $\mathcal{E}$ is actually vanishing. Thus we cannot integrate out straightforwardly all variables but the geodesic lengths. If one uses an action with a Lagrange multiplier term one will find that λ remains a free parameter, and that the on-shell action is of the form (3.12), that is given by the Hamilton–Jacobi functional of the original system plus the Lagrange multiplier term. Appendix F, explains this general mechanism.

This opens the question, why one gets a different result in Regge calculus for the case with just the outer boundary, that is for the solid torus [23]? The answer is, that in Regge calculus certain conditions, which guarantee the smoothness of the solution (in the continuum limit) around $r = 0$ are automatically implemented. We will therefore proceed by implementing similar smoothness conditions for the continuum theory.

3.1.3 Implementing smoothness conditions for the metric at $r = 0$

The smoothness conditions we are going to impose arise from assuming Taylor expandable metric perturbations around the origin in Cartesian coordinates. After transformation from Cartesian to cylindrical coordinates we can deduce a certain behaviour in the radial coordinate r:

$$\begin{aligned} \gamma_{\perp\theta} &= a^{(1)}_{r\theta}\, r + a^{(2)}_{r\theta} r^2 + O(r^3)\,, \\ \gamma_{\theta\theta} &= a^{(2)}_{\theta\theta}\, r^2 + O(r^3)\,, \\ \gamma_{\theta t} &= a^{(1)}_{\theta t} r + a^{(2)}_{\theta t}\, r^2 + O(r^3)\,, \end{aligned} \tag{3.13}$$

and all other metric perturbations starting with r^0 terms. For a detailed derivation we refer to Appendix E. We will impose these conditions for the metric perturbations, also for the case that we include the Lagrange multiplier term.

We will see that we need to consider three separate cases, namely $|k_\theta| \geq 2$, $k_\theta = \pm 1$ and $k_\theta = 0$. We will start with the generic case $|k_\theta| \geq 2$.

[3] Linearized Regge calculus on a flat background exhibits a remnant of the gauge symmetries of the continuum theory [52, 120, 121]. But these gauge symmetries are associated to bulk vertices and one can triangulate the torus ring without any such bulk vertices, but nevertheless allow for an arbitrarily fine boundary triangulation. Thus one would not find gauge symmetries for this case. Note that the triangulation invariance of 3D linearized Regge calculus (and the associated one-loop partition function) [26] allows to use the coarsest possible bulk triangulation.

3.1.4 For modes $|k_\theta| \geq 2$

For the convenience of the reader we again display the solutions for the lapse and shift variables (3.6):

$$\begin{aligned}
\gamma_{\perp\perp} &= 2\partial_\perp\left(\frac{1}{2r}\left(\gamma_{\theta\theta}+\frac{k_\theta^2}{k_t^2}\gamma_{tt}-2\frac{k_\theta}{k_t}\gamma_{\theta t}\right)\right)\,,\\
\gamma_{\perp\theta} &= \mathrm{i}k_\theta\frac{1}{2r}\left(\gamma_{\theta\theta}+\frac{k_\theta^2}{k_t^2}\gamma_{tt}-2\frac{k_\theta}{k_t}\gamma_{\theta t}\right)+r^2\partial_\perp\left(\frac{\mathrm{i}}{r^2}\left(\frac{k_\theta}{2k_t^2}\gamma_{tt}-\frac{1}{k_t}\gamma_{\theta t}\right)\right)-\mathrm{i}k_\theta\lambda\frac{1}{4k_t^2}\,,\\
\gamma_{\perp t} &= \mathrm{i}k_t\frac{1}{2r}\left(\gamma_{\theta\theta}+\frac{k_\theta^2}{k_t^2}\gamma_{tt}-2\frac{k_\theta}{k_t}\gamma_{\theta t}\right)+\partial_\perp\left(-\frac{\mathrm{i}}{2k_t}\gamma_{tt}\right)-\mathrm{i}k_t\lambda\frac{1}{4k_t^2}\quad .
\end{aligned}\tag{3.14}$$

We Taylor expand all metric perturbations in r and arrive at equations for the expansion coefficients $a_{ab}^{(n)}$. Imposing the conditions that $a_{ab}^{(n)}=0$ for $n<0$ and that $a_{a\theta}^{(0)}=0$ as well as $a_{\theta\theta}^{(1)}=0$ we arrive at the conclusions:

- In order for $a_{rr}^{(-2)}$ to vanish, we need

$$\frac{k_\theta^2}{k_t^2}a_{tt}^{(0)}=0\quad .\tag{3.15}$$

  Thus, we have $a_{tt}^{(0)}=0$ for $k_\theta\neq 0$. This also ensures that $a_{r\theta}^{(-1)}$ and $a_{rt}^{(-1)}$ vanishes.

- Notice that, according to the first equation in (3.14) the coefficient $a_{rr}^{(-1)}$ vanishes and we do allow for non–vanishing $a_{rr}^{(0)}$. The remaining requirement comes from demanding that $a_{r\theta}^{(0)}$ is vanishing. This leads to the equation (for $k_\theta\neq 0$)

$$\left(1-\frac{1}{k_\theta^2}\right)\left(\frac{k_\theta^2}{k_t^2}a_{tt}^{(1)}-2\frac{k_\theta}{k_t}a_{\theta t}^{(1)}\right)=\frac{\lambda}{2k_t^2}\quad .\tag{3.16}$$

In summary we obtain the conditions (3.15) and (3.16) for the boundary components of the metric. We also see that we need a special treatment for the case $k_\theta=0$ and $k_\theta=\pm 1$. (The case $k_t^2=\frac{4\pi^2}{\beta^2}(k_t'-\frac{\gamma}{2\pi}k_\theta)^2=0$, which arises for rational values for $\frac{\gamma}{2\pi}$ will be discussed in section 3.1.7.)

Note that both (3.15) and (3.16) are a restriction on expansion coefficients for the spatial metric perturbations. These conditions also determine the value of the r–component $\xi^\perp$ of

the diffeomorphism generating vector field at $r = 0$,

$$\begin{aligned} \xi^{\perp}(0) &= \lim_{r\to 0}\frac{1}{2r}\left(\gamma_{\theta\theta}(r)+\frac{k_\theta^2}{k_t^2}\gamma_{tt}(r)-2\frac{k_\theta}{k_t}\gamma_{\theta t}(r)\right) \\ &= \frac{1}{2}\left(\frac{k_\theta^2}{k_t^2}a_{tt}^{(1)}-2\frac{k_\theta}{k_t}a_{\theta t}^{(1)}\right) \\ &= \frac{1}{4}\frac{k_\theta^2}{(k_\theta^2-1)}\frac{\lambda}{k_t^2} \end{aligned} \tag{3.17}$$

which now is λ–dependent.

Thus, considering the equation of motion imposed by the Lagrange multiplier, we find

$$\rho = \frac{1}{2}\int_0^{r_{\rm out}} dr\,\gamma_{\perp\perp}(r) = \int_0^{r_{\rm out}} dr\,\partial_\perp\xi^{\perp}(r) = \xi^{\perp}(r_{\rm out})-\xi^{\perp}(0) \quad , \tag{3.18}$$

where

$$\xi^{\perp}(r_{\rm out}) = \frac{1}{2r_{\rm out}}\left(\gamma_{\theta\theta}(r_{\rm out})+\frac{k_\theta^2}{k_t^2}\gamma_{tt}(r_{\rm out})-2\frac{k_\theta}{k_t}\gamma_{\theta t}(r_{\rm out})\right) \tag{3.19}$$

is a function of the boundary data. As $\xi^{\perp}(0)$ is now λ–dependent, we do obtain a solution for the Lagrange multiplier

$$\lambda = 4k_t^2\left(1-\frac{1}{k_\theta^2}\right)\left(\xi^{\perp}(r_{\rm out})-\rho\right) \quad . \tag{3.20}$$

The evaluation of the action proceeds similarly as in section 3.1.2. The bulk term still leads to

$$-\kappa S^{(2)}_{\rm bulk} = \frac{1}{4}\int_{\partial\mathcal{M}} d^2y\,\lambda(y)\left(\xi^{\perp}(r_{\rm out},y)-\xi^{\perp}(0,y)\right) \quad , \tag{3.21}$$

where we have used $\epsilon = +1$ as we have only the outer boundary. The boundary term gives

$$-\kappa S^{(2)}_{\rm bdry} = -\kappa S^{(2)}_{\rm HJ}(r_{\rm out}) - \frac{1}{4}\int_{\partial\mathcal{M}} d^2y\,\lambda(y)\xi^{\perp}(r_{\rm out},y) \quad . \tag{3.22}$$

The Lagrange multiplier term vanishes on the solutions to (3.18).

Thus the terms with $\lambda\xi^\perp(r_{\rm out})$ still cancel, but we remain with the $\lambda\xi^\perp(0)$ term. We therefore obtain

$$\begin{aligned}
-\kappa S_\lambda^{(2)} &\underset{\rm solu}{=} -\kappa S_{\rm HJ}^{(2)}(r_{\rm out}) - \frac{1}{4}\int_{\partial\mathcal{M}} d^2y\,\lambda(y)\xi^\perp(0,y) \\
&= -\kappa S_{\rm HJ}^{(2)}(r_{\rm out}) + \int_{\partial\mathcal{M}} d^2y\,\left(\xi^\perp(r_{\rm out})-\rho\right)\partial_t^2\left(1+\frac{1}{\partial_\theta^2}\right)\left(\xi^\perp(r_{\rm out})-\rho\right) \\
&= -\kappa S_{\rm HJ}^{(2)}(r_{\rm out}) + \int_{\partial\mathcal{M}} d^2y\,\xi^\perp(r_{\rm out})\partial_t^2\left(1+\frac{1}{\partial_\theta^2}\right)\xi^\perp(r_{\rm out}) + \\
&\qquad \int_{\partial\mathcal{M}} d^2y\,\left(\rho\,\partial_t^2\left(1+\frac{1}{\partial_\theta^2}\right)\rho - 2\rho\,\partial_t^2\left(1+\frac{1}{\partial_\theta^2}\right)\xi^\perp(r_{\rm out})\right) \quad . \qquad (3.23)
\end{aligned}$$

The Hamilton–Jacobi functional is given by (remember that $\Delta = -2r^{-1}\partial_t^2$)

$$-\kappa S_{\rm HJ}^{(2)}(r_{\rm out}) \;=\; \frac{1}{2}\int_{\partial\mathcal{M}} d^2y\sqrt{h}\,\left(\xi^\perp\Delta\xi^\perp - \xi^A\mathcal{D}_{AB}\,\xi^B\right) \;=\; -\int_{\partial\mathcal{M}} d^2y\,\left(\,\xi^\perp\partial_t^2\xi^\perp - \xi^A h_{AB}\partial_t^2\xi^B\right) \qquad (3.24)$$

and with $\xi^\perp = \Delta^{-1}\delta({}^2\boldsymbol{R}) \;=\; -2^{-1}r\partial_t^{-2}\delta({}^2\boldsymbol{R})$ we can write

$$\begin{aligned}
-\kappa S_\lambda^{(2)} \;\underset{\rm solu}{=}\; & -\frac{1}{2}\int_{\partial\mathcal{M}} d^2y\sqrt{h}\,\left(\rho\,\Delta\left(1+\frac{1}{\partial_\theta^2}\right)\rho - 2\rho\,\left(1+\frac{1}{\partial_\theta^2}\right)\delta({}^2\boldsymbol{R})\right) + \\
& \frac{1}{2}\int_{\partial\mathcal{M}} d^2y\sqrt{h}\,\left(\xi^\perp\Delta\frac{1}{\partial_\theta^2}\xi^\perp - \xi^A\mathcal{D}_{AB}\,\xi^B\right) \quad . \qquad (3.25)
\end{aligned}$$

This does define an action for the boundary field ρ, whose on-shell value does reproduce the gravitational HJF.

We note that the ρ-dependent part of the effective action (3.25) given by

$$\kappa S'_\rho \;:=\; \frac{1}{2}\int_{\partial\mathcal{M}} d^2y\sqrt{h}\,\left(\rho\,\Delta\left(1+\frac{1}{\partial_\theta^2}\right)\rho - 2\rho\,\left(1+\frac{1}{\partial_\theta^2}\right)\delta({}^2\boldsymbol{R})\right) \qquad (3.26)$$

differs from the action S_ρ (2.33) which we found in section 2.2.1 by an insertion of the non–local operator $(1+\partial_\theta^{-2})$. (It does also reproduce $S_{\rm HJ}^{(2)}$ multiplied with this factor.) This insertion has an important consequence: the effective action for the geodesic lengths S'_ρ does vanish for modes $k_\theta = \pm 1$. The effective action is furthermore ill–defined for $k_\theta = 0$.

As we will see shortly, the modes $k_\theta = \pm 1$ have a special status, as we can have in this case a non-vanishing $\xi^\perp(r=0)$ (for vanishing λ). It can be expressed as a function of

the spatial metric components. But in the bulk these are gauge degrees of freedom. We therefore cannot determine the geodesic length at $k_\theta = \pm 1$ from the boundary data. In fact, in the Regge calculus set-up [23] the geodesic length variables at $k_\theta = \pm 1$ can be identified with gauge parameters resulting from the residual diffeomorphism symmetry of Regge calculus [52, 120, 121]. For this reason the effective action for the geodesic length should vanish — and we show below that it in fact does.

For the case $k_\theta = 0$ one has also a diffeomorphism generating vector field, which does not need to vanish at $r = 0$. But this time it is the component $\xi^\perp$ that does not need to vanish and can be furthermore identified as a gauge parameter. We will see that here we are back to a situation similar to what we described for the case with two boundaries: one cannot straightforwardly integrate out all variables except the geodesic lengths and the on-shell value of the action S_λ will reproduce the Hamilton–Jacobi functional and the Lagrange multiplier term.

The special status of these modes is also reflected in the one-loop partition function for gravity, which reproduces the vacuum character of the BMS_3 group [22, 23]. As we will discuss shortly in section 3.1.9 the one-loop determinant for gravity does coincide with the one-loop determinant of the boundary field theory (3.26). Here it is important that this determinant does only include a product over the modes $k_\theta \geq 2$, as the modes $k_\theta = 0$ and $k_\theta = \pm 1$ do describe gauge degrees of freedom [23].

3.1.5 For modes with $k_\theta = 0$

For $k_\theta = 0$ we obtain the following solutions for the lapse and shift components

$$\begin{aligned}
\gamma_{\perp\perp} &= 2\partial_\perp\left(\frac{1}{2r}\gamma_{\theta\theta}\right) = 2\partial_\perp\xi^\perp \quad , \\
\gamma_{\perp\theta} &= r^2\partial_\perp\left(-\frac{\mathrm{i}}{r^2}\frac{1}{k_t}\gamma_{\theta t}\right) = r^2\partial_\perp\xi^\theta \quad , \\
\gamma_{\perp t} &= \mathrm{i}k_t\frac{1}{2r}\gamma_{\theta\theta} + \partial_\perp\left(-\frac{\mathrm{i}}{2k_t}\gamma_{tt}\right) - \mathrm{i}k_t\lambda\frac{1}{4k_t^2} = \mathrm{i}k_t\xi^\perp + \partial_\perp\xi^t - \mathrm{i}k_t\lambda\frac{1}{4k_t^2} \quad . \qquad (3.27)
\end{aligned}$$

We see that for $k_\theta = 0$ we can have $a_{tt}^{(0)} \neq 0$. This is the only non–vanishing component of the spatial metric γ_{AB} at $r = 0$, and as it remains arbitrary, should be understood as gauge parameter. Note that this (additional) gauge parameter only appears for $k_\theta = 0$, as it is forced to vanish for $k_\theta \neq 0$ by the equations of motion.

We also see that the vector field component $\xi^\perp$ does vanish at $r = 0$. The requirement that $a^{(0)}_{r\theta}$ vanishes, imposes $a^{(1)}_{\theta t} = 0$. From the last equation in (3.27) we obtain that the only λ–dependent shift component is given by

$$a^{(0)}_{rt} \;=\; -\frac{\mathrm{i}}{2k_t}a^{(1)}_{tt} - \mathrm{i}k_t\lambda\frac{1}{4k_t^2} \quad . \tag{3.28}$$

From the Lagrange multiplier equation we obtain

$$\rho \;=\; \xi^\perp(r_{\mathrm{out}}) \;=\; \frac{1}{2r_{\mathrm{out}}}\gamma_{\theta\theta}(r_{\mathrm{out}}) \quad , \tag{3.29}$$

where different from the general case, we do not have a λ–dependent term since we have $\xi^\perp(r = 0, k_\theta = 0) = 0$.

Therefore we cannot determine λ as a function of ρ and the boundary variables. We are now in the same situation as described for the case with two boundaries in section 3.1.2. One can compute explicitly that the evaluation of the action yields the same result as in this case, namely

$$\kappa S^{(2)}_{\lambda\,|k_\theta=0} \;\underset{\text{solu}}{=}\; \kappa S^{(2)}_{\mathrm{HJ}\,|k_\theta=0} \;+\; \tfrac{1}{4}\lambda\left(\rho - \xi^\perp(r_{\mathrm{out}})\right)_{|k_\theta=0} \quad . \tag{3.30}$$

3.1.6 For modes with $k_\theta = \pm 1$

Here we find from equation (3.16) that

$$\left(1 - \frac{1}{k_\theta^2}\right)\left(\frac{k_\theta^2}{k_t^2}a^{(1)}_{tt} - 2\frac{k_\theta}{k_t}a^{(1)}_{\theta t}\right) \;=\; \frac{\lambda}{2k_t^2} \;\overset{!}{=}\; 0 \quad , \tag{3.31}$$

and thus $\lambda = 0$. The vector field component $\xi^\perp(0)$ does not need to vanish and is given by

$$\xi^\perp(0) \;=\; \frac{1}{2}\left(\frac{k_\theta^2}{k_t^2}a^{(1)}_{tt} - 2\frac{k_\theta}{k_t}a^{(1)}_{\theta t}\right) \quad . \tag{3.32}$$

Thus we have for the geodesic length variable

$$\rho \;=\; \xi^\perp(r_{\mathrm{out}}) - \xi^\perp(0) \quad . \tag{3.33}$$

But here we should understand $\xi^\perp(0)$ as a bulk variable – in fact it is a gauge parameter, that only appears at $k_\theta = \pm 1$.

Inserting the solutions into the action, we will have due to $\lambda = 0$, that

$$\kappa S^{(2)}_{\lambda}(k_\theta = \pm 1) \;\underset{\text{solu}}{=}\; \kappa S^{(2)}_{\mathrm{HJ}}(k_\theta = \pm 1) \tag{3.34}$$

and that thus the effective action for the boundary field ρ vanishes. This is also confirmed in the Regge calculus setting [23].

3.1.7 Modes with $k_t = 0$

Remember that we have defined $k_t := \frac{2\pi}{\beta}(k'_t - \frac{\gamma}{2\pi}k_\theta)$. Thus, if γ is a rational multiple of 2π there will be certain $k'_t, k_\theta \in \mathbb{Z}$ for which $k_t = 0$. At these angles and for such modes with $k_t = 0$ we do not have a well–posed boundary problem, that is solutions do not exist for all possible boundary metric fluctuations.[4] The condition of rational γ can be translated in how geodesics along the torus would wind around this torus, see [31, 32].

These modes with $k_t = 0$ will lead to divergencies of the one–loop correction, which appear for all rational angles. This can be treated with an ad-hoc regularization, as in [22]. Alternatively, one can use a discretization, e.g. Regge calculus as in [23] or the Ponzano–Regge model as in [31–33]. Such a discretization allows only rational angles γ, but the discretization does introduce a cut–off. For a given rational angle, there is a choice of (minimal) discretization, for which such modes with $k_t = 0$ do not appear.

As discussed in [31, 32] the appearance of such divergencies seems to be an artifact of the linearization, or in the quantum theory an artifact of the semiclassical (or one-loop) approximation, at least if one considers a boundary with finite radius. [31] shows however that the exact partition function, for a particular choice of boundary conditions, does reproduce the divergence structure in the limit to infinite radius.

3.1.8 The limit of large radius

We found as effective action for the geodesic length

$$\kappa S'_\rho \;:=\; \frac{1}{2}\int_{\partial\mathcal{M}} d^2y\sqrt{h}\,\left(\rho\,\Delta\left(1+\frac{1}{\partial_\theta^2}\right)\rho - 2\rho\left(1+\frac{1}{\partial_\theta^2}\right)\delta({}^2\boldsymbol{R})\right) \tag{3.35}$$

which features a non-local operator $(1+1/\partial_\theta^2)$. If we fix however the physical wave lengths of the angular modes $r^{-2}\partial_\theta^2 = \text{const.} = C$ we see that

$$\left(1+\frac{1}{r^2}\frac{1}{C}\right) \underset{r\to\infty}{\longrightarrow} 1\,, \tag{3.36}$$

and the effective action becomes local and we recover the action S_ρ as proposed in section 2.2.1.

[4] The boundary fluctuations for which one can and cannot find solutions for lapse and shift can be read off from (3.14). Eg. allowing only for non–vanishing fluctuations $\gamma_{\theta\theta}$ still allows for a solution.

In this way we define (radial) scalings

$$[k_\theta] = 1\,, \quad [\gamma_{tt}] = 0\,, \quad [\gamma_{\theta\theta}] = 2\,, \quad [\gamma_{\theta t}] = 1 \quad . \tag{3.37}$$

Then we have $[\xi^\perp] = 1$ and $[\xi^\theta] = -1$ as well as $[\xi^t] = 0$. We have also $[\Delta] = -1$ and $[\mathcal{D}_{\theta\theta}] = +1$ as well as $[\mathcal{D}_{tt}] = -1$. We thus find that $[\xi^\perp \Delta \xi^\perp] = +1$ comes with the dominant radial scaling, as compared to the terms which are not invariant under boundary tangential diffeomorphisms, which are given by $[\xi^\theta \mathcal{D}_{\theta\theta}\xi^\theta] = -1$ and $[\xi^t \mathcal{D}_{tt}\xi^t] = -1$. In this sense we have that for large radius the boundary diffeomorphism invariant term $\xi^\perp \Delta \xi^\perp$ dominates.

3.1.9 One-loop determinant of the dual boundary field theory

By construction we have that the dual action S'_ρ reproduces the (boundary diffeomorphism invariant part of the) gravitational action – modulo the insertion of $(1 + \partial_\theta^{-2})$. (To compensate, one adds the gravitational action with $-\partial_\theta^{-2}$ inserted.) Here we will show that the dual action also reproduces the one-loop determinant of gravity, which has been computed in the continuum for asymptotic boundaries in [22] and in the discrete for finite boundaries in [23].

To compute the one-loop determinant for S'_ρ given in (3.26), we will adopt a simple lattice regularization for the Hessian of the action, which is given by $k_t^2(1 - k_\theta^{-2})$:

$$\begin{aligned} k_\theta^2 \;&\to\; \left(2 - 2\cos\left(\frac{2\pi}{N_\theta}\right)\right)^{-1} \left(2 - 2\cos\left(\frac{2\pi}{N_\theta}\kappa_\theta\right)\right) \\ k_t^2 \;&\to\; \frac{N_t^2}{\beta^2}\left(2 - 2\cos\left(\frac{2\pi}{N_t}(\kappa_t - \frac{\gamma}{2\pi}\kappa_\theta)\right)\right) \quad , \end{aligned} \tag{3.38}$$

where $\kappa_\theta = 0, \ldots, N_\theta - 1$ and $\kappa_t = 0, \ldots N_t - 1$. With this choice we still have that $(1 - k_\theta^{-2}) = 0$ for $\kappa_\theta = \pm 1$. Now, as our dual action is only defined for $|k_\theta| \geq 2$ we consider

$$\prod_{\kappa_\theta=2}^{N_\theta-2}\left(1 - \frac{2 - 2\cos\left(\frac{2\pi}{N_\theta}\right)}{2 - 2\cos\left(\frac{2\pi}{N_\theta}\kappa_\theta\right)}\right) \;=\; \frac{1}{2 + 2\cos\left(\frac{2\pi}{N_\theta}\right)} \tag{3.39}$$

and

$$\prod_{\kappa_t=0}^{N_t-1}\left(2 - 2\cos\left(\frac{2\pi}{N_t}(\kappa_t - \frac{\gamma}{2\pi}\kappa_\theta)\right)\right) \;=\; 2 - 2\cos(\gamma\kappa_\theta) \quad . \tag{3.40}$$

Ignoring some inessential constants we therefore have

$$\prod_{\kappa_\theta=2}^{N_\theta-2}\prod_{\kappa_t=0}^{N_t-1}\frac{1}{\sqrt{k_t^2(1-k_\theta^{-2})}} \sim \prod_{\kappa_\theta=2}^{N_\theta/2-1}\frac{1}{|1-q^{\kappa_\theta}|^2} \tag{3.41}$$

where $q=\exp(i\gamma)$. This reproduces the one-loop determinant of the gravitational theory [22, 23]. Thus the (only) essential contribution to the one-loop determinant arises from the degrees of freedom describing the geodesic lengths from the boundary to some central point. This confirms the interpretation of the action S'_ρ as dual action for gravity.

Note that to get the correct result, it is essential to not to include the modes $k_\theta=0$ and $k_\theta=\pm1$, which in our case follows from the appearance of the non-local operator $(1-k_\theta^{-1})$. The exclusion of the $k_\theta=\pm1$ modes is a feature of the vacuum BMS_3 character [122], which is reproduced by the one-loop partition function for asymptotic boundaries [22]. Inserting a point particle in the centre, one rather expects a massive character. Indeed the insertion of a point particle will break the diffeomorphism symmetry described by the $k_\theta=\pm1$ modes. This can be also expected to happen in the current framework, as we would have to modify the smoothness conditions, which we introduced in section 3.1.3, and which were essential for obtaining a suitable dual action.

3.2 Twisted thermal AdS_3 space with finite boundary

Next we will consider as background AdS_3 space with metric

$$ds^2=\mathrm{d}r^2+\sinh^2\!r\,d\theta^2+\cosh^2\!r\,dt^2 \quad , \tag{3.42}$$

where we have fixed $\Lambda=-1$. As for the flat space metric we impose the periodicity conditions $(r,t,\theta)\sim(r,t+\beta,\theta+\gamma)$ and $\theta\sim\theta+2\pi$ for the angular variable. This defines twisted thermal AdS_3 space (see figure 3.2). The one-loop partition function for this background with asymptotic boundary has been computed from the gravity side in [21] and reproduces the vacuum character of the asymptotic symmetries of AdS_3 space [123]. This example has been intensively discussed in the literature, e.g. [14–16] and references therein. The derivation of the (Liouville) dual boundary field theory starts often with the Chern-Simons formulation of 3D gravity. One exception is [18], which derives a dual boundary theory from the breaking of diffeomorphism symmetry at the asymptotic boundary. In fact the field introduced in [18] agrees (in the linearized theory) with the geodesic distance employed here. Our derivation of the dual field theory is somewhat more direct and also applicable to finite boundaries.

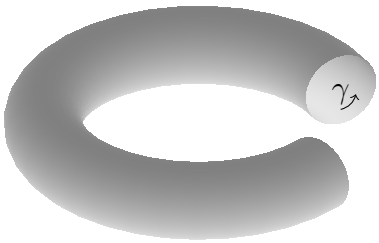

Figure 3.2: Torus boundary with twist parameter γ.

We will again consider a torus boundary at $r = r_{\text{out}}$ and thus the background intrinsic curvature of the boundary (which we constrained to be homogeneous) has to vanish.

The computation of the effective geodesic action is very similar to the flat case, and we will therefore be brief. One again, we will invoke smoothness conditions at $r = 0$ in order to obtain an effective action, which can also serve as dual boundary field theory. The modes $k_\theta = 0$ and $k_\theta = \pm 1$ will also play a special role.

One difference with the flat case is that the extrinsic curvature has now full rank

$$K_{\theta\theta} = K_{tt} = \cosh r \sinh r \quad , \qquad K_{\theta t} = 0 \quad \text{and} \quad K = \tanh r + \coth r \quad . \tag{3.43}$$

Thus

$$\Delta = 2(K^{CD} - Kh^{CD})D_C D_D \;=\; \frac{-2}{\cosh r \sinh r}\left(\partial_\theta^2 + \partial_t^2\right) \;=\; \frac{-2}{\sqrt{h}}\left(\partial_\theta^2 + \partial_t^2\right) \tag{3.44}$$

is now non-degenerate.

The Fourier transformation for the $y = (\theta, t)$ variables can be defined as for the flat background, see (3.3), which allows us to invert the various differential operators.

3.2.1 Equations of motion and evaluation of the action

The equations of motion

$$\hat{G}^{ab} \;=\; \frac{1}{4}\frac{\lambda(y)}{\sqrt{h}}\delta_\perp^a \delta_\perp^b \quad , \tag{3.45}$$

resulting from varying γ_{ab} in the Lagrange multiplier action (2.41) can be solved for the lapse and shift metric perturbations. The solutions are given by

$$\gamma_{\perp\perp} = 2\partial_\perp \xi^\perp, \qquad \gamma_{\perp A} = \mathrm{i}k_A\left(\xi^\perp - \frac{1}{4(k_t^2 + k_\theta^2)}\right) + h_{AB}\partial_\perp \xi^B \tag{3.46}$$

where the vector fields are given as functions of the boundary perturbations

$$\xi^{\perp} = \frac{k_\theta^2\gamma_{tt} + k_t^2\gamma_{\theta\theta} - 2k_t k_\theta \gamma_{t\theta}}{2\,\mathrm{cosh}r\,\mathrm{sinh}r(k_t^2+k_\theta^2)} \tag{3.47}$$

$$\xi^{\theta} = \frac{\mathrm{i}k_\theta\gamma_{tt} - \mathrm{i}k_\theta\gamma_{\theta\theta} - 2\mathrm{i}k_t\gamma_{t\theta}}{2\sinh^2 r(k_t^2+k_\theta^2)} \tag{3.48}$$

$$\xi^{t} = \frac{-\mathrm{i}k_t\gamma_{tt} + \mathrm{i}k_t\gamma_{\theta\theta} - 2\mathrm{i}k_\theta\gamma_{t\theta}}{2\cosh^2 r(k_t^2+k_\theta^2)} \quad . \tag{3.49}$$

Thus the lapse and shift perturbations arise by replacing $\xi^{\perp}$ with

$$\hat{\xi}^{\perp} = \xi^{\perp} - \frac{1}{2\Delta}\frac{\lambda}{\sqrt{h}} = \xi^{\perp} - \frac{1}{4(k_t^2+k_\theta^2)} \quad . \tag{3.50}$$

As for the flat case we have that the solution for $\gamma_{\perp\perp}$ a priori does not involve λ. Appendix C shows that this will be always the case for foliations for which ${}^{\mathrm{b}}R = 0$. Thus we will also find here that for the case of an outer and inner boundary, λ remains a free parameter and the action (2.41) evaluated on the solutions (3.46) will just reproduce the gravitational Hamilton–Jacobi functional plus the Lagrange multiplier term.

If we consider only the case of an outer boundary we have to impose smoothness conditions (see Appendix E)

$$\gamma_{\perp\theta} = r a^{(1)}_{r\theta} + r^2 a^{(2)}_{r\theta} + O(r^3)\,, \tag{3.51}$$

$$\gamma_{\theta\theta} = r^2 a^{(2)}_{\theta\theta} + O(r^3)\,, \tag{3.52}$$

$$\gamma_{t\theta} = r a^{(1)}_{t\theta} + r^2 a^{(2)}_{r\theta} + O(r^3) \quad , \tag{3.53}$$

for $r = 0$ with the remaining metric components starting with $a^{(0)}_{ab} r^0$ coefficients.

Ensuring that $a^{(-2)}_{rr} = 0$ requires again $k_\theta a^{(0)}_{tt} = 0$. To make $a^{(1)}_{r\theta}$ vanish we need

$$\lambda = (k_\theta^2 - 1)(2a^{(1)}_{tt} - 4\frac{k_t}{k_\theta}a^{(1)}_{t\theta}) \quad . \tag{3.54}$$

This leads to a non-vanishing vector component $\xi^{\perp}$ at $r = 0$:

$$\xi^{\perp}(r{=}0) = \frac{1}{4}\frac{k_\theta^2}{(k_\theta^2-1)}\frac{\lambda}{(k_t^2+k_\theta^2)}, \tag{3.55}$$

which allows us to solve the Lagrange multiplier equation $\rho = \xi^{\perp}(r_{\rm out}) - \xi^{\perp}(r=0)$ for λ:

$$\lambda = 4(k_t^2 + k_\theta^2)\left(1 - \frac{1}{k_\theta^2}\right)(\xi^{\perp}(r_{\rm out}) - \rho) \quad . \tag{3.56}$$

The evaluation of the action proceeds completely parallel to the flat case and we arrive at

$$\begin{aligned} -\kappa S_\lambda^{(2)} \underset{\text{solu}}{=} & -\frac{1}{4}\int_{\partial\mathcal{M}} d^2y\sqrt{h}\left(\rho\,\Delta\left(1+\frac{1}{\partial_\theta^2}\right)\rho - 2\rho\left(1+\frac{1}{\partial_\theta^2}\right)\delta({}^2\boldsymbol{R})\right) + \\ & \frac{1}{4}\int_{\partial\mathcal{M}} d^2y\sqrt{h}\left(\xi^{\perp}\Delta\frac{1}{\partial_\theta^2}\xi^{\perp} - \xi^A\mathcal{D}_{AB}\,\xi^B\right) \quad . \end{aligned} \tag{3.57}$$

where now $\Delta = \frac{-2}{\cosh r\,\sinh r}\,(\partial_\theta^2 + \partial_t^2)$ and $\sqrt{h} = \cosh r\,\sinh r$.

The cases $k_\theta = \pm 1$ and $k_\theta = 0$ again require special attention. For $k_\theta = \pm 1$ we find that $\lambda = 0$ and that thus the action for the field ρ vanishes. For $k_\theta = 0$ we have that $\xi^{\perp}(r=0)$ vanishes, and that thus λ remains undetermined. The on-shell evaluation of the λ–action will therefore give the same result (3.30) as in the flat case.

In summary, we find that the action for the boundary field ρ features the same insertion of the non-local differential operator $(1+\partial_\theta^{-2})$ as in the flat case

$$\kappa S'_\rho := \frac{1}{4}\int_{\partial\mathcal{M}} d^2y\sqrt{h}\left(\rho\,\Delta\left(1+\frac{1}{\partial_\theta^2}\right)\rho - 2\rho\left(1+\frac{1}{\partial_\theta^2}\right)\delta({}^2\boldsymbol{R})\right) \quad . \tag{3.58}$$

3.2.2 One-loop correction from the dual field

We have thus found an effective boundary action for the AdS_3 background. The kinetic part is describing a free scalar field on a torus. Additionally we have the operator $(1+\partial_\theta^{-2})$ but we have seen in section 3.1.9, that, apart from suppressing the $k_\theta = \pm 1$ modes, this operator does only contribute a constant to the one-loop partition function. But the Laplace operator $\Delta \sim \partial_t^2 + \partial_\theta^2$ defined on the torus leads to the one-loop correction [124]

$$\prod_{\kappa_\theta \geq 2} \frac{1}{|1 - q^{\kappa_\theta}|^2} \tag{3.59}$$

where $q = \exp(i\tau)$ with the torus modular parameter $\tau = \frac{1}{2\pi}(\gamma - i\beta)$. This agrees with the one-loop correction computed directly from gravity [21] with the structure of the Virasoro character.

3.3 Flat space with spherical boundary

We have seen that for the cases with flat boundaries, that is with ${}^{\mathrm{b}}R = 0$, we need to carefully take into account smoothness conditions at $r = 0$, to obtain an effective action, which can also be interpreted as dual field theory. This effective action does however differ by the insertion of a non-local operator from the action, which we postulated in section 2.2.1. This non-local operator plays an important role in transferring correctly the symmetries of the gravitational theory to the dual field theory.

Let us now consider a case in three dimensions with non-vanishing background intrinsic curvature ${}^2R \neq 0$. As we consider only boundaries with homogeneous curvature, we have to change the topology. We will choose a spherical one. Using Regge lengths one can argue that for a sphere boundary the effective action for the geodesic length should be local[5] and that we thus might confirm the action we postulated in section 2.2.1.

We choose as background metric

$$ds^2 \;=\; dr^2 + r^2 d\theta^2 + r^2 \sin^2\theta d\varphi^2 \tag{3.60}$$

with spherical boundary defined by $r = \text{const}$. The intrinsic boundary curvature is now non–vanishing ${}^2R = \frac{2}{r^2}$. We will see that this alters the computations in several ways from the cases with intrinsically flat boundary.

We have furthermore $K_{CD} = \frac{1}{2} K h_{CD}$ and thus $K^{AB} - K h^{AB} = -\frac{1}{2} K$. This gives

$$\begin{aligned} \Delta &= -\left(K D^C D_C + {}^2R K\right) &&= -\tfrac{2}{r}\left(D^C D_C + \tfrac{2}{r^2}\right) \quad , \\ \mathcal{D}_{AB} &= -\left(K D^C D_C + \tfrac{1}{2}{}^2R K\right) h_{AB} &&= -\tfrac{2}{r}\left(D^C D_C + \tfrac{1}{r^2}\right) h_{AB} \end{aligned} \tag{3.61}$$

with $K = \frac{2}{r}$ and ${}^2R = \frac{2}{r^2}$.

As we have now intrinsic curvature, the differential operators D_θ and D_φ are non-commuting and we cannot simultaneously diagonalize these operators. However one can use scalar, vector and tensor spherical harmonics, which allow for the diagonalization of the spherical Laplacian $\Delta_{\mathbb{S}^{(\mathrm{d}-1)}} = h^{AB} D_A D_B$ acting on scalars, vectors and second rank tensors. Furthermore one has certain properties for the divergence of the vector and tensor harmonics as well as for the trace of the tensor harmonics, see appendix G.

[5] The reason is that the one-loop partition function for 3D Regge calculus is bulk triangulation independent [26]. One can therefore choose the coarsest bulk triangulation available. For the spherical boundary one can choose a triangulation with only one bulk vertex and where all bulk edges go from the boundary to this bulk vertex. The edge lengths can therefore be interpreted as geodesic lengths and the Regge action, which is local, can be identified with the effective action for the geodesic lengths [3].

We will however not need these harmonics for most of the discussion. It will be sufficient to know that we can find the inverse of the operators Δ and $\mathcal{D}_{AB}$, e.g. by using the spherical harmonics to diagonalize these operators.

3.3.1 Solutions to the equations of motion

We again start by solving the lapse and shift components of the equations of motion

$$\hat{G}^{ab} = \frac{1}{4}\frac{\lambda(y)}{\sqrt{h}}\delta^a_\perp\delta^b_\perp \quad , \tag{3.62}$$

for the lapse and shift components of the metric perturbations. The derivation of the solutions is now more involved, due to the non-commutativity of the differential operators. We have collected the essential details in appendix C.2 (for general sphere in flat space) and reproduce here just the resulting solutions for lapse and shift:

$$\begin{aligned} \gamma_{\perp\perp} &= 2\partial_\perp\left(\xi^\perp - \frac{1}{2}\frac{1}{\Delta}\frac{\lambda}{\sqrt{h}}\right) \quad , \\ \gamma_{\perp B} &= D_B\left(\xi^\perp - \frac{1}{2}\frac{1}{\Delta}\frac{\lambda}{\sqrt{h}}\right) + h_{AB}\partial_\perp\xi^A \quad . \end{aligned} \tag{3.63}$$

We again find that the introduction of the Lagrange multiplier amounts to shifting the vector component $\xi^\perp$ to

$$\hat{\xi}^\perp = \xi^\perp - \frac{1}{2}\frac{1}{\Delta}\frac{\lambda}{\sqrt{h}} \quad . \tag{3.64}$$

But different from the cases with flat boundary we now have a λ–dependence for the lapse components $\gamma_{\perp\perp}$. Here it arises due to the fact that $\sqrt{h}\Delta$ is now r–dependent.

Let us also shortly discuss the smoothness conditions for the metric perturbations at $r = 0$. Assuming Taylor expandable metric perturbations in Cartesian coordinates and transforming these to spherical coordinates, see Appendix E, we find that $\gamma_{\perp\perp}$ has an expansion in the r–coordinate that starts with r^0, $\gamma_{\perp A}$ components start with an r^1–term and the γ_{AB}–components start with r^2.

Now assuming that the γ_{AB} components start with r^2 one will find that the solutions (3.63) ensure that the remaining conditions are satisfied. This also holds if we include a

non–vanishing λ. To see this, one can use the scaling properties of the differential operators in r, e.g.

$$\Delta = r^{-3}\tilde{\Delta} \quad , \qquad \mathcal{D}^A{}_B = r^{-3}\tilde{\mathcal{D}}^A{}_B \quad , \qquad \Pi^{AB} = r^{-4}\tilde{\Pi}^{AB} \quad , \qquad \sqrt{h} = r^2\sqrt{\tilde{h}} \tag{3.65}$$

where $\tilde{\mathcal{O}}$ is the operator $\mathcal{O}$ evaluated at $r = 1$.

Using these scaling properties we can also deduce that the vector component $\xi^\perp$ is vanishing at $r = 0$, that is we have $\xi^\perp(r = 0) = 0$ as well as $\hat{\xi}^\perp(r = 0) = 0$.

Finally we consider the Lagrange multiplier equation, which is now given by

$$\begin{aligned} \rho \;=\; \frac{1}{2}\int_{r_{\rm in}}^{r_{\rm out}} dr\, \gamma_{\perp\perp} \;&=\; \hat{\xi}^\perp(r_{\rm out}) - \hat{\xi}^\perp(r_{\rm in}) \\ &=\; \xi^\perp(r_{\rm out}) - \xi^\perp(r_{\rm in}) - \frac{(r_{\rm out} - r_{\rm in})}{2\sqrt{\tilde{h}}\tilde{\Delta}}\lambda \end{aligned} \tag{3.66}$$

Thus we obtain as a solution for λ

$$\lambda \;=\; \frac{2\sqrt{\tilde{h}}\tilde{\Delta}}{(r_{\rm out} - r_{\rm in})}\left(\xi^\perp(r_{\rm out}) - \xi^\perp(r_{\rm in}) - \rho\right) \quad , \tag{3.67}$$

where $\xi^\perp(r = 0) = 0$.

3.3.2 Evaluation of the action

Let us consider the case that we have an outer boundary at $r_{\rm out}$ and an inner boundary at $r_{\rm in}$. As we have $\hat{\xi}^\perp(r = 0) = \xi^\perp(r = 0) = 0$, it will be straightforward to derive from this the case with only an outer boundary.

For the evaluation of the boundary we need to consider the bulk and boundary term in (2.41) – the Lagrange multiplier term vanishes on solutions of (3.67). We will however treat for the moment λ as a variable, and only use the explicit solution for λ at the very end.

The bulk term gives evaluated on solutions of (3.62)

$$\begin{aligned} -\kappa S^{(2)}_{\rm bulk} \;&=\; \frac{1}{2}\int_M d^3x\sqrt{g}\,\gamma_{ab}\,\hat{G}^{ab} \;=\; \frac{1}{8}\int_M d^2y dr\;\gamma_{\perp\perp}(r,y)\lambda(y) \\ &=\; \frac{1}{4}\int_{(\partial\mathcal{M})_{\rm out}} d^2y\,\lambda\,(\hat{\xi}^\perp(r_{\rm out}) - \hat{\xi}^\perp(r_{\rm in})) \quad . \end{aligned} \tag{3.68}$$

Note that we now have $\hat{\xi}^\perp$ appearing, instead of just $\xi^\perp$. (In the cases with flat boundaries $(\hat{\xi}^\perp - \xi^\perp)$ is constant in r and we could thus use $\xi^\perp$.)

For the boundary term we find (see Appendix C.3)

$$-\kappa S^{(2)}_{\rm bdry} \;=\; -\kappa S^{(2)}_{\rm HJ} - \frac{1}{4}\int_{(\partial\mathcal{M})_{\rm out}} d^2y\,\lambda\left(\xi^\perp(r_{\rm out}) - \xi^\perp(r_{\rm in})\right) \quad . \tag{3.69}$$

We are thus left with

$$\begin{aligned} -\kappa S^{(2)}_{\lambda} &\underset{\rm solu}{=} -\kappa S^{(2)}_{\rm HJ} + \frac{1}{4}\int_{(\partial\mathcal{M})_{\rm out}} d^2y\;\lambda\left((\hat{\xi}^\perp - \xi^\perp)(r_{\rm out}) - (\hat{\xi}^\perp - \xi^\perp)(r_{\rm in})\right) \\ &= -\kappa S^{(2)}_{\rm HJ} - \frac{1}{4}\int_{(\partial\mathcal{M})_{\rm out}} d^2y\;\lambda\,\frac{(r_{\rm out}-r_{\rm in})}{2\sqrt{\tilde{h}}\tilde{\Delta}}\,\lambda \quad . \end{aligned} \tag{3.70}$$

Inserting the solution (3.67) for λ

$$\lambda \;=\; \frac{2\sqrt{\tilde{h}}\tilde{\Delta}}{(r_{\rm out}-r_{\rm in})}\left(\xi^\perp(r_{\rm out}) - \xi^\perp(r_{\rm in}) - \rho\right) \quad , \tag{3.71}$$

we obtain

$$\begin{aligned} -\kappa S^{(2)}_{\lambda} \underset{\rm solu}{=} -\kappa S^{(2)}_{\rm HJ} - \frac{1}{2}\int_{(\partial\mathcal{M})_{\rm out}} d^2y \frac{\sqrt{\tilde{h}}}{(r_{\rm out}-r_{\rm in})}\Big[\rho\tilde{\Delta}\rho - 2\rho\tilde{\Delta}\left(\xi^\perp(r_{\rm out}) - \xi^\perp(r_{\rm in})\right) + \\ \left(\xi^\perp(r_{\rm out}) - \xi^\perp(r_{\rm in})\right)\tilde{\Delta}\left(\xi^\perp(r_{\rm out}) - \xi^\perp(r_{\rm in})\right)\Big] \end{aligned} \tag{3.72}$$

The terms in $S^{(2)}_{\rm HJ}$, in which $\xi^\perp$ appears are given by

$$\begin{aligned} \sqrt{h}\xi^\perp(r_{\rm out})\Delta\xi^\perp(r_{\rm out}) &= r_{\rm out}^{-1}\sqrt{\tilde{h}}\xi^\perp(r_{\rm out})\tilde{\Delta}\xi^\perp(r_{\rm out}) \quad \text{and} \\ -\sqrt{h}\xi^\perp(r_{\rm in})\Delta\xi^\perp(r_{\rm in}) &= -r_{\rm in}^{-1}\sqrt{\tilde{h}}\xi^\perp(r_{\rm in})\tilde{\Delta}\xi^\perp(r_{\rm in}) \end{aligned} \tag{3.73}$$

Thus, for $r_{\rm in} \neq 0$ we will not have a cancellation between these terms and

$$(r_{\rm out}-r_{\rm in})^{-1}\sqrt{\tilde{h}}\left(\xi^\perp(r_{\rm out}) - \xi^\perp(r_{\rm in})\right)\tilde{\Delta}\left(\xi^\perp(r_{\rm out}) - \xi^\perp(r_{\rm in})\right) \tag{3.74}$$

appearing in (3.72).

Thus, although (3.72) is an effective action for the geodesic lengths between the outer and inner boundary, we cannot interpret the ρ–dependent part as a dual action for gravity.

This might not be a surprise as the geodesic lengths does only detect the difference between $\xi^{\perp}(r_{\rm out})$ and $\xi^{\perp}(r_{\rm in})$, whereas for the evaluation of the gravitational boundary term we need to know both $\xi^{\perp}(r_{\rm out})$ and $\xi^{\perp}(r_{\rm in})$.

These problems do not appear if we choose to have only an outer boundary, that is $r_{\rm in}=0$, in which case we have $\xi^{\perp}(r_{\rm in})=0$. Then we can write

$$\begin{aligned} -\kappa S^{(2)}_{\lambda} &\underset{\text{solu}}{=} -\kappa S^{(2)}_{\rm HJ} - \frac{1}{2}\int_{\partial\mathcal{M}} d^2y\sqrt{h}\Big[\rho\Delta\rho - 2\rho\Delta\xi^{\perp}(r_{\rm out}) + \xi^{\perp}(r_{\rm out})\Delta\xi^{\perp}(r_{\rm out})\Big] \,. \\ &= -\frac{1}{2}\int_{\partial\mathcal{M}} d^2y\sqrt{h}\left(\rho\Delta\rho - 2\rho\,\delta({}^2\boldsymbol{R})\right) - \frac{1}{2}\int_{\partial\mathcal{M}} d^2y\sqrt{h}\,\xi^A\mathcal{D}_{AB}\xi^B \quad . \end{aligned} \tag{3.75}$$

The ρ-dependent part is given by

$$S'_{\rho} = -\frac{1}{2}\int_{\partial\mathcal{M}} d^2y\sqrt{h}\left(\rho\Delta\rho - 2\rho\,\delta\left({}^2\boldsymbol{R}\right)\right) \tag{3.76}$$

and can be taken as dual boundary field theory, which reproduces the boundary-diffeomorphism invariant part of the gravitational HJF.

Thus we see that for the case of a three dimensional spherical boundary we produce exactly the action S_{ρ} which we derived in section 2.2.1, that is $S'_{\rho}=S_{\rho}$. Different from the cases with flat boundary discussed previously there is no insertion of a non-local operator in S'_{ρ}.

Note that there are also special modes, that appear for the spherical boundary. Using spherical harmonics Y^{lm} one will find that Δ is vanishing on Y^{lm} with $l=1$. One thus has three modes $l=1$ and $m=-1,0,+1$ for which S'_{ρ} is vanishing. These modes do describe the geometric position of the central point at $r=0$, which is encoded in the metric perturbations γ_{AB} around $r=0$. Thus, we can understand these three modes as (diffeomorphism) gauge parameters for the gravitational field, which do happen to affect the geodesic length variable.

As discussed above we can use the Regge calculus set-up to argue that the geodesic effective action should be indeed local. In (3.72) there is still the term $\xi^A\mathcal{D}_{AB}\xi^B$, which is a priori non-local through the expressions of ξ^A in terms of the boundary metric components γ_{BC}. Using the spherical (tensor) harmonics in Appendix G one finds however that ξ^A is determined by

$$\xi^{\Psi}=\tfrac{1}{2}\gamma^{\Psi} \quad , \qquad \xi^{\Phi}=\tfrac{1}{2}\gamma^{\Phi} \tag{3.77}$$

where we used an expansion $\gamma_{AB}=\gamma^{\Psi}\Psi_{AB}+\gamma^{\Phi}\Phi_{AB}+\gamma^{\Theta}\Theta_{AB}$ and $\xi_A=\xi^{\Psi}\Psi_A+\xi^{\Phi}\Phi_B$ of the metric and vector field into tensor and vector harmonics respectively. Note that Ψ_{AB} and Φ_{AB} are a basis for the trace free part of the metric perturbations.

Chapter 4

Twisted thermal flat space in 4D with finite boundary

The method to construct holographic duals directly from gravity, which we have employed in chapter 2, allows to study four dimensional linearized gravity. In this regard, we consider in this chapter an example of a four dimensional background spacetime which satisfies the assumptions laid out in section 2.1.1. Four dimensional gravity is not topological, the (linearized) equations of motion describe propagating degrees of freedom. Thus, the challenge is to have a description that capture the propagating degrees of freedom.

In four dimensions, the boundary metric perturbations feature a diffeomorphism sector and a graviton sector (see the discussion in section 2.1.3). The graviton sector is described by two propagating degrees of freedom. For the diffeomorphism sector, we will find a dual boundary field theory as effective action for geodesic lengths. This dual theory will turn out to be in a simple form with a coupling to the three dimensional Ricci scalar.

The example of the background we consider in this chapter also appears in [3], using the (linearized) Regge calculus certain. There, we considered a very coarse triangulation and computed directly the effective action for geodesic lengths. Thus the effective action only approximates very well the diffeomorphism sector of the theory.

As warm-up for later computing the one-loop partition function, we will determine the Hamilton–Jacobi functional (HJF) expanded around the four dimensional background which we describe next.

4.1 Twisted thermal flat space with finite boundary

The background geometry we consider here is a generalization of the twisted or spinning thermal flat space considered in section 3.1 from three to four dimensions. This background is a solution to Einstein's equation (with Euclidean signature) with a vanishing cosmological constant.

The metric of thermal spinning flat space in four dimensions is given by

$$ds^2 \;=\; dr^2 + h_{AB}dy^A dy^B = dr^2 + r^2 d\theta^2 + dt^2 + dz^2 \tag{4.1}$$

with the coordinates subject to periodic identifications

$$(r,\theta,t,z) \sim (r,\theta+\gamma_t,t+\beta_t,z) \qquad \text{and} \qquad (r,\theta,t,z) \sim (r,\theta+\gamma_z,t,z+\beta_z) \tag{4.2}$$

in addition to the usual identification $\theta \sim \theta + 2\pi$ for the angular variable and $r \geq 0$. The space time is flat, but features moduli parameters $(\beta_t, \gamma_t, \beta_z, \gamma_z)$ that turn out to lead to interesting structure for the one-loop correction.

If the space–time manifold has only an outer boundary at $r = r_{\text{out}}$ at a finite distance, then the radial coordinate takes values $r \in [0, r_{\text{out}}]$. The spacetime manifold therefore has a topology of a solid 3-torus with a 3-torus boundary topology. In the case the space–time manifold has an outer boundary at $r = r_{\text{out}}$ and an inner boundary at $r = r_{\text{in}}$, i.e., $r \in [r_{\text{in}}, r_{\text{out}}]$, the resulting topology is a toroidal annulus. A property of these annuli is that one can glue two of these together (if the outer radius of one matches the inner radius of the other), and obtain again a toroidal annulus. This gluing operation can be used to define recursion relations, that can be used to determine the path integral for the toroidal annulus, along the lines of [125].

The boundary at $r = \text{const}$ is flat (with respect to the background metric). This allows to define a 'twisted' Fourier transformation for the metric perturbation components respecting the periodic identifications in (4.2). The twisted Fourier transformed metric perturbations is given by

$$\gamma_{ab}(r,k_\theta,k_t,k_z) \;=\; \frac{1}{\sqrt{2\pi\beta_t\beta_z}} \int_{\partial\mathcal{M}} d^3y\, \gamma_{ab}(r,\theta,t,z)\, e^{-\mathrm{i}(\theta k_\theta + t k_t + z k_z)} \quad , \tag{4.3}$$

where we have the twisted frequencies k_t, k_z given by

$$k_t := \frac{2\pi}{\beta_t}(k_t' - \frac{\gamma_t}{2\pi}k_\theta), \qquad k_z := \frac{2\pi}{\beta_z}(k_z' - \frac{\gamma_z}{2\pi}k_\theta) \tag{4.4}$$

with the Fourier modes $k_\theta, k_t', k_z' \in \mathbb{Z}$. The inverse transform is given by

$$\gamma_{ab}(r,\theta,t,z) \;=\; \frac{1}{\sqrt{2\pi\beta_t\beta_z}} \sum_{k_\theta,k_t,k_z} \gamma_{ab}(r,k_\theta,k_t,k_z)\, e^{\mathrm{i}(\theta k_\theta + t k_t + z k_z)} \quad . \tag{4.5}$$

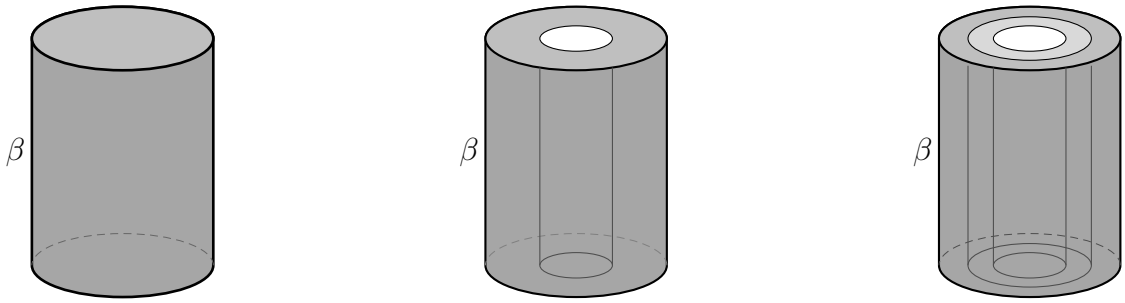

Figure 4.1: [From left to right] A solid torus, a toroidal annulus and two annuli glued together in 3D. The top and bottom are identified in all figures.

4.1.1 Parametrization of metric perturbation

As already discussed in section 2.1.3, the boundary metric fluctuations can be split into a part ζ_{AB}, which is induced by diffeomorphisms, and a part χ_{AB}, which describes graviton sector. These sectors can be described by projectors which are orthogonal with respect to to the inner product (2.19) for the boundary metric perturbations.

The diffeomorphism sector is spanned by vector fields $(\xi^{\perp}, \xi^{A})$, and the graviton sector is spanned by two functions w, x such that in the Fourier transformed picture, we obtain

$$\gamma_{AB} \;=\; \zeta_{AB} + \chi_{AB} \;=\; 2K_{AB}\xi^{\perp} + \mathrm{i}k_A\xi_B + \mathrm{i}k_B\xi_A + W_{AB}\, w + X_{AB}\, x \quad . \tag{4.6}$$

where the components of the graviton perturbations are given by

$$\begin{aligned}
(X_{\theta\theta}, X_{tt}, X_{zz}, X_{\theta t}, X_{\theta z}, X_{tz}) &= \sqrt{\frac{2}{r^2\Delta_{\mathrm{b}}}}\left(0, -\frac{k_\theta k_t k_z}{(k_t^2+k_z^2)}, \frac{k_\theta k_t k_z}{(k_t^2+k_z^2)}, \frac{r^2 k_z}{2}, -\frac{r^2 k_t}{2}, \frac{k_\theta(k_t^2-k_z^2)}{2(k_t^2+k_z^2)}\right) \\
(W_{\theta\theta}, W_{tt}, W_{zz}, W_{\theta t}, W_{\theta z}, W_{tz}) &= \frac{1}{(k_t^2+k_z^2)}\left(0, k_z^2, k_t^2, 0, 0, -k_t k_z\right) \quad ,
\end{aligned} \tag{4.7}$$

and where $\Delta_{\mathrm{b}} := \frac{k_\theta^2}{r^2} + k_t^2 + k_z^2 \equiv D^A D_A$ is the 'spatial' Laplacian. The perturbations W_{AB}[1] and X_{AB} are orthogonal to the diffeomorphism sector and also to each other with respect to the inner product

$$\langle \gamma, \gamma' \rangle := \frac{1}{{}_3V}\int d^3y\,\sqrt{h}\,\gamma_{AB}h^{AC}h^{BD}\gamma'_{CD} \;=\; \frac{1}{2\pi\beta_t\beta_z}\sum_{k_\theta,k'_t,k'_z}\gamma_{AB}(k)h^{AC}h^{BD}\gamma'_{CD}(-k) \tag{4.8}$$

[1]The perturbation $W_{AB} = \delta^i_A\delta^j_B P^T_{ij}$ where $i,j \in \{t,z\}$ and $P^T_{ij} = \delta_{ij} - \frac{\partial_i\partial_j}{(\partial_t^2+\partial_z^2)}$ is the 2D transverse projector in $t-z$ plane.

where ${}^3V := \int d^3y\,\sqrt{h} = 2\pi\beta_t\beta_z r$ is the volume for the hypersurface. The x and w parameters are therefore given by

$$\begin{aligned} w[\gamma] := \frac{\langle \gamma, W\rangle}{\langle W, W\rangle} &= \frac{1}{(k_t^2+k_z^2)}\left(k_z^2\gamma_{tt} + k_t^2\gamma_{zz} - 2k_tk_z\gamma_{tz}\right) \quad , \\ x[\gamma] := \frac{\langle \gamma, X\rangle}{\langle X, X\rangle} &= \frac{1}{r}\sqrt{\frac{2}{\Delta_{\mathrm{b}}}}\left(\frac{k_\theta k_t k_z}{k_t^2+k_z^2}(\gamma_{zz}-\gamma_{tt}) + k_z\gamma_{\theta t} - k_t\gamma_{\theta z} + \frac{k_\theta(k_t^2-k_z^2)}{k_t^2+k_z^2}\gamma_{tz}\right) . \end{aligned} \tag{4.9}$$

We have inverse differential operators (acting along a boundary component) appearing in W_{AB} and X_{AB}, the projectors constitute therefore non-local operators. The projectors can be restricted to either the outer and inner boundary component. However, to suppress bulk gravitons, we need to demand that $w = 0$ and $x = 0$ at both boundary components. Of course, bulk diffeomorphisms can appear even if we set the $\xi-$parameters at the boundary to zero. The HJF will however only depend on the boundary diffeomorphisms, and their contribution factorizes over the boundary components.

4.2 Dual boundary field theory for geodesic lengths

In section 2.1.4, we have computed the (restricted) Hamilton–Jacobi functional (HJF) for general backgrounds satisfying our assumptions in section 2.1.1. The second-order HJF (2.27) is particularly in a simple form and allowed to compute holographic dual boundary theories in chapter 3 for various three dimensional background space–time manifolds.

Here, we will restrict the boundary metric perturbations (4.6) to the diffeomorphism sector and compute the effective action for the geodesic distances (corresponding dual boundary field theory). The computations share many similarities with the 3D case and so we will be brief.

For our background metric (4.1), the (background) tensor Q^{AB} which is defined in (2.23) vanishes and hence the second-order HJF for the diffeomorphism sector is given by

$${}^{\mathrm{D}}S^{(2)}_{\mathrm{HJ}} = -\frac{1}{2\kappa}\int_{\partial\mathcal{M}} d^3y\,\sqrt{h}\,\left(\xi^\perp\Delta\xi^\perp - \xi^A\mathcal{D}_{AB}\xi^B\right) \quad , \tag{4.10}$$

where $\Delta = -\frac{2}{r}(\partial_t^2+\partial_z^2)$ and $\mathcal{D}_{AB} = -\frac{2}{r}(\partial_t^2+\partial_z^2)h_{AB}$. The second order HJF is a local functional given in terms of the diffeomorphism vector fields ξ^a and also separates into normal and tangential parts.

Considering the λ-dependent action (2.41), the solutions to the equations of motion

$$\hat{G}^{ab} = \frac{1}{4}\frac{\lambda}{\sqrt{h}}\delta^a_\perp \delta^b_\perp \quad , \tag{4.11}$$

has been determined in appendix C.1 for manifolds with flat boundaries in any dimension when the boundary metric perturbations are restricted to the diffeomorphism sector. If the manifold has one outer boundary with $0 \le r \le r_{\rm out}$, we can find the solution to the Lagrange multiplier by implementing smoothness conditions at the origin $r = 0$. The origin here describes a two dimensional (t and z directions) sub–manifold in the bulk space–time. The smoothness conditions are

$$\begin{aligned} \gamma_{ab} &= a^{(1)}_{ab}\, r + a^{(2)}_{ab}\, r^2 + \mathcal{O}(r^3) \quad \text{for } ab = r\theta, \theta t, \theta z; \\ \gamma_{\theta\theta} &= a^{(2)}_{ab}\, r^2 + \mathcal{O}(r^3) \quad , \end{aligned} \tag{4.12}$$

with the coefficients of the remaining components start with $a^{(0)}_{ab}$.

Restricting to the diffeomorphism sector, the Taylor expansions of the components $\zeta_{\perp\perp}$ and $\zeta_{\perp\theta}$ give a condition on Lagrange multiplier,

$$\xi^\perp(0) = \frac{1}{2}\frac{k_\theta^2}{1-k_\theta^2}\frac{1}{\Delta}\frac{\lambda}{\sqrt{h}} = \xi^\perp(r_{\rm out}) - \rho \quad . \tag{4.13}$$

Thus the modes $k_\theta = 0, \pm 1$ and $\sqrt{h}\Delta \sim (k_t^2 + k_z^2) = 0$ need special treatments.

Let us now discuss the modes satisfying $|k_\theta| \ge 2$ and $(k_t^2 + k_z^2) \neq 0$. The evaluation of the Lagrange multiplier equation (4.13) leads to the (restricted) effective action

$$\begin{aligned} -\kappa\, {}^{\rm D}S^{(2)}_\lambda &\underset{\rm solu}{=} -\kappa\, {}^{\rm D}S^{(2)}_{\rm HJ}(r_{\rm out}) - \frac{1}{4}\int_{\partial\mathcal{M}} d^3y\, \lambda(y)\, \xi^\perp(0,y) \\ &= -\frac{1}{4}\int_{\partial\mathcal{M}} d^3y\sqrt{h}\, \left(\rho\left(1+\frac{1}{\partial_\theta^2}\right)\Delta\,\rho - 2\rho\left(1+\frac{1}{\partial_\theta^2}\right)\delta'({}^3\boldsymbol{R})\right) + \\ &\quad \frac{1}{4}\int_{\partial\mathcal{M}} d^3y\sqrt{h}\left(\xi^\perp\Delta\frac{1}{\partial_\theta^2}\xi^\perp - \xi^A\mathcal{D}_{AB}\,\xi^B\right) \quad . \end{aligned} \tag{4.14}$$

Here, δ' represents the restriction of variations to the diffeomorphism sector ($\gamma_{AB} \equiv \zeta_{AB}$).

The $\rho-$dependent part describing the action for the boundary field ρ

$$\kappa\, {}^{\rm D}S'_\rho = \frac{1}{4}\int_{\partial\mathcal{M}} d^3y\sqrt{h}\, \left(\rho\left(1+\frac{1}{\partial_\theta^2}\right)\Delta\,\rho - 2\rho\left(1+\frac{1}{\partial_\theta^2}\right)\delta'({}^3\boldsymbol{R})\right) \tag{4.15}$$

features the same insertion of the non-local differential operator $(1+\partial_\theta^{-2})$ just as in case of a torus boundary in three dimensions.

For the modes $k_\theta = 0$, λ remains a free parameter and hence we do not get a proper dual boundary theory. For $k_\theta = \pm 1$, we get the solution $\lambda = 0$ and the effective action is

$$ {}^{\mathrm{D}}S^{(2)}_{\lambda}(k_\theta = \pm 1) \underset{\text{sol}}{=} {}^{\mathrm{D}}S^{(2)}_{\mathrm{HJ}}(k_\theta = \pm 1) \quad . \tag{4.16}$$

Hence the dual boundary action vanishes in this case. These modes are related to gauge degrees of freedom and corresponds to null vectors in the Regge setting.

In the case where we have two boundaries, $r_{\text{in}} \leq r \leq r_{\text{out}}$, the Lagrange multiplier remains a free parameter and we do not get a proper dual boundary field theory just as in the three dimensional case.

In summary, we have computed the effective action of geodesic lengths (4.15) when restricted to the diffeomorphism sector in 4D for the dual boundary theory. Surprisingly, the boundary theory is Liouville-like with a coupling of the (linearized) boundary Ricci scalar. It also has the same form as its 3D counterpart with same non-local insertion $(1+\partial_\theta^{-2})$.

The geodesic length observable which we have used to derive the dual boundary theory for the diffeomorphism sector is not capable of describing the graviton degrees of freedom. In the future, we will look for other geometric observables which can capture propagating degrees of freedom. Nonetheless, we can still compute the Hamilton–Jacobi functional and one–loop partition function (including gravitons) directly from the linearized action in section 2.1.2.

4.3 Computation of the Hamilton–Jacobi functional

As we have seen, the linearized Hamilton–Jacobi functional (HJF) is needed to determine the holographic dual boundary theory and also the gravitational one-loop partition function. The HJF also serves as 'perfect action' for gravity which is invariant under diffeomorphisms [126].

We will therefore compute here the HJF using the full metric perturbations (4.6) including the graviton sector and with Dirichlet boundary conditions. The HJF will therefore depend on the metric perturbations γ_{AB} at $r = r_{\text{out}}$, if we only have an outer boundary or at $r = r_{\text{out}}$ and $r = r_{\text{in}}$, if we have outer and inner boundaries (see figure 4.1). In the latter case, where we consider a region with two boundaries, the HJF will be shown to

be invariant under subdivisions in the radial direction, that is, if we 'glue' two regions at a common boundary, the resulting effective action after integrating out the shared bulk variables will be of the same form as the HJF for each region. (See the discussion in section 4.4.) In what follows, we will give technical details that go into computing the HJF.

4.3.1 Zeroth and First order contributions

The zeroth and first order of the HJF result from the Gibbons-Hawking-York boundary term and can be determined without solving equations of motions for the metric perturbations. The trace of the boundary extrinsic curvature is given by $K = \frac{1}{r}$ and hence the zeroth order contribution from a given boundary component to the effective action gives

$$S^{(0)}_{\mathrm{HJ}} = -\frac{1}{\kappa}\int_{\partial\mathcal{M}} d^3y\,\epsilon\sqrt{h}K = -\sum_{\epsilon}\epsilon\frac{2\pi\beta_t\beta_z}{\kappa} = -\sum_{\epsilon}\frac{\epsilon}{4G_N}\beta_t\beta_z \quad . \tag{4.17}$$

where the sum over ϵ is pertained to the boundary components, $\epsilon = +1$ for an outer boundary and $\epsilon = -1$ for an inner boundary.[2] Thus, in the case where we have two boundaries, the zeroth order contributions from both boundaries cancels out and hence vanishes.

For the background space time (4.1), the first order contribution vanishes for diffeomorphisms, whose generating vector field is normal to the boundary, and which can therefore interpreted as moving the boundary. These boundary normal diffeomorphisms are sometimes referred to as boundary gravitons (not to be confused with bulk gravitons). As shown in appendix A.2, this vanishing of the first order contribution applies to boundaries and space–times where $(2\Lambda - {}^{\mathrm{b}}R) = 0$. Thus the first order contribution to the HJF comes only from the graviton modes:

$$S^{(1)}_{\mathrm{HJ}} = -\frac{1}{2\kappa}\int_{\partial\mathcal{M}} d^3y\,\epsilon\sqrt{h}\,(K^{AB} - Kh^{AB})\gamma_{AB} = -\frac{1}{2\kappa}\int_{\partial\mathcal{M}} d^3y\,\epsilon\, w \quad . \tag{4.18}$$

where we have used the parametrization (4.6) for the boundary metric perturbations.

4.3.2 Second-order: Equations of motion

The second-order HJF quadratic in the metric perturbations encodes the linearized dynamics. Therefore, there will be different types of contributions to the HJF, which arise

[2] The sum over ϵ is also implicit in the integral over the boundary $\partial\mathcal{M}$.

from the split of the metric perturbations into the diffeomorphism sector and the sector describing (bulk) gravitons.

Let us consider the bulk equations of motion

$$\hat{G}^{ab} = 0 \tag{4.19}$$

for the linearized theory. See appendix C for definition of $\hat{G}^{ab}$. Due to diffeomorphism symmetry of the action we expect that four of the ten equations are redundant. We expect therefore only six independent equations – and we can use four to solve for lapse $\gamma_{\perp\perp}$ and shift $\gamma_{\perp A}$, and the remaining two for the graviton modes w and x.

Indeed $\hat{G}^{\perp\perp} = 0$ and $\hat{G}^{\perp A} = 0$ appear without radial derivatives acting on the lapse $\gamma_{\perp\perp}$ and shift $\gamma_{\perp A}$ components. We therefore use these equations to solve the lapse and shift components $\gamma_{\perp\perp}$ and $\gamma_{\perp A}$:

$$\begin{aligned}
\gamma_{\perp\perp} &= \partial_\perp\left(2\xi^\perp + \frac{r\Delta_{\rm b}}{(k_t^2+k_z^2)}w\right) - w \quad , \\
\gamma_{\perp\theta} &= \mathrm{i}k_\theta\left(\xi^\perp + \frac{r\Delta_{\rm b}}{2(k_t^2+k_z^2)}w\right) + r^2\partial_\perp\left(\xi^\theta + \frac{\mathrm{i}k_\theta}{2r^2(k_t^2+k_z^2)}w\right) \quad , \\
\gamma_{\perp t} &= \mathrm{i}k_t\left(\xi^\perp + \frac{r\Delta_{\rm b}}{2(k_t^2+k_z^2)}w\right) + \partial_\perp\left(\xi^t - \frac{\mathrm{i}k_t}{2(k_t^2+k_z^2)}w\right) - \mathrm{i}\sqrt{\frac{2}{\Delta_{\rm b}^3}}\frac{k_\theta k_z}{r^2}\,x \quad , \\
\gamma_{\perp z} &= \mathrm{i}k_z\left(\xi^\perp + \frac{r\Delta_{\rm b}}{2(k_t^2+k_z^2)}w\right) + \partial_\perp\left(\xi^z - \frac{\mathrm{i}k_z}{2(k_t^2+k_z^2)}w\right) + \mathrm{i}\sqrt{\frac{2}{\Delta_{\rm b}^3}}\frac{k_\theta k_t}{r^2}\,x \quad ,
\end{aligned} \tag{4.20}$$

where we have made use of the expansion (4.6). These solutions are valid away from $r = 0$ and also for $(k_t^2 + k_z^2) \neq 0$. Thus, the modes satisfying $(k_t^2 + k_z^2) = 0$ will require special treatment.

Substituting these solutions for the lapse and shift components (4.20) into the remaining equations $\hat{G}^{AB} = 0$ (the), we find that these six equations reduce to two equations for the w- and x-mode respectively:

$$\begin{aligned}
&\frac{d^2}{dr^2}w + \frac{1}{r}\frac{d}{dr}w - \Delta_{\rm b}w = 0 \quad , \\
&\frac{d^2}{dr^2}x + \frac{1}{r}\frac{d}{dr}x - \left(\Delta_{\rm b} + \frac{(k_t^2+k_z^2)}{r^2\Delta_{\rm b}}\left(1 - \frac{3\,k_\theta^2}{r^2\Delta_{\rm b}}\right)\right)x = 0 \quad .
\end{aligned} \tag{4.21}$$

Note that $\Delta_{\rm b} = \frac{1}{r^2}k_\theta^2 + k_t^2 + k_z^2 \equiv -(\frac{1}{r^2}\partial_\theta^2 + \partial_t^2 + \partial_z^2)$ includes an r-dependence.

The equation of motion for the w–graviton mode is the Laplace equation in 4D polar coordinates, hence, it is the modified Bessel differential equation whose general solution is given in terms of the modified Bessel functions[3]

$$w = c_1\, \mathcal{I}_{|k_\theta|}(r\sqrt{(k_t^2+k_z^2)}) + c_2\, \mathcal{K}_{|k_\theta|}(r\sqrt{(k_t^2+k_z^2)}) \quad , \tag{4.22}$$

where c_1 and c_2 are constants to be determined.

The equation for the x-mode can be related to the equation for the w-mode: Expressing the x-mode as $x = \frac{1}{\sqrt{\Delta_{\rm b}}}\frac{d}{dr}q$ and using this in the x-mode equation in (4.21), we find

$$\frac{1}{\sqrt{\Delta_{\rm b}}}\left(\frac{d}{dr}+\Delta_{\rm b}\frac{d}{dr}\frac{1}{\Delta_{\rm b}}\right)\left(\frac{d^2}{dr^2}+\frac{1}{r}\frac{d}{dr}-\Delta_{\rm b}\right)q \;=\; 0 \quad , \tag{4.23}$$

where the differential operator in the second bracket does coincide with the one defining the equation for the w-mode.

Thus, the general solution for the x-mode differential equation is given by

$$x = \frac{1}{\sqrt{\Delta_{\rm b}}}\left(c_3\,\frac{d}{dr}\mathcal{I}_{|k_\theta|}(r\sqrt{(k_t^2+k_z^2)}) + c_4\,\frac{d}{dr}\mathcal{K}_{|k_\theta|}(r\sqrt{(k_t^2+k_z^2)})\right) \quad , \tag{4.24}$$

where c_3 and c_4 are constants.

4.3.3 Second order: Hamilton–Jacobi functional

Here we will compute the second order HJF, by evaluating the second-order action (2.15) on solutions. As the bulk term of the second-order action vanishes for solutions of (4.19), we can restrict our attention to the boundary terms appearing in (2.15). For convenience, we rewrite the boundary action, given by

$$-\kappa S^{(2)}_{\rm bdry} = \frac{1}{2}\int_{\partial\mathcal{M}} d^3y\,\sqrt{h}\,\epsilon\,\gamma_{ab}\left(B_1^{abcd}\gamma_{cd} + B_2^{abecd}\nabla_e\gamma_{cd}\right)$$

where the (background) tensors are

$$\begin{aligned} B_1^{abcd} &= \frac{1}{2}(Kh^{ab}-K^{ab})g^{cd} - h^{ac}h^{bd}K - h^{ab}K^{cd} + h^{ac}K^{bd} + h^{bd}K^{ac} \\ B_2^{abecd} &= \frac{1}{2}\left(\left(h^{ae}h^{bd}-h^{ab}h^{ed}\right)n^c + \left(h^{ac}h^{be}-h^{ab}h^{ce}\right)n^d - \left(h^{ac}h^{bd}-h^{ab}h^{cd}\right)n^e\right) \end{aligned} \quad , \tag{4.25}$$

[3] $\mathcal{I}_{k_\theta}(r)$ and $\mathcal{K}_{k_\theta}(r)$ are modified Bessel function of order k_θ which are the two linearly independent solutions to the modified Bessel equation.

n^a is the normal to the boundary and $\epsilon = \pm 1$ denotes the orientation of the boundary component.

Using the parametrization (4.6) for the boundary metric perturbations, and the solutions (4.20), the second–order action (2.15) evaluated on solutions become

$$-\kappa S^{(2)} \underset{\text{sol}}{=} \frac{1}{2}\int_{\partial\mathcal{M}} d^3y\,\sqrt{h}\,\epsilon\,\Big(\xi^{\perp}\Delta\,\xi^{\perp} + \xi^{A}\mathcal{D}_{AB}\xi^{B} \;+ \\ 2\left(2K\partial_A\xi^A + \xi^{\perp}\Delta_{\rm b}\right)w + 2\sqrt{\frac{-2}{r^2\Delta_{\rm b}}}K(\partial_z\xi_t - \partial_t\xi_z)\partial_\theta x \;+ \\ \frac{\Delta_{\rm b} w}{\Delta}(r^2\Delta_{\rm b}-1)w + w\,\partial_\perp w - \frac{x}{2r}\left(1-\frac{\partial_\theta^2}{r^2\Delta_{\rm b}}\right)x - \frac{1}{2}x\,\partial_\perp x\Big), \quad (4.26)$$

where $\Delta = -\frac{2}{r}(\partial_t^2+\partial_z^2), \mathcal{D}_{AB} = -\frac{2}{r}(\partial_t^2+\partial_z^2)h_{AB}$, $K = \frac{1}{r}$ and $\Delta_{\rm b} = -(\frac{1}{r^2}\partial_\theta^2 + \partial_t^2 + \partial_z^2)$. In terms of Fourier modes we have

$$-\kappa S^{(2)} \underset{\text{sol}}{=} \sum_{\epsilon}\frac{\epsilon}{4}\sum_{k_\theta,k_t',k_z'}\Big(\bar{\xi}^{\perp}\tilde{\Delta}\,\xi^{\perp} + \bar{\xi}^{A}\tilde{\mathcal{D}}_{AB}\xi^{B} \;+ \\ 2\mathrm{i}\sqrt{\frac{2}{r^2\Delta_{\rm b}}}\bar{x}(k_z k_\theta\xi_t - k_t k_\theta\xi_z) - 2\bar{w}\left(r\Delta_{\rm b}\xi^{\perp} + \mathrm{i}k_A\xi^A\right) \;+ \\ \bar{w}\frac{\Delta_{\rm b}}{\tilde{\Delta}}(1-r^2\Delta_{\rm b})w + r\,\bar{w}\,\partial_\perp w - \bar{x}\left(\frac{1}{2}+\frac{k_\theta^2}{2r^2\Delta_{\rm b}}\right)x - \frac{r}{2}\bar{x}\,\partial_\perp x\Big) + cc\,, \quad (4.27)$$

where we have $\tilde{\Delta} = 2(k_t^2+k_z^2)$, $\tilde{\mathcal{D}}_{AB} = 2(k_t^2+k_z^2)h_{AB}$. The bar indicates $\bar{\xi}(r,k_\theta,k_t',k_z') = \xi(r,-k_\theta,-k_t',-k_z')$ and cc stands for complex conjugation. The sum over ϵ is a sum over orientations of the boundary components.

We see that the contributions to the second-order HJF split into three types: (a) the first is quadratic in the perturbations describing diffeomorphisms, (b) the second part mixes diffeomorphism and graviton sector, (c) the third part has terms quadratic in the graviton perturbations.

The type (a) contribution to the HJF which arises from diffeomorphism induced deformation of the background metric, can be computed for a wide class of backgrounds and boundaries, (see appendix A.2) and are localized. We have also found a (dual) boundary field theory (4.15) defined on each boundary component for these diffeomorphisms. In

summary, we get

$$\begin{aligned} -\kappa S^{(2)}_{\text{HJ-io-a}} &= \tfrac{1}{4}\sum_{k_\theta,k_t',k_z'}\Big(\big(\bar\xi^\perp\tilde\Delta\,\xi^\perp+\bar\xi^A\tilde{\mathcal{D}}_{AB}\xi^B\big)(r_{\text{out}})-\big(\bar\xi^\perp\tilde\Delta\,\xi^\perp+\bar\xi^A\tilde{\mathcal{D}}_{AB}\xi^B\big)(r_{\text{in}})\Big)+cc \\ -\kappa S^{(2)}_{\text{HJ-o-a}} &= \tfrac{1}{4}\sum_{k_\theta,k_t',k_z'}\big(\bar\xi^\perp\tilde\Delta\,\xi^\perp+\bar\xi^A\tilde{\mathcal{D}}_{AB}\xi^B\big)(r_{\text{out}})+cc \end{aligned} \tag{4.28}$$

where $S^{(2)}_{\text{HJ-io-a}}$ is contribution for the case of two (inner and outer) boundaries and $S^{(2)}_{\text{HJ-o-a}}$ is the contribution for when we have an outer boundary only (solid-torus).

Type (b) contributions to the HJF mix the diffeomorphism and the graviton sector. These terms can be read from the second line of (4.27) and are also localized to the boundary and readily given by

$$\begin{aligned} -\kappa S^{(2)}_{\text{HJ-io-b}} &= \tfrac{1}{4}\sum_{k_\theta,k_t',k_z'}\Big(2\mathrm{i}\sqrt{\frac{2}{r^2\Delta_{\text{b}}}}\bar x(k_zk_\theta\xi_t-k_tk_\theta\xi_z)-2\bar w\left(r\Delta_{\text{b}}\xi^\perp+\mathrm{i}k_A\xi^A\right)\Big)\Big|_{r_{\text{in}}}^{r_{\text{out}}}+cc \\ -\kappa S^{(2)}_{\text{HJ-o-b}} &= \tfrac{1}{4}\sum_{k_\theta,k_t',k_z'}\Big(2\mathrm{i}\sqrt{\frac{2}{r^2\Delta_{\text{b}}}}\bar x(k_zk_\theta\xi_t-k_tk_\theta\xi_z)-2\bar w\left(r\Delta_{\text{b}}\xi^\perp+\mathrm{i}k_A\xi^A\right)\Big)(r_{\text{out}})+cc\,. \end{aligned} \tag{4.29}$$

The graviton sector

The part quadratic in the graviton perturbations involve radial derivatives, and thus the solution to the graviton equation of motions. To evaluate the terms appearing in the type (c) part, we need to fix the constants c_1, c_2 and c_3, c_4 in the graviton solutions (4.22) and (4.24), respectively. To this end we have to solve the (Dirichlet) boundary value problem, so that these constants become functions of the boundary values of the graviton modes w and x respectively.

We start with the case of two boundaries (toroidal annulus) and abbreviate the boundary values as

$$w(r_{\text{in}})=w_{\text{in}},\quad w(r_{\text{out}})=w_{\text{out}},\quad x(r_{\text{in}})=x_{\text{in}},\quad x(r_{\text{out}})=x_{\text{out}}.$$

The constants c_1, c_2 and c_3, c_4 can be readily computed to be

$$\begin{aligned}
c_1 &= \frac{w_{\rm in}\,\mathcal{K}_{|k_\theta|}(\hat{r}_{\rm out}) - w_{\rm out}\,\mathcal{K}_{|k_\theta|}(\hat{r}_{\rm in})}{\mathcal{I}_{|k_\theta|}(\hat{r}_{\rm in})\,\mathcal{K}_{|k_\theta|}(\hat{r}_{\rm out}) - \mathcal{I}_{|k_\theta|}(\hat{r}_{\rm out})\,\mathcal{K}_{|k_\theta|}(\hat{r}_{\rm in})} \\
c_2 &= \frac{w_{\rm out}\,\mathcal{I}_{|k_\theta|}(\hat{r}_{\rm in}) - w_{\rm in}\,\mathcal{I}_{|k_\theta|}(\hat{r}_{\rm out})}{\mathcal{I}_{|k_\theta|}(\hat{r}_{\rm in})\,\mathcal{K}_{|k_\theta|}(\hat{r}_{\rm out}) - \mathcal{I}_{|k_\theta|}(\hat{r}_{\rm out})\,\mathcal{K}_{|k_\theta|}(\hat{r}_{\rm in})} \\
c_3 &= \frac{x_{\rm in}\,\sqrt{\Delta_{\rm b}(r_{\rm in})}\frac{d}{dr_{\rm out}}\mathcal{K}_{|k_\theta|}(\hat{r}_2) - x_{\rm out}\,\sqrt{\Delta_{\rm b}(r_{\rm out})}\frac{d}{dr_{\rm in}}\mathcal{K}_{|k_\theta|}(\hat{r}_{\rm in})}{\frac{d}{dr_{\rm in}}\mathcal{I}_{|k_\theta|}(\hat{r}_{\rm in})\frac{d}{dr_{\rm out}}\mathcal{K}_{|k_\theta|}(\hat{r}_{\rm out}) - \frac{d}{dr_{\rm out}}\mathcal{I}_{|k_\theta|}(\hat{r}_2)\frac{d}{dr_{\rm in}}\mathcal{K}_{|k_\theta|}(\hat{r}_{\rm in})} \\
c_4 &= \frac{x_{\rm out}\,\sqrt{\Delta_{\rm b}(r_{\rm out})}\frac{d}{dr_{\rm in}}\mathcal{I}_{|k_\theta|}(\hat{r}_{\rm in}) - x_{\rm in}\,\sqrt{\Delta_{\rm b}(r_{\rm in})}\frac{d}{dr_{\rm out}}\mathcal{I}_{|k_\theta|}(\hat{r}_{\rm out})}{\frac{d}{dr_{\rm in}}\mathcal{I}_{|k_\theta|}(\hat{r}_{\rm in})\frac{d}{dr_{\rm out}}\mathcal{K}_{|k_\theta|}(\hat{r}_{\rm out}) - \frac{d}{dr_{\rm out}}\mathcal{I}_{|k_\theta|}(\hat{r}_{\rm out})\frac{d}{dr_{\rm in}}\mathcal{K}_{|k_\theta|}(\hat{r}_{\rm in})}
\end{aligned} \tag{4.30}$$

where we denote $\hat{r}_i := \sqrt{(k_t^2+k_z^2)}r_i$ and $\Delta_{\rm b}(r_i) := \frac{k_\theta^2}{r_i^2} + k_t^2 + k_z^2$ for $i \in \{\text{in, out}\}$. Using (4.30) for the quadratic graviton part in (4.27) we obtain the graviton contribution to the HJF to be

$$\begin{aligned}
-\kappa S^{(2)}_{\text{HJ-io-c}}(r_{\rm out}, r_{\rm in}) &= \frac{1}{4}\sum_{k_\theta,k_t',k_z'}\Big(f_{\rm in}\,\bar{w}_{\rm in}w_{\rm in} + f_{\rm out}\,\bar{w}_{\rm out}w_{\rm out} + f_{\rm io}\,\bar{w}_{\rm in}w_{\rm out} + \\
&\qquad g_{\rm in}\,\bar{x}_{\rm in}x_{\rm in} + g_{\rm out}\,\bar{x}_{\rm out}x_{\rm out} + g_{\rm io}\,\bar{x}_{\rm in}x_{\rm out}\Big) + cc\,.
\end{aligned} \tag{4.31}$$

where

$$\begin{aligned}
f_{\rm io}(r_{\rm in}, r_{\rm out}, k) &= \frac{2}{\mathcal{I}_{|k_\theta|}(\hat{r}_{\rm in})\,\mathcal{K}_{|k_\theta|}(\hat{r}_{\rm out}) - \mathcal{I}_{|k_\theta|}(\hat{r}_{\rm out})\,\mathcal{K}_{|k_\theta|}(\hat{r}_{\rm in})} \\
f_{\rm in}(r_{\rm in}, r_{\rm out}, k) &= r_{\rm in}\frac{\partial}{\partial r_{\rm in}}\log\left(f_{\rm io}(r_{\rm in}, r_{\rm out}, k)\right) + \frac{\Delta_{\rm b}(r_{\rm in})}{2(k_t^2+k_z^2)}(r_{\rm in}^2\Delta_{\rm b}(r_{\rm in}) - 1) \\
f_{\rm out}(r_{\rm in}, r_{\rm out}, k) &= -f_{\rm in}(r_{\rm out}, r_{\rm in}, k) \\
g_{\rm io}(r_{\rm in}, r_{\rm out}, k) &= \frac{\sqrt{\Delta_{\rm b}(r_{\rm in})\Delta_{\rm b}(r_{\rm out})}}{\frac{d}{dr_{\rm in}}\mathcal{I}_{|k_\theta|}(\hat{r}_{\rm in})\,\frac{d}{dr_{\rm out}}\mathcal{K}_{|k_\theta|}(\hat{r}_{\rm out}) - \frac{d}{dr_{\rm out}}\mathcal{I}_{|k_\theta|}(\hat{r}_{\rm out})\,\frac{d}{dr_{\rm in}}\mathcal{K}_{|k_\theta|}(\hat{r}_{\rm in})} \\
g_{\rm in}(r_{\rm in}, r_{\rm out}, k) &= \frac{1}{2}\left(1 + \frac{k_\theta^2}{r_{\rm in}^2\Delta_{\rm b}(r_{\rm in})}\right) - \frac{1}{2}r_{\rm in}\frac{\partial}{\partial r_{\rm in}}\log\left(g_{\rm io}(r_{\rm in}, r_{\rm out}, k)\right) \\
g_{\rm out}(r_{\rm in}, r_{\rm out}, k) &= -g_{\rm in}(r_{\rm out}, r_{\rm in}, k) \quad ,
\end{aligned} \tag{4.32}$$

are the coefficient functions. The functions $f_{\rm io}, g_{\rm io}$ describe a coupling of the w and x graviton modes between the two boundaries.

In the case where we have only an outer boundary at $r = r_{\text{out}}$, we will require that the graviton solutions are smooth at the origin, $r = 0$. By definition, the modified Bessel function $\mathcal{K}_{|k_\theta|}(r)$ diverges[4] at $r = 0$, thus to get smoothness, we set the constants c_2 and c_4 appearing in the graviton solutions (4.22),(4.24) to zero. We therefore, only need to determine the constants c_1 and c_3. Using the boundary conditions $w(r_{\text{out}}) = w_{\text{out}}, x(r_{\text{out}}) = x_{\text{out}}$, we indeed obtain the graviton solutions:

$$w(r) = \frac{\mathcal{I}_{|k_\theta|}(\hat{r})}{\mathcal{I}_{|k_\theta|}(\hat{r}_{\text{out}})} w_{\text{out}} \ , \qquad x(r) = \sqrt{\frac{\Delta_{\text{b}}(r_{\text{out}})}{\Delta_{\text{b}}}} \frac{\mathcal{I}_{|k_\theta-1|}(\hat{r}) + \mathcal{I}_{|k_\theta+1|}(\hat{r})}{\mathcal{I}_{|k_\theta-1|}(\hat{r}_{\text{out}}) + \mathcal{I}_{|k_\theta+1|}(\hat{r}_{\text{out}})} x_{\text{out}} \quad , \tag{4.33}$$

where $\hat{r} = r\sqrt{(k_t^2 + k_z^2)}$ and the solutions are valid for all Fourier modes except $(k_t^2 + k_z^2) = 0$. These modes will require special treatment.

Using the solutions (4.33), and $\epsilon = +1$ for an outer boundary, we get the contribution to the second order HJF of the solid torus coming from the quadratic graviton part is given by

$$-\kappa S^{(2)}_{\text{HJ-o-c}}(r_{\text{out}}) \ = \ \frac{1}{4} \sum_{k_\theta, k_t', k_z'} \left(\tilde{f}_{\text{out}} \, \bar{w}_{\text{out}} w_{\text{out}} + \tilde{g}_{\text{out}} \, \bar{x}_{\text{out}} x_{\text{out}} \right) + cc \, , \tag{4.34}$$

where

$$\begin{aligned} \tilde{f}_{\text{out}}(r_{\text{out}}, k) \ &= \ r_{\text{out}} \frac{d}{dr_{\text{out}}} \left(\log \left(\mathcal{I}_{|k_\theta|}(\hat{r}_{\text{out}}) \right) \right) + \frac{\Delta_{\text{b}}(r_{\text{out}})}{\tilde{\Delta}} (1 - r_{\text{out}}^2 \Delta_{\text{b}}(r_{\text{out}})) \\ \tilde{g}_{\text{out}}(r_{\text{out}}, k) \ &= \ -\frac{1}{2} r_{\text{out}} \frac{d}{dr_{\text{out}}} \left(\log \left(\mathcal{I}_{|k_\theta-1|}(\hat{r}_{\text{out}}) + \mathcal{I}_{|k_\theta+1|}(\hat{r}_{\text{out}}) \right) \right) - \frac{1}{2} \left(1 + \frac{2\, k_\theta^2}{r_{\text{out}}^2 \Delta_{\text{b}}(r_{\text{out}})} \right) . \end{aligned} \tag{4.35}$$

Modes with $k_\theta = k_t' = k_z' = 0$

Now, we will determine the contributions to the HJF coming from special modes $(k_t^2 + k_z^2) = 0$. Note that, the twisted frequencies are given by $k_t = \frac{2\pi}{\beta_t}(k_t' - \frac{\gamma_t}{2\pi} k_\theta)$ and $k_z = \frac{2\pi}{\beta_z}(k_z' - \frac{\gamma_z}{2\pi} k_\theta)$ with $k = (k_\theta, k_t', k_z') \in \mathbb{Z}^3$. Thus $(k_t^2 + k_z^2)$ is vanishing, if $k_\theta = k_t' = k_z' = 0$ or if $\gamma_t/2\pi$ and $\gamma_z/2\pi$ are rational and the momenta satisfy $k_\theta = \frac{2\pi}{\gamma_t} k_t = \frac{2\pi}{\gamma_z} k_z$.

Let us consider the modes $k_\theta = k_t' = k_z' = 0$. The components of the (linearized) bulk

[4]The point $r = 0$ is a regular singular point for the Bessel equation.

tensor defined in appendix C have to satisfy the following equations of motion:

$$\begin{aligned}
&\hat{G}^{rr} = -\frac{1}{2r}\partial_r(\gamma_{tt}+\gamma_{zz}), \quad \hat{G}^{rA}=0, \quad \hat{G}^{\theta\theta} = -\frac{1}{2r^2}\partial_r^2(\gamma_{tt}+\gamma_{zz})\\
&\hat{G}^{\theta t} = \frac{1}{2r}\partial_r\left(\frac{1}{r}\partial_r\gamma_{\theta t}\right), \quad \hat{G}^{\theta z} = \frac{1}{2r}\partial_r\left(\frac{1}{r}\partial_r\gamma_{\theta z}\right), \quad \hat{G}^{tz} = \frac{1}{2r}\partial_r\left(r\partial_r\gamma_{tz}\right), \qquad (4.36)\\
&\hat{G}^{tt} = \frac{1}{2r}\partial_r\left(\gamma_{rr}+\frac{1}{r^2}\gamma_{\theta\theta}-\frac{1}{r}\partial_r\gamma_{\theta\theta}-r\partial_r\gamma_{zz}\right), \quad \hat{G}^{zz} = \frac{1}{2r}\partial_r\left(\gamma_{rr}+\frac{1}{r^2}\gamma_{\theta\theta}-\frac{1}{r}\partial_r\gamma_{\theta\theta}-r\partial_r\gamma_{tt}\right),
\end{aligned}$$

where the index A appearing in the first line stands for $A=\theta,t,z$.

The solutions to these equations of motion can be parametrized as follows

$$\begin{aligned}
&\gamma_{rr} = c_0 + 2\partial_r\xi^r, \quad \gamma_{r\theta} = r^2\partial_r\xi^\theta, \quad \gamma_{rB} = \partial_r\xi^B,\\
&\gamma_{\theta\theta} = 2r\xi^r, \quad \gamma_{tt} = -c_1\log(r)+c_2, \quad \gamma_{zz} = c_1\log(r)+c_3,\\
&\gamma_{\theta t} = c_4\, r^2 + c_5, \quad \gamma_{\theta z} = c_6\, r^2 + c_7, \quad \gamma_{tz} = c_8\log(r)+c_9 \qquad (4.37)
\end{aligned}$$

where $B=z,t$. Here ξ^a are the components of the diffeomorphism generating vector field and $c_i, i\in\{0,\cdots,9\}$ are additional parameters appearing in the solutions.

Substituting the solutions (4.37) into the second-order action, the bulk term vanishes and the boundary term evaluates to the second-order HJF. For the case where we have two boundary components, an inner boundary at $r=r_{\rm in}$ and an outer boundary at $r=r_{\rm out}$, the second order HJF is given by

$$\kappa S^{(2)}_{\rm HJ|_{k=0}} = \frac{1}{2}\left(C_1\left(r_{\rm out}^2-r_{\rm in}^2\right)+C_2(\log(r_{\rm out})-\log(r_{\rm in}))+C_3(\log(r_{\rm out})^2-\log(r_{\rm in})^2)\right) \qquad (4.38)$$

where the coefficients are given by

$$C_1 = 2({c_4}^2+{c_6}^2), \quad C_2 = c_1(c_1-2c_2+2c_3)+c_8(c_8+4c_9), \quad C_3 = 2({c_1}^2+{c_8}^2)\,. \qquad (4.39)$$

Using the Dirichlet boundary conditions, we determine the constants c_i to be

$$\begin{aligned}
c_1 &= -\frac{\gamma_{tt}(r_{\rm out})-\gamma_{tt}(r_{\rm in})}{\log(r_{\rm out})-\log(r_{\rm in})} = \frac{\gamma_{zz}(r_{\rm out})-\gamma_{zz}(r_{\rm in})}{\log(r_{\rm out})-\log(r_{\rm in})}\,,\\
c_2 &= \frac{\gamma_{tt}(r_{\rm out})\log(r_{\rm in})-\gamma_{tt}(r_{\rm in})\log(r_{\rm out})}{\log(r_{\rm in})-\log(r_{\rm out})}\,, \qquad c_3 = \frac{\gamma_{zz}(r_{\rm out})\log(r_{\rm in})-\gamma_{zz}(r_{\rm in})\log(r_{\rm out})}{\log(r_{\rm in})-\log(r_{\rm out})}\,,\\
c_4 &= \frac{\gamma_{\theta t}(r_{\rm in})-\gamma_{\theta t}(r_{\rm out})}{r_{\rm in}^2-r_{\rm out}^2}\,, \qquad c_5 = \frac{\gamma_{\theta t}(r_{\rm out})r_{\rm in}^2-\gamma_{\theta t}(r_{\rm in})r_{\rm out}^2}{r_{\rm in}^2-r_{\rm out}^2}\,,\\
c_6 &= \frac{\gamma_{\theta z}(r_{\rm in})-\gamma_{\theta z}(r_{\rm out})}{r_{\rm in}^2-r_{\rm out}^2}\,, \qquad c_7 = \frac{\gamma_{\theta z}(r_{\rm out})r_{\rm in}^2-\gamma_{\theta z}(r_{\rm in})r_{\rm out}^2}{r_{\rm in}^2-r_{\rm out}^2}\,,\\
c_8 &= \frac{\gamma_{tz}(r_{\rm in})-\gamma_{tz}(r_{\rm out})}{\log(r_{\rm in})-\log(r_{\rm out})}\,, \qquad c_9 = \frac{\gamma_{tz}(r_{\rm out})\log(r_{\rm in})-\gamma_{tz}(r_{\rm in})\log(r_{\rm out})}{\log(r_{\rm in})-\log(r_{\rm out})}\,. \qquad (4.40)
\end{aligned}$$

In the case of only an outer boundary, we will again require smoothness of the metric perturbations at the origin. We find that for the solutions (4.37), some parameters have to vanish

$$c_1 = 0, \quad c_5 = 0, \quad c_7 = 0, \quad c_8 = 0 \quad . \tag{4.41}$$

The contribution to the Hamilton-Jacobi Functional is then given by

$$\kappa S^{(2)}_{\mathrm{HJ}|_{k=0}} \;=\; \frac{1}{4}\left((c_2-c_3)^2 + c_0(c_2+c_3) + 4c_9^2 + 4(c_4^2+c_6^2)r_{\mathrm{out}}^2\right) . \quad , \tag{4.42}$$

where

$$c_2 = \gamma_{tt}(r_{\mathrm{out}})\,,\; c_3 = \gamma_{zz}(r_{\mathrm{out}})\,,\; c_9 = \gamma_{tz}(r_{\mathrm{out}})\,,\; c_4 = \frac{\gamma_{\theta t}(r_{\mathrm{out}})}{r_{\mathrm{out}}^2}\,,\; c_6 = \frac{\gamma_{\theta z}(r_{\mathrm{out}})}{r_{\mathrm{out}}^2} \tag{4.43}$$

and c_0 can be determined as

$$c_0 = \gamma_{rr}(r_{\mathrm{out}}) - \left[\partial_r \frac{\gamma_{\theta\theta}(r)}{r}\right]_{r=r_{\mathrm{out}}} \quad . \tag{4.44}$$

We have therefore determined in this section the continuum gravitational (linearized) HJF for space–time regions with topology of a toroidal annuli and also a solid 3-torus. In the next section, we will discuss a computation of path integrals for diffeomorphism invariant systems and for regions with boundaries via recursion relations method. This method will be used to determine the gravitational one-loop correction.

4.4 Path integrals via recursion relations

For regions with boundaries, we can 'glue' the path integrals for two neighbouring regions. In our case, we consider the path integrals $\mathcal{Z}(r_1, r_2)$ and $\mathcal{Z}(r_2, r_3)$ for the regions with radial coordinates $r \in [r_1, r_2]$ and $r \in [r_2, r_3]$, respectively. This means, we can obtain the path integral $\mathcal{Z}(r_1, r_3)$ by integrating the data associated with the shared boundary

$$\mathcal{Z}(r_3, r_1) \;=\; \int \mathcal{D}\mu(\gamma_{AB}(r_2))\; \mathcal{Z}(r_3, r_2)\mathcal{Z}(r_2, r_1) \quad , \tag{4.45}$$

where $\mathcal{D}\mu(\gamma_{AB}(r))$ is a measure over the induced metric perturbations on the $r =$ const. hypersurface. On the classical level we can 'glue' the HJF's for these two regions and obtain the HJF for $[r_3, r_1]$:

$$S^{(2)}_{\mathrm{HJ}}(r_3, r_1) \;=\; \underset{\gamma_{AB}(r_2)}{\mathrm{extremize}} \left(S^{(2)}_{\mathrm{HJ}}(r_3, r_2) + S^{(2)}_{\mathrm{HJ}}(r_2, r_1)\right) \quad , \tag{4.46}$$

where we extremize the sum of the HJF's over the induced metric perturbations $\gamma_{AB}(r_2)$.

These convolution properties motivate to define and compute the HJF and the path integral via a discretization: the input is here the path integral for a region with radial coordinate $r \in [r_i, r_{i+1}]$ where $(r_{i+1} - r_i)$ are small. One requires smallness as one most often can only provide an approximation to the path integral, but hopes that the approximation error are small for small regions. Note that for a gravitational theory, this smallness for the radial coordinate could be seen as a rather meaningless requirement, as the physical lengths of the $[r_i, r_{i+1}]$ segments are determined by the metric, which is a variable. Thus the segments could become arbitrarily large. This turns out to be a key problem for the discretization of diffeomorphism invariant theories.[5]

One can however use the convolution properties (4.45) and (4.46), and starting from an initial guess ${}^0\mathcal{Z}(r_{i+1}, r_i))$ and ${}^0S^{(2)}_{\rm HJ}(r_{i+1}, r_i)$, compute ${}^1\mathcal{Z}(r_{i+2}, r_i)$ and ${}^1S^{(2)}_{\rm HJ}(r_{i+2}, r_i)$. If we can do this computation for general values for the radii r_j, we can see that operation as either refining the discretization or as coarse graining. With the refining interpretation, ${}^n\mathcal{Z}(r_{\rm out}, r_{\rm in}))$ and ${}^nS^{(2)}_{\rm HJ}(r_{\rm out}, r_{\rm in})$ give better and better approximation for a region with fixed radial interval $[r_{\rm in}, r_{\rm out}]$.

In the limit $n \to \infty$ we can expect to obtain the continuum limit for both the HJF and path integral. Thus, ${}^\infty\mathcal{Z}(r_{\rm out}, r_{\rm in})$ and ${}^\infty S^{(2)}_{\rm HJ}(r_{\rm out}, r_{\rm in})$ satisfy the fixed point conditions

$$ {}^\infty\mathcal{Z}(r_{\rm out}, r_{\rm in}) \;=\; \int \mathcal{D}\mu(\gamma_{AB}(r_{\rm sub}))\; {}^\infty\mathcal{Z}(r_{\rm out}, r_{\rm sub}) {}^\infty\mathcal{Z}(r_{\rm sub}, r_{\rm in}) \quad , \tag{4.47} $$

and

$$ {}^\infty S^{(2)}_{\rm HJ}(r_3, r_1) \;=\; \underset{\gamma_{AB}(r_2)}{\text{extremize}} \left({}^\infty S^{(2)}_{\rm HJ}(r_3, r_2) + {}^\infty S^{(2)}_{\rm HJ}(r_2, r_1) \right) \tag{4.48} $$

respectively. One can actually attempt to directly solve the fixed point conditions and in this way obtain (a certain part of) the path integral and the HJF. This strategy has been proposed in [125] and has been successfully tested for the harmonic and anharmonic oscillator.

This strategy applies only to the part of the path integral and the HJF, which describe the propagating degrees of freedom, that is in our case the graviton modes. Indeed, for the second order HJF described in section 4.3.3, we only obtain non-trivial fixed point relations for the type (c) contributions. The contributions (a) and (b) localize to one boundary component, and come for an outer and inner boundary with different signs, and

[5] In the expansion used here, the background metric provides a meaning to "small"

thus cancel out for the glued boundaries. The fixed point condition (4.48) is therefore automatically satisfied for these contributions.

Let us illustrate how this procedure [125] works for the construction of the one-loop partition function, restricted to a graviton mode w with fixed momenta (k_θ, k'_t, k'_z). One starts with an ansatz for the path integral

$$ {}^0\mathcal{Z}_{\rm w}(r_{\rm out}, r_{\rm in}) = {}^0\mu(r_{\rm out}, r_{\rm in}) \, \exp\left(-\frac{1}{\hbar} \, {}^0S^{(2)}_{\rm HJw}(k, r_{\rm out}, r_{\rm in}) \right) \quad , \tag{4.49} $$

where

$$ {}^0S^{(2)}_{\rm HJw}(k, r_{\rm out}, r_{\rm in}) = \left({}^0f_{\rm in}(r_{\rm out}, r_{\rm in}) \, w_{\rm in}^2 + {}^0f_{\rm out}(r_{\rm out}, r_{\rm in}) \, w_{\rm out}^2 + {}^0f_{\rm io}(r_{\rm out}, r_{\rm in}) \, w_{\rm in} w_{\rm out} \right) , \tag{4.50} $$

and the ${}^0f(r_{\rm out}, r_{\rm in})$ coefficients can be for instance constructed from a discretization of the Lagrangian describing the w-mode dynamics. (See section 4.3.3.) We have chosen the measure term ${}^0\mu(r_{\rm out}, r_{\rm in})$, to depend only on the evolution parameter r and not for instance on w. This choice is justified as the form of the path integral will be stable under the iteration. The convolution property (4.45) for the path integral leads then to the following recursion relations for the ${}^nf(r_{\rm out}, r_{\rm in})$ coefficient functions and measure ${}^n\mu(r_{\rm out}, r_{\rm in})$:

$$ \begin{aligned}
{}^{n+1}f_{\rm in}(r_{\rm out}, r_{\rm in}) &= {}^nf_{\rm in}(r_{\rm sub}, r_{\rm in}) - \frac{\left({}^nf_{\rm io}(r_{\rm sub}, r_{\rm in})\right)^2}{4\left({}^nf_{\rm in}(r_{\rm out}, r_{\rm sub}) + {}^nf_{\rm out}(r_{\rm sub}, r_{\rm in})\right)} \\
{}^{n+1}f_{\rm out}(r_{\rm out}, r_{\rm in}) &= {}^nf_{\rm out}(r_{\rm out}, r_{\rm sub}) - \frac{\left({}^nf_{\rm io}(r_{\rm out}, r_{\rm sub})\right)^2}{4\left({}^nf_{\rm in}(r_{\rm out}, r_{\rm sub}) + {}^nf_{\rm out}(r_{\rm sub}, r_{\rm in})\right)} \\
{}^{n+1}f_{\rm io}(r_{\rm out}, r_{\rm in}) &= -\frac{{}^nf_{\rm io}(r_{\rm out}, r_{\rm sub}) {}^nf_{\rm io}(r_{\rm sub}, r_{\rm in})}{2\left({}^nf_{\rm in}(r_{\rm out}, r_{\rm sub}) + {}^nf_{\rm out}(r_{\rm sub}, r_{\rm in})\right)} \\
{}^{n+1}\mu(r_{\rm out}, r_{\rm in}) &= \frac{\sqrt{\pi\hbar} \; {}^n\mu(r_{\rm out}, r_{\rm sub}) \, {}^n\mu(r_{\rm sub}, r_{\rm in})}{2\sqrt{\left({}^nf_{\rm in}(r_{\rm out}, r_{\rm sub}) + {}^nf_{\rm out}(r_{\rm sub}, r_{\rm in})\right)}} \quad ,
\end{aligned} \tag{4.51} $$

where for the measure term, we considered $\mathcal{D}\mu(w(r_{\rm sub})) = {\rm d}w(r_{\rm sub}) \, \mu(r_{\rm out}, r_{\rm sub}) \mu(r_{\rm sub}, r_{\rm in})$.

Here one can choose $r_{\rm sub}$ to be some point in the interval $(r_{\rm in}, r_{\rm out})$, but we can expect to obtain a better convergence for a regular subdivision, e.g. $r_{\rm sub} = \frac{1}{2}(r_{\rm in} + r_{\rm out})$. For $n \to \infty$ we obtain the fixed point condition – which has to hold for any choice of $r_{\rm sub} \in (r_{\rm in}, r_{\rm out})$. Instead of applying the recursion relations to obtain (an approximation to) the coefficient functions ${}^\infty f$ one can also directly attempt to solve the fixed point conditions. For an example see [125].

We have already computed the coefficient functions f and g, appearing in the HJF for the w- and x-modes respectively, in (4.32). These coefficient functions do indeed satisfy the fixed point conditions derived from (4.51).[6]

4.5 The one-loop correction

Here we will utilize the convolution property (4.45)

$$\mathcal{Z}(r_3, r_1) \;=\; \int \mathcal{D}\mu(\gamma_{AB}(r_2))\; \mathcal{Z}(r_3, r_2)\mathcal{Z}(r_2, r_1) \quad , \tag{4.52}$$

to determine the one-loop correction $M(r_2, r_1)$ for the partition function

$$\mathcal{Z}(r_2, r_1) \approx \left(\prod_k M(k, r_2, r_1)\right)\; \exp\left(-\tfrac{1}{\hbar}\left(S^{(0)}_{\rm HJ}(r_2, r_1) + S^{(1)}_{\rm HJ}(r_2, r_1) + S^{(2)}_{\rm HJ}(r_2, r_1)\right)\right) \tag{4.53}$$

for a region with two boundaries. We exclude the null mode $k_\theta = k'_t = k'_z = 0$. $\mathcal{D}\mu(\gamma_{AB}(r))$ is a measure over the induced metric perturbations on the $r =$ const. hypersurface. After Fourier transform we can assume that this measure is of the form

$$\mathcal{D}\mu(\gamma_{AB}(r)) \;=\; \prod_{A\le B}\prod_k m(k, r)\, d\gamma_{AB}(k) \tag{4.54}$$

where $m(r, k)$ is some positive function of the radius r and the momenta (k_θ, k'_t, k'_z).

Next we will use the parametrization of the metric components γ_{AB} in terms of the diffeomorphism parameters $(\xi^\perp, \xi^A)$ and the graviton modes (w, x), see (4.6) . The corresponding transformation of the measure is given by

$$\prod_{A\le B} d\gamma_{AB}(k) \;=\; 2\sqrt{2}r^4(k_t^2 + k_z^2)\sqrt{\Delta_{\rm b}}\; d\xi^r \left(\prod_A d\xi^A\right) dw dx \quad . \tag{4.55}$$

As we have chosen W_{AB} and X_{AB} with components in (4.7) to be, modulo constants, orthonormal vectors spanning the graviton sector. We can understand the determinant to arise from the transformation acting on the diffeomorphism sector.

We can now discuss separately the integration over the diffeomorphism modes and the integration over the graviton modes.

[6] As a consistency check, we have checked that gluing a cylinder space–time region to an annulus space–time region (see figure 4.1), the resulting HJF is given by that of a cylinder and moreover, the coefficients satisfy fixed point conditions.

4.5.1 Gauge sector

As we discussed in section 4.4, gluing the HJF's for two regions $[r_1, r_2]$ and $[r_2, r_3]$ along r_2, the contributions coming from the diffeomorphism sector drop out, and we are only left with a non-trivial integration over the graviton modes.

Thus the diffeomorphism parameters $(\xi^r, \xi^\theta, \xi^t, \xi^z)$ are indeed gauge parameters, which parametrize non-compact gauge orbits. To obtain a finite partition function we set the integration over these orbits to 1. To this end we will assume that the measure over the gauge orbits is

$$\mathcal{D}_{go}(\gamma) \;=\; q(r)\prod_k\left(d\xi^r\prod_A d\xi^A\right) \quad , \tag{4.56}$$

so that

$$\mathcal{D}\mu(\gamma_{AB}(r)) \;=\; \mathcal{D}_{go}(\gamma)\times\prod_k\frac{m(k,r)}{q(r)}2\sqrt{2}r^4(k_t^2+k_z^2)\sqrt{\Delta_{\rm b}}\;\;dwdx \quad . \tag{4.57}$$

We split the one-loop correction $M = D \times G$ into a contribution D associated to the diffeomorphisms and a contribution G associated to the gravitons. Requiring the convolution property (4.52) to hold, leads to the following condition on M

$$\begin{aligned} D(k,r_3,r_1)G(k,r_3,r_1) \;&=\; 2\sqrt{2}\frac{m(r_2,k)}{q(r_2)}r_2^4(k_t^2+k_z^2)\sqrt{\Delta_{\rm b}(r_2)}\;D(k,r_3,r_2)D(k,r_2,r_1)\times \\ &\qquad F(k,r_3,r_2,r_1)G(k,r_3,r_2)G(k,r_2,r_1) \end{aligned} \tag{4.58}$$

where $F(k,r_3,r_2,r_1)$ results from the integration over the graviton modes. Demanding that the diffeomorphism and graviton contributions separate, we obtain the requirement

$$G(k,r_3,r_1) = F(k,r_3,r_2,r_1)G(k,r_3,r_2)G(k,r_2,r_1) \tag{4.59}$$

for the graviton modes and

$$D(k,r_2,r_1) \;=\; \frac{1}{2\sqrt{2}(k_t^2+k_z^2)}\frac{\sqrt{q(r_1)q(r_2)}}{\sqrt{m(k,r_2)m(k,r_1)}r_2^2r_1^2}\frac{1}{\Delta_b^{\frac{1}{4}}(r_2)\Delta_b^{\frac{1}{4}}(r_1)} \tag{4.60}$$

for the diffeomorphism modes.

4.5.2 Graviton sector

The recursion relation (4.59) describes the one-loop correction associated to the graviton sector. The factor F results from a Gaussian integration, defined by the second order contribution to the HJF by the w- and x graviton modes, see (4.31). Inserting this factor we obtain

$$G(k,r_3,r_1)=\sqrt{\frac{\pi\hbar}{4(f_{\rm in}(r_3,r_2)+f_{\rm out}(r_1,r_2))}}\sqrt{\frac{\pi\hbar}{4(g_{\rm in}(r_3,r_2)+g_{\rm out}(r_1,r_2))}}G(k,r_3,r_2)G(k,r_2,r_1)\,, \tag{4.61}$$

where $f_{\rm in}, f_{\rm out}, g_{\rm in}, g_{\rm out}$ are the coefficients for the second-order HJF defined in (4.32). Note that we have suppressed their dependence on the Fourier modes k_θ, k_t', k_z'. The corresponding fixed point condition is solved by

$$G(k,r_2,r_1)=\sqrt{\frac{-2\,f_{\rm io}(r_2,r_1)}{\pi\hbar}}\sqrt{\frac{-2\,g_{\rm io}(r_2,r_1)}{\pi\hbar}}\quad, \tag{4.62}$$

where $f_{\rm io}, g_{\rm io}$ are coefficients in (4.32) that couple the two boundaries.
The one-loop correction for a toroidal annulus region (4.53) is therefore given by

$$M(k,r_2,r_1)\;=\;\frac{\sqrt{q(r_1)q(r_2)}}{\sqrt{m(k,r_2)m(k,r_1)}r_2^2r_1^2}\frac{1}{2\sqrt{2}(k_t^2+k_z^2)\Delta_b^{\frac{1}{4}}(r_2)\Delta_b^{\frac{1}{4}}(r_1)}\sqrt{\frac{-2\,f_{\rm io}(r_2,r_1)}{\pi\hbar}}\sqrt{\frac{-2\,g_{\rm io}(r_2,r_1)}{\pi\hbar}} \tag{4.63}$$

where

$$\begin{aligned} f_{\rm io}(r_1,r_2,k) &= \frac{2}{\mathcal{I}_{|k_\theta|}(\hat r_1)\,\mathcal{K}_{|k_\theta|}(\hat r_2)-\mathcal{I}_{|k_\theta|}(\hat r_2)\,\mathcal{K}_{|k_\theta|}(\hat r_1)} \\ g_{\rm io}(r_1,r_2,k) &= \frac{\sqrt{\Delta_{\rm b}(r_1)\Delta_{\rm b}(r_2)}}{\frac{d}{dr_1}\mathcal{I}_{|k_\theta|}(\hat r_1)\,\frac{d}{dr_2}\mathcal{K}_{|k_\theta|}(\hat r_2)-\frac{d}{dr_2}\mathcal{I}_{|k_\theta|}(\hat r_2)\,\frac{d}{dr_1}\mathcal{K}_{|k_\theta|}(\hat r_1)}\,. \end{aligned} \tag{4.64}$$

4.5.3 Case for solid 3-torus with one boundary

Let us consider the case for one boundary. We will make use of the previous results by gluing a cylinder region with one boundary at $r=r_1$ to an annulus with two boundaries $r\in[r_1,r_2]$, such that the following convolution property holds:

$$\mathcal{Z}_\tau(r_2)\;=\;\int\mathcal{D}\mu(\gamma_{AB}(r_1))\;\mathcal{Z}(r_2,r_1)\mathcal{Z}_\tau(r_1)\quad. \tag{4.65}$$

This determines the one-loop correction $M(r_2)$ for the cylinder to be

$$\mathcal{Z}_\tau(r_2) \approx \left(\prod_k M_\tau(k,r_2)\right) \exp\left(-\tfrac{1}{\hbar}\left(S^{(0)}_{\rm HJ}(r_2)+S^{(1)}_{\rm HJ}(r_2)+S^{(2)}_{\rm HJ}(r_2)\right)\right) \quad . \tag{4.66}$$

Here, we will use the form of measure given in (4.57) and also the one-loop correction $M_\tau = D_\tau \times G_\tau$ into a diffeomorphism contribution D_τ and a graviton contribution G_τ. The convolution property (4.65) therefore, lead to the relations

$$\begin{aligned} D_\tau(k,r_2) &= 2\sqrt{2}\frac{m(r_1,k)}{q(r_1)} r_1^4 (k_t^2+k_z^2)\sqrt{\Delta_{\rm b}(r_1)}\; D(k,r_2,r_1) D_\tau(k,r_1) \quad , \\ G_\tau(k,r_2) &= F(k,r_2,r_1) G(k,r_2,r_1) G_\tau(k,r_1) \quad , \end{aligned} \tag{4.67}$$

where the factor F again results from integration over graviton modes. These relations do not specify D_τ and G_τ uniquely. For example, one could multiply these terms by an r–independent factor and still satisfy the recursion relations.

Using (4.60) for the contribution from the torus annulus, we get that the relation for the diffeomorphism part is solved by

$$D_\tau(k,r_1) = \frac{1}{2\sqrt{2}(k_t^2+k_z^2)} \frac{\sqrt{q(r_1)}}{\sqrt{m(k,r_1)} r_1^2} \frac{1}{\Delta_b^{\frac{1}{4}}(r_1)} \quad . \tag{4.68}$$

Inserting the factor from integration of the graviton modes, the relation for the graviton contribution is given by

$$G_\tau(k,r_2) = \sqrt{\frac{\pi\hbar}{4(f_{\rm in}(r_2,r_1)+\tilde{f}_{\rm out}(r_1))}} \sqrt{\frac{\pi\hbar}{4(g_{\rm in}(r_2,r_1)+\tilde{g}_{\rm out}(r_1))}} G(k,r_2,r_1) G_\tau(k,r_1) \,, \tag{4.69}$$

where $f_{\rm in}, g_{\rm in}$ are the coefficients of the HJF that couple the two boundaries (4.32), and $\tilde{f}_{\rm out}, \tilde{g}_{\rm out}$ are the coefficients (4.35) from the one boundary case. Using the solution (4.62) and the properties of the modified Bessel functions, we find that the fixed point condition is solved by

$$G_\tau(k,r_1) = \sqrt{\frac{1}{\mathcal{I}_{|k_\theta|}(\hat{r}_1)}} \sqrt{\frac{\Delta_{\rm b}^{\frac{1}{2}}(r_1)}{\frac{d}{dr_1}\mathcal{I}_{|k_\theta|}(\hat{r}_1)}} \quad . \tag{4.70}$$

The one-loop correction for a cylinder region (4.53) with one boundary is therefore given by

$$M_\tau(k,r_1) = \frac{\sqrt{q(r_1)}}{\sqrt{m(k,r_1)} r_1^2} \frac{1}{2\sqrt{2}(k_t^2+k_z^2)\Delta_b^{\frac{1}{4}}(r_1)} \sqrt{\frac{1}{\mathcal{I}_{|k_\theta|}(\hat{r}_1)}} \sqrt{\frac{\Delta_{\rm b}^{\frac{1}{2}}(r_1)}{\frac{d}{dr_1}\mathcal{I}_{|k_\theta|}(\hat{r}_1)}} \,. \tag{4.71}$$

Apart from the ambiguities in the recursion relations (4.67), we also expect some gauge parameters for the special modes $k_\theta = 0, \pm 1$, as found in [3]. We do not discuss these special cases here. However, we have demonstrated using the recursion relations method, one can compute the gravitational one-loop partition function for 4D gravity including gravitons. It is of much interest to know the one-loop correction (4.71) in the limit of small r_1 and compare results in discrete gravity [3] using Regge calculus.

We will conclude this section with the following remarks:

By construction the one-loop correction and the HJF computed via the recursion relation are invariant under subdivisions in the radial intervals. Thus the path integral and Hamilton–Jacobi functional are also discretization invariant in the radial direction and therefore, serve as a 'perfect propagator' and a 'perfect action' for gravity respectively. The results for the graviton sector is quite involved, i.e., it include modified Bessel functions and so it cannot be "guessed", but rather needs to be computed. For discretized gravity, the procedure which we have employed here will help restore diffeomorphism symmetry (not only under linearized diffeos, but in moving around subdivision in r-intervals).

We used Fourier transformation in (θ, t, z) directions, and for second order the gravitational system reduces to a one parameter system in radial direction, for which we can define a perfect discretization. The Fourier transform defines a regular subdivision in the (θ, t, z) directions. Changing to a more irregular lattice is in principle possible, but would lead to much more complicated expressions.

Chapter 5

Discussions and Outlook

In this work we determined holographic boundary theories for linearized metric gravity in three dimensions and for the gauge sector in four dimensions. We found these dual boundary theories directly by computing the effective action for a geometric observable as determined from the gravitational action. This geometric observable is the geodesic distance from the boundary to some centre or central axis and describes so–called boundary degrees of freedom [18, 127, 128], or boundary gravitons. This degree of freedom encodes the shape of the (fluctuating) boundary in the embedding space time. Together with the holographic boundary theories we also determined the Hamilton–Jacobi functional for linearized gravity, for a large class of boundaries.

The resulting boundary theories depend on the chosen type of boundary and the choice of cosmological constant. It is known that Liouville theory arises for an asymptotic AdS_3 boundary [14, 16, 18, 129]. We have shown that the effective theory for the geodesic lengths leads to Liouville like theories also for finite and more general boundaries. In particular one can always expect a Liouville-like coupling to the Ricci–scalar of the boundary. The reason is that the first variation of the Ricci–scalar is proportional to the first variation of the lengths of geodesics that start normal to the boundary.

For the examples we have considered, the boundary theories are furthermore defined by a quadratic form given by $\Delta = 2(K^{CD} - Kh^{CD})D_C D_D - {}^{\mathrm{b}}R^{AB}K_{AB}$. For background space–times with vanishing boundary intrinsic curvature, this gives a (non-degenerate) flat Laplacian for the torus boundary in AdS_3 space and a degenerate Laplacian for the torus boundary in flat space. For a spherical boundary in 3D flat space we obtain a differential operator proportional to the Laplacian on the sphere, but also a mass term resulting from ${}^{\mathrm{b}}R^{AB}K_{AB}$.

We have seen that in the case of a manifold with a torus boundary the derivation of the effective action for the geodesic lengths requires some subtle procedure. This is the imposition of smoothness condition at the central axis at $r = 0$. It leads to the insertion of a non-local operator $(1 + \partial_\theta^{-2})$ into the effective action.

This has an important consequence, namely that the modes $k_\theta = \pm 1$ describe a gauge freedom of the boundary field theory. Indeed this follows from diffeomorphism symmetry modes, which affect the precise definition of the central axis. Accordingly the geodesic length at these modes is a gauge parameter and the geodesic effective action is independent of the boundary field and just given by the gravitational Hamilton–Jacobi functional, which does not depend on the boundary field, for $k_\theta = \pm 1$. The $k_\theta = 0$ mode is also affected by diffeomorphism symmetry – but here it is a diffeomorphism along the central axis, which to first order does not affect the lengths of the geodesics. In this case the geodesic effective action is given by the gravitational Hamilton–Jacobi functional, but with the addition of the Lagrange multiplier term, which imposes that the boundary field mode reproduces the geodesic length at $k_\theta = 0$.

This illustrates an interesting interplay between the bulk and the possibly asymptotic boundary. It deserves further study: for instance the inclusion of a point particle at $r = 0$ should change the smoothness conditions, and in fact break the gauge symmetry at $k_\theta = \pm 1$. Correspondingly one would expect that the one–loop partition function now reproduces a massive BMS_3 character instead of the vacuum one, see also [32, 130]. This has been confirmed in the Regge calculus certain [131].The one–loop partition function which we have computed for the flat torus also reproduces the vacuum BMS_3 character (the symmetry group at asymptotic infinity).

Another interesting direction is to investigate other geometric observables. For the asymptotically flat [17] and AdS boundaries [16] one can employ certain angle variables, which are better suited to capture the BMS or Virasoro symmetry respectively. It would be interesting to see whether one can also identify germs for these symmetries at finite boundaries. It would also be interesting to study Lorentzian space–times, null boundaries, BTZ black holes and different boundary conditions [132–134].

The method to construct holographic duals directly from gravity, which we employed here allowed to study the 4D case. In this regard we have computed the geodesic length effective action for a 4D generalization of twisted thermal flat space. We restricted to boundary conditions which impose flat perturbations, that is excluded propagating bulk gravitons and the resulting boundary action is then however a straightforward generalization of the 3D result, that is given by the same action with a Liouville like coupling to the boundary Ricci scalar and a degenerate kinetic term. The next step is to study how the

inclusion of bulk gravitons affects the geodesic effective action, and in particular whether non-localities arise [2]. One might also be led to introduce additional boundary fields, which encode (better than the geodesic length) the dynamics of the bulk gravitons. A key question will be which kind of geometric observables are best suited for such boundary fields.

To compute the gravitational one-loop correction, we introduced a new method which relied on recursion relations. This method was motivated by the convolution property of the gravitational path integral. This allowed us also also to compute the so called perfect action and perfect propagator for discrete gravity. This is the first time such a computation has been carried out for a 4D theory involving graviton degrees of freedom. (See [135] paper for earlier results, which include scalar fields, vector fields but only 3D linearized gravity.) The results show that perfect actions for theories with propagating degrees of freedom cannot be guessed but rather need to be computed in a suitable truncation scheme. Discretization of gravitational systems usually break diffeomorphism symmetry [126]. Our method applied to discrete gravitational systems can help restore the broken symmetries and also ensure discretization independence.

We hope that these investigations will help for the understanding of the renormalization flow of quantum gravity models, e.g. [136–138]. A key issue is to find suitable truncations, as one otherwise has to deal with an infinite dimensional space of possible couplings. The framework introduced in [38, 139–141] employs boundaries and boundary Hilbert spaces to determine dynamically preferred truncation maps. Here a crucial question is to identify geometric boundary observables which encode efficiently the bulk dynamics, which is also a key point in the quasi-local holography program.

Part II

Quantum geometry based on area variables

This part of the thesis is based on materials from the following two papers:

- The Degrees of Freedom of Area Regge Calculus: Dynamics, Non-metricity, and Broken Diffeomorphisms (with Bianca Dittrich and Hal M Haggard) [4].
- Effective Spin Foam Models for Four-Dimensional Quantum Gravity (with Bianca Dittrich and Hal M Haggard) [5].

Chapter 6

Actions for discretized gravity

Regge in [25] formulated a discretization of gravity based on a simplicial decomposition of the continuum manifold. Here, we introduce a different discrete theory inspired by Regge calculus and playing a prominent role in the dynamics of spin foams. In this theory areas (instead of lengths) are taken as fundamental [43]. This leads to quite a different dynamics from length Regge calculus. The original version of area Regge calculus [43] suffers from ambiguities. These ambiguities appear due to certain configurations with right-angles make the action based on area variables ill-defined. We cure this problem by constructing a first order formulation for area Regge calculus. We will also analyze gauge symmetries and dynamics of the linearized area Regge calculus. Our analysis will lead to tools to distinguish between length and area Regge dynamics in (the semi classical limit of) spin foams.[1]

Let us start with a review of Length Regge Calculus (LRC). In LRC one substitutes the metric by lengths l_e assigned to the edges e of a triangulation Δ of a four dimensional manifold with a boundary triangulation $\partial\Delta$ of the boundary manifold. The l_e determine the triangle areas $A_t(l_e)$ and the 4D (internal) dihedral angles $\theta_t^\sigma(l_e)$ in 4-simplices σ. Varying the LRC action

$$\begin{aligned} S_{\rm LRC} &= \sum_{t\in\partial\Delta} \pi A_t(l_e) + \sum_{t\in\Delta} 2\pi A_t(l_e) - \sum_\sigma \sum_{t\supset\sigma} A_t(l_e)\theta_t^\sigma(l_e) \\ &\equiv \tfrac{1}{2}\sum_{t\in\partial\Delta} S_t^e(l_e) + \sum_{t\in\Delta} S_t^e(l_e) + \sum_\sigma S_\sigma^e(l_e) \end{aligned} \tag{6.1}$$

[1] Although this can be generalized to Lorentz signature, here we adopt Euclidean signature geometries.

with respect to the bulk lengths leads to the dynamics

$$\sum_{t\supset e} \frac{\partial A_t(l_e)}{\partial l_e}\epsilon_t(l_e) = 0\,, \quad \text{with} \quad \epsilon_t = 2\pi - \sum_{\sigma\supset t}\theta_t^\sigma(l_e)\,, \tag{6.2}$$

where the deficit angle ϵ_t is a measure of the curvature concentrated on the triangle t. The boundary term is known as the Gibbons-Hawking-Hartle-Sorkin boundary term [142] which is analogous to the Gibbons-Hawking-York boundary term in Einstein Hilbert action. In the limit of a very fine triangulation one recovers Einstein's equations [143].

In part II of this thesis, we will mostly employ a formulation in terms of area variables. We, thus, define the Area Regge Calculus (ARC) action [43] for 4D triangulations, whose value on configurations with $A_t = A_t(l_e)$ agrees with the LRC action

$$S_{\text{ARC}} \;=\; \tfrac{1}{2}\sum_{t\in\partial\Delta} S_t^A(A_t) + \sum_{t\in\Delta} S_t^A(A_t) + \sum_{\sigma} S_\sigma^A(A_t), \tag{6.3}$$

where $S_t^A(A_t) = 2\pi A_t$ and $S_\sigma^A(A_t) = A_t\,\theta_t^\sigma(A_{t'})$. Strikingly, freely varying the bulk areas one finds the equations of motion $\epsilon_t = 0$, which impose flatness. This is due to the Schläfli identity [144] (for a modern symplectic proof see [145])

$$\sum_{t\subset\sigma} A_t\,\delta\theta_t^\sigma \;=\; 0 \quad , \tag{6.4}$$

which holds for arbitrary variations $\delta\theta_t^\sigma$ of the dihedral angles in a simplex σ and, in effect, leads to a vanishing of the variations of the deficit angles $\sum_t A_t\,\delta\epsilon_t = 0$.

The dihedral angles θ_t^σ are uniquely determined from the (flat) geometry of the simplex σ, which is defined by its 10 edge lengths. The action (6.3), however, requires the dihedral angles as functions of the 10 triangle areas of the simplex. Unfortunately, the 10 areas of a four-simplex do not uniquely determine the 10 length variables. This is due to the fact that the areas are quadratic functions of the edge lengths. A particular example of this ambiguity is the "Tuckey–configuration," which has all edge lengths equal to 1 except for one edge with length $\sqrt{b}$, [43]. For both the values b and $4-b$, triangles sharing the latter edge have equal areas. Nonetheless, in configuration space and away from right angle configurations, one can locally[2] invert the 10 functions $A_t(l_e)$ that give the simplex's areas in terms of its lengths. We will denote the resulting functions $L_e^\sigma(A)$, where A collectively signifies the 10 areas associated to σ.

[2]These functions also depend on a discrete parameter that accounts for the multiple roots that appear in the inversion of $A_t(l_e)$. This discrete parameter appears as a summation variable for the (constrained) Area Regge path integral. To ease notation we will suppress this parameter.

To cure the problem with the ambiguities of the action we will consider first order Regge calculus. An alternative, presented in section 6.2, is to replace flat simplices by simplices with homogeneous curvature. This framework is useful for modeling space–times with a cosmological constant. We will work here mostly with the flat simplex version. There are also other versions of Regge calculus based on area and angle variables [44], which we do not consider in this chapter.

6.1 First order Area–Regge calculus

To circumvent the problem of finding the dihedral angles as functions of the areas we will treat these dihedral angles θ_t^σ as independent variables. This amounts to a first order area Regge calculus. First order frameworks for the standard length Regge calculus were defined by Barrett [146] for the flat case and in [147] for the case of homogeneously curved simplices.

The mechanism behind our first order formulation is the same as in [146], with the important difference that here the equations of motion impose flatness. On a given simplex the full set of dihedral angles and areas provides more data than necessary to determine the geometry of the simplex. Hence these variables cannot be specified completely independently, or the dihedral angles might not be compatible with the areas. Consistency of these data will be imposed by an equation of motion that follows from the variation of the dihedral angles.

The dihedral angles of a (flat) simplex are also not independent. Define the angle Gram matrix

$$G^\sigma_{ij} := \begin{cases} 1 & \text{for} \quad i = j \\ -\cos(\theta^\sigma_{ij}) & \text{for} \quad i \neq j \end{cases}, \tag{6.5}$$

where $i, j \in \{1, \ldots, 5\}$ label the five vertices of the simplex σ and θ^σ_{ij} is the dihedral angle opposite the edge connecting vertices i and j. Then the dihedral angles must satisfy the constraint that the determinant of the angle Gram matrix G^σ vanishes. In Appendix I we prove this claim and give a general structural characterization of the Gram matrix.

As in [146], we impose this constraint on each simplex using a Lagrange multiplyer Λ_σ. The action is

$$S_{\text{FOA}} = \sum_{t \in \partial\Delta} \pi A_t + \sum_{t \in \Delta} 2\pi A_t - \sum_\sigma \sum_{t \supset \sigma} A_t \, \theta^\sigma_t \; + \; \sum_\sigma \Lambda_\sigma \det G^\sigma \quad . \tag{6.6}$$

This action leads to the equations of motion

$$\begin{aligned} \delta A_t : \qquad & \epsilon_t = 2\pi - \sum_{\sigma \supset t} \theta^\sigma_t \; = \; 0 \quad , \\ \delta \Lambda_\sigma : \qquad & \det G^\sigma = 0 \quad , \\ \delta \theta^\sigma_t : \qquad & A_t = \Lambda_\sigma \, \frac{\partial \det G^\sigma}{\partial \theta^\sigma_t} \quad . \end{aligned} \tag{6.7}$$

In Appendix I we find the derivative of the determinant of the angle Gram matrix

$$\frac{\partial \det G^\sigma}{\partial \theta^\sigma_{ij}} \; = \; [c V_i V_j](\theta^\sigma_{kl}) \; \sin \theta^\sigma_{ij} \; = \; [c' V_{ij}](\theta^\sigma_{kl}) \quad , \tag{6.8}$$

where V_i is the volume of the tetrahedron obtained by removing from σ the vertex i and V_{ij} is the area of the triangle obtained by removing vertices i and j. The coefficients c and c' are defined in Appendix I and depend on the full simplex. They are dimensionful, as we have a dimensionless quantity on the left hand side of (6.8). On the right hand side we have made the dependencies on the angles θ^σ explicit, but, as the dihedral angles cannot determine the scale of the simplex, it is only the combined quantities in square brackets that are well defined functions of the dihedral angles.

Thus, the last equation of motion in (6.7) does, in fact, impose that the dihedral angles are compatible with the areas. This will be more manifest in the homogeneously curved case considered below. The second equation of motion imposes that the dihedral angles come from a simplex. In general (away from right angles) the last two equations of (6.7) can be solved for the dihedral angles and the Lagrange multiplier in terms of the areas. This can be achieved locally on each simplex.

6.2 Area Regge calculus for homogeneously curved simplices

A second approach is to use homogeneously curved simplices. For a curved four-simplex, the curvature scale breaks the overall scaling symmetry of the flat case and both the edge lengths and the areas can be expressed as functions of the dihedral angles. Actions that impose the dynamics for length Regge calculus with homogeneously curved simplices have been investigated in [147], see also [148–158] for spin foam models and loop gravity techniques based on homogeneously curved simplices.

Homogeneously curved simplices allow for a simple solution to the dynamics of length Regge calculus with a cosmological constant. While in the flat case it is intricate to arrive at expressions for the Hessian of the action, they are immediate in the constant curvature case. This will allow us to easily find a second order formulation as well. In the first order action it will not be necessary to introduce a Lagrange multiplier as the cosmological constant and curved Schläfli identity address the associated issues completely.

The first order action with cosmological constant $\Lambda = 3\kappa$ is

$$S_{\rm HC} = \sum_{t\in\partial\Delta} \pi A_t + \sum_{t\in\Delta} 2\pi A_t - \sum_{\sigma}\sum_{t\supset\sigma} A_t\,\theta_t^\sigma \; + 3\kappa \sum_{\sigma} V_\sigma(\theta^\sigma) \quad . \tag{6.9}$$

Here $V_\sigma(\theta^\sigma)$ is the volume of the simplex σ, viewed as a function of all of its dihedral angles. The curved Schläfli identity gives the variation of this volume under an arbitrary variation of the dihedral angles

$$3\kappa\delta V_\sigma = \sum_{t\subset\sigma} A_t \delta\theta_t^\sigma \quad . \tag{6.10}$$

Note that this properly reduces to the flat Schläfli identity, Eq. (6.4), in the $\kappa \to 0$ limit. Using the Schläfli identity, we have

$$\frac{\partial V_\sigma}{\partial\theta_t^\sigma} = \frac{1}{3\kappa} A_t(\theta^\sigma) \tag{6.11}$$

and the equations of motion follow immediately

$$\begin{aligned} \delta A_t: &\qquad \epsilon_t = 0 \\ \delta\theta_t: &\qquad -A_t + A_t(\theta^\sigma) = 0. \end{aligned} \tag{6.12}$$

The second of these equations imposes the area agreement, namely, that the independent area variables A_t agree with the areas determined by the dihedral angles $A_t(\theta^\sigma)$.

In anticipation of the more complicated linearization of the next section, we conclude this section by briefly considering linearization of the constant curvature area Regge calculus. First, split the variables into background values and perturbations

$$\begin{aligned} A_t &= A_t^0 + a_t \quad , \\ \theta_t^\sigma &= (\theta_t^\sigma)^0 + \vartheta_t^\sigma \quad . \end{aligned} \tag{6.13}$$

The quadratic part of the action can be written as a contribution for each simplex

$$S^{(2)}_{\rm HC} = \sum_\sigma S^{(2)}_{{\rm HC}\sigma} \tag{6.14}$$

with the quadratic simplex action

$$S^{(2)}_{\mathrm{HC}\sigma} = -\sum_{t\subset\sigma} a_t\vartheta^\sigma_t + \frac{3\kappa}{2}\sum_{t,t'\subset\sigma}\vartheta^\sigma_t\frac{\partial^2 S_c}{\partial\theta^\sigma_t\partial\theta^\sigma_{t'}}\vartheta^\sigma_{t'} = -\sum_{t\subset\sigma} a_t\vartheta^\sigma_t + \frac{3\kappa}{2}\sum_{t,t'\subset\sigma}\vartheta^\sigma_t\frac{\partial A_{t'}(\theta^\sigma)}{\partial\theta^\sigma_t}\vartheta^\sigma_{t'} \quad , \tag{6.15}$$

where in the second equality we have used the curved Schläfli identity (6.11) again. The inverse function theorem guarentees that, at least locally, the Hessian

$$H^\sigma_{tt'} = \frac{\partial^2 S_c}{\partial\theta^\sigma_t\partial\theta^\sigma_{t'}} = \frac{\partial A_{t'}(\theta^\sigma)}{\partial\theta^\sigma_t} \tag{6.16}$$

is invertible and has inverse

$$(H^\sigma)^{-1}_{tt'} = \frac{\partial\theta^\sigma_t}{\partial A_{t'}} \quad . \tag{6.17}$$

These explicit forms allow us to integrate out the ϑ^σ_t to obtain the second order linearized action

$$S^{(2)}_{\mathrm{HC}} = -\frac{1}{3\kappa}\sum_{t,t'\subset\sigma} a_t(H^\sigma)^{-1}_{tt'}a_{t'} \quad . \tag{6.18}$$

While we have found $A_t(\theta^\sigma)_{t'}$ analytically, see Appendix H, inverting these functions to $\theta^\sigma_{t'}(A_t)$ has so far remained impractical. Nonetheless the Hessians are straightforward to work with numerically and our results on the homogeneously curved case are found this way.

6.3 Linearized theory

To analyze the symmetries of the theory and distinguish between physical and gauge degrees of freedom we will consider the linearized theory for flat simplices. (We have also tested some features for the curved simplex case, which we will comment on throughout.) To this end we will assume a background given by a flat and metric configuration. Flatness is imposed by the equations of motion. Metricity means that all the areas are determined from a consistent set of length variables. In chapter 8, we consider more general backgrounds, and we will see that this is a very special choice of background with an enhanced symmetry content. This is closely analogous to the special character of flat backgrounds in length Regge calculus [120, 121].

Let us consider splitting the variables into background plus perturbations

$$\begin{aligned} A_t &= A_t^0 + a_t \quad , \\ \Lambda^\sigma &= \Lambda_\sigma^0 + \lambda_\sigma \quad , \\ \theta_t^\sigma &= (\theta_t^\sigma)^0 + \vartheta_t^\sigma \quad . \end{aligned} \tag{6.19}$$

The quadratic part of the action can be written as a contribution for each simplex (with a boundary there might also be a linear boundary term for the expanded action)

$$S^{(2)}_{\rm FOA} \,=\, \sum_\sigma S_\sigma \tag{6.20}$$

with

$$S_\sigma \,=\, -\sum_{t\subset\sigma} a_t \vartheta_t^\sigma \,+\, \lambda_\sigma \sum_{t\subset\sigma} \frac{\partial \det G^\sigma}{\partial\theta_t^\sigma}\vartheta_t^\sigma \,+\, \frac{\Lambda_\sigma^0}{2}\sum_{t,t'\subset\sigma} \vartheta_t^\sigma \frac{\partial^2 \det G^\sigma}{\partial\theta_t^\sigma \partial\theta_{t'}^\sigma}\vartheta_{t'}^\sigma \quad . \tag{6.21}$$

This can be written as

$$S_\sigma \,=\, -\sum_{\tilde t\supset\sigma} a_{\tilde t}\vartheta_{\tilde t}^\sigma \,+\, \frac{1}{2}\sum_{\tilde t,\tilde t'} \vartheta_{\tilde t}^\sigma H^\sigma_{\tilde t\tilde t'}\vartheta_{\tilde t}^\sigma \quad , \tag{6.22}$$

where we have introduced the extended index $\tilde t = (0,t)$ with $\vartheta^\sigma_{\tilde t=0} = \lambda_\sigma$ and $a_{\tilde t=0} = 0$. The matrix $(H^\sigma)_{\tilde t\tilde t'}$ is given by

$$\begin{aligned} H^\sigma_{00} = 0 \quad , \qquad H^\sigma_{0t} &= H_{t0} \,=\, \frac{\partial \det G^\sigma}{\partial\theta_t^\sigma} \,, \\ \text{and} \qquad H^\sigma_{tt'} &= \Lambda^0_\sigma \frac{\partial^2 \det G^\sigma}{\partial\theta_t^\sigma\partial\theta_{t'}^\sigma} \quad . \end{aligned} \tag{6.23}$$

Generically (away from right angles) this matrix can be inverted, that is, we can integrate out the dihedral angles and the λ variables. This gives an effective simplex action expressed in terms of the area perturbations alone

$$S^\sigma_a \,=\, -\frac{1}{2}\sum_{\tilde t,\tilde t'\subset\sigma} a_{\tilde t}\,((H^\sigma)^{-1})_{\tilde t\tilde t'}\,a_{\tilde t'} = -\frac{1}{2}\sum_{t,t'\subset\sigma} a_t\,((H^\sigma)^{-1})_{tt'}\,a_{t'} \quad , \tag{6.24}$$

where $((H^\sigma)^{-1})_{tt'}$ are the tt'-components of the inverse of the full matrix $H^\sigma_{\tilde t\tilde t'}$.

Leveraging the bordered structure of $H^\sigma_{\tilde{t}\tilde{t}'}$, the matrix $((H^\sigma)^{-1})_{tt'}$ satisfies the condition

$$\begin{aligned} 0 &= \sum_{t\in\sigma} \frac{\partial \det G^\sigma}{\partial \theta^\sigma_t} ((H^\sigma)^{-1})_{tt'} \\ &= \sum_{t\in\sigma} c' A_t(\theta^\sigma)\ ((H^\sigma)^{-1})_{tt'}, \end{aligned} \tag{6.25}$$

where in the second line we used (6.8). We are hence looking for a set of vectors $\{v^t\}_{t'}$ which are orthogonal to the vector with components the areas, $w^t = A_t$. The Schläfli identity does indeed provide such vectors: $v^t = \delta\theta^\sigma_t$ for any variation δ. Additionally $((H^\sigma)^{-1})_{tt'}$ is a symmetric matrix, which suggests

$$((H^\sigma)^{-1})_{tt'} = \frac{\partial \theta^\sigma_t}{\partial A_{t'}} \quad . \tag{6.26}$$

This is confirmed by the fact that the same Hessian arises from the second order action (6.3) for one simplex, which also shows that $\partial\theta^\sigma_t/\partial A_{t'}$ is a symmetric matrix. Note that we obtain the same expression for the Hessian in the flat and in the homogeneously curved cases. The difficulty for the flat case is that the functions $A_t(\theta^\sigma_{t'})$ are ill-defined—only $\theta^\sigma_t(A_t)$ can be expected to exist locally in configuration space. However, there is no explicit expression available for these functions, and thus the route to obtain expressions for (6.26) is by inverting $H^\sigma_{\tilde{t}\tilde{t}'}$, the matrix of (double) derivatives of the angle Gram matrix.

From a computational perspective calculating the first and second derivatives of the determinant of the angle Gram matrix is straightforward (see Appendix I) and the matrix H^σ can be inverted numerically on explicit backgrounds. The alternative of computing $\partial\theta/\partial l$ and multiplying with the (numerically obtained) inverse of $\partial A/\partial l$ is cumbersome; although explicit expressions for $\partial\theta/\partial l$ are available [159], they are quite involved.

6.3.1 Identifying metric and non-metric perturbations

Generically, a three- or four-dimensional triangulation will have more triangles than edges and therefore we have more area variables than length variables. A single four-simplex has the same number, namely 10, of length and area variables and given the areas we can—modulo ambiguities arising from right angle configurations—compute its length variables. But, already for the case of two glued four-simplices we have 16 area and 14 length variables. Computing the lengths for each of the two simplices one will find that the lengths of the edges of the shared tetrahedron do not necessarily agree. We will refer to configurations with such a mismatch of length variables non-metric.

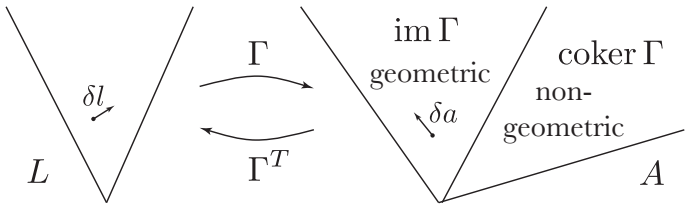

Figure 6.1: The space of length perturbations maps under Γ to the space of metric area perturbations. The complement defines the non-metric perturbations.

For the linearized theory, and for a general triangulation, we consider the matrix of derivatives

$$\Gamma^t{}_e := \frac{\partial A_t}{\partial L_e} \quad , \tag{6.27}$$

where A_t are the areas and L_e are the length variables. We assume a metric background and thus the (background) length variables L_e are well defined. We will use Γ to identify the vector space of non-metric area perturbations as the space spanned by its left null vectors. Note that we can apply this characterization to all lengths and areas of a given complex, or to only the set of boundary areas and boundary lengths. In the latter case we will speak of boundary non-metricity.

In more detail, if we call the space of edge lengths L and that of the areas A then Γ can be seen as a linear map $\Gamma : TL \to TA$; these spaces are illustrated in Fig. 6.1. In addition to the usual kernel of this map, which is spanned by the right null vectors of the matrix $\Gamma^t{}_e$, we will also consider the cokernel, namely the quotient space $TA/\mathrm{im}(\Gamma)$. Equivalently, this cokernel can be characterized as the kernel of the transpose map $\Gamma^T : TA \to TL$. Thus it is spanned by the left null vectors of $\Gamma^t{}_e$. The cokernel can be thought of as the extra combinations of areas that go beyond the edge lengths in a given simplicial complex. More precisely, it measures the degree to which Γ fails to be surjective.

The dimensions of the kernel and cokernel of a linear map are not independent,

$$\dim \mathrm{coker}(\Gamma) = \dim TA - \dim \mathrm{im}(\Gamma) = \dim TA - \dim TL + \dim \ker(\Gamma), \tag{6.28}$$

which serves as a useful sanity check when you find the various null spaces.

6.3.2 Gauge Symmetries

We turn to potential gauge symmetries of the linearized area Regge action. A quadratic action features gauge symmetries if its Hessian has null modes that can be localized to the bulk degrees of freedom. The presence of these null modes means that the solution under consideration is not uniquely determined by the boundary data—a gauge choice is required to uniquely specify the solution.

As emphasized in [52] the choice of background on which the Hessian is evaluated is important. The number of null modes, and therefore the number of gauge symmetries, might depend on the solution being considered. In this section we consider metric (background) solutions, while in Section 8 we consider more general backgrounds. On the latter backgrounds we show that the gauge symmetries of the metric backgrounds are broken.

Because of the equations of motion the deficit angles ϵ_t vanish on all bulk triangles. Thus the background is given by a flat piecewise linear geometry. For any vertex v in the bulk we can translate its position in the embedding flat geometry without changing the fact that the geometry is flat; in our four-dimensional triangulation there are four possible directions in which to do this. This will affect the lengths of the adjacent edges $l_e \to l_e + \delta_v^I l_e$, with $I = 1, \ldots 4$. These translations maintain zero deficit angles and leave the boundary areas and dihedral angles invariant, that is, they do not change the intrinsic or extrinsic geometry of the boundary. Thus the area Regge action remains invariant under (bulk) vertex translations. This gives four gauge symmetries per bulk vertex.[3] Note that the same kind of argument can be made if we use simplices with homogeneous curvature and the appropriate action (6.9).

In our investigations of Hessians on various metric backgrounds we did not find any additional gauge symmetries. Examples can be found in section 7.1. As the equations of motion impose flatness and would seem to suggest a topological theory, which would require more gauge symmetries, one could ask why there are not more gauge symmetries. In fact, the action

$$S_{\mathrm{BF}} = \sum_t \mathcal{A}_t \, \epsilon_t(L_e) \quad , \tag{6.29}$$

constructed by Baratin and Freidel [41], is topological. Here the L_e are lengths associated to the edges of a triangulation, and $\epsilon_t(L_e)$ is the deficit angle calculated from these lengths. The $\mathcal{A}_t$ are not areas *a priori*, but are treated as independent variables. Thus the $\mathcal{A}_t$ are

[3] Redundancies could occur, but only globally and thus depending on the topology of the manifold. For the four-sphere there are 10 such symmetries, 6 rotations and 4 translations.

Lagrange multipliers imposing the vanishing of the deficit angles. The equations of motion arising from variations of the length variables are

$$\sum_{\sigma} \sum_{t \in \sigma} \mathcal{A}_t \frac{\partial \theta_t^\sigma}{\partial L_e} = 0 \quad . \tag{6.30}$$

One class of solutions is provided by the Schläfli identity (6.4): choosing $\mathcal{A}_t = \alpha A_t(L_e)$, where α is a constant, ensures that Eq. (6.30) is satisfied. These solutions are called Regge solutions in [41].

Baratin and Freidel analyze the symmetries of this action on the Regge backgrounds. Apart from the vertex translation symmetry discussed above, there are also three symmetries per edge. These arise from perturbations of the Lagrange multipliers $\mathcal{A}_t \to \mathcal{A}_t + \varepsilon n_t^{e',I}$, with $I = 1, 2, 3$. The $n_t^{e',I}$ are specific perturbations satisfying

$$\sum_t n_t^{e',I} \frac{\partial \epsilon_t}{\partial L_e} = 0 \quad \text{for all } e, \tag{6.31}$$

and therefore constitute an additional three gauge symmetries per edge. There are local redundancies between the gauge parameters, which are thoroughly discussed in [41].

Are there similar symmetries for area Regge calculus? It turns out there are not. Here we have to consider the Hessian $\partial \epsilon_t / \partial A_{t'}$. This Hessian can be obtained from

$$\frac{\partial \epsilon_t}{\partial L_e} = \sum_\sigma \frac{\partial \theta_t^\sigma}{\partial L_e^\sigma} \tag{6.32}$$

by multiplying the Hessians associated to each simplex by $\partial L_e^\sigma / \partial A_t$. However, for the action (6.29), the condition $L_e^\sigma = L_e$ is imposed on all edges, which is not the case for the area Regge action. Instead when we multiply these Hessians by $\partial L_e^\sigma / \partial A_t$ there are more equations to satisfy, precisely one for each triangle.

Indeed in the numerical examples studied in the next section we find that $\partial \epsilon_t / \partial L_e$ has the (left) null vectors resulting from Eq. (6.31) whereas $\partial \epsilon_t / \partial A_{t'}$ has only the null vectors (which are null from the left and right) resulting from the vertex translation symmetry. The disappearance of the left null vectors in going from $\partial \epsilon_t / \partial L_e$ to $\partial \epsilon_t / \partial A_{t'}$ is a consequence of the fact that there are more areas than length variables and thus more conditions to satisfy in order to be a left null vector.

Chapter 7

Covariant and Canonical analysis

Here, we shall consider certain aspects of the dynamics of linearized area Regge calculus both in the covariant formalism and the canonical formalism. In the covariant analysis, we shall employ the 'Pachner moves' which are local changes of the bulk triangulation that finitely generate any change of the bulk triangulation, [160].

The canonical framework which we will be employing, [45], uses discrete time evolution steps. The action will serve as a generating function for the canonical transformation that represents the time evolution [161]. This has the advantage that the covariant equations of motion are exactly reflected in the canonical framework. The symmetry content is also mirrored exactly [45], and thus we will find that the vertex translation symmetry leads to (first order) constraints. The latter can be used to define a notion of continuous time transformations. (Again here we consider metric background solutions and these features will only hold on such backgrounds.)

7.1 Pachner moves

We will now study the equations of motion of linearized area Regge calculus on small simplicial complexes, those that support Pachner moves.

In d dimensions there are $(d+1)$ different types of moves referred to as $(d+1)-1, d-2, \cdots, 1-(d+1)$. An $x-y$ Pachner move with $x+y=d+2$ changes a complex of x d–simplices into a complex of y d–simplices. A $y-x$ move is the inverse of an $x-y$ move. In four dimensions we have therefore the $5-1$ move, the $4-2$ move, their inverses, and the $3-3$ move. The subsections below treat each of these moves in turn.

The Pachner moves allow us to efficiently check the symmetry content of the theory. We also compare the behavior of the area and length Regge calculi under Pachner moves and find that there are significant differences. This could be a useful test to classify spin foam models.

Note that for this analysis we only consider the linearized theory on flat and *metric* background solutions. Explicit expressions for the Hessians we have used can be found in our open-source Area Regge Calculus (ARC) Mathematica code, available at https://github.com/Seth-Kurankyi/Area-Regge-Calculus.

7.1.1 5–1 move

We start with the 5–1 move. Its properties in area Regge calculus turn out to be very similar to the 5–1 move in length Regge calculus. The 5–1 move starts with an initial configuration of 5 four-simplices sharing a common vertex in the bulk of the triangulation and removes the bulk vertex to get a single simplex (see Fig. 7.1). As in length Regge calculus, a solution with 5 four-simplices is most simply constructed by subdividing a single flat simplex. There is a free choice in this subdivision, namely where to place the bulk vertex. This leads to the four-dimensional gauge symmetry discussed above and can be seen as a remnant of the continuum diffeomorphisms.

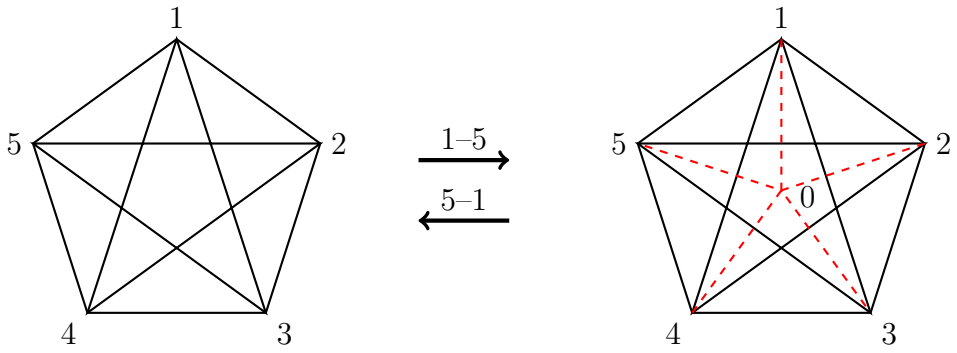

Figure 7.1: A 1–5 move splits a 4-simplex into five 4-simplices by introducing a bulk vertex 0. The 5–1 Pachner move is the inverse and reduces the five 4-simplices on the right to the one 4-simplex at left by removing the bulk vertex and its associated bulk edges (dashed).

The simplicial complex for the initial configuration of the 5–1 move has 20 triangles and 15 edges. Of these, 10 triangles and 10 edges are in the boundary, which coincides with the boundary of a four–simplex. Thus we have 5 bulk edges and 10 bulk triangles.

We label the vertices of our background solution by $(0, 1, \ldots, 5)$, with 0 the bulk vertex. The background edge lengths are chosen to be $l_{\text{bdry}} = 1$ for edges (i, j) and $l_{\text{bulk}} = \sqrt{2/5}$ for edges $(0, i)$ with $i, j \in \{1, \ldots, 5\}$. The effective Hessian matrix describing the linearized action in terms of area perturbations is

$$M^{51}_{tt'} := -\frac{1}{2}\sum_{\sigma}((H^{\sigma})^{-1})_{tt'}, \tag{7.1}$$

as described in section 6.3, and can be found explicitly for our background.[1]

As expected, see the discussion in Section 6.3.2, the bulk part of the Hessian has exactly four null vectors; these correspond to the four vertex translations of the bulk vertex and are the discrete remnant of diffeomorphism symmetry. The full Hessian has five null vectors: the four null vectors describing vertex translations and a global scaling symmetry, that affects also the boundary areas.

We have also considered the (linearized) theory with homogeneously curved simplices. In this case one also finds four null vectors for the bulk Hessian. There is however no global null vector, as the scaling symmetry is broken by the homogeneous curvature. Again see the ARC code for the explicit computations in both the flat and homogeneously curved cases.

Metricity

As explained in Section 6.3.1, the area perturbations split into metric and non-metric types. For the 5–1 move all boundary area perturbations are metric (away from right angle configurations). Conversely, the boundary length perturbations determine the boundary area perturbations uniquely. Considering the full complex, including bulk areas, there are 5 non-metric area perturbations.

On our chosen background the solutions to the equations of motion are orthogonal to these non-metric directions. In fact, this holds for general 5–1 backgrounds due to the subdivision construction introduced above: The boundary data specify (away from right angle configurations) a metric 4-simplex and thus do not admit non-metric directions. Meanwhile, the equations of motion impose flatness for the deficit angles appearing in a subdivision of this metric simplex. Thus the subdivision determines a 4-parameter set of flat and metric solutions.

[1] This, and all other explicit calculations can be found in our open-source Area Regge Calculus (ARC) code.

This argument shows that, like the length Regge action, the area Regge action is invariant under the 5–1 Pachner move. In particular, evaluating the action for a complex consisting of five simplices on the solution for the bulk variables we find the same value as for the final configuration consisting of only one simplex.

7.1.2 4–2 move

The 4–2 move starts with a configuration of four 4-simplices sharing a common edge and, by removing the common edge, ends up with a configuration of two 4-simplices glued along a (new) shared tetrahedron.

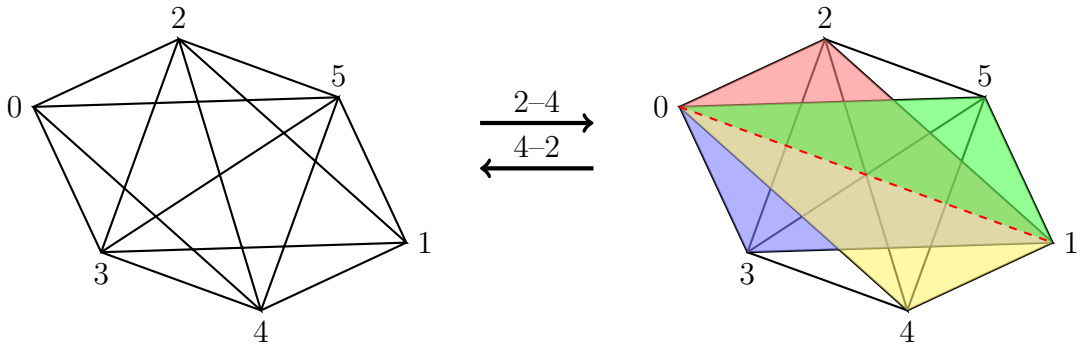

Figure 7.2: The 2–4 Pachner move takes two 4-simplices $\sigma^0 = (1,2,3,4,5)$ and $\sigma^1 = (0,2,3,4,5)$, which share the boundary tetrahedron $(2,3,4,5)$, to four simplices $\sigma^2, \sigma^3, \sigma^4, \sigma^5$ by introducing a bulk edge $e(01)$. The inverse procedure gives the 4–2 move.

The 4–2 move in area Regge calculus has quite different properties from that in length Regge calculus. The main reason is that the boundary of the complex, which agrees with the boundary of two glued 4-simplices, admits non-metric data. As we will see this possibility will be responsible for the non-invariance of the area Regge action under the 4–2 move. The boundary data for the 4–2 move in length Regge calculus, which are given by the lengths of the edges of the two glued simplices, do not induce curvature. This means that the solution for the initial configuration of the 4–2 move is flat, and leads to the invariance of the length Regge action.

The simplicial complex for the initial configuration of the 4–2 move has 20 triangles and 15 edges. Of these, 16 triangles and 14 edges are in the boundary, which coincides with the boundary of two glued four–simplices. Thus we have one bulk edge and four bulk triangles (see Fig. 7.2).

Again we label vertices $(0, 1, \ldots, 5)$ with (01) the bulk edge. Consider the background edge lengths $l_{\text{bdry}} = 1$ for edges (i, j) and edges (I, i) with $i, j \in \{2, \ldots, 5\}$ and $I \in \{0, 1\}$. For the bulk edge $(0, 1)$, $l_{\text{bulk}} = \sqrt{5/2}$.

The solution for the bulk areas is unique, that is, the bulk Hessian has no null vectors. The full Hessian has one null vector corresponding to a global scaling symmetry.

Metricity

Amongst the 20 area perturbations of the full complex, five combinations describe non-metric directions. These are determined by the left null vectors of the matrix ${\Gamma^t}_e$. When restricted to the boundary triangles and edges, there are two null vectors and hence two non-metric directions. In both cases there are no right null vectors, which means the metric area perturbations determine the length perturbations uniquely.

Let us first consider a restriction to metric boundary perturbations. (We remind the reader that these are over a metric background.) We again find a solution by subdivision in a flat embedding. The embedding determines the bulk edge of the subdivision and as before the action is invariant when restricted to metric boundary data.

However, this changes if we consider non-metric boundary data. These can be isolated through a variable transformation for the boundary variables; the new variables will also be useful for the analysis of the 4–valent tent move in section 7.2. The 16 boundary areas can be taken to define the areas of two simplices $\sigma^0 = (0, 2, 3, 4, 5)$ and $\sigma^1 = (1, 2, 3, 4, 5)$ that share a tetrahedron $\tau = (2, 3, 4, 5)$. This allows us to consider the following transformation

$$(\{a_{0ij}\}, \{a_{1ij}\}, \{a_{kij}\}) \;\to\; (\{l_{0i}\}, \{\phi^0_\alpha\}, \{l_{1i}\}, \{\phi^1_\alpha\}, \{a_{kij}\}) \quad , \tag{7.2}$$

where the indices i, j, k take values in $\{2, 3, 4, 5\}$. The variables ϕ^0_α with $\alpha \in \{1, 2\}$ are two 3D dihedral angles at non-opposite edges in the tetrahedron τ and are determined by the areas of the simplex σ^0. The ϕ^1_α describe dihedral angles at the same edges, but are computed from the areas of the simplex σ^1. Finally the l_{mn} are the edge lengths between vertices m and n. We can construct such a transformation by splitting it into two steps: For each simplex we first transform the 10 areas to the 10 length variables. We then consider separately the 6 length variables l_{ij}, which determine the tetrahedron τ in σ^0 and in σ^1. From these 6 length variables we can define the four areas a_{kij} and the dihedral angles ϕ^0_α and ϕ^1_α. See Appendix J for the explicit transformation needed in the second step.

Clearly, we have a non-metric configuration if $\phi^0_\alpha \neq \phi^1_\alpha$, as these dihedral angles describe the same geometric quantity, but are computed from the data of different 4-simplices. The

metricity condition is thus that these 3D dihedral angles in the shared tetrahedron coincide. This is analogous to the metricity condition for tetrahedra identified in [44], which demands that the 2D dihedral angles of shared triangles should coincide.

We can now introduce two variables $t_\alpha = \phi^1_\alpha - \phi^0_\alpha$ which isolate the non-metric directions. For boundary data that give non-vanishing t_α the action will fail to be invariant under the 4–2 move. Interestingly, the effective action for the configuration with four simplices couples the angles ϕ^1_α and ϕ^0_α. This coupling cannot appear for the action with two simplices, as it is just a sum of two terms $S(\sigma^0)$ and $S(\sigma^1)$ which only depend on the quantities in σ^0 and σ^1 respectively.

In summary, for general boundary data the area Regge action is not invariant under the 4–2 Pachner moves and the reason is that the boundary admits non-metric perturbations.

7.1.3 3–3 move

The 3–3 Pachner move transforms a configuration of three 4-simplices in a triangulation to a different configuration also made up of three simplices. See Fig. 7.3.

In length Regge calculus the 3–3 move is the only one that admits curvature. The boundary lengths can be chosen such that the bulk triangle has a non-zero deficit angle. Note that there is no bulk edge and hence no equation of motion to impose in length Regge calculus. The presence of curvature leads to non-invariance of the action under 3–3 Pachner moves [26].

This leads to a puzzling question for area Regge calculus: if we can choose boundary data that lead to curvature in the bulk, how are the equations of motion, which demand flatness, imposed? The resolution will be a subtle interplay between the geometric data described by the boundary areas on the one hand and the geometric data described by the boundary lengths on the other.

There are *only* 19 triangles in this complex—the triangle $(3, 4, 5)$ does *not* appear. There are 15 edges and the boundary includes all 15 edges and 18 of the triangles. There is one bulk triangle.

We consider again the vertices $(0, 1, \ldots, 5)$ and the three four-simplices $\sigma(01234), \sigma(01235)$ and $\sigma(01245)$ which share the bulk triangle $t(012)$. For our background solution the edge length are $l_{\text{bdry}} = 1$ for edges (i, j) and (I, J) with $i, j \in \{3, \ldots, 5\}$ and $I, J \in \{0, 1, 2\}$. The edges (I, i) have length $l_{\text{bdry}} = \sqrt{2/3}$.

With our background solution we find that the solution for the bulk area is unique and that the full Hessian has one null vector corresponding to the global scaling symmetry.

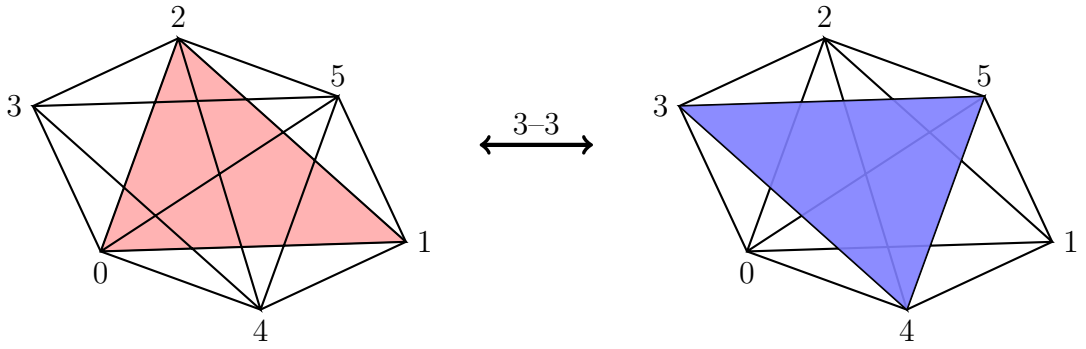

Figure 7.3: The 3–3 Pachner move changes a configuration of three simplices with one bulk triangle $t(0,1,2)$ to a different configuration of three simplices with a bulk triangle $t(3,4,5)$ keeping the boundary geometry fixed.

Metricity

As before the surfeit of area variables allows for area perturbations that are non-metric. These behave much as before and rather than treat them in detail we will focus on an issue that is unique to the 3–3 move.

We have just shown that the boundary data uniquely determine the bulk triangle. Thus even for a metric boundary perturbation of the areas that one would expect to lead to boundary edge lengths that induce curvature we find a particular bulk triangle. As all area solutions require flatness, it seems the only possibility is that this solution is non-metric.

However, it turns out that this is not the case!

Considering ${\Gamma^t}_e$ we have now to take into account one triangle less than for the other complexes. It has a co-image of dimension four, but, none of these non-metric perturbations has a component in the bulk area. The co-image is orthogonal to the vector describing the solution (i.e. the bulk row of the effective Hessian).

Restricting ${\Gamma^t}_e$ to boundary triangles and boundary edges we find, surprisingly, that although it is an 18×15 matrix, it has a one–dimensional kernel. This means that despite their number, the 18 boundary areas do *not* uniquely determine the 15 boundary edge lengths. If we add the bulk area to the boundary areas—and the resulting set is metric—it will uniquely determine the (boundary) length perturbations.

Thus, if we solve the equations of motion for a fixed and metric area-perturbation, we actually fully determine the corresponding (boundary) length perturbation, and, as it

must, it determines a zero curvature solution.

Considering the background solution cited above one finds that the area Regge action is invariant under the 3–3 move. That is, the actions for both configurations of the 3–3 move agree after one has included, for each configuration, the bulk area. However, this invariance is due to the highly symmetric nature of the background. We have studied less symmetric backgrounds and found that the area Regge action is not invariant. This can again be traced back to the non-metric boundary perturbations.

7.1.4 Summary: Pachner moves in area vs. length Regge calculus

In summary, we have found that both for length and area Regge calculus only the initial configuration of the 5–1 move features gauge symmetries; these are remnants of the diffeomorphism symmetry. Both actions are also invariant under the 5–1 move.

For the other Pachner moves one finds however differences: the boundary configuration for the 4–2 Pachner moves admits non-metric directions. This leads to a non–invariance of the area Regge action. In contrast, the length Regge action is invariant under the 4–2 Pachner move as the boundary configuration admits only flat solutions.

The 3–3 move is the only one under which the length Regge action is not invariant. The reason is that the boundary length data generically prescribe a non-vanishing deficit angle for the bulk triangle. A vanishing deficit angle requires special boundary data. There is no bulk edge and thus no equation to solve in length Regge calculus.

There is however a bulk triangle and thus an equation of motion—imposing flatness—in area Regge calculus. Given the fact that the length boundary data generically induce curvature one might wonder how this flatness is realized. It turns out however that the area boundary data do not fully determine the length boundary data even though there are 18 areas and only 15 lengths in the boundary. In fact, it is exactly the bulk area that is needed to fully determine the boundary lengths, and its value is fixed by the equation of motion which demands a vanishing deficit angle.

Nevertheless, the area Regge action is also (generically) not invariant under the 3–3 move. The reason again is that non-metric area perturbations can appear in the area boundary data.

7.2 Tent moves

We now analyze the linearized dynamics of area Regge calculus in a canonical framework. This will tell us whether, apart from the constraints expected from the vertex translation symmetries, there are any further (e.g. second class) constraints, that would reduce the number of physical degrees of freedom. We will find that this is not the case, and that, as the number of area variables is typically larger than the number of length variables, area Regge calculus has a larger number of physical degrees of freedom than length Regge calculus.

With the discrete time evolution steps that we will employ here for the canonical framework, we need to decide how to evolve the triangulation stepwise. We use local evolution moves, which do not change the connectivity of the spatial triangulation, and are called tent moves [162]. Consider all tetrahedra $\{\tau_i\}$ that share the vertex v_0 in the triangulation of an equal time hypersurface. The union of these tetrahedra defines the three-dimensional star of v_0. We glue an edge $e(v_0, v_1)$—the tent pole—to v_0 and thus obtain a new vertex v_1. This new vertex will be connected by new edges with all vertices adjacent to v_0 in the initial (equal-time) triangulation. For each τ_i we glue a simplex σ_i onto τ_i so that all these simplices share the tent pole e. The tent moves change the geometric data of the triangulated hypersurface by replacing the three-dimensional star of v_0 with the three-dimensional star of v_1.

The canonical framework developed in [45] provides a setting in which to analyze these tent moves.[2] To this end one needs to consider the action S_{T} associated to the triangulation piece T that is glued onto the hypersurface during the tent move. This piece of triangulation carries 4 types of variables:

(a) Variables associated to the 'lower' boundary of T that will be glued and thus 'disappear'. These variables are associated to the initial time and the simplices sharing the vertex v_0.

(b) Exactly the same number of 'new' variables are associated to the 'upper' boundary of T, and can be associated to the final time.

(c) There will also be variables associated to the corner of the tent T; these are variables that appear at both the initial and final time. They do not change under the tent move evolution and, hence, are non-dynamical.

[2] The more general framework of [45] also allows for Pachner moves of the spatial triangulation. These can be seen as time evolution steps in which the number of degrees of freedom change.

(d) Finally, there are variables associated to the bulk of the tent T. In length Regge calculus the only such variable is the length of the tent pole, while in area Regge calculus there are all the areas of the triangles that hinge on the tent pole.

The bulk variables can be incorporated into the canonical framework, but the conjugated momenta will always be constrained to vanish. This imposes the equations of motion for the bulk variables, and coincides with the covariant equations of motion. Using the solutions in the remaining equations gives a reduced phase space. Equivalently one can integrate out the bulk variables from the action. This leaves only the variables of the types (a), (b) and (c). We will proceed along the latter path and denote by S_{T} the (effective) action with the bulk variables integrated out.

The 'corner' variables, type (c), are non-dynamical and do not have associated momenta. For the remaining variables, x_0^i at the initial time and x_1^i at the final time, the equations

$$p_0^i \;=\; -\frac{\partial S_{\mathrm{T}}}{\partial x_0^i} \quad , \qquad p_1^i \;=\; \frac{\partial S_{\mathrm{T}}}{\partial x_1^i} \tag{7.3}$$

serve both to define the momenta and as equations of motion. Solving for the final data (x_1^i, p_1^i) in terms of the initial data (x_0^i, p_0^i) proceeds in two steps: the first set of equations in (7.3) is solved for the x_1^i and then these solutions are used in the second set to find the p_1^i.

It can, however, happen that a solution of the first set of equations in terms of x_1^i is not possible. Similarly one might not be able to solve the second set of equations for x_0^i. This will be the case if the matrix

$$\frac{\partial^2 S_{\mathrm{T}}}{\partial x_0^i \partial x_1^j} \tag{7.4}$$

is not invertible, i.e. we have a degenerate Lagrangian system. The matrix will thus have left null vectors Y_I^i. By contracting the first set of equations in (7.3) with such a null vector

$$\sum_i Y_I^i p_0^i \;=\; -\sum_i Y_I^i \frac{\partial S_{\mathrm{T}}}{\partial x_0^i} \tag{7.5}$$

we can project out any linear dependence on perturbations in the variables x_1^j around points where (7.4) is non-invertible. In fact, for a linear theory these equations (7.5) are linear and thus they will lead directly to constraints.[3] These constraints are equations (of

[3] An in-depth analysis of the various types of constraints that can appear can be found in [163].

motion) that hold between the configuration variables and momenta at one time. Thus left null vectors of (7.4) lead to constraints for the data at the initial time. Similarly, right null vectors Z^j_I of (7.4) will lead to constraints at the final time. Gauge symmetries, which correspond to localizable null vectors for the (bulk) Hessian of the action, always lead to constraints [45]. The gauge constraints are preserved by the time evolution, or more precisely, initial data satisfying the initial constraints will be mapped to data satisfying the final constraints. Correspondingly, the equations of motion will not lead to a unique solution for the final data in terms of the initial data. Instead we have a gauge freedom, involving the same number of parameters as we have constraints. This is an expected consequence of the gauge symmetry of the action.

The main result of our tent move analysis is that we find only constraints resulting from the gauge symmetry of the action. As in the continuum, we will differentiate between gauge and physical degrees of freedom. The evolution of the physical degrees of freedom—in contrast to that of the gauge degrees of freedom—is determined by the tent move equations of motion. More precisely these are phase space functions that Poisson commute with the constraints (with the canonical Poisson structure $\{x^i, p^j\} = \delta^{ij}$ between variables at one time).

Note that the definition of a physical degree of freedom depends on the notion of tent move. For example, we might find that tent moves have physical degrees of freedom, whereas a more global notion of time evolution might find only gauge degrees of freedom. The reason is that we consider the 'corner' variables (type (c) above) as constant and thus freeze gauge symmetries that affect these variables (or variables outside the region of the tent move). In contrast, the notion of a gauge degree of freedom will remain the same even with a more global time evolution.

As an example, consider the degrees of freedom of length Regge calculus in $(2+1)$ and $(3+1)$ dimensions. The $(2+1)$-dimensional Regge calculus is topological: using a global time evolution one finds that the number of physical degrees of freedom does not depend on the size of the triangulation, but only on the topology of the underlying space. There are no local physical degrees of freedom. However, a tent move over a vertex with n adjacent edges, which we call an n-valent tent move, will have $n-3$ physical and three gauge degrees of freedom. The appearance of physical degrees of freedom for the tent moves is, nevertheless, consistent with the finding that there are no local physical degrees of freedom under a global time evolution. The tent moves show that there are three constraints (or three gauge degrees of freedom) per vertex and modulo a topological constant this agrees with the number of edges in a two-dimensional triangulation.

Similarly, for $(3+1)$–dimensional Regge calculus an n–valent tent move gives $n-4$

physical and four gauge degrees of freedom. In this case, one also finds local physical degrees of freedom under global time evolution—the reason is that for a sufficiently large three-dimensional triangulation the number of edges is generically greater than four times the number of vertices.[4]

In the examples considered here we find no additional constraints, beyond those resulting from the vertex translation symmetry. There are more dynamical area than dynamical length variables, and so we have more physical degrees of freedom for area Regge calculus than in the length calculus. This will also hold in a global time evolution, as generically there are more triangles than edges in three-dimensional triangulations. We have thus more kinematical variables in area than in length Regge calculus, but the same gauge freedoms (in the theories linearized on a metric or flat background respectively).

Here we have studied the 4-valent and 5-valent tent moves in detail. These already exemplify all the dynamical features that appear in length Regge calculus and those that we expect to appear in the area calculus. In length Regge calculus the 4-valent tent move only admits a flat dynamics and all four dynamical degrees of freedom turn out to be gauge. In contrast, in the area calculus version the 4-valent tent move has six dynamical degrees of freedom, of which four are gauge and two are physical; the latter represent non-metric degrees of freedom.

The 5-valent tent move in length Regge calculus admits curvature and out of the five dynamical degrees of freedom one is physical. In area Regge calculus we find four gauge and five physical degrees of freedom. Four of these physical degrees of freedom describe non-metric motions.

One can obtain the equal time triangulated hypersurfaces for higher valent tent moves from those for lower valent tent moves by subdividing tetrahedra adjacent to the vertex v_0 with 1–4 Pachner moves. In going from an n-valent to an $(n+1)$-valent tent move you add one edge and three triangles all adjacent to v_0. This counting shows that an n–valent tent move has $(3n-6)$ dynamical area variables, which can be compared to the n dynamical length variables in the length calculus. As we have found no indication of gauge symmetries beyond vertex translation nor additional (possibly second class) constraints for the 4–valent and 5–valent tent moves we expect that there are only four gauge degrees of freedom for all the tent moves. This leads to $(3n-10)$ physical degrees of freedom for an n–valent tent move in area Regge calculus, significantly more than the $(n-4)$ physical degrees of freedom one finds in length Regge calculus.

[4]The exceptions are so-called stacked triangulations of the three-sphere, see [45].

7.2.1 The 4-valent tent move

For a 4-valent tent move at a vertex v we glue four 4-simplices that share the tent pole onto the 4 tetrahedra that make up the 3D star of the vertex v, see Fig. 7.4. As these four simplices share an edge they turn out to coincide with the 4 simplex configuration of the 4–2 Pachner move. The bulk areas that appear in the 4–2 move are the 'lapse' areas of the triangles sharing the tent pole. Thus the effective action for the 4–2 move defines also the effective action for the tent move. We will denote this action by S_{4V}. Because we integrate out all bulk variables, S_{4V} only depends on the variables in the boundary of the complex.

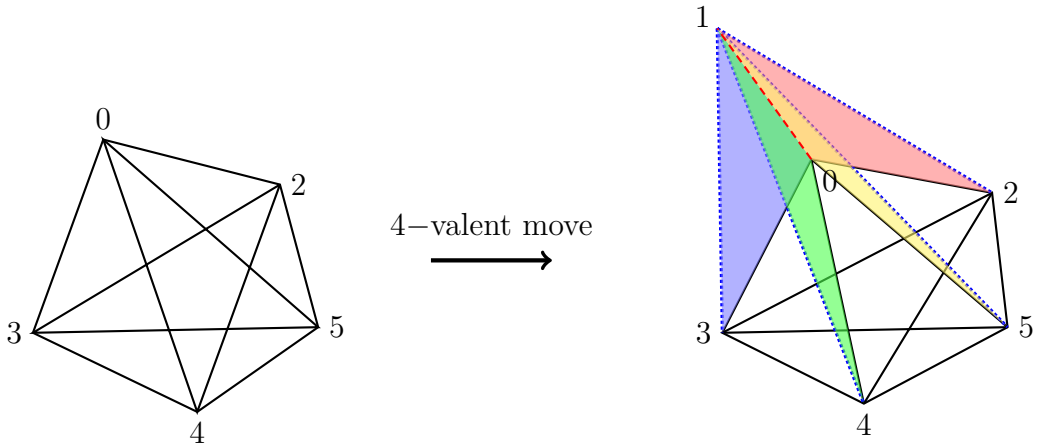

Figure 7.4: A tent move at the 4-valent vertex 0. Introducing a tent pole $e(01)$ and connecting the vertex 1 to the vertices in $\tau(2345)$ yields the final configuration. This introduces four bulk areas.

This relation with the 4–2 Pachner move allows us to work again with the background introduced in Section 7.1.2. (In that background the two simplices that make up the final configuration of the 4–2 move have positive orientation. For the tent move it is more typical to consider one simplex with positive and the other (initial) simplex with negative orientation. This describes a larger tent being erected on top of a smaller base. However, the tent move is well defined for any choice of orientation. The background chosen here corresponds to putting up a tent over a pit.)

With a tent move like that depicted in Figure 7.4 we have the following configuration variables:

(a) At time 0 we have six areas a_{0ij} (we will use $i, j, k \in \{2, 3, 4, 5\}$ and $\alpha \in \{1, 2\}$). In length Regge calculus we have four lengths l_{0i}.

(b) At time 1 we also have six areas a_{1ij} and four lengths l_{1i}.

(c) In addition there are four areas a_{ijk} that are non-dynamical 'corner' variables, and appear at both times. There would be six such variables l_{ij} in length Regge calculus.

As for the 4–2 move, we have 16 area variables in the boundary of the tent move complex and 14 length variables.

The boundary of the tetrahedron $\tau(2, 3, 4, 5)$ defines the 'corner' for the tent move. We therefore have to keep the four areas of this tetrahedron constant, as its boundary defines the 'corner' for the tent move. This is different from length Regge calculus, where all six edge lengths of this tetrahedron are fixed. Hence there are two degrees of freedom associated to this tetrahedron that are dynamical in area Regge calculus but not in the length calculus. As the areas have to be constant we can identify these two degrees of freedom as 3D dihedral angles hinging at two non-opposite edges. (Four areas and two non-opposite 3D dihedral angles determine all the lengths of a tetrahedron, see Appendix J.) The fact that the 3D dihedral angles can change is key to non-metricity: changing an angle affects the lengths of the edges of the tetrahedron. These edges are however part of the 'corner' which constitutes the boundary of both equal time hypersurfaces.

We will therefore apply the same variable transformation as in the discussion for the 4–2 move, that is, (remember $i, j, k \in \{2, 3, 4, 5\}$ and $\alpha \in \{1, 2\}$)

$$(\{a_{0ij}\}, \{a_{1ij}\}, \{a_{ijk}\}) \;\to\; (\{l_{0i}\}, \{\phi^0_\alpha\}, \{l_{1i}\}, \{\phi^1_\alpha\}, \{a_{kij}\}) \tag{7.6}$$

where the (l_{0i}, ϕ^0_α) and the (l_{1i}, ϕ^1_α) appear now as dynamical variables at time 0 and time 1, respectively. The a_{kij} are the non-dynamical 'corner' variables.

The canonical evolution equations have the following form

$$p^l_{0i} = -\frac{\partial S_{4V}}{\partial l_{0i}} =: -\sum_j M^{00}_{i,j} l_{0j} - \sum_\alpha M^{00}_{i,\alpha}\phi^0_\alpha - \sum_{(jkl)} M^{0b}_{i,jkl} a_{jkl} \quad , \tag{7.7}$$

$$p^\phi_{0\alpha} = -\frac{\partial S_{4V}}{\partial \phi^0_\alpha} =: -\sum_j M^{00}_{\alpha,j}\, l_{0j} - \sum_\beta M^{00}_{\alpha,\beta}\phi^0_\beta - \sum_\beta M^{01}_{\alpha,\beta}\phi^1_\beta - \sum_{(jkl)} M^{0b}_{\alpha,jkl} a_{jkl} \quad , \tag{7.8}$$

$$p^l_{1i} = \frac{\partial S_{4V}}{\partial l_{1i}} =: \sum_j M^{11}_{i,j}\, l_{1j} + \sum_\alpha M^{11}_{i,\alpha}\phi^1_\alpha - \sum_{(jkl)} M^{1b}_{i,jkl} a_{jkl} \quad , \tag{7.9}$$

$$p^\phi_{1\alpha} = \frac{\partial S_{4V}}{\partial \phi^1_\alpha} =: \sum_j M^{11}_{\alpha,j}\, l_{1j} + \sum_\beta M^{11}_{\alpha,\beta}\phi^1_\beta + \sum_\beta M^{10}_{\alpha,\beta}\phi^0_\beta + \sum_{(jkl)} M^{1b}_{\alpha,jkl} a_{jkl} \tag{7.10}$$

Here we made use of the fact that the mixed time block of the Hessian for the action, expressed in terms of x_I^A with $A = 0, 1$ at time 0 or 1 respectively,

$$M_{IJ}^{01} := \frac{\partial^2 S_{4V}}{\partial x_I^0 \partial x_J^1} \quad , \tag{7.11}$$

has four left and four right null vectors. These are given by the length perturbations l_{0i} and l_{1i}, respectively. These null vectors result from the vertex translation symmetry discussed in Sec. 6.3.2.

The presence of these null vectors can be explained as follows: Consider an extension of the tent move triangulation so that, e.g., the vertex v_1 appears as a bulk vertex of the extended triangulation. Such an extension can be obtained via a second tent move from time 1 to time 2. The action for the extended triangulation is a sum of two terms S_{01} and S_{12}—one for the first tent move from time 0 to time 1 and one for the second tent move between times 1 and 2. As discussed in section 6.3.2, the Hessian of the full action $S_{01} + S_{12}$ has four null vectors corresponding to the vertex translation symmetry of v_1, and thus these null vectors have entries only for variables at time 1. (We assume we have integrated out all lapse like variables.) Being null vectors for the full Hessian they are also annihilated by the non-diagonal block M^{01} of the Hessian for the action $S_{01} + S_{12}$, which coincides with the non-diagonal block of the Hessian for S_{01} alone. Likewise the null vectors are annihilated by the non–diagonal block M^{21} of S_{12}. By time translating the argument we have that M^{01} has at least four left null vectors and at least four right null vectors.

We have not found any further null vectors for the Hessian (7.11) evaluated on the background described above nor on the other backgrounds we investigated. For the background described above $M_{i,\alpha}^{00}$ vanishes, but this is due to the high symmetry of this background and we did find non-vanishing entries on more general backgrounds.

The null vectors of M_{IJ}^{01} correspond exactly to the perturbations described by the four length variables l_{0i} or l_{1j}, as these are independent parameters for the gauge action resulting from vertex translation of v_0 or of v_1.

Thus equation (7.7) only involves variables at time 0 (including the non–dynamical variables), whereas equation (7.9) only involves variables at time 1. These constitute constraints

$$C_i^A := \; p_{Ai}^l + (-1)^A \sum_j M_{i,j}^{AA} l_{Aj} + (-1)^A \sum_\alpha M_{i,\alpha}^{AA} \phi_\alpha^A + (-1)^A \sum_{(jkl)} M_{i,jkl}^{Ab} a_{jkl} \tag{7.12}$$

and these constraints are also preserved by time evolution. The constraints (at a fixed time) are first class, i.e. they Poisson commute. This follows from the fact that the matrix $M^{AA}_{i,j}$ is symmetric.

This also means that given a set of initial data that satisfy the constraint equations the length variables at time 1 are not determined by the equations of motion (7.7). We can rather choose these freely. These four length variables represent the lapse and shift gauge degrees of freedom and describe the position of the 'tip of the tent', by giving its distance to its (four) adjacent vertices.

Non-trivial dynamics will be confined to the angle variables ϕ^A_α. Changes of these variables under time evolution means that non-metricity is being generated.

We can however alter the dynamics and impose constraints that ensure $\phi^0_\alpha = \phi^1_\alpha$. This can be done by hand, but a more elegant procedure is to replace the action we were considering by the action $S^{01} := S(\sigma^0) + S(\sigma^1)$ for the 2 simplex configuration of the 4–2 move. (Remember that the effective actions for the 4 simplex and the 2 simplex configurations agree when projected onto the space of metric boundary perturbations.) By defining the dynamics using the action S^{01}, all variables at time step 0 decouple from the variables at time step 1. This leads to constraints for the momenta conjugated to the angle variables. These momenta at, say, time 0 would only involve the action of the simplex σ^0. The angle variables at time 1 will now also appear as gauge parameters and can be chosen to agree with the angle variables at time 0.

7.2.2 5–valent tent move

Next we will discuss the 5-valent tent move. In length Regge calculus this move has one physical degree of freedom and the canonical data, or equivalently, the boundary data, can be chosen so that the configuration has curvature. As area Regge calculus imposes flatness, we expect that—as in the 3–3 move—the boundary areas do not completely fix the lengths on the boundary.

To be more precise we consider a tent move that puts up a tent pole between 0 and 1. The triangulation at time 0 can be obtained from gluing two simplices (02345) and (02346) along the tetrahedron (0234). Note that this shared tetrahedron (0234) is not part of the 3D 'equal time' hypersurface. In particular, the triangle (234) will not be part of the boundary data. However, the edges (23), (24), and (34) are part of the tent move complex.

The tent move is performed by gluing 6 simplices $(01ij5)$ and $(01ij6)$, with $i, j \in \{2, 3, 4\}$, onto the 'equal time' hypersurface. The background we will be considering is

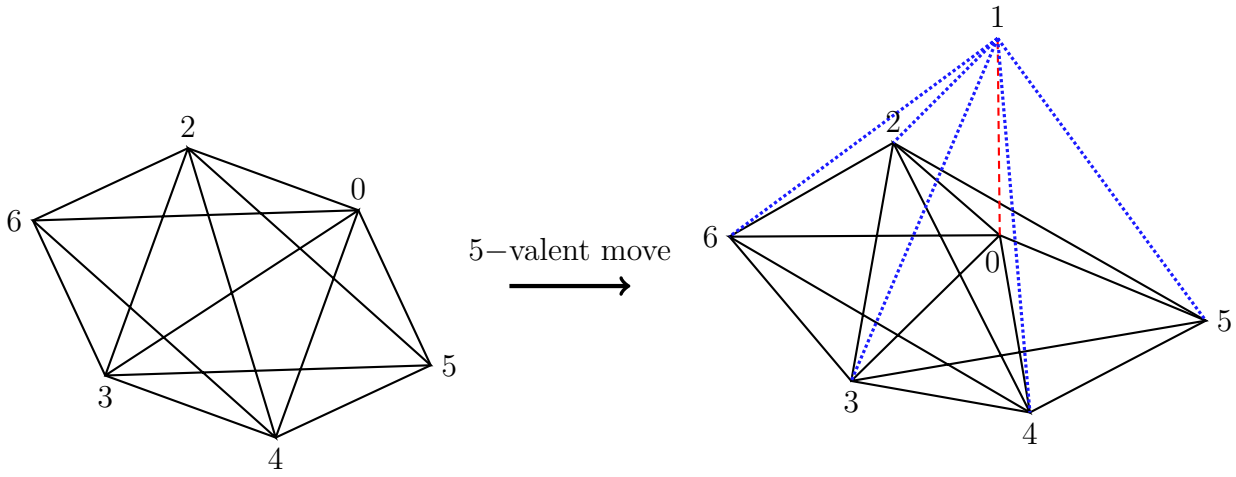

Figure 7.5: A five-valent tent move at the vertex 0 starting from a configuration of two simplices $\sigma^6 = (0, 2, 3, 4, 5)$ and $\sigma^5 = (0, 2, 3, 4, 6)$ and gluing six simplices on the 3D star of vertex 0.

given by $L_{0i} = L_{05} = L_{06} = L_{ij} = L_{i5} = L_{i6} = 1$ and $L_{1i} = \sqrt{9/2}$ as well as $L_{15} = L_{16} = 2$. The length of the tent pole can then be computed to be $L_{01} = \sqrt{3/2}$.

In the following table 7.1 we give the number of triangles for the full tent move complex and for the various sub-triangulations ($T = 0$ and $T = 1$ indicate the vertices 0 and 1 and again $i, j \in \{2, 3, 4\}$):

	Full complex	Boundary	Equal time: bulk	Equal time: boundary
Areas	29	24	9: $\{a_{Tij}, a_{0i5}, a_{Ti6}\}$	6: $\{a_{ij5}, a_{ij6}\}$
Lengths	20	19	5: $\{l_{Ti}, l_{T5}, l_{T6}\}$	9: $\{l_{ij}, l_{i5}, l_{i6}\}$

Table 7.1: Number of edges and triangles for the 5-valent tent move complex

The boundary of the tent move complex has 24 triangles and only 19 edges. Considering the ${\Gamma^t}_e$ matrix of derivatives of areas with respect to lengths we find one right null vector and six left null vectors.

Restricting to the data at time $T = 0$ we have $15 = (9 + 6)$ triangles and $14 = (5 + 9)$ edges. For this case we find that ${\Gamma^t}_e|_{T=0}$ has one right null vector and two left null vectors. The right null vector can indeed be identified with the 'missing' area a_{234}. That is, it represents the linearized expression for this area in terms of the length perturbations. The two left null vectors can be identified with the differences between a pair of 3D dihedral

angles in the shared tetrahedron as computed from the 4-simplex containing $v = 5$ and the 4-simplex containing $v = 6$, respectively.

Hence, as for the 3–3 move, the area boundary data do not completely determine the (length) geometry of the boundary. This allows for a dynamics that imposes vanishing deficit angles.

The fact that one of the areas is not available makes a transformation, similar to the one we performed for the 4-valent tent move, impossible. We already have non-metric degrees of freedom at a single time step, those picked out by the two left null vectors of $\Gamma^t{}_e(0)$ or of $\Gamma^t{}_e(1)$. Additionally there are non-metric degrees of freedom that can occur upon gluing the two time step complexes together.

As in the case of the 4-valent tent move we find exactly four null vectors for the Hessian block between variables at time $T = 0$ and at time $T = 1$. These four null vectors represent metric perturbations as they are in the image of the map Γ. Hence there are four constraints that result from each of the vertex translation symmetries of v_0 and v_1. This leaves five physical degrees of freedom that split into a metric perturbation (the fifth edge length) and four non-metric perturbations. The latter describe the (two) non-metric degrees of freedom appearing within an equal time hypersurface and another two degrees of freedom describing non-metricity due to time evolution. We also encountered this last type in the 4-valent tent move.

Length Regge calculus has only one physical degree of freedom in the 5-valent tent move: four of the edge lengths can be viewed as gauge parameters and the fifth as the physical degree of freedom.[5] In area Regge calculus we have four additional degrees of freedom that arise from the various ways non-metricities can occur, namely, within an equal time hypersurface and as a result of time evolution.

[5] A pair of phase space functions that commute with the constraints and thus represent Dirac observables can be defined using the methods of [28]. These observables can be made to give the values of the fifth edge length and its conjugated momentum at the point in the gauge orbit where the other four edge lengths have prescribed values.

Chapter 8

Non-metricity breaks diffeomorphism symmetry

For our explorations of the dynamics and of the symmetries of area Regge calculus we have so far assumed a metric background solution where the length variables can be consistently defined. For each four-simplex σ (and away from right angle configurations) we can define 10 functions L_e^σ, which depend on the 10 area variables A_t, and evaluate to the length of the edges e of the simplex. Metric configurations are such that the length functions for the same edge, but coming from different four-simplices, agree.

The presence of gauge symmetries depends on the solution one is considering: the gauge symmetries specify in which ways we can deform this solution and still obtain a solution to the equations of motion (with the same boundary data).

The dependence of the number of gauge symmetries on the solution appears, in particular, if we consider discretizations of continuum systems with gauge symmetries. Often, and certainly for diffeomorphism symmetry, discretization breaks these gauge symmetries. There may be, however, special solutions, e.g. flat space in (length) Regge calculus, which exactly mirror a solution of the continuum theory. In this case the gauge symmetries around this solution are preserved. A necessary and sufficient criterion for the existence of gauge symmetries is that the Hessian of the action, evaluated on this solution, has null vectors localized to the bulk degrees of freedom. Moving away from these special solutions there is no guarantee that the gauge symmetries still exist.

For (length) Regge calculus reference [121] identified the vertex translation symmetries as gauge symmetries using a flat background. This work also showed that the vertex translation symmetries can be matched in a continuum limit to the diffeomorphism symmetry

of the continuum. Motivated by these findings, [164] and other references argued that the vertex translation symmetries exist generally for (length) Regge calculus, i.e. for arbitrary backgrounds.

This turned out not to be the case. Reference [120] considered solutions with curvature and explicitly evaluated the Hessian of the Regge action on these solutions. This showed that the vertex translation symmetries are broken by curvature. More precisely, in the example considered in [120] the lowest eigenvalues grew quadratically with a deficit angle in the bulk of the triangulation.

The breaking of diffeomorphism symmetry has considerable repercussions for discrete quantum gravity approaches such as Regge calculus and spin foams [120, 165].

In a canonical quantization, diffeomorphism symmetry leads to constraints. A long-standing problem has been to provide an anomaly free representation of this constraint algebra in the quantum theory. The breaking of diffeomorphism symmetry by discretization, which is often used as a regulator, leads to inconsistent constraints. An alternative formulation, that of 'consistent discretizations' [161], is what we used here. In this framework broken gauge symmetries lead to pseudo-constraints, which are equations of motion that weakly couple the canonical data of neighboring time slices. (Constraints are equations of motion that involve the data of only one time.) The replacement of the constraints by pseudo-constraints means that one has more propagating degrees of freedom than in the continuum. Degrees of freedom that are gauge in the continuum are now physical. For example, in Regge calculus the position of the vertices in the embedding space–time become physical if vertex translation symmetry is broken.

In the covariant formalism, breaking diffeomorphism symmetry leads to an unwanted dependence on the choice of triangulation. In fact, in [125, 126] it was conjectured that diffeomorphism symmetry and triangulation invariance are equivalent and shown that diffeomorphism symmetry implies triangulation invariance for one-dimensional systems. Restoring diffeomorphism symmetry is crucial in order to remove discretization or regulator dependence [165].

To regain diffeomorphism symmetry the work [126] suggested the construction of an improved dynamics by coarse graining. The key point here is that, given fixed boundary data,[1] refinement of the triangulation leads to smaller deficit angles as the fixed total curvature is distributed over more simplices. Diffeomorphism symmetry is then violated to a lesser extent, and potentially restored, for an infinitely fine triangulation. One constructs

[1] Refinement and coarse graining of the boundary also plays an important role in the coarse graining process [139].

an effective action for a coarser triangulation by taking into account the dynamics of the finer one. As the coarse lattice now reflects the dynamics of the refined one, it also exhibits the same amount of diffeomorphism symmetry. Thus one can hope to restore diffeomorphism symmetry for the effective action in the infinite refinement limit.

This was illustrated successfully in [126] using the example of three-dimensional Regge calculus with a cosmological constant. Starting from a discretization with flat simplices, in which diffeomorphism symmetry is broken, the coarse graining procedure yielded as its fixed point an action describing simplices with homogeneous curvature. This action features diffeomorphism symmetry, is triangulation invariant, and leads to an anomaly free constraint algebra [23, 126].

This has triggered the development of a program for coarse graining spin foam models [115,135,141,165–170]. Here the hope is to construct amplitudes for which the regulator dependence is removed and that explicitly display diffeomorphism symmetry. As discussed above, one dynamical quantity that leads to a breaking of diffeomorphism symmetry is curvature, [120]. Spin foam models so far seem to display non-metricity (see the introduction section 1.2). The question we answer here is whether non-metricity can also lead to breaking of diffeomorphism symmetry. That it does could be expected due to the connection between triangulation (non-)invariance and (breaking of) diffeomorphism symmetry, and the fact that we found that the area Regge action is not invariant under two of the Pachner moves. Below we show explicitly that diffeomorphism symmetry is broken for non-metric solutions. This is important for spin foams as it necessitates understanding the dynamics of the non-metric degrees of freedom. It also explains the breaking of diffeomorphism symmetry and the triangulation dependence of the spin foam models conjectured to admit no curvature degrees of freedom. We explore the implications of these findings in more detail in the discussion, Section 10.

8.1 Constructing a non-metric solution

To analyze diffeomorphism symmetry for a non-metric solution we have to construct these solutions explicitly. We then evaluate the Hessian on such a background and check whether there are any vanishing eigenvalues. We could, for instance, consider two consecutive 4-valent tent moves such that we have a bulk vertex at the intermediate time step. But, there is a short cut we can exploit: in Section 7.2.1, where we analyzed the 4-valent tent moves, we showed that null vectors for the bulk Hessian lead to null vectors for the non-diagonal-in-time block of the Hessian for the piece of triangulation that is glued onto the initial triangulation. This piece of triangulation coincides with the initial configuration of the

4–2 Pachner move. It is therefore sufficient to consider this initial Pachner configuration and to evaluate a certain part of the Hessian of the associated action to see if any of its eigenvalues vanish.

To construct a solution with a non-metric area configuration we must first construct non-metric boundary data for the initial 4–2 Pachner move configuration. To this end we consider the matrix of derivatives $\Gamma^t{}_e = \partial A_t / \partial L_e$. Recall that this matrix identifies the vector space of non-metric area directions. Restricting to the set of boundary areas and boundary edge lengths of the triangulation, the left null vectors n^I_{bdry} of the corresponding matrix $(\Gamma^t{}_e)_{\text{bdry}}$ describe the boundary area non-metric directions. Here I labels which null vector is being considered.

Starting from a metric set of boundary areas A_t, we generate a set of non-metric boundary areas by adding multiples of these null vectors

$$A_{\text{bdry}} \to A^\kappa_{\text{bdry}} = A_{\text{bdry}} + \kappa_I \cdot n^I_{\text{bdry}}, \tag{8.1}$$

with κ_I arbitrary, but small parameters. The set of areas A^κ_{bdry}, for non-zero κ_I, are non-metric in the sense that the corresponding edge lengths are not well defined (i.e., the length of a single edge will have different values depending on which simplex it is computed from).

Having fixed the non-metric areas (8.1), we use them to construct a solution to the equations of motion. Here we use the equations of motion (6.7) derived from the first order action (6.6). These are solved for the dihedral angles $(\theta^\sigma_t)^\kappa$, a Lagrange multiplier Λ^κ_σ for each four–simplex σ, and the bulk area variables A^κ_{bulk}. By construction, the set of dihedral angles computed in this way will automatically be compatible with the areas and will satisfy the closure condition for each simplex σ. The equations of motion impose flatness for each of the bulk triangles.

We consider the initial configuration of the 4–2 Pachner move (see Fig. 7.4). The boundary of this configuration is made up of the two simplices $\sigma^0 = (1,2,3,4,5)$ and $\sigma^1 = (0,2,3,4,5)$, which share the tetrahedron $\tau = (2,3,4,5)$. There are 16 triangles and 14 edge lengths contained in this boundary. As in section 7.1.2, we consider the variable transformation (with $i,j,k \in \{2,3,4,5\}$ and $\alpha \in \{1,2\}$)

$$\big(\{A^\kappa_{0ij}\}, \{A^\kappa_{1ij}\}, \{A^\kappa_{kij}\}\big) \to \big(\{L^\kappa_{0i}\}, \{(\Phi^0_\alpha)^\kappa\}, \{L^\kappa_{1i}\}, \{(\Phi^1_\alpha)^\kappa\}, \{A^\kappa_{kij}\}\big) \quad , \tag{8.2}$$

but now for the fully non-perturbative variables (see Appendix J). Here $(\Phi^0_\alpha)^\kappa$ and $(\Phi^1_\alpha)^\kappa$ are the 3D dihedral angles for any choice of two adjacent edges in the tetrahedron shared by the two simplices in the final configuration of the 4–2 Pachner move, the first viewed from σ^1 and the second from σ^2. The difference between these dihedral angles, $\Delta\Phi^\kappa_\alpha := (\Phi^1_\alpha - \Phi^0_\alpha)^\kappa$, will make non-metricity transparent (c.f. Fig. 8.1).

We have chosen an asymmetric, metric background configuration with boundary edge lengths $L_{1i} = L_{04} = L_{05} = 1$, $L_{02} = \sqrt{\frac{8}{9}}$, and $L_{03} = \sqrt{\frac{9}{8}}$, with $i \in \{2, 3, 4, 5\}$. The matrix $(\Gamma^t{}_e)_{\text{bdry}}$ for this configuration has two left null vectors $n^I_{\text{bdry}}, (I \in \{1, 2\})$, the non-metric directions for these boundary areas. Using these null vectors, we construct the non-metric areas A^κ_t using (8.1) and then transform them to length and 3D dihedral angles, as in Eq. (8.2).

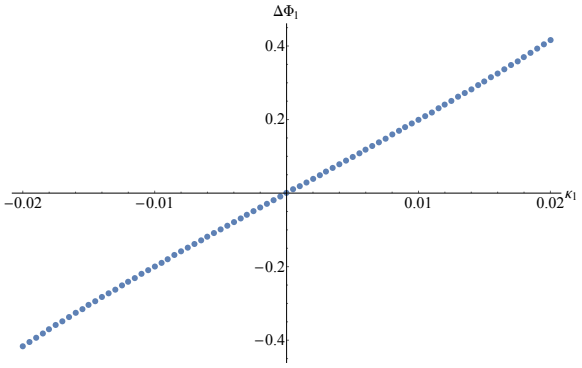

(a) $\Delta\Phi^\kappa_1$ vs. κ_1 at fixed $\kappa_2 = 0$.

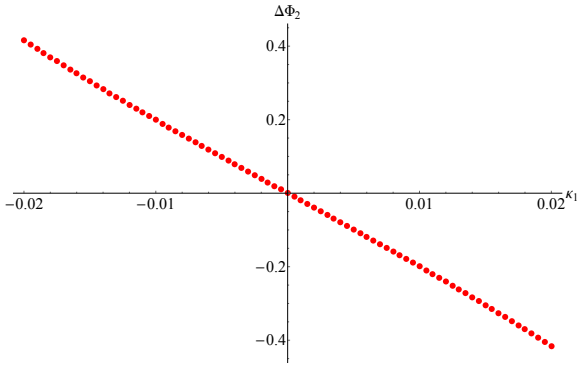

(b) $\Delta\Phi^\kappa_2$ vs. κ_1 at fixed $\kappa_2 = 0$.

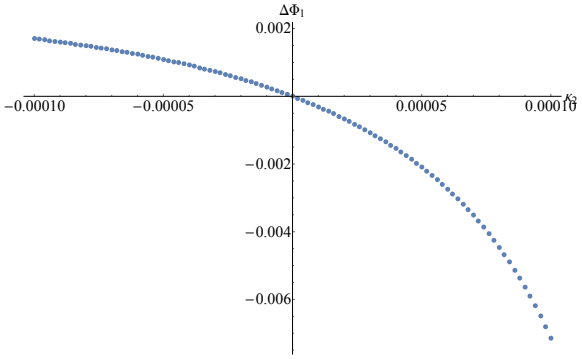

(c) $\Delta\Phi^\kappa_1$ vs. κ_2 at fixed $\kappa_1 = 0$.

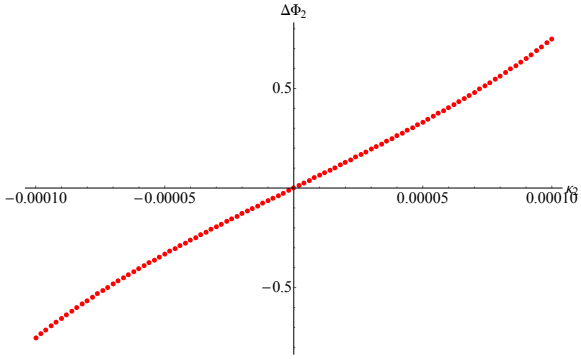

(d) $\Delta\Phi^\kappa_2$ vs. κ_2 at fixed $\kappa_1 = 0$.

Figure 8.1: Differences of the 3D dihedral angles $\Delta\Phi^\kappa_\alpha = \Phi^\kappa_\alpha(\sigma^0) - \Phi^\kappa_\alpha(\sigma^1)$ of tetrahedron $\tau(2, 3, 4, 5)$ computed from the simplices σ^0 and σ^1 as functions of the non-metricity parameters κ_I.

In Figure 8.1, we have plotted the two parameters $\Delta\Phi^\kappa_\alpha$ against κ_I for the edges (24) and (25). Fixing $\kappa_2 = 0$, $\Delta\Phi^\kappa_1$ increases linearly with κ_1 while $\Delta\Phi^\kappa_2$ decreases, see panels (a) and (b). On the other hand, fixing $\kappa_1 = 0$, $\Delta\Phi^\kappa_2$ grows monotonically with κ_2 and $\Delta\Phi^\kappa_1$ decreases monotonically, panels (c) and (d).

8.2 Breaking of diffeomorphism symmetry

Having produced a non-metric boundary configuration, we numerically solve for the bulk variables $(A^\kappa_{\text{bulk}}, (\theta^\sigma_t)^\kappa, \Lambda^\kappa_\sigma)$. These bulk variables belong to the configuration consisting of the four simplices $\sigma^2, \sigma^3, \sigma^4$, and σ^5 that share the bulk edge (01). We can now evaluate the Hessian of the area Regge action on these solutions, and, as in Section 7.2.1, compute an effective, linearized action for the 4-valent tent move, but now on a non-metric background. We find that the mixed time block of the effective Hessian is not singular for non-vanishing non-metricity parameters. In particular, all eigenvalues of the mixed time block of the Hessian are non-vanishing.[2] The gauge symmetries (vertex translation) are therefore broken by the non-metric boundary data.

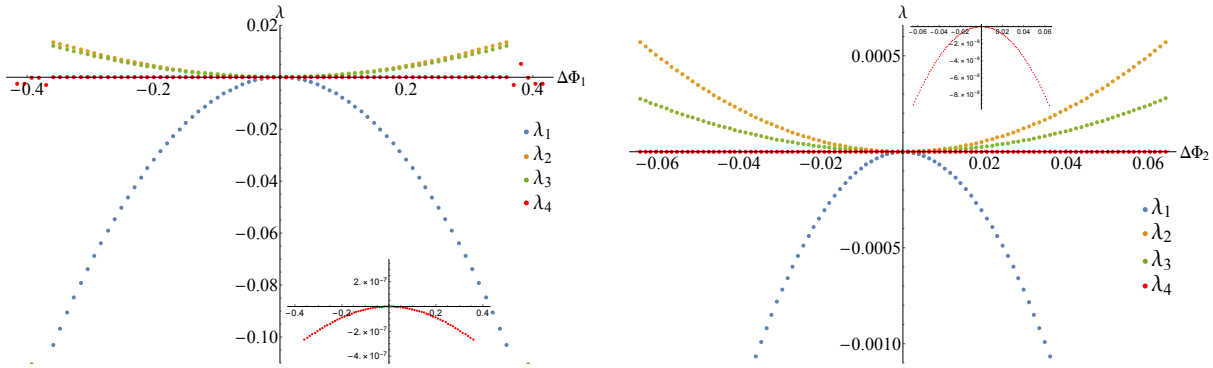

(a) The smallest eigenvalues as a function of $\Delta\Phi^\kappa_1$ with $\kappa_1 = 0$.

(b) The smallest eigenvalues as a function of $\Delta\Phi^\kappa_2$ with $\kappa_2 = 0$.

Figure 8.2: Eigenvalues of the mixed time block of Hessian as a function of $\Delta\Phi^\kappa_\alpha$. The lowest eigenvalues are zoomed in at the bottom right corner of (a) and the top right corner of (b) .

The panels of Figure N.1 show the four smallest eigenvalues as a function of the non-metricity parameters $\Delta\Phi^\kappa_\alpha$. We observe that all these eigenvalues, including the lowest eigenvalue λ_4 (shown with a separate scale), grow quadratically with the non-metricity parameters. Panel (a) is plotted at fixed $\kappa_1 = 0$, while panel (b) is for $\kappa_2 = 0$. Similar behaviors appear for the other two combinations of non-metricity parameter and κ_I. All

[2]Using the highly symmetric background from Section 7.1.2 as a starting point, one finds that 1 of the 4 eigenvalues, which vanished on a metric background, remains zero under a deformation to a non-metric boundary. Here we have a less symmetric configuration but, as it is close to the very symmetric background, one of the eigenvalues is growing slowly compared to the others.

the eigenvalues vanish identically only in the metric case $\Delta\Phi_1^\kappa = \Delta\Phi_2^\kappa = 0$ (or $\kappa_I = 0$). In practice the eigenvalues are computed numerically and never exactly vanish; at $\kappa_I = 0$ the two non-vanishing eigenvalues are seven orders of magnitude larger than the largest 'vanishing' eigenvalue.

We thus can conclude that the vertex translation symmetry, which is present on metric backgrounds, is broken for non-metric backgrounds. In the examples we considered here, the relevant Hessian eigenvalues grow quadratically with our non-metricity parameter, the difference of 3D dihedral angles seen from two different 4-simplices. This is similar to the findings on diffeomorphism breaking in length Regge calculus [120], where the eigenvalues also grew quadratically with one of the deficit angles in the bulk triangulation.

Chapter 9

Effective Spinfoam models

As already discussed in the introduction section 1.2, the quantization of quantum geometry based on areas as fundamental variables give a discrete area spectrum. This is because the area variables are conjugated to compact angles variables.[1] In spin foam models, which are discrete geometry path integrals derived from loop quantum gravity (LQG), area variables are fundamental and have discrete spectra. Area variables also play a central role in holography [58, 59], in particular, for the reconstruction of geometry from entanglement [60, 61]. Discrete area spectra are also key in many approaches to black hole entropy counting.

There is however, a tension between the choice of area variables and the dynamics of general relativity (GR): the area variables must be constrained to avoid a suppression of curvature. In this chapter, we will show that the discreteness of area spectra hinders the sharp imposition of these constraints.

Here we tackle directly the question of whether a discrete, locally independent, area spectrum is consistent with the dynamics of general relativity. To this end we propose a family of 'effective' models that (a) incorporate a discrete area spectrum, (b) impose the constraints between the areas as strongly as allowed by the LQG Hilbert space structure, and (c) use—more directly than current spin foam models—a discretized gravity action for the amplitudes.

These effective models allow us to show that the flatness problem can be overcome, but to do so also imposes certain restrictions involving the discretization scale, curvature per triangle, and the Barbero–Immirzi parameter, which controls the area spectral gap.

[1] We are considering here Euclidean signature geometries.

Future work will show whether this is sufficient to ensure general relativistic dynamics in the continuum limit.

9.1 Discrete, locally-independent areas

We will propose a path integral for 4D quantum gravity regulated by a triangulation of space–time. We work with quantum amplitudes for Euclidean signature simplices, leaving the Lorentzian case to future work. Our key assumption is that the areas have a discrete, prescribed spectrum. Further, we will take these area eigenvalues to be independent, more precisely (apart from triangle inequalities) the measured values in the kinematical Hilbert space will not depend on the state away from the measured triangle.

The particular area spectrum we work with is

$$A(j) = \gamma \ell_P^2 \sqrt{j(j+1)} \sim \gamma \ell_P^2 (j + 1/2), \tag{9.1}$$

where j is a half-integer (spin label), $\ell_P = \sqrt{8\pi\hbar G/c^3}$ is the Planck length, γ is the dimensionless Barbero-Immirzi parameter, and $\sim$ indicates the large-j asymptotic limit. We focus on the equispaced asymptotic spectrum. This form for the area spectrum was first established in LQG [49–51, 55–57], but discrete area spectra have been also discussed in the context of black hole spectroscopy [62].

Before taking up the path integral, we review the use of area variables in simplicial discretization of GR. These discretizations were first considered by Regge [25] and used length variables. A wide array of reformulations have been considered [3, 43, 44, 46, 47, 146, 147, 171], and we use descriptive adjectives to capture the variables used in each form. The change from length to area variables turns out to be far more subtle than one might expect. A treatment in the more transparent context of Regge calculus will illuminate the issues before discussing the path integral.

9.2 Actions for discretized gravity

To make this section self-contained, we will repeat and summarize discrete actions for gravity which were partially discussed in chapter 6. In length Regge calculus (LRC), the fundamental variables are lengths l_e assigned to edges e of a triangulation. The l_e determine

the triangle areas $A_t(l)$ and the 4D (internal)dihedral angles θ_t^σ in each 4-simplex σ. The action

$$S_{\text{LRC}} = \sum_t n_t \pi A_t(l) - \sum_\sigma \sum_{t \supset \sigma} A_t(l) \theta_t^\sigma(l) \equiv \sum_t S_t^l + \sum_\sigma S_\sigma^l \tag{9.2}$$

is a discretization of the Einstein-Hilbert action and the corresponding equations of motion approximate Einstein's equations [143]. The factor $n_t \in \{1, 2\}$ allows for triangulations with boundary and is 1 for triangles on the boundary and 2 for triangles in the bulk.

The 4-simplices, which are the basic building blocks of the triangulation, each have 10 edges and 10 triangles. One can thus (locally) invert the 10 functions $A_t(l)$ to give a simplex's areas in terms if its lengths. These functions will also depend on a discrete parameter that account for the multiple roots appearing in the inversion of $A_t(l)$. This discrete parameter is a summation variable for the (constrained) Area Regge path integral. To simplify notation we suppress this parameter here. We will denote the resulting functions $L_e^\sigma(A)$, where A collectively signifies the 10 areas associated to σ. This allows to define the Area Regge Calculus (ARC) action whose configuration with $A_t = A_t(l_e)$ agrees with the LRC action

$$S_{\text{ARC}} = \sum_t S_t^A + \sum_\sigma S_\sigma^A \tag{9.3}$$

where $S_t^A = n_t \pi A_t$ and $S_\sigma^A = S_\sigma^l(L_e^\sigma(A))$. Strikingly, freely varying the bulk action one finds the deficit angles $\epsilon_t = 2\pi - \sum_{\sigma \supset t} \theta_t^\sigma$, which measure curvature, have to vanish (see also chapter 6). That is the ARC equations of motion impose flatness.

Despite these equations of motion, the theory features propagating degrees of freedom, which are, however, of a non-geometrical nature. We have analyzed this is detail in section 6.3.1. These arise because the number of matching conditions, when gluing two 4-simplices, differ between LRC and ARC. For this gluing we need to identify the data of the shared tetrahedron. As it has six edges and four triangles we match six pairs of lengths in LRC, but only four pairs of areas in ARC.

This mismatch can be resolved by introducing 3D dihedral angles $\Phi_e^{\tau,\sigma}$ associated to edges e in the tetrahedron τ. These angles are determined by the lengths of the tetrahedron, and can also be expressed as functions of the areas A_t of the 4-simplex σ. They allow us to introduce two constraints per bulk tetrahedron

$$C_i^{\sigma,\sigma'}(A) = \Phi_{e_i}^{\tau,\sigma}(A) - \Phi_{e_i}^{\tau,\sigma'}(A) \quad i = 1, 2, \tag{9.4}$$

where (e_1, e_2) is any choice of a pair of non-opposite edges in τ. Together with matching of the four areas, the two matching conditions (9.4) ensure that the geometries imposed on

τ by σ, on the one hand, and by σ' on the other, agree. Varying the ARC action (9.3) on the corresponding constraint hypersurface gives equations of motion equivalent to LRC. (See Appendix L) The constraints (9.4) involve pairs of 4-simplices, and this makes the specification of free boundary data difficult.

This can be alleviated by introducing auxiliary variables that allow one to localize the constraints onto pairs of tetrahedra. Indeed, as the constraints feature 3D dihedral angles, it is natural to introduce these as explicit variables[2] $\phi^\tau_{e_i}, i = 1, 2$. We demand for each pair (τ, σ) with $\tau \subset \sigma$ the new constraints

$$C_i^{\sigma,\tau}(\phi, A) = \phi^\tau_{e_i} - \Phi^{\tau,\sigma}_{e_i}(A) \quad i = 1, 2. \tag{9.5}$$

This imposes the constraints (9.4) for each bulk tetrahedron and adds for each boundary tetrahedron two dihedral angles as boundary data as well as two constraints. In contrast to (9.4) the constraints (9.5) localize onto 4-simplices. This allows path integral amplitudes that factorize over the 4-simplices.

An even more local reformulation of the constraints isolates the conditions on the 3D boundary data. It uses the matching for the geometry of a triangle t induced by the neighbouring tetrahedra τ and τ', respectively. This geometry is specified by three variables, in addition to the area matching we need two constraints

$$C_k^{\tau,\tau'}(\phi, A) \;=\; \alpha^{t,\tau}_{v_k}(\phi, A) - \alpha^{t,\tau'}_{v_k}(\phi, A) \quad k = 1, 2, \tag{9.6}$$

where $\alpha^{t,\tau}_{v_k}$ denotes the 2D angles at two vertices v_1, v_2 of t, determined by the geometric data of τ. Imposing the constraints (9.6) for all 10 pairs of neighbouring tetrahedra (τ, τ') in a simplex σ is equivalent[3] to imposing the constraints (9.5) for all 5 tetrahedra in σ [44].

The original form of Area Angle Regge Calculus (AARC) [44] featured the constraints (9.6). These specify in concrete terms the enlargement of the LQG phase space [53, 71] as compared to the LRC phase space [45]. We will however see that it is much easier to implement the versions (9.5) into the path integral. Armed with these understandings, we take up the path integral.

9.3 Path integral

Next, we construct a path integral quantization, which is based on the Constrained Area Regge formulation. To incorporate a discrete area spectrum (9.1), we parametrize areas

[2] Here we introduce two dihedral angles per tetrahedron. One can also introduce all six dihedral angles, but would then have to add four closure constraints per tetrahedron [44].

[3] There are (10) redundancies between the (20) constraints (9.6) associated to a simplex.

by spins, and thus sum over the spin labels j_t:

$$\mathcal{Z} \;=\; \sum_{\{j_t\}} \mu(j) \prod_t \mathcal{A}_t(j) \prod_\sigma \mathcal{A}_\sigma(j) \prod_{\tau\in\text{blk}} G_\tau^{\sigma,\sigma'}(j)\,. \tag{9.7}$$

Here

$$\mathcal{A}_t = \exp(\mathrm{i}\gamma\, X \pi(j_t + \tfrac{1}{2})) \tag{9.8}$$

is the weight for the bulk (with $X = 2$) and boundary ($X = 1$) triangles. The simplex amplitude is

$$\mathcal{A}_\sigma = \exp\left(-\mathrm{i}\gamma \sum_{t\in\sigma} (j_t + \tfrac{1}{2})\theta_t^\sigma(j)\right) T_\sigma(j)\,, \tag{9.9}$$

where $T_\sigma(j) = 1$, if the lengths defined by the areas satisfy the generalized triangle inequalities[4], and is vanishing otherwise. The precise form of the measure factor $\mu(j)$ will not be important for the discussion here.[5] The product over the $\mathcal{A}_t$ and $\mathcal{A}_\sigma$ amplitudes gives the exponentiated Area Regge action.[6]

The factors $G_\tau^{\sigma,\sigma'}$ implement the constraints (9.4), and are therefore crucial for imposing the dynamics of length Regge calculus (LRC) instead of area Regge calculus (ARC).

However, imposing the constraints (9.4) sharply, i.e. setting $G_\tau^{\sigma,\sigma'}(j) = 1$ if the constraints are satisfied, and $G_\tau^{\sigma,\sigma'}(j) = 0$ otherwise, leads to a severe problem: As we allow only discrete (asymptotically equispaced) values for the areas, the constraints (9.4) constitute diophantine conditions for the spin labels. These can only be satisfied for a very small set of labels with accidental symmetries, e.g. if all 10 pairs of labels match. The resulting reduction in the density of states prevents a suitable semiclassical limit.

One way out is to weaken the constraints (9.4), e.g. by allowing a certain error interval. But, one has to navigate between Scylla—reducing too much the density of states—and Charybdis—imposing a dynamics which does not match GR.

Here we will take guidance from loop quantum gravity. The associated phase space includes areas a_t and 3D dihedral angles ϕ_e^τ as variables [53,66,67]. Crucially, the 3D dihedral

[4]The squared volumes of the various sub-simplices of σ and of σ itself, as defined by the appropriate Caley-Menger determinants, has to be non-negative.

[5]It can be specified by requiring a discrete remnant of (approximate) diffeomorphism invariance [26].

[6]One can also describe a version where one sums over orientation and thus the exponential is replaced by a cosine.

angles at two non-opposite edges (e_1, e_2) in a tetrahedron τ do not Poisson commute

$$\hbar\{\phi^\tau_{e_1}, \phi^\tau_{e_2}\} = \ell_P^2\gamma\frac{\sin\alpha_v^{t,\tau}}{A_t} = \frac{\sin\alpha_v^{t,\tau}}{(j_t+\frac{1}{2})}\,, \tag{9.10}$$

where $\alpha_v^{t,\tau}$ is the angle between (e_1, e_2). (See appendix K for a proof.) This non-commutativity[7] arises as the geometry of a tetrahedron is encoded into the set of normals to its triangles, which are then quantized as (non-commuting) angular momentum operators [55, 56, 173, 175, 176].

Respecting the uncertainty relations resulting from (9.10), we can impose the constraints only weakly. To achieve an as-strong-as-possible imposition we will employ coherent states in the angle variables. There are different constructions available for tetrahedral states[8] that are coherent in the two degrees of freedom encoding the 3D dihedral angles, but are eigenstates for the area operators [77, 177–179]. We will denote such states $\mathcal{K}_\tau(\phi_1, \phi_2; \Phi_1, \Phi_2)$, where (ϕ_1, ϕ_2) are the arguments of the wave functions and (Φ_1, Φ_2) are the angles on which the wave function is peaked. With the associated measure $d\mu^\tau_{\mathcal{K}}(\phi_1, \phi_2)$ we define

$$\mathcal{Z}' \;=\; \sum_{\{j_t\}}\mu(j)\int\prod_\tau d\mu^\tau_{\mathcal{K}}(\phi)\prod_t\mathcal{A}_t(j)\prod_\sigma\mathcal{A}'_\sigma(j,\phi)\,, \tag{9.11}$$

where the new simplex amplitude[9] is given by

$$\mathcal{A}'_\sigma(j,\phi) = \mathcal{A}_\sigma(j)\prod_{\tau\in\sigma}\mathcal{K}_\tau(\phi^\tau_{e_i}; \Phi^{\tau,\sigma}_{e_i}(j))\,. \tag{9.12}$$

Integrating out the dihedral angles for the bulk tetrahedra we regain—modulo boundary contributions[10]—a path integral of the form (9.7) where now

$$G^{\sigma,\sigma'}_\tau(j) = \langle\mathcal{K}_\tau(\cdot; \Phi^{\tau,\sigma}_{e_i}(j)) \,|\, \mathcal{K}_\tau(\cdot; \Phi^{\tau,\sigma'}_{e_i}(j))\rangle\,. \tag{9.13}$$

This inner product is peaked on the matching conditions (9.4) and provides a precise sense in which these conditions are weakly imposed.

[7] This Poisson bracket (with $\gamma = 1$) also appears in the Kapovich-Millson phase space describing linkages [172]. This phase space can be used to describe the space of shapes of a tetrahedron with fixed areas [55, 56, 173]. This non-commutativity was anticipated early on in the length picture [174].

[8] These are states on the intertwiner Hilbert space $\mathcal{H}_{\{j_i\}} = \mathrm{Inv}\left(\otimes_{i=1}^4 V_{j_i}\right)$, where V_j is a spin-j representation space for $SU(2)$ and Inv denotes invariance under the global $SU(2)$ action.

[9] Here we assume that the tetrahedra have an outward orientation. Changing the orientation leads to a complex conjugated $\mathcal{K}_\tau$.

[10] These are given by a coherent state $\mathcal{K}_\tau$ for each boundary tetrahedron.

To further simplify the models we can approximate $G_\tau^{\sigma,\sigma'}$ by, e.g., Gaussians in the angles $\Phi_{e_i}^{\tau,\sigma}$. Even more drastically, to count the number of configurations not suppressed by the $G_\tau^{\sigma,\sigma'}$ factor we approximate it with a Heaviside function. That is, we allow $(\Phi_{e_i}^{\tau,\sigma}, \Phi_{e_i}^{\tau,\sigma'})$ to mismatch by as much as

$$\sigma(\Phi) = \beta\sqrt{\ell_P^2\gamma\frac{\sin\alpha_v^{t,\tau}}{A_t}} = \beta\sqrt{\frac{\sin\alpha_v^{t,\tau}}{(j_t+\frac{1}{2})}}\ . \tag{9.14}$$

Here we have introduced a parameter β which can be tuned between (unconstrained) Area Regge dynamics and a sharp imposition of the matching constraints.

We have also used this criterion to determine the number of allowed configurations on a complex of two glued 4-simplices, see Appendix M. The configuration we have studied is symmetry reduced wtih 3 length and 3 area parameters on each of its simplices. For the two glued simplices there are 4 length and 5 area parameters. The number of length configurations for the two glued simplices, with area values $A_t \in \{\frac{1}{2}, 1, \cdots, N\}$, scales as $N^{1.03\times p}$, where $p = 3$ for $\beta = 0$ (the shape matching constraints hold exactly), and $p = 5$ for $\beta = \infty$ (the shape matching conditions need not hold). A scaling with N^4 arises for $\beta \approx 0.15$. We also considered just one (symmetry reduced) simplex with $p = 2, 3$ and 4 lengths and area parameters. The number of configurations scales with $N^{1.03\times p}$. This test suggests that the weakened matching condition (9.14) does lead to a reasonable number of configurations.

9.4 Relation to spin foams

Spin foams arise from a discretized $SO(4)$-gauge formulation of GR [54]. The main object is a simplex amplitude [76] depending on the spin labels j_t and, for the more recent models [180], on intertwiner labels associated to the tetrahedra. A number of key works have shown that in the limit of large spins the simplex amplitude includes saddle points peaked on the cosine of the Regge action [85, 86, 89, 113, 181, 182]. The cosine results from a sum over orientation, in addition there are further saddle points describing degenerate simplex configurations. In practice the large spin limit is already obtained with spin values around $j = 10$.

The simplex amplitudes require, however, a huge effort for their numerical evaluation [183], and this has hindered deeper insight into the dynamics of spin foams, including a resolution of the flatness problem [83, 88, 105–109]. Other open questions include whether

summing over orientations[11] or including degenerate configurations prevent a suitable semiclassical dynamics [109, 184, 185].

Here we rather propose to test a key assumption of LQG, namely a Hilbert space describing independent area variables with a discrete (asymptotically equidistant) spectrum. As we have argued, this allows only a weak imposition of the shape matching constraints. It is not clear whether such a weak imposition is consistent with a (semiclassical) gravitational dynamics. To tackle this question, we need workable amplitudes. Thus we propose to use, instead of the involved spin foam simplex amplitudes, the exponentiated (Area) Regge action[12] together with a mechanism to impose the shape matching constraints. If it becomes clear that such a model leads to a gravitational dynamics, one can go to more complicated versions, and e.g. study the effects of including a sum over orientations.

In the following we will elaborate more on a possible relation of our proposed family of models to various spin foam models. Note that the large j limit of the spin foam amplitudes reveals only a limited amount of information. For example, one finds that for the EPRL-FK models the saddle point conditions include the shape matching equations (9.6) for non-degenerate configurations [85, 86, 89, 113, 181, 182]. However, it is not known how weakly or strongly these constraints are imposed [109]. Another possible source for flatness problems is the imposition of the closure (Gauß) constraints [83, 88, 105–109]. Here we disregard possible issues with the Gauß constraints and assume that the shape matching constraints are as strongly implemented as allowed by the LQG kinematics.

The first spin foam amplitude, known as the Barrett-Crane (BC) model [76], featured only a sum over areas (no sum over 3D dihedral angles). In this model amplitudes factorize over simplices and thus cannot include a gluing factor $G_\tau^{\sigma,\sigma'}$, as in our proposal (9.7). It is therefore conjectured that the BC model describes the dynamics of ARC [3, 43]. Thus, including the factors (9.13) can be seen as correcting the BC model.[13]

A newer class of models [180], known as EPRL-FK, include a summation over area and angle variables. Crucially the boundary Hilbert space for these models is the LQG Hilbert space. With the assumptions outlined above for these spin foam models, we conjecture that our model (9.11) describes the behavior of these models for larger spins, if sums over orientations and degenerate configurations can be ignored.

[11] In 3D the sum over orientations still allows for a semiclassical and continuum limit, which reproduces continuum GR [35].

[12] Another possibility is to not take the exponentiated area Regge action as the simplex amplitude $\mathcal{A}_\sigma$, but an action resulting from a gauge-reduced SU(2) BF theory, which involves areas and 3D dihedral angles and leads to a topological theory.

[13] This would also lead to a boundary Hilbert space coinciding with the LQG Hilbert space (with $\gamma = 1$).

A special feature for our model (9.11) is that it includes an integration over two dihedral angles per tetrahedron. These two dihedral angles are encoded into only one quantum number (e.g. if one uses a spin network basis). This is why the coherent states are crucial: using a Segal-Bargmann (like) transform one can change the amplitudes and integration from two variables to one quantum number per tetrahedron. This will then allow a more direct comparison with the EPRL-FK amplitudes.

Instead of a gauge formulation, one can also employ a higher gauge formulation to study gravity [6, 186, 187]. A related topological state sum model [6, 188] features an amplitude factor given by the cosine of the Regge action (without having to take a semiclassical limit). But the model sums over both (discrete) area variables and (continuous) length variables. Constraining the areas to be functions of the lengths one does obtain a formulation of gravity. However, insisting on discrete areas leads to the same problem as discussed here [187], namely a drastic reduction in the density of states. In fact, a canonical analysis [189] reveals that the corresponding constraint system is, like the shape matching constraints, second class.

9.5 On the flatness problem

We now take up the question of whether the constraints are implemented sufficiently strongly to avoid flatness. We consider a first test case consisting of a triangulation where we can control the scale for the bulk area variable and the bulk curvature through the boundary data. Specifically we consider a complex consisting of three 4-simplices sharing a (bulk) triangle. There are no bulk edges, thus no bulk variables to sum over in LRC, and the (bulk) deficit angle is determined by the boundary lengths. Nonetheless in ARC, there is one bulk variable to sum over, which imposes a vanishing deficit angle for the internal triangle.

The shape matching constraints restrict the (effective) summation range for the area variable and the question arises as to whether this restriction is sufficient to allow for a non-vanishing expectation value for the bulk deficit angle.

In the following we will perform a more detailed analysis and identify a regime in which curved configurations can dominate. We will be applying only scaling arguments and approximate the imposition of the constraints with Gaussians. For the minimal triangulations investigated here, the boundary spins j and the bulk spins j_{blk} have similar scaling, that is $j \sim j_{\text{blk}}$; future work will show how these scales separate in larger triangulations.

From (9.14) we see that the G- functions come with a deviation scaling as $\sigma(\Phi) \sim 1/\sqrt{j}$

for the 3D dihedral angle, where we assume that the boundary areas have approximately equal values determined by the spin value j. Meanwhile, as the dihedral angles $\Phi(j)$ and deficit angles $\epsilon(j)$ are dimensionless, their derivatives scale as $\partial\Phi/\partial j_{\rm blk} \sim 1/j$ and $\partial\epsilon/\partial j_{\rm blk} \sim 1/j$. Thus the deviation $\sigma(j_{\rm blk})$ for the (bulk) spin labels and the deficit angle ϵ will scale as

$$\begin{aligned} \sigma(j_{\rm blk}) &\sim \left[\frac{\partial\Phi(j_{\rm blk})}{\partial j_{\rm blk}}\right]^{-1} \times \sigma(\Phi) \sim j \times \frac{1}{\sqrt{j}} = \sqrt{j}\,, \\ \sigma(\epsilon) &\sim \left[\frac{\partial\epsilon(j_{\rm blk})}{\partial j_{\rm blk}}\right] \times \sigma(j_{\rm blk}) \sim \frac{1}{j} \times \sqrt{j} = \frac{1}{\sqrt{j}}\,. \end{aligned} \tag{9.15}$$

As angles are invariant under global rescaling, we can choose boundary data that induce a given deficit angle ϵ, and then choose a sufficiently large scale j, so that the $\epsilon = 0$ value is outside the deviation interval. Thus by going to sufficiently large spins j, the constraint part of the amplitudes can peak sharply on non-vanishing curvature values.

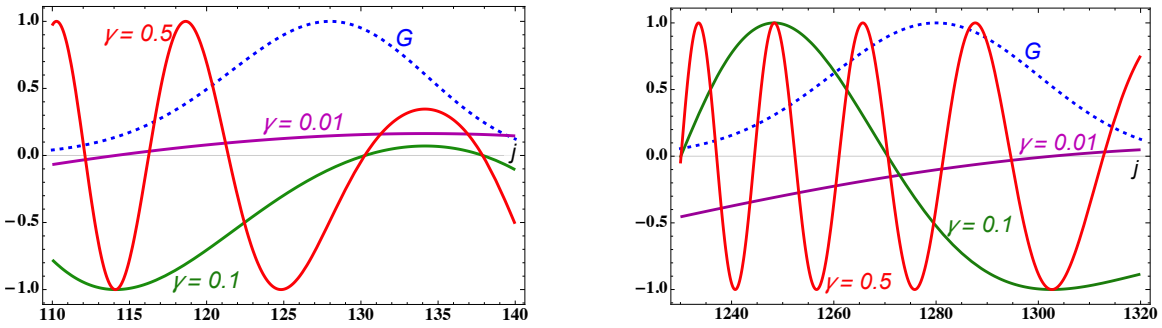

(a) $j = 99.5$ (b) $j = 999.5$

Figure 9.1: The G function (dashed), which imposes the matching conditions weakly, and the real part of the product of the amplitude factors $\mathcal{A}_t$ and $\mathcal{A}_\sigma$ as a function of the bulk spin $j_{\rm blk}$. The solid graphs show the amplitude for $\epsilon \approx 0.5$. Larger γ's lead to a more oscillatory behaviour. This example is described in more detail in Appendix **B**.

The oscillatory behavior resulting from the variation of the action over the $\sigma(j_{\rm blk})$ interval should also be considered, see Fig. 9.1. Having a highly oscillatory amplitude, the expectation value for the deficit angle will average out to some value different from the one in LRC. As the action scales with the spin j, this in particular applies in the large j-limit (away from the stationary points of the ARC action).

This large j-limit is often identified with the semi classical limit for spin foams. The condition for stationary of the ARC action leads to the flatness—and thus to the flatness

problem. To avoid this mechanism, we demand a bound n the variation of the action. The corresponding contribution to the LRC path integral is rather given by a fixed value of the amplitude, therefore, we demand that

$$\sigma(\tfrac{S_{\mathrm{ARC}}}{\ell_P^2}) = \frac{1}{\ell_P^2}\frac{\partial(S_{\mathrm{ARC}})}{\partial j_{\mathrm{blk}}} \times \sigma(j_{\mathrm{blk}}) \sim \gamma\epsilon\sqrt{j} \overset{!}{\lesssim} \mathcal{O}(1)\,. \tag{9.16}$$

Thus, whereas the scaling for the deficit angle (9.15) requires a choice of larger j, (9.16) demands that with growing j we choose smaller γ. These expectations are confirmed by an explicit example, see Appendix N.

To distinguish a small ϵ from a vanishing ϵ we also need—due to $\sigma(\epsilon) \sim 1/\sqrt{j}$—a scaling with $|\epsilon| \sim 1/\sqrt{j}$. Thus choosing smaller γ, which makes the area spectrum denser, allows for a larger range of accessible curvature angles.

We can also interpret (9.16) as a bound on the curvature per triangle $\epsilon \lesssim 1/(\gamma\sqrt{j})$, which—uncharacteristically—decreases with increasing j, the discretization scale. Note that a similar bound has been derived by [190] for the EPRL model using an improved version of the saddle point analysis. Here we have shown that this restriction holds for a broad range of models, which implement a (locally independent) almost equidistant area discrete spectra as encountered in LQG.

We have considered the simplest triangulation that differentiates between LRC and ARC. As we only employed scaling arguments, the conclusions apply also for larger triangulations. For larger triangulations, however, the scale set by the boundary spins will not determine a unique scale for the bulk spins that lead to significant amplitude contributions. Larger triangulations must, therefore, be studied explicitly. In future work we will investigate examples including bulk edges and bulk vertices. Finally, to make definite conclusions on the continuum limit it will be necessary to see how the implementation of the constraints changes under refining and coarse graining. The models proposed here simplify this task considerably.

Chapter 10

Discussion

With the aim of reaching a better understanding of spin foam dynamics, we have revisited area Regge calculus. We have provided a well-defined action principle for flat, as well as homogeneously curved, simplices and analyzed certain aspects of the covariant dynamics, in particular, the behavior of area Regge calculus under Pachner moves. The invariance properties of area Regge calculus under these moves differ from those of length Regge calculus. Obtaining a semiclassical limit of Pachner moves seems feasible for spin foams [102,191–193], and so our results can be used as a test to differentiate between the different types of dynamics in spin foam models.

Interestingly, the equations of motion can impose flatness in the 3–3 move even when boundary data would seem to induce curvature. This is due to the surprising fact that, although there are more area than length variables in the boundary, the boundary areas do not always uniquely determine the boundary lengths.

We have also performed a canonical analysis of area Regge calculus using tent moves. For the linearized dynamics over a metric background we find the constraints resulting from the diffeomorphism symmetry of the (linearized) action. The same constraints arise for (linearized) length Regge calculus on a flat background. We have not found additional constraints. As there are generically far more areas than lengths, area Regge calculus has far more physical degrees of freedom then length Regge calculus. In particular, for an n–valent tent move we expect $3n-10$ physical degrees of freedom in area Regge calculus and $n-4$ physical degrees of freedom in length Regge calculus. We have provided an in-depth analysis of how the non-metric degrees of freedom appear and discussed how they can be parametrized in the 4-valent tent move. Our results suggest that the differences of 3D dihedral angles as determined from different four-simplices is a good measure for the

non-metricity in general.

We analyzed the gauge symmetry content of area Regge calculus and found that on metric backgrounds area Regge calculus features (discrete remnants of) diffeomorphism symmetry. These symmetries are broken if one considers non-metric backgrounds. The breaking can be quantified via the size of the eigenvalues of the Hessian evaluated on these backgrounds. There is a quadratic dependence on our non-metricity parameter, the difference of certain 3D dihedral angles.

We also considered in the quantum theory a path integral formulation with discrete area spectra. Area operators are central in a number of approaches to 4D quantum gravity, notably LQG and holography. Discrete area spectra are a key result of LQG and crucial for various black hole entropy countings [62–65]. To achieve a quantum dynamics that reproduces GR constraints between the areas need to hold. This is, however, hindered if areas have an asymptotically equispaced spectrum and are (kinematically) locally independent.

The imposition of these constraints is pivotal in spin foam quantization. This leads to highly involved amplitudes, which has so far prevented a satisfactory resolution of key dynamical questions, most pressingly whether the models suppress curvature excitations. Here we proposed a class of effective models, with a transparent encoding of the dynamics and much more amenable for numerical investigations. In these models the constraints are imposed as strongly as allowed by the LQG Hilbert space structure, from which the discrete, locally independent, area spectra result. We emphasize 'locally independent' for the following reason: strong imposition of the constraints (that is, first solving the constraints classically and then quantizing the reduced phase space) should also lead to a discrete area spectrum. This follows from Bohr's correspondence principle, as the areas are also conjugated to (dihedral) angles on the reduced phase space. However, the Dirac brackets, which define the canonically conjugated pairs, have a non-local structure [53, 66, 67, 189] and one would expect a reflection of this non-locality in the resulting Hilbert space.

Insisting on the local structure of the (kinematical) Hilbert space and a prescribed area spectrum we can impose the constraints only weakly. Whether such a weak imposition of second class constraints leads to the correct dynamics is not understood (even in much simpler models than gravity) and should be further tested. In particular, for spin foam models, a too weak imposition of the constraints could lead to suppression of curvature.

Using the effective spin foam models we have found that for triangulations in which the scale for the areas can be controlled, curvature is not necessarily suppressed. This result comes with restrictions connecting the average area $a \sim \ell_P^2 \gamma j$, the Barbero-Immirzi parameter γ, and the curvature ϵ_t per triangle. The peakedness of the constraints on a given curvature value does improve with growing spin j, as $1/\sqrt{j}$, but is independent of γ.

And, to avoid a highly oscillatory behaviour of the amplitudes over the regime allowed by the constraints, we need $\gamma\sqrt{j}\epsilon_t \leq \mathcal{O}(1)$. Not surprisingly, this last condition prefers small γ, and hence a small spacing in the area spectrum. Furthermore, it can be seen as a bound on curvature, one which is more stringent for larger spins.

In our example, in Appendix N we need large spin values (and correspondingly small γ) to obtain an expectation value for the deficit angle that approximates well the classical value. This justifies our focus on 'effective' models, where we replace the full spin foam simplex amplitude with its large spin asymptotics, given by the cosine (replaced here with the exponential) of the Regge action. It has been argued in [194], that a double scaling limit that takes γ small and spins j large, with γj fixed, reproduces the Length Regge equations of motion. Here, we find also that γ should be small and j large, but that we need for the combination $\gamma\sqrt{j}\epsilon_t$ to be of order one or smaller. Such a combination, and the related bound on curvature has also been identified in [190], based on a generalized stationary phase analysis of the EPRL/FK amplitudes. Using much simpler inputs, we have shown that such a bound does not depend on specific choices for the spin foam amplitudes. The reason for this bound is rather tied to the LQG Hilbert space and the area spectrum it leads to. On this Hilbert space the shape matching constraints are non-commutative and can therefore be imposed only weakly.

The conclusions for the expectation value of the deficit angle hold in general, but assume that we can control the scale of bulk spin and deficit angles, e.g. via the choice of boundary data. This is not necessarily the case for larger triangulations. Moreover, to understand the continuum limit, we would have to investigate how these arguments are impacted by a coarse graining and renormalization process [195]. The investigation of corresponding continuum actions [196], in which the geometricity (simplicity) constraints are also imposed only weakly, might elucidate how these constraints behave under renormalization.

The effective models presented here will make the study of the coarse graining and renormalization flow [195] much more feasible than for the full spin foam models [180] and will help to establish whether loop quantum gravity and spin foams allow for a satisfactory continuum limit.

References

[1] S. K. Asante, B. Dittrich, and F. Hopfmueller, *Holographic formulation of 3D metric gravity with finite boundaries*, *Universe* **5** no. 8, (2019) 181, arXiv:1905.10931 [gr-qc].

[2] S. K. Asante and B. Dittrich, *One-loop partition functions for bounded regions and perfect discretizations for 4D gravity*,. To appear.

[3] S. K. Asante, B. Dittrich, and H. M. Haggard, *Holographic description of boundary gravitons in (3+1) dimensions*, *JHEP* **01** (2019) 144, arXiv:1811.11744 [hep-th].

[4] S. K. Asante, B. Dittrich, and H. M. Haggard, *The Degrees of Freedom of Area Regge Calculus: Dynamics, Non-metricity, and Broken Diffeomorphisms*, *Class. Quant. Grav.* **35** no. 13, (2018) 135009, arXiv:1802.09551 [gr-qc].

[5] S. K. Asante, B. Dittrich, and H. M. Haggard, *Effective Spin Foam Models for Four-Dimensional Quantum Gravity*, arXiv:2004.07013 [gr-qc].

[6] S. K. Asante, B. Dittrich, F. Girelli, A. Riello, and P. Tsimiklis, *Quantum geometry from higher gauge theory*, *Classical and Quantum Gravity* (07, 2020) , arXiv:1908.05970 [gr-qc].

[7] R. Oeckl, *A 'General boundary' formulation for quantum mechanics and quantum gravity*, *Phys. Lett. B* **575** (2003) 318–324, arXiv:hep-th/0306025.

[8] E. Witten, *(2+1)-Dimensional Gravity as an Exactly Soluble System*, *Nucl. Phys. B* **311** (1988) 46.

[9] E. Witten, *Quantum Field Theory and the Jones Polynomial*, *Commun. Math. Phys.* **121** (1989) 351–399.

[10] G. Moore and N. Seiberg, *Taming the conformal zoo*, *Physics Letters B* **220** no. 3, (1989) 422 – 430.

[11] S. Elitzur, G. W. Moore, A. Schwimmer, and N. Seiberg, *Remarks on the Canonical Quantization of the Chern-Simons-Witten Theory*, *Nucl. Phys. B* **326** (1989) 108–134.

[12] P. Forgacs, A. Wipf, J. Balog, L. Feher, and L. O'Raifeartaigh, *Liouville and Toda Theories as Conformally Reduced WZNW Theories*, *Phys. Lett. B* **227** (1989) 214–220.

[13] A. Alekseev and S. L. Shatashvili, *Path Integral Quantization of the Coadjoint Orbits of the Virasoro Group and 2D Gravity*, *Nucl. Phys. B* **323** (1989) 719–733.

[14] O. Coussaert, M. Henneaux, and P. van Driel, *The Asymptotic dynamics of three-dimensional Einstein gravity with a negative cosmological constant*, *Class. Quant. Grav.* **12** (1995) 2961–2966, arXiv:gr-qc/9506019.

[15] A. Maloney and E. Witten, *Quantum Gravity Partition Functions in Three Dimensions*, *JHEP* **02** (2010) 029, arXiv:0712.0155 [hep-th].

[16] J. Cotler and K. Jensen, *A theory of reparameterizations for AdS_3 gravity*, *JHEP* **02** (2019) 079, arXiv:1808.03263 [hep-th].

[17] G. Barnich, A. Gomberoff, and H. A. González, *Three-dimensional Bondi-Metzner-Sachs invariant two-dimensional field theories as the flat limit of Liouville theory*, *Phys. Rev. D* **87** no. 12, (2013) 124032, arXiv:1210.0731 [hep-th].

[18] S. Carlip, *Dynamics of asymptotic diffeomorphisms in (2+1)-dimensional gravity*, *Class. Quant. Grav.* **22** (2005) 3055–3060, arXiv:gr-qc/0501033.

[19] K. Bautier, *Diffeomorphisms and Weyl transformations in AdS(3) gravity*, *PoS* **tmr99** (1999) 006, arXiv:hep-th/9910134.

[20] K. Skenderis and S. N. Solodukhin, *Quantum effective action from the AdS / CFT correspondence*, *Phys. Lett. B* **472** (2000) 316–322, arXiv:hep-th/9910023.

[21] S. Giombi, A. Maloney, and X. Yin, *One-loop Partition Functions of 3D Gravity*, *JHEP* **08** (2008) 007, arXiv:0804.1773 [hep-th].

[22] G. Barnich, H. A. Gonzalez, A. Maloney, and B. Oblak, *One-loop partition function of three-dimensional flat gravity*, *JHEP* **04** (2015) 178, arXiv:1502.06185 [hep-th].

[23] V. Bonzom and B. Dittrich, *3D holography: from discretum to continuum*, *JHEP* **03** (2016) 208, arXiv:1511.05441 [hep-th].

[24] G. Barnich, A. Gomberoff, and H. A. Gonzalez, *The Flat limit of three dimensional asymptotically anti-de Sitter spacetimes*, *Phys. Rev. D* **86** (2012) 024020, arXiv:1204.3288 [gr-qc].

[25] T. Regge, *GENERAL RELATIVITY WITHOUT COORDINATES*, *Nuovo Cim.* **19** (1961) 558–571.

[26] B. Dittrich and S. Steinhaus, *Path integral measure and triangulation independence in discrete gravity*, *Phys. Rev. D* **85** (2012) 044032, arXiv:1110.6866 [gr-qc].

[27] B. Dittrich, *Partial and complete observables for canonical general relativity*, *Class. Quant. Grav.* **23** (2006) 6155–6184, arXiv:gr-qc/0507106.

[28] B. Dittrich, *Partial and complete observables for Hamiltonian constrained systems*, *Gen. Rel. Grav.* **39** (2007) 1891–1927, arXiv:gr-qc/0411013.

[29] C. Pagani and M. Reuter, *Composite Operators in Asymptotic Safety*, *Phys. Rev. D* **95** no. 6, (2017) 066002, arXiv:1611.06522 [gr-qc].

[30] M. Becker and C. Pagani, *Geometric operators in the asymptotic safety scenario for quantum gravity*, *Phys. Rev. D* **99** no. 6, (2019) 066002, arXiv:1810.11816 [gr-qc].

[31] B. Dittrich, C. Goeller, E. Livine, and A. Riello, *Quasi-local holographic dualities in non-perturbative 3d quantum gravity I – Convergence of multiple approaches and examples of Ponzano–Regge statistical duals*, *Nucl. Phys. B* **938** (2019) 807–877, arXiv:1710.04202 [hep-th].

[32] B. Dittrich, C. Goeller, E. R. Livine, and A. Riello, *Quasi-local holographic dualities in non-perturbative 3d quantum gravity II – From coherent quantum boundaries to BMS_3 characters*, *Nucl. Phys. B* **938** (2019) 878–934, arXiv:1710.04237 [hep-th].

[33] B. Dittrich, C. Goeller, E. R. Livine, and A. Riello, *Quasi-local holographic dualities in non-perturbative 3d quantum gravity*, *Class. Quant. Grav.* **35** no. 13, (2018) 13LT01, arXiv:1803.02759 [hep-th].

[34] A. Riello, *Quantum edge modes in 3d gravity and 2+1d topological phases of matter*, *Phys. Rev. D* **98** no. 10, (2018) 106002, arXiv:1802.02588 [hep-th].

[35] C. Goeller, E. R. Livine, and A. Riello, *Non-Perturbative 3D Quantum Gravity: Quantum Boundary States and Exact Partition Function*, *Gen. Rel. Grav.* **52** no. 3, (2020) 24, arXiv:1912.01968 [hep-th].

[36] W. Wieland, *Conformal boundary conditions, loop gravity and the continuum*, *JHEP* **10** (2018) 089, arXiv:1804.08643 [gr-qc].

[37] G. Ponzano and T. Regge, *Semiclassical limit of racah coefficients.*, *Spectroscopic and Group Theoretical Methods in Physics. Block, F. (ed.). New York, John Wiley and Sons, Inc.* (10, 1969) 1–58.

[38] B. Dittrich, *The continuum limit of loop quantum gravity - a framework for solving the theory*, pp. 153–179. WSP, 2017. arXiv:1409.1450 [gr-qc].

[39] E. R. Livine and S. Speziale, *Group Integral Techniques for the Spinfoam Graviton Propagator*, *JHEP* **11** (2006) 092, arXiv:gr-qc/0608131.

[40] B. Dittrich, W. Kamiński, and S. Steinhaus, *Discretization independence implies non-locality in 4D discrete quantum gravity*, *Class. Quant. Grav.* **31** no. 24, (2014) 245009, arXiv:1404.5288 [gr-qc].

[41] A. Baratin and L. Freidel, *Hidden Quantum Gravity in 4-D Feynman diagrams: Emergence of spin foams*, *Class. Quant. Grav.* **24** (2007) 2027–2060, arXiv:hep-th/0611042.

[42] H. Waelbroeck and J. A. Zapata, *Translation symmetry in 2+1 Regge calculus*, *Class. Quant. Grav.* **10** (1993) 1923–1932.

[43] J. W. Barrett, M. Rocek, and R. M. Williams, *A note on area variables in regge calculus*, *Classical and Quantum Gravity* **16** no. 4, (Jan, 1999) 1373–1376, arXiv:gr-qc/9710056.

[44] B. Dittrich and S. Speziale, *Area-angle variables for general relativity*, *New J. Phys.* **10** (2008) 083006, arXiv:0802.0864 [gr-qc].

[45] B. Dittrich and P. A. Hohn, *From covariant to canonical formulations of discrete gravity*, *Class. Quant. Grav.* **27** (2010) 155001, arXiv:0912.1817 [gr-qc].

[46] J. Makela, *Variation of area variables in Regge calculus*, *Class. Quant. Grav.* **17** (2000) 4991–4998, arXiv:gr-qc/9801022.

[47] J. Makela and R. M. Williams, *Constraints on area variables in Regge calculus*, *Class. Quant. Grav.* **18** (2001) L43, arXiv:gr-qc/0011006.

[48] A. Ashtekar, *New Variables for Classical and Quantum Gravity*, *Phys. Rev. Lett.* **57** (1986) 2244–2247.

[49] C. Rovelli and L. Smolin, *Discreteness of area and volume in quantum gravity*, *Nucl. Phys. B* **442** (1995) 593–622, arXiv:gr-qc/9411005.

[50] A. Ashtekar and J. Lewandowski, *Quantum theory of geometry. 1: Area operators*, *Class. Quant. Grav.* **14** (1997) A55–A82, arXiv:gr-qc/9602046.

[51] A. Ashtekar and J. Lewandowski, *Quantum theory of geometry. 2. Volume operators*, *Adv. Theor. Math. Phys.* **1** (1998) 388–429, arXiv:gr-qc/9711031.

[52] B. Dittrich, *Diffeomorphism symmetry in quantum gravity models*, *Adv. Sci. Lett.* **2** (10, 2008) 151, arXiv:0810.3594 [gr-qc].

[53] B. Dittrich and J. P. Ryan, *Phase space descriptions for simplicial 4d geometries*, *Class. Quant. Grav.* **28** (2011) 065006, arXiv:0807.2806 [gr-qc].

[54] A. Perez, *The Spin Foam Approach to Quantum Gravity*, *Living Rev. Rel.* **16** (2013) 3, arXiv:1205.2019 [gr-qc].

[55] E. Bianchi and H. M. Haggard, *Discreteness of the volume of space from Bohr-Sommerfeld quantization*, *Phys. Rev. Lett.* **107** (2011) 011301, arXiv:1102.5439 [gr-qc].

[56] E. Bianchi and H. M. Haggard, *Bohr-Sommerfeld Quantization of Space*, *Phys. Rev. D* **86** (2012) 124010, arXiv:1208.2228 [gr-qc].

[57] W. Wieland, *Fock representation of gravitational boundary modes and the discreteness of the area spectrum*, *Annales Henri Poincare* **18** no. 11, (2017) 3695–3717, arXiv:1706.00479 [gr-qc].

[58] G. 't Hooft, *Dimensional reduction in quantum gravity*, *Conf. Proc. C* **930308** (1993) 284–296, arXiv:gr-qc/9310026.

[59] L. Smolin, *Four principles for quantum gravity*, vol. 187, pp. 427–450. Fundam.Theor.Phys., 2017. arXiv:1610.01968 [gr-qc].

[60] S. Ryu and T. Takayanagi, *Holographic derivation of entanglement entropy from AdS/CFT*, *Phys. Rev. Lett.* **96** (2006) 181602, arXiv:hep-th/0603001.

[61] E. Bianchi and R. C. Myers, *On the Architecture of Spacetime Geometry*, *Class. Quant. Grav.* **31** (2014) 214002, arXiv:1212.5183 [hep-th].

[62] J. D. Bekenstein and V. F. Mukhanov, *Spectroscopy of the quantum black hole*, *Phys. Lett. B* **360** (1995) 7–12, arXiv:gr-qc/9505012.

[63] A. Ashtekar, J. Baez, A. Corichi, and K. Krasnov, *Quantum geometry and black hole entropy*, *Phys. Rev. Lett.* **80** (1998) 904–907, arXiv:gr-qc/9710007.

[64] J. D. Bekenstein, *Statistics of black hole radiance and the horizon area spectrum*, *Phys. Rev. D* **91** no. 12, (2015) 124052, arXiv:1505.03253 [gr-qc].

[65] J. Barbero G. and A. Perez, *Quantum Geometry and Black Holes*, pp. 241–279. WSP, 2017. arXiv:1501.02963 [gr-qc].

[66] B. Dittrich and J. P. Ryan, *Simplicity in simplicial phase space*, *Phys. Rev. D* **82** (2010) 064026, arXiv:1006.4295 [gr-qc].

[67] B. Dittrich and J. P. Ryan, *On the role of the Barbero-Immirzi parameter in discrete quantum gravity*, *Class. Quant. Grav.* **30** (2013) 095015, arXiv:1209.4892 [gr-qc].

[68] J. A. Zapata, *Topological lattice gravity using selfdual variables*, *Class. Quant. Grav.* **13** (1996) 2617–2634, arXiv:gr-qc/9603030.

[69] T. Thiemann, *Quantum spin dynamics (QSD): 7. Symplectic structures and continuum lattice formulations of gauge field theories*, *Class. Quant. Grav.* **18** (2001) 3293–3338, arXiv:hep-th/0005232.

[70] B. Dittrich and M. Geiller, *Flux formulation of loop quantum gravity: Classical framework*, *Class. Quant. Grav.* **32** no. 13, (2015) 135016, arXiv:1412.3752 [gr-qc].

[71] L. Freidel and S. Speziale, *Twisted geometries: A geometric parametrisation of SU(2) phase space*, *Phys. Rev. D* **82** (2010) 084040, arXiv:1001.2748 [gr-qc].

[72] A. Ashtekar and J. Lewandowski, *Representation theory of analytic holonomy C* algebras*, arXiv:gr-qc/9311010.

[73] B. Dittrich and M. Geiller, *A new vacuum for Loop Quantum Gravity*, *Class. Quant. Grav.* **32** no. 11, (2015) 112001, arXiv:1401.6441 [gr-qc].

[74] J. Lewandowski and H. Sahlmann, *Loop quantum gravity coupled to a scalar field*, *Phys. Rev. D* **93** no. 2, (2016) 024042, arXiv:1507.01149 [gr-qc].

[75] B. Bahr, B. Dittrich, and M. Geiller, *A new realization of quantum geometry*, arXiv:1506.08571 [gr-qc].

[76] J. W. Barrett and L. Crane, *Relativistic spin networks and quantum gravity*, *J. Math. Phys.* **39** (1998) 3296–3302, arXiv:gr-qc/9709028.

[77] E. R. Livine and S. Speziale, *A New spinfoam vertex for quantum gravity*, *Phys. Rev. D* **76** (2007) 084028, arXiv:0705.0674 [gr-qc].

[78] J. Engle, E. Livine, R. Pereira, and C. Rovelli, *LQG vertex with finite Immirzi parameter*, *Nucl. Phys. B* **799** (2008) 136–149, arXiv:0711.0146 [gr-qc].

[79] L. Freidel and K. Krasnov, *A New Spin Foam Model for 4d Gravity*, *Class. Quant. Grav.* **25** (2008) 125018, arXiv:0708.1595 [gr-qc].

[80] M. Dupuis and E. R. Livine, *Holomorphic Simplicity Constraints for 4d Spinfoam Models*, *Class. Quant. Grav.* **28** (2011) 215022, arXiv:1104.3683 [gr-qc].

[81] A. Baratin and D. Oriti, *Group field theory and simplicial gravity path integrals: A model for Holst-Plebanski gravity*, *Phys. Rev. D* **85** (2012) 044003, arXiv:1111.5842 [hep-th].

[82] J. W. Barrett and T. Foxon, *Semiclassical limits of simplicial quantum gravity*, *Class. Quant. Grav.* **11** (1994) 543–556, arXiv:gr-qc/9310016.

[83] F. Conrady and L. Freidel, *On the semiclassical limit of 4d spin foam models*, *Phys. Rev. D* **78** (2008) 104023, arXiv:0809.2280 [gr-qc].

[84] J. W. Barrett, R. Dowdall, W. J. Fairbairn, H. Gomes, and F. Hellmann, *Asymptotic analysis of the EPRL four-simplex amplitude*, *J. Math. Phys.* **50** (2009) 112504, arXiv:0902.1170 [gr-qc].

[85] J. W. Barrett, R. Dowdall, W. J. Fairbairn, F. Hellmann, and R. Pereira, *Lorentzian spin foam amplitudes: Graphical calculus and asymptotics*, *Class. Quant. Grav.* **27** (2010) 165009, arXiv:0907.2440 [gr-qc].

[86] M.-X. Han and M. Zhang, *Asymptotics of Spinfoam Amplitude on Simplicial Manifold: Euclidean Theory*, *Class. Quant. Grav.* **29** (2012) 165004, arXiv:1109.0500 [gr-qc].

[87] M. Han and T. Krajewski, *Path Integral Representation of Lorentzian Spinfoam Model, Asymptotics, and Simplicial Geometries*, *Class. Quant. Grav.* **31** (2014) 015009, arXiv:1304.5626 [gr-qc].

[88] M. Han, *On Spinfoam Models in Large Spin Regime*, *Class. Quant. Grav.* **31** (2014) 015004, arXiv:1304.5627 [gr-qc].

[89] P. Doná, M. Fanizza, G. Sarno, and S. Speziale, *SU(2) graph invariants, Regge actions and polytopes*, *Class. Quant. Grav.* **35** no. 4, (2018) 045011, arXiv:1708.01727 [gr-qc].

[90] C. Rovelli, *The Basis of the Ponzano-Regge-Turaev-Viro-Ooguri quantum gravity model in the loop representation basis*, *Phys. Rev. D* **48** (1993) 2702–2707, arXiv:hep-th/9304164.

[91] E. Alesci and C. Rovelli, *The Complete LQG propagator. I. Difficulties with the Barrett-Crane vertex*, *Phys. Rev. D* **76** (2007) 104012, arXiv:0708.0883 [gr-qc].

[92] A. Baratin and D. Oriti, *Quantum simplicial geometry in the group field theory formalism: reconsidering the Barrett-Crane model*, *New J. Phys.* **13** (2011) 125011, arXiv:1108.1178 [gr-qc].

[93] S. Alexandrov, *The new vertices and canonical quantization*, *Phys. Rev. D* **82** (2010) 024024, arXiv:1004.2260 [gr-qc].

[94] M. Geiller and K. Noui, *Testing the imposition of the Spin Foam Simplicity Constraints*, *Class. Quant. Grav.* **29** (2012) 135008, arXiv:1112.1965 [gr-qc].

[95] S. Alexandrov, M. Geiller, and K. Noui, *Spin Foams and Canonical Quantization*, *SIGMA* **8** (2012) 055, arXiv:1112.1961 [gr-qc].

[96] M. Geiller and K. Noui, *A note on the Holst action, the time gauge, and the Barbero-Immirzi parameter*, *Gen. Rel. Grav.* **45** (2013) 1733–1760, arXiv:1212.5064 [gr-qc].

[97] V. Bonzom, *From lattice BF gauge theory to area-angle Regge calculus*, *Class. Quant. Grav.* **26** (2009) 155020, arXiv:0903.0267 [gr-qc].

[98] L. Freidel and J. Ziprick, *Spinning geometry = Twisted geometry*, *Class. Quant. Grav.* **31** no. 4, (2014) 045007, arXiv:1308.0040 [gr-qc].

[99] L. Freidel and S. Speziale, *From twistors to twisted geometries*, *Phys. Rev. D* **82** (2010) 084041, arXiv:1006.0199 [gr-qc].

[100] E. R. Livine, S. Speziale, and J. Tambornino, *Twistor Networks and Covariant Twisted Geometries*, *Phys. Rev. D* **85** (2012) 064002, arXiv:1108.0369 [gr-qc].

[101] W. M. Wieland, *Twistorial phase space for complex Ashtekar variables*, *Class. Quant. Grav.* **29** (2012) 045007, arXiv:1107.5002 [gr-qc].

[102] A. Banburski, L.-Q. Chen, L. Freidel, and J. Hnybida, *Pachner moves in a 4d Riemannian holomorphic Spin Foam model*, *Phys. Rev. D* **92** no. 12, (2015) 124014, arXiv:1412.8247 [gr-qc].

[103] F. Anzá and S. Speziale, *A note on the secondary simplicity constraints in loop quantum gravity*, *Class. Quant. Grav.* **32** no. 19, (2015) 195015, arXiv:1409.0836 [gr-qc].

[104] H. M. Haggard, C. Rovelli, W. Wieland, and F. Vidotto, *Spin connection of twisted geometry*, *Phys. Rev. D* **87** no. 2, (2013) 024038, arXiv:1211.2166 [gr-qc].

[105] V. Bonzom, *Spin foam models for quantum gravity from lattice path integrals*, *Phys. Rev. D* **80** (2009) 064028, arXiv:0905.1501 [gr-qc].

[106] F. Hellmann and W. Kaminski, *Holonomy spin foam models: Asymptotic geometry of the partition function*, *JHEP* **10** (2013) 165, arXiv:1307.1679 [gr-qc].

[107] J. R. Oliveira, *EPRL/FK Asymptotics and the Flatness Problem*, *Class. Quant. Grav.* **35** no. 9, (2018) 095003, arXiv:1704.04817 [gr-qc].

[108] P. Donà, F. Gozzini, and G. Sarno, *Searching for classical geometries in spin foam amplitudes: a numerical method*, *Classical and Quantum Gravity* **37** no. 9, (Apr, 2020) 094002.

[109] E. Bianchi, J. Engle, and S. Simone, *ILQGS online seminar (March 3rd 2020): Panel on the status of the vertex*,. Link to slides.

[110] J. W. Barrett, *Refractive gravitational waves and quantum fluctuations*, arXiv:gr-qc/0011051.

[111] C. Wainwright and R. M. Williams, *Area Regge calculus and discontinuous metrics*, *Class. Quant. Grav.* **21** (2004) 4865–4880, arXiv:gr-qc/0405031.

[112] Y. Neiman, *A look at area Regge calculus*, arXiv:1308.1012 [gr-qc].

[113] J. W. Barrett and C. M. Steele, *Asymptotics of relativistic spin networks*, *Class. Quant. Grav.* **20** (2003) 1341–1362, arXiv:gr-qc/0209023.

[114] J. W. Barrett, W. J. Fairbairn, and F. Hellmann, *Quantum gravity asymptotics from the SU(2) 15j symbol*, *Int. J. Mod. Phys. A* **25** (2010) 2897–2916, arXiv:0912.4907 [gr-qc].

[115] B. Bahr and S. Steinhaus, *Investigation of the Spinfoam Path integral with Quantum Cuboid Intertwiners*, *Phys. Rev. D* **93** no. 10, (2016) 104029, arXiv:1508.07961 [gr-qc].

[116] F. P. Schuller and M. N. Wohlfarth, *Geometry of manifolds with area metric: multi-metric backgrounds*, *Nucl. Phys. B* **747** (2006) 398–422, arXiv:hep-th/0508170.

[117] M. Van Raamsdonk, *Building up spacetime with quantum entanglement*, *Gen. Rel. Grav.* **42** (2010) 2323–2329, arXiv:1005.3035 [hep-th].

[118] N. Lashkari, M. B. McDermott, and M. Van Raamsdonk, *Gravitational dynamics from entanglement 'thermodynamics'*, *JHEP* **04** (2014) 195, arXiv:1308.3716 [hep-th].

[119] S. Ryu and T. Takayanagi, *Holographic derivation of entanglement entropy from AdS/CFT*, *Phys. Rev. Lett.* **96** (2006) 181602, arXiv:hep-th/0603001.

[120] B. Bahr and B. Dittrich, *(Broken) Gauge Symmetries and Constraints in Regge Calculus*, *Class. Quant. Grav.* **26** (2009) 225011, arXiv:0905.1670 [gr-qc].

[121] M. Rocek and R. M. Williams, *QUANTUM REGGE CALCULUS*, *Phys. Lett. B* **104** (1981) 31.

[122] B. Oblak, *Characters of the BMS Group in Three Dimensions*, *Commun. Math. Phys.* **340** no. 1, (2015) 413–432, arXiv:1502.03108 [hep-th].

[123] J. Brown and M. Henneaux, *Central Charges in the Canonical Realization of Asymptotic Symmetries: An Example from Three-Dimensional Gravity*, *Commun. Math. Phys.* **104** (1986) 207–226.

[124] P. Di Francesco, P. Mathieu, and D. Senechal, *Conformal Field Theory*. Graduate Texts in Contemporary Physics. Springer-Verlag, New York, 1997.

[125] B. Bahr, B. Dittrich, and S. Steinhaus, *Perfect discretization of reparametrization invariant path integrals*, *Phys. Rev. D* **83** (2011) 105026, arXiv:1101.4775 [gr-qc].

[126] B. Bahr and B. Dittrich, *Improved and Perfect Actions in Discrete Gravity*, *Phys. Rev. D* **80** (2009) 124030, arXiv:0907.4323 [gr-qc].

[127] W. Donnelly and L. Freidel, *Local subsystems in gauge theory and gravity*, *JHEP* **09** (2016) 102, arXiv:1601.04744 [hep-th].

[128] A. Riello, *Soft charges from the geometry of field space*, *JHEP* **05** (2020) 125, arXiv:1904.07410 [hep-th].

[129] G. Barnich and H. A. Gonzalez, *Dual dynamics of three dimensional asymptotically flat Einstein gravity at null infinity*, *JHEP* **05** (2013) 016, arXiv:1303.1075 [hep-th].

[130] B. Oblak, *BMS Particles in Three Dimensions*. PhD thesis, Brussels U., 2016. arXiv:1610.08526 [hep-th].

[131] A. Castro and B. Dittrich, *Point particle in 3D discrete gravity and holography,*. *PSI essay*.

[132] S. Carlip, *The dynamics of supertranslations and superrotations in 2 + 1 dimensions*, *Class. Quant. Grav.* **35** no. 1, (2018) 014001, arXiv:1608.05088 [gr-qc].

[133] F. Hopfmueller and L. Freidel, *Null Conservation Laws for Gravity*, *Phys. Rev. D* **97** no. 12, (2018) 124029, arXiv:1802.06135 [gr-qc].

[134] W. Wieland, *Generating functional for gravitational null initial data*, *Class. Quant. Grav.* **36** no. 23, (2019) 235007, arXiv:1905.06357 [gr-qc].

[135] B. Bahr, B. Dittrich, and S. He, *Coarse graining free theories with gauge symmetries: the linearized case*, *New J. Phys.* **13** (2011) 045009, arXiv:1011.3667 [gr-qc].

[136] O. Lauscher and M. Reuter, *Ultraviolet fixed point and generalized flow equation of quantum gravity*, *Phys. Rev. D* **65** (2002) 025013, arXiv:hep-th/0108040.

[137] M. Reuter and F. Saueressig, *Renormalization group flow of quantum gravity in the Einstein-Hilbert truncation*, *Phys. Rev. D* **65** (2002) 065016, arXiv:hep-th/0110054.

[138] M. Reuter and F. Saueressig, *Quantum Gravity and the Functional Renormalization Group: The Road towards Asymptotic Safety*. Cambridge University Press, 12, 2018.

[139] B. Dittrich, *From the discrete to the continuous: Towards a cylindrically consistent dynamics*, *New J. Phys.* **14** (2012) 123004, arXiv:1205.6127 [gr-qc].

[140] B. Dittrich and S. Steinhaus, *Time evolution as refining, coarse graining and entangling*, *New J. Phys.* **16** (2014) 123041, arXiv:1311.7565 [gr-qc].

[141] C. Delcamp and B. Dittrich, *Towards a phase diagram for spin foams*, *Class. Quant. Grav.* **34** no. 22, (2017) 225006, arXiv:1612.04506 [gr-qc].

[142] J. Hartle and R. Sorkin, *Boundary Terms in the Action for the Regge Calculus*, *Gen. Rel. Grav.* **13** (1981) 541–549.

[143] L. C. Brewin and A. P. Gentle, *On the convergence of Regge calculus to general relativity*, *Class. Quant. Grav.* **18** (2001) 517–526, arXiv:gr-qc/0006017.

[144] S. Ludwig, *On the multiple integral* $\int^n dxdy\dots dz$ *whose limits are* $p = a_1x + b_1y + \dots + h_1z > 0, p_2 > 0, \dots, p_n > 0$, *and* $x^2 + y^2 + \dots + z^2 < 1$, *Quart. J. Pure Appl. Math.* **2** (1858) 269.

[145] A. Hedeman, H. M. Haggard, E. Kur, and R. G. Littlejohn, *Symplectic and semiclassical aspects of the Schläfli identity*, *J. Phys. A* **48** no. 10, (2015) 105203, arXiv:1409.7117 [math-ph].

[146] J. W. Barrett, *First order Regge calculus*, *Class. Quant. Grav.* **11** (1994) 2723–2730, arXiv:hep-th/9404124.

[147] B. Bahr and B. Dittrich, *Regge calculus from a new angle*, *New J. Phys.* **12** (2010) 033010, arXiv:0907.4325 [gr-qc].

[148] V. Turaev and O. Viro, *State sum invariants of 3 manifolds and quantum 6j symbols*, *Topology* **31** (1992) 865–902.

[149] L. Crane, L. H. Kauffman, and D. N. Yetter, *State sum invariants of four manifolds. 1.*, arXiv:hep-th/9409167.

[150] S. Major and L. Smolin, *Quantum deformation of quantum gravity*, *Nucl. Phys. B* **473** (1996) 267–290, arXiv:gr-qc/9512020.

[151] J. W. Barrett, *Geometrical measurements in three-dimensional quantum gravity*, *Int. J. Mod. Phys. A* **18S2** (2003) 97–113, arXiv:gr-qc/0203018.

[152] M. Dupuis and F. Girelli, *Observables in Loop Quantum Gravity with a cosmological constant*, *Phys. Rev. D* **90** no. 10, (2014) 104037, arXiv:1311.6841 [gr-qc].

[153] V. Bonzom, M. Dupuis, and F. Girelli, *Towards the Turaev-Viro amplitudes from a Hamiltonian constraint*, *Phys. Rev. D* **90** no. 10, (2014) 104038, arXiv:1403.7121 [gr-qc].

[154] H. M. Haggard, M. Han, W. Kamiński, and A. Riello, *SL(2,C) Chern–Simons theory, a non-planar graph operator, and 4D quantum gravity with a cosmological constant: Semiclassical geometry*, *Nucl. Phys. B* **900** (2015) 1–79, arXiv:1412.7546 [hep-th].

[155] H. M. Haggard, M. Han, and A. Riello, *Encoding Curved Tetrahedra in Face Holonomies: Phase Space of Shapes from Group-Valued Moment Maps*, *Annales Henri Poincaré* **17** no. 8, (2016) 2001–2048, arXiv:1506.03053 [math-ph].

[156] H. M. Haggard, M. Han, W. Kaminski, and A. Riello, *SL(2,C) Chern-Simons Theory, Flat Connections, and Four-dimensional Quantum Geometry*, arXiv:1512.07690 [hep-th].

[157] B. Dittrich and M. Geiller, *Quantum gravity kinematics from extended TQFTs*, *New J. Phys.* **19** no. 1, (2017) 013003, arXiv:1604.05195 [hep-th].

[158] B. Dittrich, *(3 + 1)-dimensional topological phases and self-dual quantum geometries encoded on Heegaard surfaces*, *JHEP* **05** (2017) 123, arXiv:1701.02037 [hep-th].

[159] B. Dittrich, L. Freidel, and S. Speziale, *Linearized dynamics from the 4-simplex Regge action*, *Phys. Rev. D* **76** (2007) 104020, arXiv:0707.4513 [gr-qc].

[160] U. Pachner, *P.l. homeomorphic manifolds are equivalent by elementary shellings*, *European Journal of Combinatorics* **12** no. 2, (1991) 129 – 145.

[161] C. Di Bartolo, R. Gambini, and J. Pullin, *Canonical quantization of constrained theories on discrete space-time lattices*, *Class. Quant. Grav.* **19** (2002) 5275–5296, arXiv:gr-qc/0205123.

[162] J. W. Barrett, M. Galassi, W. A. Miller, R. D. Sorkin, P. A. Tuckey, and R. M. Williams, *A Paralellizable implicit evolution scheme for Regge calculus*, *Int. J. Theor. Phys.* **36** (1997) 815–840, arXiv:gr-qc/9411008.

[163] B. Dittrich and P. A. Hoehn, *Constraint analysis for variational discrete systems*, *J. Math. Phys.* **54** (2013) 093505, arXiv:1303.4294 [math-ph].

[164] H. W. Hamber and R. M. Williams, *Gauge invariance in simplicial gravity*, *Nucl. Phys. B* **487** (1997) 345–408, arXiv:hep-th/9607153.

[165] B. Dittrich, *How to construct diffeomorphism symmetry on the lattice*, *PoS* **QGQGS2011** (2011) 012, arXiv:1201.3840 [gr-qc].

[166] B. Bahr, B. Dittrich, F. Hellmann, and W. Kaminski, *Holonomy Spin Foam Models: Definition and Coarse Graining*, *Phys. Rev. D* **87** no. 4, (2013) 044048, arXiv:1208.3388 [gr-qc].

[167] B. Dittrich, M. Martin-Benito, and S. Steinhaus, *Quantum group spin nets: refinement limit and relation to spin foams*, *Phys. Rev. D* **90** (2014) 024058, arXiv:1312.0905 [gr-qc].

[168] B. Bahr, *On background-independent renormalization in spin foam models*, *POS* **FFP14** (2016) 157.

[169] B. Dittrich, S. Mizera, and S. Steinhaus, *Decorated tensor network renormalization for lattice gauge theories and spin foam models*, *New J. Phys.* **18** no. 5, (2016) 053009, arXiv:1409.2407 [gr-qc].

[170] B. Dittrich, E. Schnetter, C. J. Seth, and S. Steinhaus, *Coarse graining flow of spin foam intertwiners*, *Phys. Rev. D* **94** no. 12, (2016) 124050, arXiv:1609.02429 [gr-qc].

[171] R. M. Williams, *Recent progress in Regge calculus*, *Nucl. Phys. B Proc. Suppl.* **57** (1997) 73–81, arXiv:gr-qc/9702006.

[172] M. Kapovich and J. J. Millson, *The symplectic geometry of polygons in euclidean space*, *Journal of Diff. Geometry* **44** (1998) 479–513.

[173] E. Bianchi, P. Dona, and S. Speziale, *Polyhedra in loop quantum gravity*, *Phys. Rev. D* **83** (2011) 044035, arXiv:1009.3402 [gr-qc].

[174] E. Bianchi, *The Length operator in Loop Quantum Gravity*, *Nucl. Phys. B* **807** (2009) 591–624, arXiv:0806.4710 [gr-qc].

[175] A. Barbieri, *Quantum tetrahedra and simplicial spin networks*, *Nucl. Phys. B* **518** (1998) 714–728, arXiv:gr-qc/9707010.

[176] J. C. Baez and J. W. Barrett, *The Quantum tetrahedron in three-dimensions and four-dimensions*, *Adv. Theor. Math. Phys.* **3** (1999) 815–850, arXiv:gr-qc/9903060.

[177] F. Conrady and L. Freidel, *Quantum geometry from phase space reduction*, *J. Math. Phys.* **50** (2009) 123510, arXiv:0902.0351 [gr-qc].

[178] V. Bonzom and E. R. Livine, *Generating Functions for Coherent Intertwiners*, *Class. Quant. Grav.* **30** (2013) 055018, arXiv:1205.5677 [gr-qc].

[179] L. Freidel and J. Hnybida, *A Discrete and Coherent Basis of Intertwiners*, *Class. Quant. Grav.* **31** (2014) 015019, arXiv:1305.3326 [math-ph].

[180] J. Engle, R. Pereira, and C. Rovelli, *The Loop-quantum-gravity vertex-amplitude*, *Phys. Rev. Lett.* **99** (2007) 161301, arXiv:0705.2388 [gr-qc].

[181] J. W. Barrett and R. M. Williams, *The Asymptotics of an amplitude for the four simplex*, *Adv. Theor. Math. Phys.* **3** (1999) 209–215, arXiv:gr-qc/9809032.

[182] W. Kaminski, M. Kisielowski, and H. Sahlmann, *Asymptotic analysis of the EPRL model with timelike tetrahedra*, *Class. Quant. Grav.* **35** no. 13, (2018) 135012, arXiv:1705.02862 [gr-qc].

[183] P. Doná, M. Fanizza, G. Sarno, and S. Speziale, *Numerical study of the Lorentzian Engle-Pereira-Rovelli-Livine spin foam amplitude*, *Phys. Rev. D* **100** no. 10, (2019) 106003, arXiv:1903.12624 [gr-qc].

[184] J. Engle, *Proposed proper Engle-Pereira-Rovelli-Livine vertex amplitude*, *Phys. Rev. D* **87** no. 8, (2013) 084048, arXiv:1111.2865 [gr-qc].

[185] J. Engle, *A spin-foam vertex amplitude with the correct semiclassical limit*, *Physics Letters B* **724** (01, 2012) .

[186] F. Girelli, H. Pfeiffer, and E. Popescu, *Topological Higher Gauge Theory - from BF to BFCG theory*, *J. Math. Phys.* **49** (2008) 032503, arXiv:0708.3051 [hep-th].

[187] A. Mikovic and M. Vojinovic, *Poincare 2-group and quantum gravity*, *Class. Quant. Grav.* **29** (2012) 165003, arXiv:1110.4694 [gr-qc].

[188] A. Baratin and L. Freidel, *A 2-categorical state sum model*, *J. Math. Phys.* **56** no. 1, (2015) 011705, arXiv:1409.3526 [math.QA].

[189] B. Dittrich, *Quantum geometries in* $(3+1)$ *dimensions*,. *To appear.*

[190] M. Han, *Semiclassical Analysis of Spinfoam Model with a Small Barbero-Immirzi Parameter*, *Phys. Rev. D* **88** (2013) 044051, arXiv:1304.5628 [gr-qc].

[191] A. Riello, *Radiative corrections to the Lorentzian Engle-Pereira-Rovelli-Livine and Freidel-Krasnov spinfoam graviton*, *Phys. Rev. D* **89** no. 6, (2014) 064021, arXiv:1310.2174 [gr-qc].

[192] A. Riello, *Self-energy of the Lorentzian Engle-Pereira-Rovelli-Livine and Freidel-Krasnov model of quantum gravity*, *Phys. Rev. D* **88** no. 2, (2013) 024011, arXiv:1302.1781 [gr-qc].

[193] L.-Q. Chen, *Bulk amplitude and degree of divergence in 4d spin foams*, *Phys. Rev. D* **94** no. 10, (2016) 104025, arXiv:1602.01825 [gr-qc].

[194] E. Magliaro and C. Perini, *Regge gravity from spinfoams*, *Int. J. Mod. Phys. D* **22** (2013) 1–21, arXiv:1105.0216 [gr-qc].

[195] B. Bahr, G. Rabuffo, and S. Steinhaus, *Renormalization of symmetry restricted spin foam models with curvature in the asymptotic regime*, *Phys. Rev. D* **98** no. 10, (2018) 106026, arXiv:1804.00023 [gr-qc].

[196] K. Krasnov, *Gravity as BF theory plus potential*, *Int. J. Mod. Phys. A* **24** (2009) 2776–2782, arXiv:0907.4064 [gr-qc].

[197] V. D. Sandberg, *Tensor spherical harmonics on s2 and s3 as eigenvalue problems*, *Journal of Mathematical Physics* **19** no. 12, (1978) 2441–2446, https://doi.org/10.1063/1.523649.

[198] E. R. Livine and S. Speziale, *Consistently Solving the Simplicity Constraints for Spinfoam Quantum Gravity*, *EPL* **81** no. 5, (2008) 50004, arXiv:0708.1915 [gr-qc].

[199] P. Dona and G. Sarno, *Numerical methods for EPRL spin foam transition amplitudes and Lorentzian recoupling theory*, *Gen. Rel. Grav.* **50** (2018) 127, arXiv:1807.03066 [gr-qc].

[200] S. Speziale, *Boosting Wigner's nj-symbols*, *J. Math. Phys.* **58** no. 3, (2017) 032501, arXiv:1609.01632 [gr-qc].

[201] M. Vojinović, *Causal Dynamical Triangulations in the Spincube Model of Quantum Gravity*, *Phys. Rev. D* **94** no. 2, (2016) 024058, arXiv:1506.06839 [gr-qc].

[202] E. Magliaro and C. Perini, *Emergence of gravity from spinfoams*, *EPL* **95** no. 3, (2011) 30007, arXiv:1108.2258 [gr-qc].

[203] K. Krasnov, *Effective metric Lagrangians from an underlying theory with two propagating degrees of freedom*, *Phys. Rev. D* **81** (2010) 084026, arXiv:0911.4903 [hep-th].

[204] H. M. Haggard, M. Han, W. Kamiński, and A. Riello, *Four-dimensional Quantum Gravity with a Cosmological Constant from Three-dimensional Holomorphic Blocks*, *Phys. Lett. B* **752** (2016) 258–262, arXiv:1509.00458 [hep-th].

[205] B. Dittrich and P. A. Hohn, *Canonical simplicial gravity*, *Class. Quant. Grav.* **29** (2012) 115009, arXiv:1108.1974 [gr-qc].

[206] B. Bahr and B. Dittrich, *Breaking and restoring of diffeomorphism symmetry in discrete gravity*, *AIP Conf. Proc.* **1196** no. 1, (2009) 10, arXiv:0909.5688 [gr-qc].

[207] A. Ashtekar and J. Lewandowski, *Differential geometry on the space of connections via graphs and projective limits*, *J. Geom. Phys.* **17** (1995) 191–230, arXiv:hep-th/9412073.

[208] P. Drobiński and J. Lewandowski, *Continuum approach to the BF vacuum: The U(1) case*, *Phys. Rev. D* **96** no. 12, (2017) 126011, arXiv:1705.09836 [gr-qc].

[209] M. Han and M. Zhang, *Asymptotics of Spinfoam Amplitude on Simplicial Manifold: Lorentzian Theory*, *Class. Quant. Grav.* **30** (2013) 165012, arXiv:1109.0499 [gr-qc].

[210] S. Alexandrov, *Degenerate Plebanski Sector and Spin Foam Quantization*, *Class. Quant. Grav.* **29** (2012) 145018, arXiv:1202.5039 [gr-qc].

[211] S. Speziale and W. M. Wieland, *The twistorial structure of loop-gravity transition amplitudes*, *Phys. Rev. D* **86** (2012) 124023, arXiv:1207.6348 [gr-qc].

[212] R. Punzi, F. P. Schuller, and M. N. Wohlfarth, *Area metric gravity and accelerating cosmology*, *JHEP* **02** (2007) 030, arXiv:hep-th/0612141.

[213] M. Rocek and R. Williams, *The Quantization of Regge Calculus*, *Z. Phys. C* **21** (1984) 371.

[214] R. Gambini and J. Pullin, *Consistent discretization and canonical classical and quantum Regge calculus*, *Int. J. Mod. Phys. D* **15** (2006) 1699–1706, arXiv:gr-qc/0511096.

[215] B. Bahr and S. Steinhaus, *Numerical evidence for a phase transition in 4d spin foam quantum gravity*, *Phys. Rev. Lett.* **117** no. 14, (2016) 141302, arXiv:1605.07649 [gr-qc].

[216] B. Bahr and S. Steinhaus, *Hypercuboidal renormalization in spin foam quantum gravity*, *Phys. Rev. D* **95** no. 12, (2017) 126006, arXiv:1701.02311 [gr-qc].

[217] P. A. Hoehn, *Classification of constraints and degrees of freedom for quadratic discrete actions*, *J. Math. Phys.* **55** (2014) 113506, arXiv:1407.6641 [math-ph].

[218] B. Dittrich and J. Tambornino, *A Perturbative approach to Dirac observables and their space-time algebra*, *Class. Quant. Grav.* **24** (2007) 757–784, arXiv:gr-qc/0610060.

[219] B. Dittrich and J. Tambornino, *Gauge invariant perturbations around symmetry reduced sectors of general relativity: Applications to cosmology*, *Class. Quant. Grav.* **24** (2007) 4543–4586, arXiv:gr-qc/0702093.

[220] V. Bonzom and B. Dittrich, *Dirac's discrete hypersurface deformation algebras*, *Class. Quant. Grav.* **30** (2013) 205013, arXiv:1304.5983 [gr-qc].

[221] I. Rivin, *A multidimensional law of sines*, arXiv:0211261 [math].

[222] S. Kokkendorff, *Polar duality and the generalized law of sines*, *Journal of Geometry* **86** (04, 2007) 140–149.

APPENDICES FOR PART I

Appendix A

Proof of results for diffeomorphism induced perturbations

In this appendix, we will give a proof of **Results 1** given in equations (2.22) relating the diffeomorphism induced perturbations ζ_{AB} and the components $\xi^{\perp}, \xi^{A}\partial_{A} = \xi^{\parallel}$ of the diffeomorphism inducing vector field. The result holds for a background space–time satisfying the vacuum Einstein equations. We shall also give a proof of the first and second order Hamilton–Jacobi action **Results 2** in equations (2.27).

A.1 Vector basis for induced perturbations

From (2.18) we see that a vector field $\xi^{\perp}\partial_{\perp} + \xi^{A}\partial_{A}$ acting on the background metric leads to an induced perturbation

$$\zeta_{AB} = 2\xi^{\perp}K_{AB} + D_{A}\xi_{B} + D_{B}\xi_{A}, \tag{A.1}$$

where K_{AB}, D_{A} and $\xi_{A} = h_{AB}\xi^{B}$ pertain to the background.

Our first claim is:

Claim:

$$\begin{aligned} \Pi^{AB}\zeta_{AB} &= \Delta\xi^{\perp} + 2D^{B}({}^{\mathrm{b}}R_{AB})\xi^{A} \qquad \text{where} && \text{(A.2)}\\ \Pi^{AB} &= D^{A}D^{B} - D_{C}D^{C}h^{AB} - {}^{\mathrm{b}}R^{AB}\,, && \text{(A.3)}\\ \Delta &= 2(K^{AB} - Kh^{AB})D_{A}D_{B} - 2\,{}^{\mathrm{b}}R^{AB}K_{AB} \quad . && \text{(A.4)} \end{aligned}$$

Proof:
For any background and dimensions we have

$$\begin{aligned}(D^A D^B - D_C D^C h^{AB})(D_A\xi_B + D_B\xi_A) &= (D^A D^B - D^B D^A)D_B\xi_A + 2D^B(D_A D_B - D_B D_A)\xi^A \\ &= 2D^B({}^{\rm b}R_{AB}\xi^A)\ . \end{aligned} \tag{A.5}$$

Using ${}^{\rm b}R^{AB}(D_A\xi_B + D_B\xi_A) = 2\,{}^{\rm b}R^{AB}D_A\xi_B$, we get that

$$\Pi^{AB}(D_A\xi_B + D_B\xi_A) = 2D^B({}^{\rm b}R_{AB})\xi^A. \tag{A.6}$$

which vanishes for our (background) homogeneous boundary assumption. Now for the term proportional to $\xi^\perp$, we obtain

$$\begin{aligned}(D^A D^B - D_C D^C h^{AB})(2K_{AB}\xi^\perp) &= 2D_A D_B\big(\tilde\pi^{AB}\xi^\perp\big) \\ &= 2\tilde\pi^{AB}D_A D_B\xi^\perp\ , \end{aligned} \tag{A.7}$$

where $\tilde\pi^{AB} = (K^{AB} - Kh^{AB})$ and for the second lines we have used the momentum constraint $D_A\tilde\pi^{AB} = 0$ (which follows from the $(\perp A)$–components of the Einstein equations). Putting together equations (A.6) and (A.7), we obtain

$$\Pi^{AB}\zeta_{AB} = \Delta\xi^\perp + 2D^B({}^{\rm b}R_{AB})\xi^A \quad . \tag{A.8}$$

This proves our first claim. □

We also get the first result in (2.22) if we apply the homogeneous curvature assumption.

Our second claim is the following:

Claim:

$$2\tilde\pi^{BC}\,\delta'\,{}^{\rm b}\Gamma^A_{BC} = \mathcal{D}^A{}_B\,\xi^B - 2D_B({}^{\rm b}R^{AB})\xi^\perp + Q^{AB}D_B\xi^\perp \qquad \text{where} \tag{A.9}$$

$$\begin{aligned}\mathcal{D}^A{}_B &= 2\tilde\pi^{CD}\left(D_C D_D h^A_B - {}^{\rm b}R^A{}_{CDB}\right) \\ Q^{AB} &= 2\left(2\tilde\pi^{BC}K^A_C - \tilde\pi^{CD}K_{CD}h^{AB}\right) \quad . \end{aligned} \tag{A.10}$$

Proof:

We consider the term with the variation of the boundary Christoffel symbol given by

$$\begin{aligned} 2\tilde{\pi}^{BC}\delta' {}^{\mathrm{b}}\Gamma^{A}_{BC} &= \tilde{\pi}^{BC}h^{AD}(D_B\zeta_{CD} + D_C\zeta_{BD} - D_D\zeta_{BC}) \\ &= \tilde{\pi}^{BC}\left(D_BD_C\xi_D + D_BD_D\xi_C + D_CD_B\xi_D + D_CD_D\xi_B - D_DD_B\xi_C - D_DD_C\xi_B\right) \\ &\quad + 2\tilde{\pi}^{BC}\left(D_B(K^A_C\xi^{\perp}) + D_C(K^A_B\xi^{\perp}) - D^A(K_{BC}\xi^{\perp})\right) \end{aligned} \tag{A.11}$$

Using the momentum constraint $D_A\tilde{\pi}^{AB} = 0$, the Gauss-Codazzi condition $D_AK_{BC} - D_BK_{AC} = 0$ and the formula for boundary Riemann tensor in term of spatial covariant derivatives, we can simplify the variation of the boundary Christoffel symbol further:

$$\begin{aligned} 2\tilde{\pi}^{BC}\delta' {}^{\mathrm{b}}\Gamma^{A}_{BC} &= 2\tilde{\pi}^{BC}\left(D_BD_C\xi^A - {}^{\mathrm{b}}R^A{}_{BCD}\xi^D\right) + 2D_B(\tilde{\pi}^{BC}K^A_C)\xi^{\perp} \\ &\quad + 2\left(2\tilde{\pi}^{BC}K^A_C - \tilde{\pi}^{CD}K_{CD}h^{AB}\right)D_B\xi^{\perp} \end{aligned} \tag{A.12}$$

Using the contracted Guass-Codazzi relations, the third term in (A.12) is equal to $-2D_B({}^{\mathrm{b}}R^{AB})\xi^{\perp}$ and then we finally get

$$2\tilde{\pi}^{BC}\delta' {}^{\mathrm{b}}\Gamma^{A}_{BC} = \mathcal{D}^A_B\,\xi^B - 2D_B({}^{\mathrm{b}}R^{AB})\xi^{\perp} + Q^{AB}D_B\xi^{\perp} \tag{A.13}$$

where we have used the definitions in (A.10). Hence we have proved our second claim. □

We get the second result in equation (2.22) if we apply the homogeneous curvature assumption. Now, using $\tilde{\pi}^{BC}K^A_C = \left(K^{BC}K^A_C - KK^{AB}\right)$, $\tilde{\pi}^{CD}K_{CD} = \left(K^{CD}K_{CD} - K^2\right)$ from the Gauss-Codazzi relations and the assumptions on the background, we have

$$Q^{AB} = 2\left(\left({}^{\mathrm{b}}Rh^{AB} - 2{}^{\mathrm{b}}R^{AB}\right) - 2\Lambda\frac{(d-3)}{(d-1)}h^{AB}\right) \quad . \tag{A.14}$$

Note that Q^{AB} vanishes identically in three dimensions since two dimensional metrics satisfy ${}^{\mathrm{b}}R^{AB} = \frac{1}{2}{}^{\mathrm{b}}Rh^{AB}$.

Also, we can expand the boundary Riemann curvature in the $\mathcal{D}^A_B$ term using the Gauss-Codazzi relations to get

$$\mathcal{D}^A{}_B = 2\tilde{\pi}^{CD}D_CD_Dh^A_B + 2\left(R^{AC}K_{BC} - RK^A_B + \frac{2(d-3)\Lambda}{(d-2)}\left(K^A_B - \frac{1}{(d-1)}Kh^A_B\right)\right) \tag{A.15}$$

A.2 Restricted Hamilton–Jacobi functional

Here we shall prove the equations for the first and second order Hamilton–Jacobi functionals given in **Results 2**.

A.2.1 First order Hamilton–Jacobi functional

Using the parametrization $\gamma_{ab} = \mathcal{L}_\xi g_{ab}$ for the (projected) boundary metric fluctuations, the first order of the on-shell action evaluates to

$$\begin{aligned} {}^{\mathrm{D}}S^{(1)}_{\mathrm{HJ}} &= \frac{1}{2\kappa}\int_{\partial\mathcal{M}} d^{(d-1)}y\sqrt{h}\epsilon\,\tilde{\pi}^{AB}(\nabla_A\xi_B + \nabla_B\xi_A) \\ &= \frac{1}{\kappa}\int_{\partial\mathcal{M}} d^{(d-1)}y\sqrt{h}\epsilon\,\tilde{\pi}^{AB}\left(D_A\xi_B + K_{AB}\xi^\perp\right) \\ &\simeq \frac{1}{\kappa}\int_{\partial\mathcal{M}} d^{(d-1)}y\sqrt{h}\epsilon\left(-D_A\tilde{\pi}^{AB}\xi_B + \tilde{\pi}^{AB}K_{AB}\xi^\perp\right) \\ &= \frac{1}{\kappa}\int_{\partial\mathcal{M}} d^{(d-1)}y\sqrt{h}\epsilon\,\left(2\Lambda - {}^{\mathrm{b}}R\right)\,\xi^\perp \quad . \end{aligned} \tag{A.16}$$

where $\simeq$ represents modulo corner terms and we have used the Gauss–Codazzi relations (2.10) and (2.11) to arrive at the last line.

A.2.2 Second order Hamilton–Jacobi functional

We consider a $(d-1)$–dimensional boundary $\partial\mathcal{M}$ of a d–dimensional space–time satisfying the vacuum Einstein equations. We assume the parametrization (A.1) for the (projected) boundary fluctuations ζ_{AB} in terms of the diffeomorphism generating vector field ξ^a. We will furthermore assume that the boundary has homogeneous curvature.

The second order of the (restricted) Hamilton–Jacobi functional is then given by

$${}^{\mathrm{D}}S^{(2)}_{\mathrm{HJ}} = -\frac{1}{4\kappa}\int_{\partial\mathcal{M}} d^{(d-1)}y\,\sqrt{h}\epsilon\left(\xi^\perp(\Delta + Q^{AB}K_{AB})\xi^\perp + \xi^\perp Q^{AB}D_A\xi_B - \xi_A Q^{AB}D_B\xi^\perp - \xi^A\mathcal{D}_{AB}\xi^B\right) \tag{A.17}$$

where

$$\begin{aligned} \Delta &= 2\tilde{\pi}^{AB}D_AD_B - 2{}^{\mathrm{b}}R^{AB}\,K_{AB} \quad , \\ \mathcal{D}^A{}_B &= 2\tilde{\pi}^{CD}\left(D_CD_Dh^A_B - {}^{\mathrm{b}}R^A{}_{CDB}\right) \\ Q^{AB} &= 2\left(2\tilde{\pi}^{BC}K^A_C - \tilde{\pi}^{CD}K_{CD}h^{AB}\right) \quad . \end{aligned} \tag{A.18}$$

We remind the reader that we defined the extrinsic curvature tensor through the foliation, which with our choice of Gaussian coordinates amounts to $K_{AB} = \frac{1}{2}\partial_\perp h_{AB}$. We thus introduced ϵ, which is equal to $+1$ for boundary components where the outward pointing

normal in the background geometry is given by $n \equiv \partial_\perp$ (that is the outer boundary), and $\epsilon = -1$ if $n \equiv -\partial_\perp$ (that is the inner boundary).

Proof: We have to evaluate

$$ {}^{\rm D}S^{(2)}_{\rm HJ} \;=\; \frac{1}{2\kappa}\int_{\partial\mathcal{M}} d^{(d-1)}y\,\epsilon\,\delta'(\sqrt{h}\,\tilde{\pi}^{AB})\zeta_{AB}\,. \tag{A.19}$$

with $\delta'\boldsymbol{h}_{AB} = \zeta_{AB} = 2K_{AB}\xi^\perp + D_A\xi_B + D_B\xi_A$.

Let us also use the abbreviation $\tilde{\pi}^{AB} = (\boldsymbol{K}^{AB} - \boldsymbol{K}\boldsymbol{h}^{AB})$ for the spatial tensors, then we find for the integrand in (A.19)

$$\begin{aligned}\mathcal{F} \;&:=\; \delta'\left(\sqrt{h}\tilde{\pi}^{AB}\right)\zeta_{AB}\\ &=\; \sqrt{h}\left(\frac{1}{2}\tilde{\pi}^{AB}\zeta_{AB}h^{CD}\delta' h_{CD} + \delta'\left(\tilde{\pi}^{AB}\zeta_{AB}\right) - \tilde{\pi}^{AB}\delta'\zeta_{AB}\right)\end{aligned} \tag{A.20}$$

Now we will use that by definition $\delta'\xi^\perp = \delta'\xi^A = 0$ and that $\tilde{\pi}^{AB}D_A\xi_B$ is, modulo a total divergence, given by $\xi_B D_A\tilde{\pi}^{AB}$, where $D_A\tilde{\pi}^{AB}$ is the momentum constraint and hence vanishes. Thus also the variation of $\tilde{\pi}^{AB}D_A\xi_B$ vanishes. We also have that the variation $\delta'(D_A\xi_B) = -\xi_C\delta'{}^{\rm b}\Gamma^C_{AB}$ and we get :

$$\mathcal{F} \;\simeq\; \sqrt{h}\left(\xi^\perp\tilde{\pi}^{AB}K_{AB}h^{CD}\delta' h_{CD} + 2\delta'\left(\tilde{\pi}^{AB}K_{AB}\right)\xi^\perp - 2\tilde{\pi}^{AB}\delta' K_{AB}\xi^\perp + 2\tilde{\pi}^{AB}\xi_C\delta'{}^{\rm b}\Gamma^C_{AB}\right)\,. \tag{A.21}$$

We have used $\simeq$ to indicate equivalence up to total divergences. Now let us consider the variation appearing in the second term above

$$\begin{aligned}\delta'\left(\tilde{\pi}^{AB}K_{AB}\right) \;&=\; \delta'\left((h^{AC}h^{BD} - h^{AB}h^{CD})K_{AB}K_{CD}\right)\\ &=\; 2\tilde{\pi}^{AB}\,\delta' K_{AB} - 2\tilde{\pi}^{CA}K_A{}^D\delta' h_{CD}\quad .\end{aligned} \tag{A.22}$$

Therefore, the integrand simplifies to

$$\mathcal{F} \;\simeq\; \sqrt{h}\left(\xi^\perp\left(\tilde{\pi}^{AB}K_{AB}h^{CD} - 2\tilde{\pi}^{AC}K^D_A\right)\delta' h_{CD} + \delta'\left(\tilde{\pi}^{AB}K_{AB}\right)\xi^\perp + 2\tilde{\pi}^{AB}\xi_C\delta'{}^{\rm b}\Gamma^C_{AB}\right)\,. \tag{A.23}$$

The first two terms in the integrand above can be written as $-\frac{1}{2}\xi^\perp Q^{AB}\zeta_{AB}$ using the expression in (A.10). We also have that $\tilde{\pi}^{AB}K_{AB} = 2\Lambda - {}^{\rm b}R$ and hence $\delta'(\tilde{\pi}^{AB}K_{AB}) = \delta'({}^{\rm b}\boldsymbol{R})$. The variation of the boundary Riemann curvature satisfies $\delta'({}^{\rm b}\boldsymbol{R}) = \Pi^{AB}\zeta_{AB}$. Thus, we can use the results in (A.2). For the last term, we will use the results in (A.9) and then get

$$\mathcal{F} \;\simeq\; -\sqrt{h}\left(\xi^\perp\delta'({}^{\rm b}\boldsymbol{R}) + \tfrac{1}{2}\xi^\perp Q^{AB}\zeta_{AB} - \xi_A Q^{AB}D_B\xi^\perp + 2\xi_A D_B({}^{\rm b}R^{AB})\xi^\perp - \xi_A\mathcal{D}^A_B\xi^B\right)\,. \tag{A.24}$$

This form of the Hamilton–Jacobi action holds for a generic boundaries without any assumptions on the boundary space–time. Now if we assume that the boundary curvature is homogeneous, $D_B({}^{\mathrm{b}}R^{AB}) = 0$, and then we finally get the second order restricted Hamilton–Jacobi functional

$$
\begin{aligned}
{}^{\mathrm{D}}S^{(2)}_{\mathrm{HJ}} \;=\; -\frac{1}{2\kappa}\int_{\partial\mathcal{M}} d^{(d-1)}y\,\sqrt{h}\epsilon\Big(&\xi^{\perp}(\Delta + Q^{AB}K_{AB})\xi^{\perp} + \xi^{\perp}Q^{AB}D_A\xi_B - \\
&\xi_A Q^{AB}D_B\xi^{\perp} - \xi^A\mathcal{D}_{AB}\xi^B\Big) \quad .
\end{aligned}
\tag{A.25}
$$

Hence the proof. □

The explicit forms of the background tensors and the boundary differential operators appearing in the second order functional are given in Appendix A.1 with simplified terms in equations (A.14) and (A.15).

Appendix B

Useful formulas

In this chapter, we will derive some formulas that will be needed for computations in the next appendices. We mostly use the Gauss and Codazzi relations which are given in section 2.1.1 and the metric (2.2) given in Gaussian coordinates to derive these formulas here.

B.1 Expanding space–time covariant derivatives

First, consider the metric in Gaussian coordinates with the Christoffel symbols (2.4) given in terms of the extrinsic curvature.The space–time covariant derivatives can be expanded as

$$\begin{aligned}
\nabla_A \gamma_{\perp\perp} &= D_A \gamma_{\perp\perp} - 2K_A^B \gamma_{\perp B}, \\
\nabla_A \gamma_{\perp B} &= D_A \gamma_{\perp B} - K_A^C \gamma_{BC} + K_{AB} \gamma_{\perp\perp}, \\
\nabla_A \gamma_{BC} &= D_A \gamma_{BC} + K_{AB} \gamma_{\perp C} + K_{AC} \gamma_{\perp B}, \\
\nabla_\perp \gamma_{AB} &= \partial_\perp \gamma_{AB} - K_A^E \gamma_{BE} - K_B^E \gamma_{AE}, \\
\nabla_\perp \gamma_{\perp A} &= \partial_\perp \gamma_{A\perp} - K_A^E \gamma_{\perp E},
\end{aligned} \tag{B.1}$$

where the spatial covariant derivative D_A acts on only the spatial indices B. Note that $\nabla_\perp \gamma_{AB}$ involves only the spatial metric perturbations.

Employing the equations above (B.1), we can expand the following expressions quadratic

in the covariant derivatives:

$$\begin{aligned}
\nabla_A\nabla_B\gamma_{CD} &= D_AD_B\gamma_{CD} + D_A\left(K_{BC}\gamma_{\perp D} + K_{BD}\gamma_{\perp C}\right) + K_{AC}D_B\gamma_{\perp D} + K_{AD}D_B\gamma_{\perp C} \\
&\quad + K_{AB}\nabla_\perp\gamma_{CD} + (K_{AC}K_{BD} + K_{AD}K_{BC})\gamma_{\perp\perp} - K_{AC}K^E_B\gamma_{DE} - K_{AD}K^E_B\gamma_{CE}, \\
\nabla_D\nabla_C\gamma_{\perp B} &= D_DD_C\gamma_{\perp B} + D_D\left(K_{BC}\gamma_{\perp\perp}\right) - D_D(K^E_C\gamma_{BE}) + K_{CD}\nabla_\perp\gamma_{\perp B} + K_{BD}D_C\gamma_{\perp\perp} \\
&\quad - 2K^E_CK_{BD}\gamma_{\perp E} - K^E_D\left(D_C\gamma_{BE} + K_{BC}\gamma_{\perp E} + K_{CE}\gamma_{\perp B}\right), \\
\nabla_B\nabla_\perp\gamma_{CD} &= D_B\nabla_\perp\gamma_{CD} + K_{BC}\nabla_\perp\gamma_{\perp D} + K_{BD}\nabla_\perp\gamma_{\perp C} \\
&\quad - K^E_B\left(D_E\gamma_{CD} + K_{CE}\gamma_{\perp D} + K_{DE}\gamma_{\perp C}\right) \quad . \qquad \text{(B.2)}
\end{aligned}$$

B.2 Radial derivatives of boundary tensors

With the abbreviation $\tilde{\pi}^{AB} = K^{AB} - Kh^{AB}$, the contracted Gauss relations satisfy

$$\begin{aligned}
\tilde{\pi}^{AB}K_{AB} &= 2\Lambda - {}^{\mathrm{b}}R \qquad \text{(B.3)} \\
\tilde{\pi}^{AC}K^B_C &= \frac{2\Lambda}{(d-1)}h^{AB} - {}^{\mathrm{b}}R^{AB} \quad . \qquad \text{(B.4)}
\end{aligned}$$

The contracted Codazzi relation is also given by $D_A\tilde{\pi}^{AB} = 0$ and its equivalent to the momentum constraint of the Einstein equations. We have assumed the boundary space–time is homogeneous and hence $D_A(\tilde{\pi}^{BC}K_{BC}) = 0$ and $D_A(\tilde{\pi}^{BD}K^C_D) = 0$.

We will compute the radial derivatives for various background boundary tensors. Our convention is such that the boundary extrinsic curvature is given in terms of the radial derivative of the boundary metric, that is $\partial_\perp h_{AB} = 2K_{AB}$ and $\partial_\perp h^{AB} = -2K^{AB}$.

The Ricci equation adapted to the Gaussian coordinates satisfies

$$\begin{aligned}
R_{A\perp B}{}^{\perp} &= \partial_\perp\Gamma^\perp_{AB} - \Gamma^C_{\perp B}\Gamma^\perp_{CA} \\
&= -\partial_\perp K_{AB} + K_{AC}K^C_B \quad . \qquad \text{(B.5)}
\end{aligned}$$

Using for maximally symmetric solutions $R_{A\perp B}{}^{\perp} = \frac{2\Lambda}{(d-1)(d-2)}h_{AB}$, we obtain the derivative of the extrinsic curvature to be

$$\partial_\perp K_{AB} = K_{AC}K^C_B - \frac{2\Lambda}{(d-1)(d-2)}h_{AB} \quad . \qquad \text{(B.6)}$$

Contractions of (B.6) with the boundary metric and its radial derivative give the following:

$$\begin{aligned}
\partial_\perp K &= -K^{AB}K_{AB} - \tfrac{2\Lambda}{(d-2)} \\
\partial_\perp K^{AB} &= -3K^{AC}K^B_C - \tfrac{2\Lambda}{(d-1)(d-2)}h^{AB} \\
\partial_\perp\tilde{\pi}^{AB} &= 3({}^{\mathrm{b}}R^{AB}) - {}^{\mathrm{b}}Rh^{AB} - K\tilde{\pi}^{AB} + 2\Lambda\tfrac{(d-3)}{(d-1)}h^{AB} \quad . \qquad \text{(B.7)}
\end{aligned}$$

where we have used the Gauss-Codazzi relations to simplify the last expression.

For the radial derivative of the boundary Christoffel symbols we compute

$$\begin{aligned}\partial_\perp {}^{\mathrm{b}}\Gamma^A_{BC} &= \frac{1}{2}h^{AE}\left(D_A\partial_\perp h_{BE} + D_B\partial_\perp h_{AE} - D_E\partial_\perp h_{AB}\right)\\ &= h^{AE}\left(D_A K_{BE} + D_B K_{AE} - D_E K_{AB}\right)\\ &\underset{\text{G.-C.}}{=} D_B K^A_C = D_C K^A_B = D^A K_{BC} \quad .\end{aligned} \tag{B.8}$$

Consider the abbreviation $H^{ABCD} = h^{AB}h^{CD} - h^{AC}h^{BD}$. The following identities hold for contractions with the extrinsic curvature

$$\begin{aligned}&H^{ABCD}K_{CD} = -\tilde{\pi}^{AB}, \qquad H^{ABCD}K_{BC} = 0, \qquad H^{ABCD}K^E_B K_{CE} = 0\\ &H^{ABCD}(K^E_C D_B\gamma_{DE} + K^E_D D_B\gamma_{CE} + K^E_B D_E\gamma_{CD} + K^E_D D_C\gamma_{BE}) = \tfrac{1}{2}(\partial_\perp H^{ABCD})D_B\gamma_{CD}\,.\end{aligned} \tag{B.9}$$

Also, using the Guass-Codazzi relations repeatedly we obtain

$$\begin{aligned}\tfrac{1}{2}(\partial_\perp H^{ABCD})D_A D_B K_{CD} &= 0\\ \tfrac{1}{2}(\partial_\perp H^{ABCD})D_A D_B(D_C\xi_D + D_D\xi_C) &= 2(K_{CD}{}^{\mathrm{b}}R^{ADBC} + {}^{\mathrm{b}}R^{AC}K^B_C)D_A\xi_B\\ \tfrac{1}{2}(\partial_\perp H^{ABCD})K_{CD} &= 2\,{}^{\mathrm{b}}R^{AB} - {}^{\mathrm{b}}R h^{AB} - K\tilde{\pi}^{AB} + 2\Lambda\tfrac{(d-3)}{(d-1)}h^{AB} \quad .\end{aligned} \tag{B.10}$$

B.3 The commutator between radial derivative and spatial operators

To commute radial derivatives and spatial derivatives, we will make use of the derivatives of Christoffel symbols in equation (B.8) to get

$$\begin{aligned}\partial_\perp D_A\xi_B &= D_A\partial_\perp\xi_B - \partial_\perp({}^{\mathrm{b}}\Gamma^C_{AB})\xi_C = D_A\partial_\perp\xi_B - D_A K^C_B\xi_C\\ \partial_\perp D_A\gamma_{BC} &= D_A\partial_\perp\gamma_{BC} - D_A K^E_B\gamma_{CE} - D_A K^E_C\gamma_{BE}\\ \partial_\perp D_A D_B\gamma_{CD} &= D_A\partial_\perp D_B\gamma_{CD} - D_A K^E_B D_E\gamma_{CD} - D_A K^E_C D_B\gamma_{DE} - D_A K^E_D D_B\gamma_{CE} \quad .\end{aligned} \tag{B.11}$$

We will also need the following commutator

$$\left[\partial_\perp, \Delta^{-1}\right] = -\Delta^{-1}\left[\partial_\perp, \Delta\right]\Delta^{-1} \tag{B.12}$$

where $\Delta = 2\tilde{\pi}^{AB} D_A D_B - 2\,{}^{\mathrm{b}}R^{AB} K_{AB}$. This commutator can be simplified by considering its action on a scalar function f. The radial derivative acting on the differential operator Δ satisfies

$$\begin{aligned} \partial_\perp \Delta f &= \Delta \partial_\perp f - 2\tilde{\pi}^{AB} D_A(K_B^C) D_C f + 2\partial_\perp(\tilde{\pi}^{AB}) D_A D_B f - 2\partial_\perp({}^{\mathrm{b}}R^{AB} K_{AB}) f \\ &= \Delta \partial_\perp f - 2 D_A({}^{\mathrm{b}}R^{AB}) D_B f + 2\partial_\perp(\tilde{\pi}^{AB}) D_A D_B f - 2\partial_\perp({}^{\mathrm{b}}R^{AB} K_{AB}) f \quad . \end{aligned} \tag{B.13}$$

where we have used the identities in (B.11) to commute radial and spatial covariant derivatives. Let us consider the case where the intrinsic geometry on the boundary is flat, i.e ${}^{\mathrm{b}}R = 0$, then the commutator simplifies to

$$[\partial_\perp, \Delta]\, f = \left(-2K\tilde{\pi}^{AB} + 4\Lambda \tfrac{(d-3)}{(d-1)} h^{AB}\right) D_A D_B f = -K\Delta f + 4\Lambda \tfrac{(d-3)}{(d-1)} D^A D_A f \tag{B.14}$$

where we have used the formula for $\partial_\perp \tilde{\pi}^{AB}$ given in (B.7) and also that $\Delta = 2\tilde{\pi}^{AB} D_A D_B$ for flat boundaries.

In the case where the boundary geometry is a spherical $\mathbb{S}^{\mathrm{d}-1}$, the extrinsic curvature and boundary Ricci curvature satisfies $K_{AB} = \frac{1}{r} h_{AB}$ and ${}^{\mathrm{b}}R^{AB} = \frac{1}{(d-1)} {}^{\mathrm{b}}R h^{AB} = \frac{(d-2)}{r^2} h^{AB}$ respectively. Hence we get the following radial derivatives

$$\partial_\perp \tilde{\pi}^{AB} = \tfrac{1}{r} \tilde{\pi}^{AB} \quad , \qquad \partial_\perp {}^{\mathrm{b}}R^{AB} = 0 \quad , \qquad \partial_\perp K_{AB} = -\tfrac{1}{r} K_{AB} \tag{B.15}$$

Using these identities, we can simplify the equations in (B.13) to get the commutator

$$[\partial_\perp, \Delta]\, f = \tfrac{2}{r} \tilde{\pi}^{AB} D_A D_B f + \tfrac{2}{r} {}^{\mathrm{b}}R^{AB} K_{AB} f = -\tfrac{1}{r} \Delta f + \tfrac{4}{r} \tilde{\pi}^{AB} D_A D_B f \tag{B.16}$$

which holds for a spherical boundary.

Appendix C

Solutions to equations of motion

Here, we will give a general procedure for solving the (linearized) Einstein equations of motion and then specialize to the cases for which the background boundary is a) flat and b) spherical. In both cases, we shall consider the diffeomorphism sector of the equations of motion and find solutions to the lapse and shift ($\zeta_{\perp\perp}$ and $\zeta_{\perp A}$) metric perturbations.

The second order gravitational action with Lagrange multiplier term (2.41) is given by

$$\begin{aligned} -\kappa S_\lambda^{(2)} &= \frac{1}{2}\int_M d^dx\sqrt{g}\;\gamma_{ab}\left(V^{abcd}\,\gamma_{cd} \;+\; \tfrac{1}{2}\,G^{abcdef}\,\nabla_c\nabla_d\gamma_{ef}\right) \;+ \\ &\quad \frac{1}{2}\int_{\partial\mathcal{M}} d^{(d-1)}y\sqrt{h}\,\epsilon\,\gamma_{ab}\left(\,(B_1)^{abcd}\gamma_{cd} + \,(B_2)^{abecd}\nabla_e\gamma_{cd}\right) \;+ \\ &\quad \frac{1}{2}\int_{(\partial\mathcal{M})_{r_{\rm out}}} d^{(d-1)}y\;\lambda(y)\,(\rho(y)-\ell_{\rm g}[\gamma_{\perp\perp}]) \end{aligned} \tag{C.1}$$

where we have

$$\begin{aligned} V^{abcd} &= \frac{1}{2}\left[\frac{1}{2}\,(R-2\Lambda)\left(g^{ab}g^{cd}-2g^{ac}g^{bd}\right) - R^{ab}g^{cd} - g^{ab}R^{cd} + 2\left(g^{ac}R^{bd}+g^{bc}R^{ad}\right)\right] \\ G^{abcdef} &= g^{ab}g^{ce}g^{df}+g^{ad}g^{bc}g^{ef}+g^{ae}g^{bf}g^{cd}-g^{ab}g^{cd}g^{ef}-g^{ad}g^{bf}g^{ce}-g^{af}g^{bd}g^{ce} \\ B_1^{abcd} &= \frac{1}{2}(Kh^{ab}-K^{ab})g^{cd}-h^{ac}h^{bd}K-h^{ab}K^{cd}+h^{ac}K^{bd}+h^{bd}K^{ac} \\ B_2^{abecd} &= \frac{1}{2}\left(\left(h^{ae}h^{bd}-h^{ab}h^{ed}\right)n^c+\left(h^{ac}h^{be}-h^{ab}h^{ce}\right)n^d-\left(h^{ac}h^{bd}-h^{ab}h^{cd}\right)n^e\right). \end{aligned} \tag{C.2}$$

The derivation for the second order expansion of the boundary term can be found in [23].

Using the form of the Ricci tensor and Ricci scalar for vacuum solutions, we can write

$$V^{abcd} = \frac{\Lambda}{d-2}\left(2g^{ac}g^{bd} - g^{ab}g^{cd}\right) \quad . \tag{C.3}$$

The variation of the action (C.1) with respect to the metric perturbations γ_{ab} leads to the equations of motion

$$\hat{G}^{ab} := \left(V^{abcd}\,\gamma_{cd} \;+\; \tfrac{1}{2}\,G^{abcdef}\,\nabla_c\nabla_d\gamma_{ef}\right) \;=\; \frac{1}{4}\frac{\lambda(y)}{\sqrt{h}}\delta^a_\perp\delta^b_\perp \quad . \tag{C.4}$$

One can show that $\gamma_{ab} = \nabla_a\xi_b + \nabla_b\xi_a$ satisfies (C.4) for $\lambda = 0$. Here we want to solve the equations including the Lagrange multiplier term. As explained in section 2.3 it is sufficient to solve the $(\perp\perp)$ and $(\perp\, A)$ components of the equations of motion and solve for the lapse and shift perturbations.

We therefore, consider the Hamiltonian constraint

$$H \;:=\; -2V^{\perp\perp cd}\,\gamma_{cd} \;-\; G^{\perp\perp cdef}\,\nabla_c\nabla_d\gamma_{ef} \quad , \tag{C.5}$$

as well as the momentum constraint

$$M^A \;:=\; 2V^{\perp Acd}\,\gamma_{cd} \;+\; G^{\perp Acdef}\,\nabla_c\nabla_d\gamma_{ef} \quad . \tag{C.6}$$

To rewrite the constraints we will make use of the fact that we have a maximally symmetric background solution (2.6) and that the Gauss–Codazzi relations (2.9,2.10,2.11) hold. Using the shorthand $H^{ABCD} = h^{AB}h^{CD} - h^{AC}h^{BD}$, we simplify the constraints as

$$\begin{aligned} H &= \left(\tfrac{2\Lambda}{(d-1)}h^{AB}\gamma_{AB} + H^{ABCD}\nabla_A\nabla_B\gamma_{CD}\right) \\ M^A &= \left(\tfrac{4\Lambda}{(d-1)}h^{AB}\gamma_{\perp B} + H^{ABCD}(\nabla_B\nabla_\perp\gamma_{CD} + \nabla_D\nabla_C\gamma_{\perp B})\right) \quad . \end{aligned} \tag{C.7}$$

We will make use of the formulas in (B.2) to simplify further the space–time covariant derivative terms in the Hamiltonian and momentum constraints. After some algebra these constraints become

$$H \;=\; \tilde{\pi}^{AB}K_{AB}\gamma_{\perp\perp} + 2\tilde{\pi}^{AB}D_A\gamma_{\perp B} - \tilde{\pi}^{AB}\partial_\perp\gamma_{AB} + H^{ABCD}D_AD_B\gamma_{CD} + R^{AB}\gamma_{AB}\,, \tag{C.8}$$

$$\begin{aligned} M^A \;=\;& 2\,{}^{\mathrm{b}}R^{AB}\gamma_{\perp B} + \tilde{\pi}^{AB}D_B\gamma_{\perp\perp} + H^{ABCD}(D_DD_C\gamma_{\perp B} + \partial_\perp D_B\gamma_{CD} - D_D(K^E_C\gamma_{BE})) \\ &+ \tfrac{1}{2}\left(\partial_\perp H^{ABCD}\right)D_B\gamma_{CD} \quad . \end{aligned} \tag{C.9}$$

In deriving these equations, we have used the formulas in equation (B.11) to commute radial and spatial covariant derivatives and also the last identity in (B.9) to simplify the momentum constraint. In the case of vanishing λ one can solve the Hamiltonian and momentum constraint equations for the lapse and shift perturbations which will determine the solutions to the equations of motions (C.4).

The divergence of the momentum constraint M^A can be simplified further by using the following :

$$H^{ABCD}D_AD_DD_C\gamma_{\perp B} = \left(D^AD^B - D^BD^A\right)D_A\gamma_{\perp B} = 0 \tag{C.10}$$

which is satisfied since the curvature tensors in its expansion cancel out. Furthermore $H^{ABCD}D_AK^E_D = 0$ as we have $D_AK^E_D = D_DK^E_A = D^EK_{AD}$ due to the Codazzi relation (2.11). The following identity also holds:identity

$$\begin{aligned} D_A(H^{ABCD}\partial_\perp D_B\gamma_{CD} + \tfrac{1}{2}\partial_\perp H^{ABCD}D_B\gamma_{CD}) &= H^{ABCD}\partial_\perp D_AD_B\gamma_{CD} + \tfrac{1}{2}\partial_\perp H^{ABCD}D_AD_B\gamma_{CD} \\ &= \partial_\perp(H^{ABCD}D_AD_B\gamma_{CD}) - \tfrac{1}{2}\partial_\perp H^{ABCD}D_AD_B\gamma_{CD} \end{aligned} \tag{C.11}$$

We therefore obtain the divergence of the momentum constraint

$$D_AM^A = 2\,{}^{\mathrm{b}}R^{AB}D_A\gamma_{\perp B} + \tilde{\pi}^{AB}D_AD_B\gamma_{\perp\perp} + \partial_\perp(H^{ABCD}D_AD_B\gamma_{CD}) - \tfrac{1}{2}\partial_\perp H^{ABCD}D_AD_B\gamma_{CD} \tag{C.12}$$

where we have also used that the boundary is homogeneous, that is $D_A{}^{\mathrm{b}}R^{AB} = 0$.

C.1 Equations of motion for flat boundaries

We will now restrict to the case where the background boundary has vanishing curvature. The divergence of the momentum constraint in this case satisfies

$$D_AM^A = \tfrac{1}{2}\Delta\gamma_{\perp\perp} - \partial_\perp(\Pi^{AB}\gamma_{AB}) - \tfrac{1}{2}\partial_\perp(H^{ABCD})D_AD_B\gamma_{CD} \tag{C.13}$$

where $\Delta = 2\tilde{\pi}^{AB}D_AD_B$ and $\Pi^{AB}\gamma_{AB} = -H^{ABCD}D_AD_B\gamma_{CD}$, which apply for a flat background boundary. We have assumed that the operator Δ is invertible and hence we can easily find the solution of the lapse $\gamma_{\perp\perp}$ from the divergence of the momentum constraint (C.13).

We will now consider the restriction to the diffeomorphism sector where we adopt a parametrization

$$\gamma_{AB} \equiv \zeta_{AB} = 2K_{AB}\xi^\perp + D_A\xi_B + D_B\xi_A \tag{C.14}$$

for the boundary metric perturbations such that we have $\Pi^{AB}\zeta_{AB} = \Delta\xi^{\perp}$.

The last term in the divergence of the momentum (C.13) restricted to the diffeomorphism sector can be simplified using the formulas in (B.10) applied to flat boundaries to get

$$\tfrac{1}{2}\partial_{\perp}(H^{ABCD})D_AD_B\zeta_{CD} = \partial_{\perp}(H^{ABCD})K_{CD}D_AD_B\xi^{\perp} = (-2K\tilde{\pi}^{AB} + 4\Lambda\tfrac{(d-3)}{(d-1)}h^{AB})D_AD_B\xi^{\perp} \quad .(C.15)$$

using the parametrization (C.14). The term on right hand side of (C.15) is equal to the commutator $[\partial_{\perp}, \Delta]$ which we have computed in (B.14) for the case of vanishing intrinsic curvature. Hence we get from the divergence D_AM^A, the solution for the lapse

$$\zeta_{\perp\perp} = 2\partial_{\perp}\xi^{\perp} \quad , \tag{C.16}$$

We now insert this solution into the linearized Hamiltonian constraint

$$H \;\; = \;\; \tilde{\pi}^{AB}K_{AB}\zeta_{\perp\perp} + 2\tilde{\pi}^{AB}D_A\zeta_{\perp B} - \Pi^{AB}\zeta_{AB} - \tilde{\pi}^{AB}\partial_{\perp}\zeta_{AB}\,. \tag{C.17}$$

Substituting furthermore $\zeta_{\perp A} = D_A\xi^{\perp} + h_{AB}\partial_{\perp}\xi^B$, and making use of the identities we have derived in Appendix B one gets $H = 0$. To take into account the Lagrange multiplier term consider the ansatz $\zeta_{\perp A} = D_A\xi^{\perp} + h_{AB}\partial_{\perp}\xi^B + t_A$. We then have to solve

$$H = 2\tilde{\pi}^{AB}D_At_B \stackrel{!}{=} -\frac{1}{2}\frac{\lambda}{\sqrt{h}} \quad . \tag{C.18}$$

Choosing $t_B = -D_B\frac{1}{2\Delta}\frac{\lambda}{\sqrt{h}}$ we see that we satisfy this equation. The addition of such a t_B to $\zeta_{\perp B}$ does leave the momentum constraint (C.9) invariant, if we use that boundary Ricci curvature tensor vanishes and spatial covariant derivatives commute. Hence the general solution of the lapse and shift perturbations for the case where the boundary manifold is flat, i.e., ${}^bR = 0$ is given by

$$\zeta_{\perp\perp} = 2\partial_{\perp}\xi^{\perp}\,, \qquad \zeta_{\perp A} = D_A\left(\xi^{\perp} - \frac{1}{2\Delta}\frac{\lambda}{\sqrt{h}}\right) + h_{AB}\partial_{\perp}\xi^B \quad . \tag{C.19}$$

In three dimensions or in the case for vanishing cosmological constant we get from (B.14) the commutator

$$\partial_{\perp}\frac{1}{\Delta}\frac{\lambda}{\sqrt{h}} = \frac{1}{\Delta}\partial_{\perp}\frac{\lambda}{\sqrt{h}} + \frac{1}{\Delta}K\frac{\lambda}{\sqrt{h}} = 0 \tag{C.20}$$

where $\partial_{\perp}\sqrt{h} = -K\sqrt{h}$ and $\partial_{\perp}\lambda = 0$. Hence, in three dimensions or in $d \geq 3$ with vanishing cosmological constant, the lapse solution can be accommodated by

$$\zeta_{\perp\perp} = 2\partial_{\perp}\hat{\xi}^{\perp} = 2\partial_{\perp}\left(\xi^{\perp} - \frac{1}{2\Delta}\frac{\lambda}{\sqrt{h}}\right) \quad . \tag{C.21}$$

C.2 Equations of motion in spherical coordinates

Here we will consider the diffeomorphism sector of the equations of motions with Lagrange multiplier term (C.4) for the case with spherical boundary embedded in Euclidean flat space–time, where we have non-vanishing intrinsic curvature. The metric in spherical coordinates is given by

$$ds^2 = dr^2 + h_{AB}dy^A dy^B = dr^2 + r^2 d\Omega_{\mathbb{S}^{d-1}} \quad , \tag{C.22}$$

where $d\Omega_{\mathbb{S}^{d-1}}$ is the metric on the spherical boundary. The extrinsic curvature is given by $K_{AB} = \frac{1}{r}h_{AB}$ whiles the Ricci curvature is ${}^{b}R_{AB} = \frac{1}{(d-1)}{}^{b}R h_{AB} = \frac{(d-2)}{r^2}h_{AB}$, hence we have the identities

$$R^{AB} + \tfrac{1}{r}\tilde{\pi}^{AB} \;=\; 0 \quad , \quad \tfrac{1}{2}\partial_\perp H^{ABCD} = -\tfrac{2}{r}H^{ABCD} \quad . \tag{C.23}$$

Using the definitions of the Hamiltonian H in (C.8) and the divergence of the momentum $D_A M^A$ in (C.12), we obtain

$$\begin{aligned} D_A M^A + \frac{1}{r}\left(H + \frac{1}{2}\frac{\lambda}{\sqrt{h}}\right) \;=\; & \frac{1}{2}\Delta\gamma_{\perp\perp} - \partial_\perp(\Pi^{AB}\gamma_{AB}) - \frac{1}{2r}\partial_\perp(H^{ABCD})D_A D_B\gamma_{CD} \\ & -\frac{1}{r}\Pi^{AB}\gamma_{AB} + \frac{1}{2r}\frac{\lambda}{\sqrt{h}}\,. \end{aligned} \tag{C.24}$$

Now consider the induced perturbation with $\gamma_{AB} \equiv \zeta_{AB}$ restricted to the diffeomorphism sector in (C.14). We can use the equations (B.10) and the form of the curvature tensor for the sphere to express the following

$$\tfrac{1}{2}\partial_\perp(H^{ABCD})D_A D_B(D_C\xi_D + D_D\xi_C) = 2(K_{CD}{}^{b}R^{ADBC} + {}^{b}R^{AC}K^B_C)D_A\xi_B = 0 \tag{C.25}$$

since ${}^{b}R^{ADBC}K_{CD} = \frac{1}{r^2}\tilde{\pi}^{AB}$ holds for a spherical boundary. Using the last expression in (C.23) and the fact that the left hand side of (C.24) vanishes, we get

$$\frac{1}{2}\Delta\zeta_{\perp\perp} = \partial_\perp\Delta\xi^\perp + \frac{1}{r}\Delta\xi^\perp - \frac{4}{r}\pi^{AB}D_A D_B\xi^\perp - \frac{1}{2r}\frac{\lambda}{\sqrt{h}} \quad . \tag{C.26}$$

The commutator $[\partial_\perp, \Delta]$ for the spherical boundary is given in (B.16) and hence the solution for the lapse for a spherical boundary space–time is given by

$$\zeta_{\perp\perp} = 2\partial_\perp\xi^\perp - \frac{1}{r}\frac{1}{\Delta}\frac{\lambda}{\sqrt{h}} \tag{C.27}$$

Inserting the lapse solution (C.27) and $\zeta_{\perp A} = D_A\xi^\perp + h_{AB}\partial_\perp\xi^B + t_B$ into the $\perp\perp$ component of the equation of motion (C.4), we get

$$H = -\frac{1}{r}\frac{1}{\Delta}\frac{\lambda}{\sqrt{h}}\tilde{\pi}^{AB}K_{AB} + 2\tilde{\pi}^{AB}D_A t_B = R^{AB}K_{AB}\frac{1}{\Delta}\frac{\lambda}{\sqrt{h}} + 2\tilde{\pi}^{AB}D_A t_B \stackrel{!}{=} -\frac{1}{2}\frac{\lambda}{\sqrt{h}} \quad . \tag{C.28}$$

which is again solved by $t_B = -D_B\frac{1}{2\Delta}\frac{\lambda}{\sqrt{h}}$. Thus the solution to the shift perturbations are given by

$$\zeta_{\perp A} \;=\; D_A(\xi^\perp - \frac{1}{2\Delta}\frac{\lambda}{\sqrt{h}}) + h_{AB}\partial_\perp\xi^B \quad . \tag{C.29}$$

These solutions can be inserted into the spatial–spatial part of the Einstein equations, and one will find that these evaluate to zero, $\hat{G}^{AB} = 0$. This can be also expected from the fact that the divergence of the Einstein equations, including the Lagrange multiplier term, vanishes identically.

For the geometry of a sphere, we have the scaling properties $\Delta = r^{-3}\bar{\Delta}$, $\sqrt{h} = r^{d-1}\sqrt{\bar{h}}$ where $\bar{\Delta}$ and $\sqrt{\bar{h}}$ are both independent of the radial coordinate r, and hence we have

$$\partial_\perp\left(\frac{1}{\Delta}\frac{\lambda}{\sqrt{h}}\right) = \frac{(4-d)}{r}\frac{1}{\Delta}\frac{\lambda}{\sqrt{h}} \quad . \tag{C.30}$$

In summary, we obtain that for three dimensions, for all the backgrounds we consider in chapter 3 of the thesis, the solutions are given by

$$\zeta_{\perp\perp} \;=\; 2\partial_\perp\hat{\xi}^\perp \quad , \quad \zeta_{\perp A} = D_A\hat{\xi}^\perp + h_{AB}\partial_\perp\xi^B \tag{C.31}$$

with

$$\hat{\xi}^\perp = \xi^\perp - \frac{1}{2\Delta}\frac{\lambda}{\sqrt{h}} \tag{C.32}$$

and $\xi^\perp$ and ξ^A defined in (2.22).

C.3 Lagrange multiplier dependent boundary terms

We have considered the Einstein equations with Lagrange multiplier term

$$\hat{G}^{ab} \;=\; \frac{1}{4}\frac{\lambda(y)}{\sqrt{h}}\delta^a_\perp\delta^b_\perp \quad , \tag{C.33}$$

computed from $G^{\perp\perp}$ and $G^{\perp A}$ equations, the lapse and shift perturbations $\gamma_{\perp\perp}$ and $\gamma_{\perp A}$. In all the examples we consider, we find that the solutions of the diffeomorphism sector can be expressed as

$$\begin{aligned} \zeta_{\perp\perp} &= 2\partial_\perp \xi^\perp + \beta \frac{1}{r}\frac{1}{\Delta}\frac{\lambda}{\sqrt{h}} \quad , \\ \zeta_{\perp A} &= D_A \hat{\xi}^\perp + h_{AB}\partial_\perp \xi^B \quad , \end{aligned} \tag{C.34}$$

where

$$\hat{\xi}^\perp = \xi^\perp - \frac{1}{2\Delta}\frac{\lambda}{\sqrt{h}} \quad , \tag{C.35}$$

and $\beta = 0$ for background with a flat boundary and $\beta = 1$ for a spherical boundary. The components ξ^a are understood as functionals of the spatial metric perturbations γ_{AB}, as defined in (2.22).

Here we are going to evaluate the (second order) boundary term on solutions of the form (C.34). We already know the result for λ=0 (see Appendix A.2), we therefore need only keep track of the λ–dependent terms.

These terms only arise through the lapse and shift components. The only terms where these appear in the second order contribution to the boundary action (C.1) are given by

$$\begin{aligned} &\zeta_{AB}\left(B_1^{AB\perp\perp}\zeta_{\perp\perp} + B_2^{ABC\perp D}\nabla_C\zeta_{\perp D} + B_2^{ABCC\perp}\nabla_D\zeta_{C\perp}\right) \\ &= \zeta_{AB}\left(-\tfrac{1}{2}\tilde{\pi}^{AB}\zeta_{\perp\perp} + (h^{AC}h^{BD} - h^{AB}h^{CD})\nabla_C\zeta_{\perp D}\right) \\ &= \zeta_{AB}\left(\tfrac{1}{2}\tilde{\pi}^{AB}\zeta_{\perp\perp} - H^{ABCD}D_C\zeta_{\perp D}\right) \end{aligned} \tag{C.36}$$

where $\tilde{\pi}^{AB} = K^{AB} - Kh^{AB}$. For boundaries with vanishing intrinsic curvature $\zeta_{\perp\perp}$ is independent of λ whiles for spherical boundaries we have ${}^{\mathrm{b}}R^{AB} = -\frac{1}{r}\tilde{\pi}^{AB}$. Using the definition of Π^{AB} in (2.23), we get that the $\lambda-$dependent terms are of the form

$$\zeta_{AB}\left(\tfrac{1}{2}\tilde{\pi}^{AB}\zeta_{\perp\perp} - H^{ABCD}D_C\zeta_{\perp D}\right) = \zeta_{AB}\Pi^{AB}\left(\frac{1}{2\Delta}\frac{\lambda}{\sqrt{h}}\right) \quad , \tag{C.37}$$

for all the background examples we consider. We therefore obtain the $\lambda-$dependent boundary term

$$\begin{aligned} \frac{1}{2}\int_{\partial\mathcal{M}} d^{(d-1)}y\,\sqrt{h}\epsilon\,\zeta_{AB}\Pi^{AB}\left(\frac{1}{2\Delta}\frac{\lambda}{\sqrt{h}}\right) &= \frac{1}{4}\int_{\partial\mathcal{M}} d^{(d-1)}y\,\sqrt{h}\epsilon\,(\Delta^{-1}\Pi^{AB}\zeta_{AB})\frac{\lambda}{\sqrt{h}} \\ &= \frac{1}{4}\int_{\partial\mathcal{M}} d^{(d-1)}y\,\epsilon\,\lambda\,\xi^\perp \end{aligned} \tag{C.38}$$

Appendix D

Geodesic length to first order in metric perturbations

We are interested in the geodesic distance between two fixed coordinate points, for a given (Euclidean) metric. The full metric will differ from a background metric by a perturbation, and we need the expansion of the geodesic distance in the metric perturbations to first order.

The background metric is g_{ab}, and the background geodesic $x^a(\tau)$ with $\tau \in [0,1]$. The full metric is $\boldsymbol{g}_{ab}$ and the $\boldsymbol{g}$–geodesic will be called $\boldsymbol{x}(\tau) = x(\tau) + \delta\boldsymbol{x}(\tau)$. We will assume that $\boldsymbol{x}$ is affinely parametrized, so it has constant modulus w.r.t $\boldsymbol{g}$ and thus satisfies

$$\nabla_{\dot{\boldsymbol{x}}}\dot{\boldsymbol{x}}^a = 0, \qquad \frac{d}{d\tau}(\dot{\boldsymbol{x}}^a\dot{\boldsymbol{x}}^b\boldsymbol{g}_{ab}) = 0. \tag{D.1}$$

These equations continue to hold under variations.

We will consider the variation of the square of the geodesic length

$$L^2 = \int_0^1 d\tau\, \dot{\boldsymbol{x}}^a\dot{\boldsymbol{x}}^b\boldsymbol{g}_{ab} \quad . \tag{D.2}$$

This is indeed the square length as $z(\tau)$ has constant modulus. The variation is given by

$$\delta L^2 = \int_0^1 \mathrm{d}\tau\Big[2\frac{d}{d\tau}\big(\delta\boldsymbol{x}^a\dot{x}^b g_{ab}\big) - 2\delta\boldsymbol{x}^a\frac{d}{d\tau}\big(g_{ab}\dot{x}^b\big) + \delta\boldsymbol{x}^c\partial_c g_{ab}\dot{x}^a\dot{x}^b + \dot{x}^a\dot{x}^b\delta\boldsymbol{g}_{ab}\Big] \tag{D.3}$$

$$= 2\Big[\delta\boldsymbol{x}^a\dot{x}^b g_{ab}\Big]_{\tau=0}^1 - 2\int_0^1 d\tau\,\delta\boldsymbol{x}^a(\nabla_{\dot{x}}\dot{x}_a) + \int_0^1 \mathrm{d}\tau\dot{x}^a\dot{x}^b\delta\boldsymbol{g}_{ab} \quad , \tag{D.4}$$

where second and third term in the first line combine to the covariant derivative in the second line.

Since $\delta\boldsymbol{x}$ vanishes at the end points, we can drop the first term. Furthermore as x is an affine geodesic, we can also drop the second term and are left with

$$\delta L^2 = \int_0^1 d\tau\, \dot{x}^a \dot{x}^b \gamma_{ab} \quad , \tag{D.5}$$

where $\delta\boldsymbol{g}_{ab} = \gamma_{ab}$.

With $x^a = (r_{\rm in} + (r_{\rm out} - r_{\rm in})\tau, 0, 0)$ we therefore have for the first order perturbation of the geodesic length

$$\ell_{\rm g} := \delta L = \frac{1}{2(r_{\rm out} - r_{\rm in})} \int_0^1 d\tau\, (r_{\rm out} - r_{\rm in})^2\, \gamma_{\perp\perp} \;=\; \frac{1}{2} \int_{r_{\rm in}}^{r_{\rm out}} d\tau\, \gamma_{\perp\perp}(r) \quad . \tag{D.6}$$

Appendix E

Smoothness conditions for the metric at $r = 0$

Consider the metric perturbations $\gamma_{\mu\nu}$ expressed in Cartesian coordinates (x, y, t) such that the components of the metric $\gamma_{\mu\nu}$ are smooth at the origin and can thus be expanded in a Taylor series in the coordinates. We shall transform the metric from flat into polar coordinates (r, θ, t) and spherical coordinates (r, θ, φ) and study the behaviour of the metric components near the origin $r \to 0$. Let us denote the components of the metric perturbations in polar or spherical coordinates by γ_{ab}.

In polar coordinates, we have the transformation of the coordinates and the components of the metric are given by

$$x = r\cos\theta, \quad y = r\sin\theta, \quad \gamma_{ab} = \gamma_{\mu\nu}\frac{\partial x^\mu}{\partial x^a}\frac{\partial x^\nu}{\partial x^b} \quad . \tag{E.1}$$

The components of the metric in polar coordinates are therefore given by

$$\begin{aligned}
\gamma_{\perp\perp} &= \gamma_{xx}\cos^2\theta + \gamma_{yy}\sin^2\theta + \gamma_{xy}\sin 2\theta, \\
\gamma_{\theta\theta} &= r^2\left(\gamma_{xx}\sin^2\theta + \gamma_{yy}\cos^2\theta - \gamma_{xy}\sin 2\theta\right), \\
\gamma_{tt} &= \gamma_{tt}, \\
\gamma_{\perp\theta} &= r\left(\tfrac{1}{2}\sin(2\theta)(\gamma_{yy} - \gamma_{xx}) + \gamma_{xy}\cos 2\theta\right), \\
\gamma_{\perp t} &= \gamma_{xt}\cos\theta + \gamma_{yt}\sin\theta, \\
\gamma_{\theta t} &= r\left(\gamma_{yt}\cos\theta - \gamma_{xt}\sin\theta\right) \quad .
\end{aligned} \tag{E.2}$$

Given that the metric components $(\gamma_{xx}, \gamma_{yy}, \gamma_{tt}, \gamma_{xy}, \gamma_{xt}, \gamma_{yt})$ are smooth functions near the origin, a Taylor expansion of the metric perturbations around the origin for the thermal

flat spinning space is given by

$$\begin{aligned}
\gamma_{ab} &= a^{(0)}_{ab} + a^{(1)}_{ab}\, r + a^{(2)}_{ab}\, r^2 + \mathcal{O}(r^3) \quad \text{for } ab = rr, tt, rt; \\
\gamma_{ab} &= a^{(1)}_{ab}\, r + a^{(2)}_{ab}\, r^2 + \mathcal{O}(r^3) \quad \text{for } ab = r\theta, \theta t; \\
\gamma_{\theta\theta} &= a^{(2)}_{\theta\theta}\, r^2 + \mathcal{O}(r^3) \quad .
\end{aligned} \tag{E.3}$$

In spherical coordinates, we have the coordinate transformation

$$x = r\sin\theta\cos\varphi, \quad y = r\sin\theta\sin\varphi, \quad t = r\cos\theta \quad . \tag{E.4}$$

The components of the metric in spherical coordinates are given by

$$\begin{aligned}
\gamma_{\perp\perp} &= \sin^2\theta(\gamma_{xx}\cos^2\varphi + \gamma_{yy}\sin^2\varphi) + \gamma_{tt}\cos^2\theta + \gamma_{xy}\sin^2\theta\sin 2\varphi + \sin 2\theta(\gamma_{yt}\sin\varphi + \gamma_{xt}\cos\varphi), \\
\gamma_{\theta\theta} &= r^2\left(\cos^2\theta(\gamma_{xx}\cos^2\varphi + \gamma_{yy}\sin^2\varphi) + \gamma_{tt}\sin^2\theta + \gamma_{xy}\cos^2\theta\sin 2\varphi - \sin 2\theta(\gamma_{yt}\sin\varphi + \gamma_{xt}\cos\varphi)\right), \\
\gamma_{\varphi\varphi} &= r^2\left(\sin^2\theta(\gamma_{xx}\sin^2\varphi + \gamma_{yy}\cos^2\varphi) - \gamma_{xy}\sin^2\theta\sin 2\varphi\right), \\
\gamma_{\perp\theta} &= r\left(\tfrac{1}{2}\sin 2\theta(\gamma_{xx}\cos^2\varphi + \gamma_{yy}\sin^2\varphi - \gamma_{tt} + \gamma_{xy}(\sin 2\varphi + \cos 2\theta)) - 2\sin^2\theta(\gamma_{xt}\cos\varphi + \gamma_{yt}\sin\varphi)\right), \\
\gamma_{\perp\varphi} &= r\sin^2\theta\left(\tfrac{1}{2}\sin 2\varphi(\gamma_{yy} - \gamma_{xx}) + \gamma_{xy}\cos^2\varphi\right), \\
\gamma_{\theta\varphi} &= r^2\sin 2\theta\left(\tfrac{1}{4}\sin 2\varphi(\gamma_{yy} - \gamma_{xx}) + \gamma_{xy}\cos^2\varphi\right) \quad .
\end{aligned} \tag{E.5}$$

The Taylor expansion for the metric perturbations in spherical space–time region around the origin $r = 0$ is thus

$$\begin{aligned}
\gamma_{\perp\perp} &= a^{(0)}_{rr} + a^{(1)}_{rr}\, r + a^{(2)}_{rr}\, r^2 + \mathcal{O}(r^3); \\
\gamma_{ab} &= a^{(1)}_{ab}\, r + a^{(2)}_{ab}\, r^2 + \mathcal{O}(r^3) \quad \text{for } ab = r\theta, r\varphi; \\
\gamma_{ab} &= a^{(2)}_{ab}\, r^2 + \mathcal{O}(r^3) \quad \text{for } ab = \theta\theta, \varphi\varphi, \theta\varphi \quad .
\end{aligned} \tag{E.6}$$

The Euclidean AdS_3 space–time can be described as a hyperbolic hypersurface in a four dimensional Euclidean manifold $\mathbb{R}^4$ with a pseudo-Riemannian metric $\eta_{\mu\nu} = \mathrm{diag}(-,+,+,+)$[1] described by

$$\mathrm{AdS}_3 = \{x^\mu = (t_1, t_2, x_1, x_2) \in \mathbb{R}^{(1,3)} \mid -t_1^2 + t_2^2 + x_1^2 + x_2^2 = -1\} \tag{E.7}$$

The hypersurface can be parametrized by

$$\begin{aligned}
t_1 &= \cosh r\cosh t, \quad x_1 = \sinh r\cos\theta, \\
t_2 &= \cosh r\sinh t, \quad x_2 = \sinh r\sin\theta \quad .
\end{aligned} \tag{E.8}$$

[1] In Lorentzian AdS_3 space–time, the metric is $\mathbb{R}^{(2,2)}$

Since we are only interested in the coefficients of the radial coordinates r, we get that the metric perturbations for the AdS_3 metric using the transformation (E.1) gives,

$$\begin{aligned}
\gamma_{\perp\perp} &= a_1 \cosh^2 r + b_1 \sinh(2r) + c_1 \sinh^2 r \ , & \gamma_{\theta\theta} &= a_4 \sinh^2 r \ , \\
\gamma_{\perp\theta} &= a_2 \sinh(2r) + b_2 \sinh^2 r \ , & \gamma_{\theta t} &= a_5 \sinh(2r) \ , \\
\gamma_{\perp t} &= a_3 \sinh(2r) + b_3 \cosh^2 r \ , & \gamma_{tt} &= a_6 \cosh^2 r \ .
\end{aligned} \tag{E.9}$$

where the coefficients $a_i, b_i, c_i, i = 1, \cdots 6$ are functions of angular coordinate θ and time coordinate t. Performing a series expansion of the hyperbolic trigonometric functions of r in the equations (E.9) above, we get

$$\begin{aligned}
\gamma_{ab} &= a^{(0)}_{ab} + a^{(1)}_{ab}\, r + a^{(2)}_{ab}\, r^2 + \mathcal{O}(r^3) \quad \text{for } ab = rr, rt, tt; \\
\gamma_{ab} &= a^{(1)}_{ab}\, r + a^{(2)}_{ab}\, r^2 + \mathcal{O}(r^3) \quad \text{for } ab = r\theta, \theta t; \\
\gamma_{\theta\theta} &= a^{(2)}_{ab}\, r^2 + \mathcal{O}(r^3) \quad .
\end{aligned} \tag{E.10}$$

Appendix F

On effective actions

Here we will consider a quadratic dynamical system with two dynamical variables (x, y) and integrate out one of these variables y in order to define an effective action for the remaining variable x. We will then consider the case that the action for the variable y is degenerate and show that the effective action will take a special form. This can be easily generalized to systems with more variables.

We start with an action

$$S_\lambda = \frac{1}{2} \begin{pmatrix} x \\ y \end{pmatrix}^{\mathrm{t}} \cdot M \cdot \begin{pmatrix} x \\ y \end{pmatrix} + \begin{pmatrix} x \\ y \end{pmatrix}^{\mathrm{t}} \cdot \begin{pmatrix} b_x \\ b_y \end{pmatrix} + \begin{pmatrix} (\rho - x) \\ 0 \end{pmatrix}^{\mathrm{t}} \cdot \begin{pmatrix} \lambda \\ 0 \end{pmatrix} \tag{F.1}$$

with dynamical variables (x, y), "boundary values" (b_x, b_y) and a Lagrange multiplier term, which enforces $x = \rho$. We will assume that the matrix M is invertible.

Variation with respect to x and y leads to equations of motion, which are solved by

$$\begin{pmatrix} x \\ y \end{pmatrix} \;=\; -M^{-1} \cdot \begin{pmatrix} b_x \\ b_y \end{pmatrix} + M^{-1} \cdot \begin{pmatrix} \lambda \\ 0 \end{pmatrix} \quad . \tag{F.2}$$

We will now differentiate two cases, firstly the case (i) $M_{yy} \neq 0$ (or in the higher–dimensional case $\det M_{yy} \neq 0$) and secondly the case (ii), which is that $M_{yy} = 0$.

In case (i), as

$$(M^{-1})_{xx} \;=\; \frac{M_{yy}}{\det M} \tag{F.3}$$

we find that the solution for x is λ–dependent. Let us denote by $x_0[b_x, b_y]$ the solution for $\lambda = 0$. Then we have the solution

$$x = x_0[b_x, b_y] + \frac{M_{yy}}{\det M}\lambda \quad , \tag{F.4}$$

which we insert into the Lagrange multiplier equation $\rho = x$ and solve for λ:

$$\lambda = \frac{\det M}{M_{yy}} \left(\rho - x_0[b_x, b_y]\right) \quad . \tag{F.5}$$

Inserting these solutions back into the action we find

$$\begin{aligned} S_\lambda &\underset{\text{sol. for } x,y}{=} -\frac{1}{2}\begin{pmatrix} b_x \\ b_y \end{pmatrix}^{\mathrm{t}} \cdot M^{-1} \cdot \begin{pmatrix} b_x \\ b_y \end{pmatrix} + \frac{1}{2}\begin{pmatrix} \lambda \\ 0 \end{pmatrix}^{\mathrm{t}} \cdot M^{-1} \cdot \begin{pmatrix} \lambda \\ 0 \end{pmatrix} + \lambda(\rho - x_0[b_x, b_y] - \tfrac{M_{yy}}{\det M}\lambda) \\ &\underset{\text{sol. for } \lambda}{=} \frac{\det M}{M_{yy}}\left(\frac{1}{2}\rho^2 - \rho\, x_0[b_x, b_y]\right) + \frac{1}{2}\frac{\det M}{M_{yy}}(x_0[b_x, b_y])^2 - \frac{1}{2}\begin{pmatrix} b_x \\ b_y \end{pmatrix}^{\mathrm{t}} \cdot M^{-1} \cdot \begin{pmatrix} b_x \\ b_y \end{pmatrix} \end{aligned} \tag{F.6}$$

which can be adopted as effective action for the dynamical variable $\rho = x$.

For case (ii) we will however find that the solution for x does not depend on λ, but is determined only by the boundary values $x = x_0[b_x, b_y]$. Thus we *cannot* solve the Lagrange multiplier equation $\rho = x = x_0[b_x, b_y]$ for λ. We have rather to understand this equation as a condition on the parameter ρ. Evaluating the action on the solution we obtain

$$S_\lambda \underset{\text{sol. for } x,y}{=} -\frac{1}{2}\begin{pmatrix} b_x \\ b_y \end{pmatrix}^{\mathrm{t}} \cdot M^{-1} \cdot \begin{pmatrix} b_x \\ b_y \end{pmatrix} + \lambda(\rho - x_0[b_x, b_y]) \tag{F.7}$$

where λ remains a free variable, enforcing $\rho = x_0[b_x, b_y]$. The term quadratic in λ which appears in (F.6) is now vanishing, as we have $(M^{-1})_{xx} = 0$. Thus the on-shell action is just given by the on-shell action of $S_{\lambda=0}$ plus the Lagrange multiplier term, with the solution for x inserted.

Appendix G

Spherical tensor harmonics

Here we define scalar, vector and tensor spherical harmonics. These spherical harmonics are eigenfunctions of the Laplace operator and are furthermore characterized by their divergence and their trace [197]. We denote by Y^{lm} the scalar spherical harmonics (and omit the indices (l,m)). Furthermore we consider here a unit sphere, that is fix $r=1$. The vector and tensor harmonics are defined by

$$\begin{aligned} &\Psi_A = D_A Y, && \Phi_A = \epsilon_A{}^B D_B Y, \\ &\Psi_{AB} = D_B D_A Y + \tfrac{1}{2} l(l+1) h_{AB} Y, && \Phi_{AB} = \tfrac{1}{2}\left(D_A \Phi_B + D_B \Phi_A\right), \qquad \Theta_{AB} = h_{AB} Y \end{aligned} \tag{G.1}$$

with $\epsilon_\theta{}^\varphi = \sin^{-1}\theta$ and $\epsilon_\varphi{}^\theta = -\sin\theta$.

We have the following properties for $\Box = D^A D_A$:

$$\begin{aligned} &\Box Y = -l(l+1) Y\,, \\ &\Box \Psi_B = (1 - l(l+1))\Psi_A\,, \qquad \Box \Phi_B = (1 - l(l+1))\Phi_A\,, \\ &\Box \Psi_{BC} = (4 - l(l+1))\Psi_{BC}, \quad \Box \Phi_{BC} = (4 - l(l+1))\Phi_{BC}\,, \quad \Box \Theta_{BC} = -l(l+1)\Theta_{BC} \end{aligned} \tag{G.2}$$

Furthermore

$$\begin{aligned} &D^A \Psi_A = -l(l+1) Y\,, && D^A \Phi_A = 0 \\ &D^A \Psi_{AB} = \tfrac{1}{2}(2 - l(l+1))\Psi_B, && D^A \Phi_{AB} = \tfrac{1}{2}(2 - l(l+1))\Phi_B, \quad D^A \Theta_{AB} = \Psi_B\,. \end{aligned} \tag{G.3}$$

Finally we have for the trace of the tensor modes

$$h^{AB}\Psi_{AB} = 0\,, \quad h^{AB}\Phi_{AB} = 0\,, \quad h^{AB}\Theta_{AB} = 2Y \quad . \tag{G.4}$$

APPENDICES FOR PART II

Appendix H

Curved simplex areas as functions of the dihedral angles

We use the drop vertex notation, where $\sigma(k)$ is the tetrahedron obtained from the four-simplex $(ijklm)$ by dropping the vertex k and $\sigma(kl)$ is the triangle obtained by dropping vertices k and l. This triangle contains edges $\sigma(ikl)$ and $\sigma(jkl)$. Denote the 2D face angle between these two edges by $\alpha_{ij,kl}$, where the second index pair indicates the triangle $\sigma(kl)$ and the first pair indicates the vertices dropped to obtain each of the edges. Similarly, the 3D dihedral angle in tetrahedron $\sigma(k)$ between triangles $\sigma(ik)$ and $\sigma(jk)$ and hinged at the edge $\sigma(ijk)$ is denoted $\phi_{ij,k}$. Finally, the 4D dihedral angle between the tetrahedra $\sigma(i)$ and $\sigma(j)$ and hinged at $\sigma(ij)$ is θ_{ij}.

Because all of these angles are defined in the appropriate tangent space many of the properties of flat simplices can be carried over to the spherical case. For example, by intersecting a small enough neighborhood of the vertex m (contained in simplex $(ijklm)$) by a sphere, the spherical cosine law yields

$$\cos\alpha_{ij,kl} = \frac{\cos\phi_{ij,k} + \cos\phi_{il,k}\cos\phi_{jl,k}}{\sin\phi_{il,k}\sin\phi_{jl,k}}. \tag{H.1}$$

Carrying out the analogous argument in one higher dimension also yields

$$\cos\phi_{ij,k} = \frac{\cos\theta_{ij} + \cos\theta_{ik}\cos\theta_{jk}}{\sin\theta_{ik}\sin\theta_{jk}}. \tag{H.2}$$

Using these two results we can relate the 2D face angles and the 4D dihedral angles. First note that all of these dihedral angles take values in the range $\theta \in [0, \pi]$ and we can

safely exchange $\sin\theta = \sqrt{1-\cos^2\theta}$. Then after a little algebra, and briefly adopting the shorthand $\cos\theta \equiv \mathrm{c}\theta$, we have

$$\mathrm{c}\alpha_{ij,kl} = \frac{\mathrm{c}\theta_{ij} + \mathrm{c}\theta_{ik}\mathrm{c}\theta_{jk} + \mathrm{c}\theta_{il}\mathrm{c}\theta_{jl} - \mathrm{c}\theta_{ij}\mathrm{c}^2\theta_{kl} + \mathrm{c}\theta_{il}\mathrm{c}\theta_{jk}\mathrm{c}\theta_{kl} + \mathrm{c}\theta_{jl}\mathrm{c}\theta_{ik}\mathrm{c}\theta_{kl}}{\sqrt{(1-\mathrm{c}^2\theta_{il}-\mathrm{c}^2\theta_{ik}-\mathrm{c}^2\theta_{kl}-2\mathrm{c}\theta_{il}\mathrm{c}\theta_{ik}\mathrm{c}\theta_{kl})(1-\mathrm{c}^2\theta_{il}-\mathrm{c}^2\theta_{ik}-\mathrm{c}^2\theta_{kl}-2\mathrm{c}\theta_{il}\mathrm{c}\theta_{ik}\mathrm{c}\theta_{kl})}}. \tag{H.3}$$

Combining this result with the spherical excess formula for the area of a triangle, $A_t = \alpha + \beta + \gamma - \pi$, gives a general expression for $A_t(\theta^\sigma)$. With the appropriate change to the formula for the area, the same results apply to a finite simplex in the hyperbolic case.

Appendix I

The Gram matrix and the derivatives of its determinant

Consider an n-simplex σ. It has $(n+1)$ vertices v_i, $i \in \{1 \cdots n+1\}$ and $(n+1)$ faces f_i (defined as the $(n-1)$-simplex obtained by removing the vertex v_i from the simplex σ), each face with a corresponding volume V_i. Let $\hat{n}_i$ be the outward unit normal to the face f_i. Each pair of faces f_i and f_j share a common hinge h_{ij} (the $(n-2)$-simplex obtained by removing the vertices v_i and v_j) and the angle between the unit normals $\hat{n}_i$ and $\hat{n}_j$ defines the dihedral angle at the hinge h_{ij}

$$\cos\theta_{ij} \;=\; -\langle \hat{n}_i, \hat{n}_j \rangle \quad , \tag{I.1}$$

where θ_{ij} is the dihedral angle between the faces f_i and f_j. The *Gram matrix* is defined as the symmetric matrix G^σ whose elements are given by

$$G^\sigma_{ij} = -\cos(\theta^\sigma_{ij}) \quad , \qquad G^\sigma_{ii} = 1.$$

Every closed flat simplex σ satisfies the closure constraint

$$\sum_i V_i \, \hat{n}_i = 0 \quad , \tag{I.2}$$

where V_i is the volume of the face f_i. Using (I.2), the Gram matrix has a null space given by the vector with entries $\{V_i\}$, i.e.

$$\sum_j G^\sigma_{ij} V_j \;=\; \sum_j \langle \hat{n}_i, \hat{n}_j \rangle V_j \;=\; \sum_j \langle \hat{n}_i, V_j \, \hat{n}_j \rangle \;=\; 0. \tag{I.3}$$

It follows that the Gram matrix is singular and $\det(G^\sigma) = 0$. Any other null vector of G^σ is proportional to V_i, therefore V_i is the only null vector for G^σ. For a non-degenerate simplex the $(n+1)$ vectors $\hat{n}_i$ span an n-dimensional space, thus there are no further null vectors for the Gram matrix in this case.

Using Jacobi's formula for matrices, we can express the derivative of the determinant of the Gram matrix in terms of its adjugate matrix $\mathrm{adj}(G^\sigma)$:

$$d\det(G^\sigma) = \mathrm{Tr}\left(\mathrm{adj}(G^\sigma)\, dG^\sigma\right) \quad , \tag{I.4}$$

and the second derivative is given by

$$dd\det(G^\sigma) = \mathrm{Tr}\left(d\mathrm{adj}(G^\sigma)\, dG^\sigma\right) + \mathrm{Tr}\left(\mathrm{adj}(G^\sigma)\, ddG^\sigma\right) \quad . \tag{I.5}$$

The adjugate matrix of any matrix A is defined as the transpose of the matrix of cofactors of A, with the cofactor matrix given by $C_{ij} = (-1)^{i+j}\det A(ij)$ where $A(ij)$ is the matrix A with the i^{th} row and j^{th} column removed. The adjugate matrix satisfies the relation

$$\mathrm{adj}(A)A = A\,\mathrm{adj}(A) = \det(A)\mathbb{I} \quad , \tag{I.6}$$

where $\mathbb{I}$ is the identity matrix.

For the second derivative of the Gram matrix we thus need the derivative of the adjugate of the Gram matrix. The usual trick of taking the derivative of equation (I.6) does not help, as G^σ is not invertible. We thus have to use the explicit definition of the adjugate in terms of the determinants of sub-matrices and use again Jacobi's formula

$$d(\mathrm{adj}(G^\sigma))_{ij} = (-1)^{i+j} d\det G^\sigma(ji) = (-1)^{i+j}\,\mathrm{Tr}\left(\mathrm{adj}(G^\sigma(ji))\, dG^\sigma(ji)\right) \quad . \tag{I.7}$$

Following [221] we will now determine the structure of the adjugate ot the Gram matrix. As noted above the Gram matrix for a non–degenerate simplex has exactly one null vector. For a symmetric matrix A which has a unique null vector N, the adjugate is given by

$$\mathrm{adj}(A)_{ij} = c\, N_i N_j \quad , \tag{I.8}$$

with c a constant that we will determine below.

Proof

Since A has only one null vector and $\det(A) = 0$, the relation given in (I.6) implies that the image of $\mathrm{adj}(A)$ is contained in the kernel of A, which is given by N. Hence $\mathrm{adj}(A)$ has rank 1. As A and therefore adj$A$ is symmetric we can conclude that $\mathrm{adj}(A)_{ij} = c\, N_i N_j$.

By definition, the principal n minors of an $(n+1)\times(n+1)$ matrix A are given by the diagonal elements of $\mathrm{adj}(A)$. If A has only one zero eigenvalue, then from the characteristic polynomial, the product of non-zero eigenvalues equals the sum of the principal n minors of A

$$c\sum_i N_i N_i = \prod_{\lambda_i\neq 0}\lambda_i. \tag{I.9}$$

For the Gram matrix the null vector is given by $N_i = V_i$ and the adjugate is thus $\mathrm{adj}(G^\sigma) = cV_iV_j$. The constant c is given by

$$c \;=\; \frac{\prod_{\lambda_i\neq 0}\lambda_i}{\sum_k V_k^2} \;=\; \frac{\det(G^\sigma_{ij}+V_iV_j)}{\left(\sum_k V_k^2\right)^2} \quad . \tag{I.10}$$

Therefore the derivate of the Gram matrix is

$$d\det(G^\sigma) \;=\; 2c\sum_{i<j} V_iV_j\sin(\theta^\sigma_{ij})d\theta^\sigma_{ij} \;=\; 2c\sum_{i<j}\frac{n}{n-1}VV_{ij}d\theta^\sigma_{ij} \tag{I.11}$$

where we used the generalized law of sines (see e.g. [159, 222] for a derivation)

$$\sin\theta_{ij} \;=\; \frac{n}{n-1}\frac{V_{ij}V}{V_iV_j} \quad , \tag{I.12}$$

V is the volume of the simplex σ, and V_{ij} is the volume of the hinge h_{ij}.

We thus have

$$\frac{\partial\det(G^\sigma)}{\partial\theta_{ij}} \;=\; c'\,V_{ij}\;, \qquad c' = 2\,\frac{n}{n-1}V\,\frac{\det(G^\sigma_{ij}+V_iV_j)}{\left(\sum_k V_k^2\right)^2} \quad . \tag{I.13}$$

Appendix J

Edge lengths from areas and dihedral angles of a tetrahedron

We derive a formula for the edge lengths of a tetrahedron expressed as a function of its four triangle areas and any two of its dihedral angles along non-opposite edges. As was explained in Appendix I, the Gram matrix has one null vector whose components are given by V_i. For a tetrahedron this gives a set of four equations for the 3D dihedral angles ϕ_{ij}

$$\sum_{i \neq j} V_i \cos \phi_{ij} - V_j \; = \; 0 \tag{J.1}$$

where V_i is the area of the triangle obtained from τ by dropping the vertex i. We can solve for four of the dihedral angles as a function of the four areas and two of the dihedral angles.[1] The remaining two dihedral angles must be such that they are non-opposite. In general, for an n-simplex, $n+1$ dihedral angles can be solved for and n of these must be the dihedral angles of the n hinges of any face f_i. As an example, for a tetrahedron τ with

[1] One might wonder why the closure relations (J.1), which constitute only 3 independent equations for a tetrahedron, allow one to solve for 4 quantities. The reason is that the ϕ_{ij} are also not independent; they satisfy $\det G^\tau = 0$.

vertices $(1,2,3,4)$ one can solve for the 3D (interior) dihedral angles ϕ_{ij}

$$\cos\phi_{14} = \frac{V_1 - V_2\cos\phi_{12} - V_3\cos\phi_{13}}{V_4} \quad , \tag{J.2}$$

$$\cos\phi_{23} = \frac{V_1^2 + V_2^2 + V_3^2 - V_4^2 - 2V_1\left(V_2\cos\phi_{12} + V_3\cos\phi_{13}\right)}{2V_2V_3} \quad , \tag{J.3}$$

$$\cos\phi_{24} = \frac{-V_1^2 + V_2^2 - V_3^2 + V_4^2 + 2V_1V_3\cos\phi_{13}}{2V_2V_4} \quad , \tag{J.4}$$

$$\cos\phi_{34} = \frac{-V_1^2 - V_2^2 + V_3^2 + V_4^2 + 2V_1V_2\cos\phi_{12}}{2V_3V_4} \quad . \tag{J.5}$$

Heron's formula gives the area of a triangle as a function of its edge lengths. For the triangle $\tau(i)$,

$$V_i = \frac{1}{4}\sqrt{\sum_{j,k\neq i} V_{ij}^2V_{ik}^2 - 2\sum_{j\neq i} V_{ij}^4} \quad , \tag{J.6}$$

where V_{ij} is the length of the edge obtained by dropping the vertices i and j from τ. We shall also make use of the generalized law of sines in three dimensions

$$V_{ij} = \frac{2}{3}\frac{V_iV_j\sin\phi_{ij}}{V} \quad , \tag{J.7}$$

with V the volume of the tetrahedron. Using the generalized law of sines and Heron's formula, Eqs. (J.6) and (J.7), one can compute the volume of the tetrahedron as a function of its four areas and all 6 dihedral angles. The result is given by (N.B. $\sin\phi_{ii} = 0$)

$$V = \frac{1}{3}\sqrt[4]{V_i^2\left(\sum_{j,k} V_j^2V_k^2\sin^2\phi_{ij}\sin^2\phi_{ik} - 2\sum_j V_j^4\sin^4\phi_{ij}\right)} \quad . \tag{J.8}$$

Substituting this formula into the generalized law of sines, one obtains a formula for the edge lengths of a tetrahedron as a function of its four areas and all its dihedral angles. Then, using the four solutions for the dihedral angles from (C2-C5), we get the edge lengths of the tetrahedron as a function of the areas of the face triangles and two non-opposite dihedral angles.

As an example, we compute the edge length $e(34)$ of the tetrahedron $\tau(1,2,3,4)$ as a function of the four areas and the dihedral angles ϕ_{12} and ϕ_{13}. Using the short hand notation $\sin\phi_{ij} \equiv \mathrm{s}\phi_{ij}$, we have

$$V_{12} = \frac{2\sqrt{V_1}V_2\,\mathrm{s}\phi_{12}}{\left(2\left[V_2^2V_3^2\,\mathrm{s}\phi_{12}^2\mathrm{s}\phi_{13}^2 + V_2^2V_4^2\,\mathrm{s}\phi_{12}^2\mathrm{s}\phi_{14}^2 + V_3^2V_4^2\,\mathrm{s}\phi_{13}^2\mathrm{s}\phi_{14}^2\right] - V_2^4\,\mathrm{s}\phi_{12}^4 - V_3^4\,\mathrm{s}\phi_{13}^4 - V_4^4\,\mathrm{s}\phi_{14}^4\right)^{1/4}}, \tag{J.9}$$

where

$$\sin^2 \phi_{14} = 1 - \left(\frac{V_1 - V_2 \cos \phi_{12} - V_3 \cos \phi_{13}}{V_4} \right)^2 \quad . \tag{J.10}$$

Appendix K

Derivation of the brackets between dihedral angles

.

The Poisson bracket on N copies of the dual to the Lie algebra of $\mathfrak{su}(2)$ is

$$\{f, g\} = \sum_{I=1}^{N} \vec{J}_I \cdot \left(\frac{\partial f}{\partial \vec{J}_I} \times \frac{\partial g}{\partial \vec{J}_I} \right), \tag{K.1}$$

where each of the $\{\vec{J}_I\}_{I=1}^N$ can be thought of as an angular momentum vector $\vec{J}_I = (J_{I1}, J_{I2}, J_{I3})$. Consider the case $N = 4$, which gives the phase space of a tetrahedron described in terms of the Minkowski area vectors $\vec{A}_I = \gamma \vec{J}_I$ whose magnitudes A_I are equal to the tetrahedron's face areas and whose directions are normal to the faces. (References [8] of the main text provide additional details about this phase space and how it connects to the geometry of the tetrahedron.) The (internal) dihedral angle ϕ_{IK} between the triangles labelled by I and K is determined by

$$\vec{A}_I \cdot \vec{A}_K = -A_I A_K \cos \phi_{IK}.$$

Define $B_{12,23} \equiv \{\vec{A}_1 \cdot \vec{A}_2, \vec{A}_2 \cdot \vec{A}_3\}$ and note that

$$B_{12,23} = A_1 A_2^2 A_3 \sin \phi_{12} \sin \phi_{12} \{\phi_{12}, \phi_{23}\}, \tag{K.2}$$

where we used the derivation property of the bracket. On the other hand, we can make

use of Eq. (K.1) to compute

$$\begin{aligned} B_{12,23} &= \sum_I \epsilon_{ijk} J_{Ii} \frac{\partial}{\partial J_{Ij}} (A_{1m} A_{2m}) \frac{\partial}{\partial J_{Ik}} (A_{2n} A_{3n}) \\ &= -\gamma \ \vec{A}_1 \cdot (\vec{A}_2 \times \vec{A}_3) \ = \ -\gamma \frac{9}{2} V^2 \end{aligned} \tag{K.3}$$

where we drew on the following expression for the volume of a tetrahedron $V^2 = \frac{2}{9}\vec{A}_1 \cdot (\vec{A}_2 \times \vec{A}_3)$. This volume can be also computed through $V = \frac{2}{3} l_{IK}^{-1} A_I A_K \sin\phi_{IK}$,where l_{IK} is the length of the edge shared by triangles I and K. Using this formula twice gives

$$B_{12,23} = -\frac{2\gamma}{l_{12} l_{23}} A_1 A_2^2 A_3 \sin\phi_{12} \sin\phi_{23}. \tag{K.4}$$

Setting the two expressions (K.2) and (K.4) equal gives

$$\{\phi_{12}, \phi_{23}\} = -\frac{2\gamma}{l_{12} l_{23}}. \tag{K.5}$$

Finally, noting that $A_2 = \frac{1}{2} l_{12} l_{23} \sin\alpha_{12,23}$, where $\alpha_{12,23}$ is the angle between the edges with lengths l_{12} and l_{23}, yields the result quoted in the text, Eq. (6),

$$\{\phi_{12}, \phi_{23}\} = -\gamma \frac{\sin\alpha_{12,23}}{A_2}. \tag{K.6}$$

Of course, the minus sign in this result is just due to the choice of an increasing index ordering for the bracket.

Appendix L

Equations of motion from Area-Angle action

We will show that the equations of motion coming from the area-angle Regge action evaluated on a constraint hypersurface coincides with the length Regge equations of motions. To start, let us consider a version of the area-angle action given by

$$S_{\rm AA1} = \sum_t A_t\, \epsilon_t(A_{t'}) + \sum_\tau \sum_{\sigma\supset\tau} \sum_i \lambda^i_{(\sigma,\tau)} \left(\phi^i_\tau - \Phi^i_{(\sigma,\tau)}(A_t)\right) \tag{L.1}$$

where $\Phi^i_{(\sigma,\tau)}(A_t)$ is the 3D dihedral angle in the tetrahedron τ as computed from the areas in the 4-simplex σ. The Lagrange multiplier term $\lambda^i_{(\sigma,\tau)}$, imposes the constraints (9.5) for each bulk tetrahedra with i labelling two (non-opposite) 3D angles per tetrahedron ϕ^i_τ which is shared by two 4-simplices. Also, $\epsilon_t = 2\pi - \sum_{\sigma\supset t} \theta^\sigma_t(A_{t'})$ is the deficit angle hinged at the triangle t and ϕ^i_τ are the 3D angle variables .

A version without explicit 3D angle variables arises after integrating out ϕ^i_τ. The corresponding equations of motion demands that

$$\lambda^i_{(\sigma,\tau)} + \lambda^i_{(\sigma',\tau)} = 0 \tag{L.2}$$

where σ, σ' are the two 4-simplices sharing τ. Reinserting these solutions into the action (L.1) leads to

$$S_{\rm AA2} = \sum_t A_t \epsilon_t(A_{t'}) + \sum_\tau \sum_i \lambda^i_{(\sigma,\tau)} \left(\Phi^i_{(\sigma,\tau)}(A_t) - \Phi^i_{(\sigma',\tau)}(A_t)\right) \quad . \tag{L.3}$$

Note that we have suppressed discrete degeneracy parameters, which distinguish different roots of the Area-Length system. Variation of the action (L.3) with respect to the areas A_t (using Schläfli identity) gives

$$\frac{\delta S_{\mathrm{AA2}}}{\delta A_t} = \epsilon_t(A_{t'}) + \sum_\tau \sum_i \lambda^i_\tau \left(\frac{\partial \Phi^i_{(\sigma,\tau)}(A_t)}{\partial A_t} - \frac{\partial \Phi^i_{(\sigma',\tau)}(A_t)}{\partial A_t} \right) \quad . \tag{L.4}$$

Now, we have

$$\frac{\partial \Phi^i_{(\sigma,\tau)}(A_t)}{\partial A_t} \underset{\text{if } \tau \subset \sigma}{=} \frac{\partial \Phi^i_\tau(l_e)}{\partial l_e} \cdot \frac{\partial L^\sigma_e(A_t)}{\partial A_t} \tag{L.5}$$

where $\Phi^i_\tau(l_e)$ is the 3D dihedral angles defined by lengths in τ and $L^\sigma_e(A_t)$ are the lengths computed in the simplex σ from its areas. Contracting the equations of motion (L.4) with $\frac{\partial A_t(l_e)}{\partial l_e}$ and evaluating on 'geometric' configurations, $A_t = A_t(l_e)$, the constraint term becomes

$$\frac{\partial \Phi^i_\tau(l_e)}{\partial l_e} - \frac{\partial \Phi^i_\tau(l_e)}{\partial l_e} = 0 \tag{L.6}$$

and hence drops out. Thus, we remain with

$$\sum_t \epsilon_t \frac{\partial A_t(l_e)}{\partial l_e} = 0 \tag{L.7}$$

which give the length Regge equations of motion. As $\frac{\partial A_t(l_e)}{\partial l_e}$ has left null vectors (corresponding to area oreintations of the constraint hypersurface), there are more equations of motions which involve λ's and can be expected to therefore fix these Lagrange multipliers.

Appendix M

Counting of length configurations

We consider a triangulation with certain edge lengths chosen to be equal and then compute the number of allowed edge length solutions given locally independent discrete asymptotically equidistant area spectra. To start with we consider one 4-simplex with vertices (12345) and $p = 2, 3, 4$ length parameters. For $p = 2$, we set $l_{ij} = x$ and $l_{i5} = y$, where $i, j = 1, 2, 3, 4$. For the $p = 3$ case we choose: $l_{ij} = x, l_{mn} = y$ and $l_{im} = z$ where $i, j = 1, 2, 3$ and $m, n = 4, 5$. For $p = 4$ we have $l_{ij} = w, l_{i4} = x, l_{i5} = y$ and $l_{45} = z$ where $i, j = 1, 2, 3$. We count all edge length solutions where the triangle areas take discrete values $A_t \in \{\frac{1}{2}, 1, \cdots, N\}$ for $N \in \mathbb{N}$. The left panel of Figure M.1 shows a semilog plot of the number of length solutions for a simplex having $p = 2, 3, 4$ length parameters. The number of length configurations scale as $N^{1.03p} \approx N^p$.

We also consider a gluing of two simplices with vertices $\sigma = (12345)$ and $\sigma' = (12346)$. For the shared tetrahedron we allow two length parameters u for the edges (12) and (34) and v for the remaining four edges. All four areas of the tetrahedron therefore agree, and we are left with one area parameter $a = A(u, v, v)$. Here $A(x_1, x_2, x_3)$ denotes the area of a triangle with edge lengths (x_1, x_2, x_3). For the simplex σ we introduce additional edge lengths w for edges $(i5)$ with $i = 1, 2, 3, 4$. This introduces two more area parameters $b = A(u, w, w)$ and $c = A(v, w, w)$, giving us three length and three area parameters for σ. We make the same kind of choices for σ', that is, w' gives the length of the edges $(i6)$ leading to area parameters $b' = A(u, w', w')$ and $c' = A(v, w', w')$. After gluing the complex has four lengths parameters (u, v, w, w') and five area parameters (a, b, c, b', c').

We proceed to count the number of configurations with all areas valued in $\{\frac{1}{2}, 1, \cdots, N\}$, and which have a maximum deviation (9.14) for the pairs $(\Phi^{\tau,\sigma}_{e_i}, \Phi^{\tau,\sigma'}_{e_i})$ of 3d dihedral angles in the shared tetrahedron. The right panel of Fig. M.1 shows the results for various choices

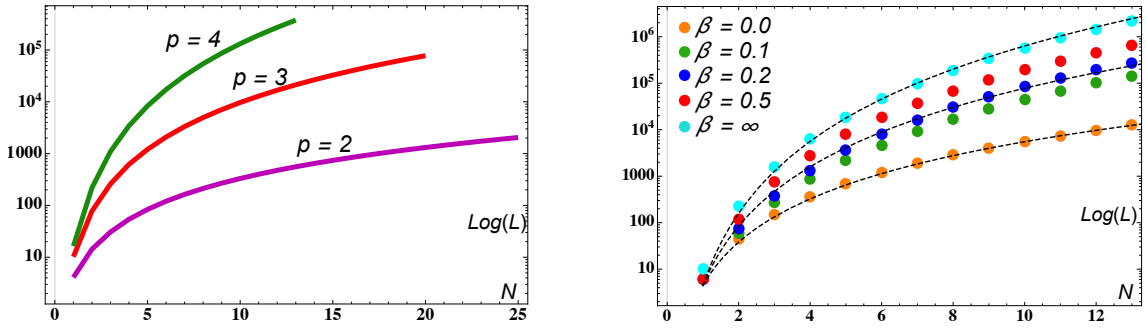

(a) (b)

Figure M.1: Log-linear plots of the number L of length configurations as a function of the maximal area. (a) Count of length configurations with areas up to N in a simplex with p length parameters. (b) The count for two glued simplices with four length parameters. The dashed lines show N^3, N^4 and N^5 power law scaling.

of the parameters β. For $\beta = 0$, where shape matching is imposed exactly, we find a scaling N^3. This is explained by the fact that requiring exact shape matching forces $w = w'$, and thus we have only three parameters. Not imposing the shape matching conditions, we find a scaling N^5 reflecting the five area parameters for the two glued simplices. For $\beta \approx 0.15$ we find a scaling of N^4, see Fig. M.1.

Appendix N

Triangulations with three and with six 4-simplices

Take three 4-simplices with vertices $(12345), (12356)$ and (13456) respectively, and glue these around the shared triangle (135). Here all edges and all but the triangle (135) are in the boundary. Thus we have one bulk triangle and no bulk edge.

We will assume some lengths to be equal, so that we have overall only three length parameters: $x = l_{ij}, y = l_{mn}$ and $z = l_{im}$, where $i, j = 1, 3, 5$ and $m, n = 2, 4, 6$. Correspondingly, we have three area parameters $a = A(x, x, x), b = A(x, z, z)$ and $c = A(y, z, z)$ where $A(x_1, x_2, x_3)$ denotes the area of a triangle with lengths (x_1, x_2, x_3).

Note that with this special choice of boundary data the boundary areas (b, c) do not determine the boundary lengths (x, y, z). To do so one also needs the bulk area a. In Area Angle Regge calculus one has also 3D dihedral angles as boundary data. With the given symmetry reduction, all boundary tetrahedra have the same geometry, determined by edge lengths (z, y, z, z, x, z). We can choose a pair of non-opposite edges, both with length z. Due to our choice of symmetric boundary data, the 3D dihedral angles ϕ_z for the z–edges are all the same—thus we have boundary data (b, c, ϕ_z). These determine a bulk deficit angle $\epsilon_a(b, c, \phi_z)$.

The matching conditions (9.4) for the bulk tetrahedra are all satisfied due to our symmetry reduction. Thus, if we start from the AARC path integral (9.11), and integrate out the bulk 3D dihedral angles, we will just obtain a multiplicative factor, given by the norm of the coherent states $\mathcal{K}_\tau(\cdot, \Phi)$.

We can now consider the AARC path integral with boundary, which, after integrating out the bulk 3D angles, involves only a summation over one spin j_a.

Alternatively, we can take two such complexes consisting of three 4-simplices each, and glue these so that we obtain a triangulation of S^4. After integrating out all 3D dihedral angles we will have four area parameters, the areas b, c and the bulk areas a and a' from the two complexes respectively. We will compute the expectation value for the deficit angle $\langle\epsilon_a\rangle$—while keeping the areas (a', b, c) fixed. Classically, i.e. with sharp shape-matching constraints and fixed (a', b, c), these data determine the deficit angles $\epsilon_{a'}$ and ϵ_a with $\epsilon_a = \epsilon_{a'}$.

The summation for the path integral thus involves only the bulk area parameter a. There are two contributions to the amplitudes: the exponential of the (Area) Regge action, as well as the inner product $G(a, a')$ between the coherent states, which impose the matching constraints $\Phi_z(a, b, c) = \Phi_z(a', b, c)$. (If we consider the path integral with boundary this factor is given by the coherent state itself, peaked on $\Phi_z(a)$.) We approximate the factor arising from these inner products between the coherent states by

$$G(a, a') = \exp\left(-\frac{9}{2\sigma^2(\Phi)}(\Phi_z(a, b, c) - \Phi_z(a', b, c))^2\right)$$

with

$$\sigma^2(\Phi) = \frac{1}{2}\frac{\sin\alpha(a, b, c)}{(j_b + 1/2)} + \frac{1}{2}\frac{\sin\alpha(a', b, c)}{(j_b + 1/2)}\,. \tag{N.1}$$

where $\sin\alpha(a, b, c) = 2b/Z^2(a, b, c)$ with $Z(a, b, c)$ the length of a z-edge in the complex with areas (a, b, c). The factor 9 in the exponential arises because we have 9 boundary tetrahedra and therefore 9 inner products.

For the computation of the expectation value $\langle\epsilon_a\rangle(a', b, c)$ we use

$$\langle\epsilon_a\rangle(a', b, c) = \frac{1}{\mathcal{Z}}\sum_{j_a}\epsilon_a\; G(a, a')\prod_t \mathcal{A}_t\prod_\sigma \mathcal{A}_\sigma \tag{N.2}$$

with

$$\mathcal{Z} = \sum_{j_a} G(a, a')\prod_t \mathcal{A}_t\prod_\sigma \mathcal{A}_\sigma \tag{N.3}$$

and $\mathcal{A}_t$ and $\mathcal{A}_\sigma$ defined in (9.8) and (9.9) above.

The resulting expectation values are shown in Tables N.1 and N.2. Here we have set $j_b = j_c = j$. Thus the pair $(j, j_{a'})$ determine the scale as well as the deficit angle $\epsilon_{a'}$. Classically we have $\epsilon_a = \epsilon_{a'}$. To reproduce this result for the expectation value we need a

$(j+\frac{1}{2}, j_{a'}+\frac{1}{2}, \epsilon_{a'})$	$\gamma = 0.01$	$\gamma = 0.1$	$\gamma = 0.5$
$(30, 38.5, 0.52)$	$0.78 - 0.03\mathrm{i}$	$0.68 - 0.26\mathrm{i}$	$0.17 - 0.32\mathrm{i}$
$(100, 128, 0.54)$	$0.62 - 0.062\mathrm{i}$	$0.55 - 0.19\mathrm{i}$	$0.17 - 0.27\mathrm{i}$
$(300, 384, 0.54)$	$0.57 - 0.02\mathrm{i}$	$0.51 - 0.17\mathrm{i}$	$0.16 - 0.25\mathrm{i}$
$(1000, 1280, 0.54)$	$0.55 - 0.01\mathrm{i}$	$0.50 - 0.16\mathrm{i}$	$0.16 - 0.24\mathrm{i}$

Table N.1: Expectation value for the deficit angle ϵ_a with classical value ≈ 0.5.

$(j+\frac{1}{2}, j_{a'}+\frac{1}{2}, \epsilon_{a'})$	$\gamma = 0.01$	$\gamma = 0.1$	$\gamma = 0.5$
$(30, 40, 0.08)$	$0.39 - 0.02\mathrm{i}$	$0.33 - 0.15\mathrm{i}$	$0.03 - 0.14\mathrm{i}$
$(100, 133.5, 0.06)$	$0.14 - 0.01\mathrm{i}$	$0.13 - 0.05\mathrm{i}$	$0.03 - 0.06\mathrm{i}$
$(300, 400, 0.08)$	$0.11 - 0.00\mathrm{i}$	$0.09 - 0.03\mathrm{i}$	$0.03 - 0.5\mathrm{i}$
$(1000, 1335, 0.06)$	$0.07 - 0.00\mathrm{i}$	$0.06 - 0.02\mathrm{i}$	$0.02 - 0.03\mathrm{i}$

Table N.2: Expectation value for the deficit angle ϵ_a with classical value ≈ 0.07.

sufficiently large scale j and a sufficiently small value for the Barbero-Immirzi parameter, in particular if we consider data leading to a small deficit angle.

In this example the averaging of the deficit angle with the $G(a, a')$ factor (but without the $\mathcal{A}_t$ and $\mathcal{A}_\sigma$ factors) tends to over-estimate the curvature angle. This is due to a certain asymmetry in the example that partially originates with the generalized triangle inequalities, which restrict a to $a \leq \frac{3}{2}b = \frac{3}{2}c$. The oscillatory behavior of the $\mathcal{A}_t$ and $\mathcal{A}_\sigma$ factors tends to average out the expectation values—more so for larger Barbero–Immirzi parameter γ, which leads to more oscillations over the interval where $G(a, a')$ is sufficiently large, see Fig. N.1 and Fig. 9.1 (in the main text). Note that the expectation values do have imaginary contributions. These arise as the $G(a, a')$ factor peaks away from the stationary point of the action (where $\epsilon_a = 0$), so the imaginary parts do not average out. As the imaginary contributions are sourced by the oscillatory behaviour of the amplitudes, they grow with γ. Having imaginary contributions on the order of the real contributions indicates that the regime is unreliable, even if the (real part of the) expectation value happens to be near the classical value.

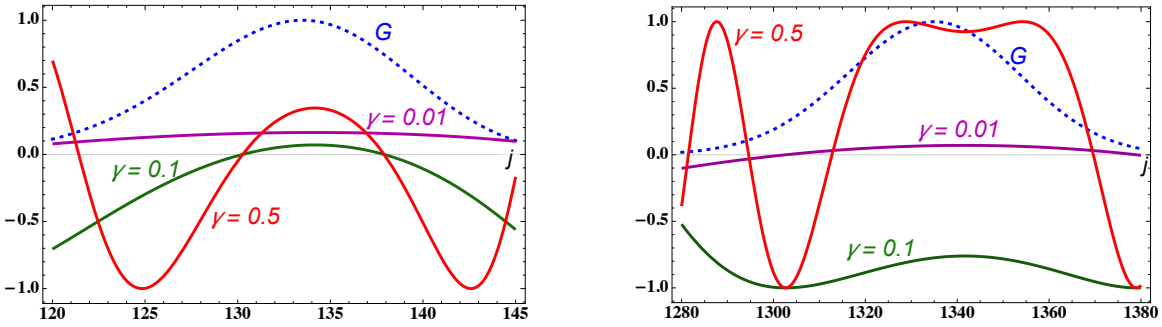

(a) $j = 99.5$ (b) $j = 999.5$

Figure N.1: The $G(a, a')$ factor (dashed) and the real part of the product of the amplitude factors $\mathcal{A}_t$ and $\mathcal{A}_\sigma$ as a function of j_a for $\epsilon_{a'} \sim 0.07$ and different γ–values.